THE UNIVERSITY
of ADELAIDE

Spectroscopic Imaging of Multiplex Bioassays Encoded by Raman and SERS Tags

A Thesis Submitted

By

Umar Azhar, *PMP*

B.E (Hons), MS (Chem. Eng.), MBA (Finance)

For the Degree of Doctor of Philosophy

School of Chemical Engineering

Faculty of Engineering, Computer and Mathematical Sciences

The University of Adelaide, Australia

17th January 2019

I dedicate this whole thesis to my late mother who died from cancer, and my beloved

wife for her support, encouragement and ongoing love.

DECLARATION

I certify that this work contains no material which has been accepted for the award of any other degree or diploma in any university or other tertiary institution and, to the best of my knowledge and belief, contains no material previously published or written by another person, except where due reference has been made in the text. In addition, I certify that no part of this work will, in the future, be used in a submission for any other degree or diploma in any university or other tertiary institution without the prior approval of the University of Adelaide and where applicable, any partner institution responsible for the joint-award of this degree.

I give consent to this copy of my thesis when deposited in the University Library, being made available for loan and photocopying, subject to the provisions of the Copyright Act 1968.

The author acknowledges that copyright of published works contained within this thesis resides with the copyright holder(s) of those works.

I also give permission for the digital version of my thesis to be made available on the web, via the University's digital research repository, the Library catalogue and also through web search engines, unless permission has been granted by the University to restrict access for a period of time.

Name: Umar Azhar

Signed: UMAR AZHAR   Date: 17th January 2019

ACKNOWLEDGEMENTS

ABSTRACT

Suspension microsphere multiplex immunoassays are rapidly gaining recognition in immunoglobulin G (IgG) identification. Detection of multiple analytes from a single sample is critical in modern bioanalytical technique, which always requires complex encoding. However, traditional fluorescent technology has various limitations in such multiplex encoding systems. The aim of this study is to use Raman and surface enhanced Raman scattering (SERS) signatures as novel encoding elements in immunoassays to overcome various problems associated with fluorescence labels. In addition to the amplified capacity of Raman/SERS encoding elements, the use of Raman imaging aimed at reinforcement of qualitative analysis has been demonstrated for the first time. This holds great promise in biomedical applications. In this thesis, a series of IgGs were selected as model proteins, and gold nanoparticles (AuNPs) served as the "hotspot" of SERS-active substrates. Three different Raman-active molecules namely, 4-aminothiophenol (4-ATP), 4-mercaptobenzoic acid (4-MBA), and 3-mercaptopropionic acid (3-MPA) can be easily self-assembled on the AuNPs to form functional SERS tags. Various polymer microbeads (prepared by dispersion polymerization) were utilized as the immune-solid supports together with providing Raman signatures. Additionally, focus was laid on the fabrication of different SERS nanotags and Raman spectroscopic-encoded polymer microbeads for the multiplex, specific and selective detection of biomarkers in dual encoded immunoassay systems.

Raman imaging of different uniform polymer microbeads were evaluated. Polymers are long chain molecules containing many repeating monomer units, which give rise to the strong Raman signals of these monomers. In addition, different monomers can be polymerised together to produce co-polymer microbeads to provide different Raman signatures. The development of polymer microbeads not only improves the detection sensitivity significantly, but also makes these microbeads to be more multiplexed in lieu of specific post-reaction

labelling. Four Raman spectroscopic-encoded copolymer microbeads were fabricated by dispersion polymerization with their average diameters of 1.1 to 1.7 µm. These synthesised microbeads namely, poly(Sty-co-AA), poly(4tBS-co-AA), poly(4MS-co-AA) and poly(GMA-co-AA) revealed narrow size distribution and unique Raman fingerprints, which rendered them to be suitable for Raman imaging and immunoassay analysis. Furthermore, microbeads combining the Raman and SERS signals were successfully fabricated by conjugating a SERS nanotag (4-ATP on the surface of AuNPs) to two Raman encoded polymer microbeads of poly(Sty-co-AA) and poly(4tBS-co-AA). The spectroscopic and imaging results reinforce the suitability of such dual coding systems for immunoassays, which further expands the possibility of Raman/SERS multiplex systems for biological analysis. Finally, a practical demonstration of multiplex IgG immunoassay system based on carboxylated Raman encoded polymer microbeads and SERS nanotags was developed. Antibodies (donkey anti-goat IgG & donkey anti-rabbit IgG) were conjugated to polymer microbeads by EDC coupling chemistry. Two different batches of SERS nanotags comprising of Raman-active molecules (4-MBA & 3-MPA) with AuNPs were synthesised. Moreover, antigens (goat anti-human IgG and rabbit anti-human IgG) were conjugated on SERS tags to form SERS reporters. The immunoassays were performed by mixing the protein conjugated polymer microbeads and SERS reporters. Due to the specific recognition between antibody and antigen, SERS nanotags attached on the surface of their specific antibody polymer microbeads. The results were positively verified from both Raman imaging and spectroscopic analysis.

In summary, a series of SERS nanotags and Raman spectroscopic-encoded copolymer microbeads were successfully synthesised. The thesis further demonstrates Raman imaging analysis as a new strategy for qualitative analysis of complicated multiplex immunoassay with high sensitivity and specificity.

Table of Contents

LIST OF FIGURES

LIST OF TABLES

Chapter 1   **Introduction**

1.1   **Background**

Diseases as noxious as cancer are shadowed by the requisite for therapeutic treatment with side effects inflicted after incurring costly surgeries and medicines. The present time cancer diagnostic tests include physical examination, serological tests, biopsy, imaging (X-ray, PET/CT, MRI, and Ultrasound etc.), nuclear medicine scans, endoscopy and genetic tests. However, these customary technologies are tedious, expensive, limited in their ability to multiplex and to detect cancer in its early stages [1]. To curtail these drawbacks recent times has been stressed upon to undertake extensive research and technological advancements in biomolecular assays. The advancements particularly need to meet the stringent errands such as minimal sample, high sensitivity, rapid diagnosis, multiplex and label-free bioassays.

In context to the above, Raman spectroscopy initially established its viability as a powerful analytical tool with no sample preparation. To date, Raman scattering has been popularly employed in the fields of biology, chemistry, environment, pharmaceuticals, forensics, and materials science [2]. Another obvious advantage of Raman scattering is that it can be applied in aqueous environment, which makes Raman scattering an important analytical tool for biological analysis. Studies have been performed to apply Raman scattering on cancer diagnostics [3-5]. The broad applications of Raman scattering indicate that it is a competitive technique compared to infrared and fluorescence. However, botched to progress due to its inherently weak sensitivity, caused by its small cross-section and weak emission, making it unlikely to achieve measurements with high signal-to-noise (S/N) ratios.

The advent of surface enhanced Raman spectroscopy (SERS) augments Raman spectroscopy with enhanced sensitivity making it once again a frontline contender for bioassay characterization and a bio-imaging modality [6-9]. This enhancement is achieved by adsorbing

sample molecules on a roughened metal surface. This coincidental revelation revived the "Raman effect" in the world of spectroscopy. SERS as a surface-sensitive "Raman effect" enhancement technique helps overcome low sensitivity setback of Raman scattering, and at the same time compliments the multiplexing capabilities. The enhancement factor can be as much as 10^{10} to 10^{11}, which means the technique is able to detect single molecules. Technologies using SERS has experienced significant growth in immunoassay leading its way into clinical translation. Here, it is intended to provide a classifiable understanding of SERS probes and SERS based immunoassay along with its consolidated bio-imaging applications related to cancer detection.

SERS-based immunoassays are developed for complex disease detection. Typically, abnormal cells generate various antigens as the first sign of abnormality in organism. The most representative method for analyses of such disease biomarkers is immunoassays, realized by the immune recognition between antigens (IgG's) and relevant specific antibodies. Traditional labels, including enzyme, fluorescence, isotopes, and luminescence, are normally employed to assist the detection of specific antibody and antigen interaction during the immunoassays. Markedly, SERS labels have many advantages over these traditional labels, such as no photobleaching, narrow emission spectra, high sensitivity and throughput. This type of assay consists of two major structural parts, to capture the target analyte: (1) SERS tags/probes used to specially bind to the target analyte attached to the SERS substrate providing SERS spectra, and (2) Immune substrate used to provide a stable platform to specifically bind and immobilize the target analyte. In practice, solid surfaces have to be used as immune substrates, but their application is limited by the extended incubation time and repeated washing process [10]. Alternatively, living cells or solids particles can also be used as the immune supports [11]. The antigen concentration at the early-stage of disease is relatively low and the complex

environment of the cell conceals the Raman signals of the analytes. However, particle-based SERS immunoassays can overcome these complications.

Polymers have marked their profound use in our daily life, industries and biotechnology. Their unique molecular structure, stability and ability to be bioconjugated make them an ideal contender for use in latex immunoassays [12]. Surface functionalized polymer beads covalently bonded to bio-ligands have been widely pragmatic, as a diagnosis of rheumatoid and detection of human rotaviruses. Moreover, polymers micro- and nano- beads have been reported for sandwich immunoassays [13-14]. The development of different polymers with unique Raman signature will result in a large pool of barcoded library, which can be applied in the multiplex detection system [15]. Therefore, the combination of Raman encoded polymer beads and SERS allows the development of a large pool of combinatorial chemistry and multiplexing diagnostics for complex disease diagnosis. To date, there are insufficient reports on the Raman/SERS spectroscopy especially imaging of particle-based SERS immunoassays.

1.2 Aims and Objectives

This project aims at developing a rapid, reproducible and highly selective multiplex imaging from Raman encoded polymer microbeads and SERS-dual coded immunoassays. Different Raman spectroscopic-encoded polymer microbeads conjugated to SERS-reporters are going to be prepared. The microbeads can serve as immune-solid supports and provide unique Raman signatures during the Raman imaging. It is expected that this research project can develop a new technique for ultrasensitive biomedical imaging as well as improving the feasibility and efficiency of polymer and nanomaterials in bioassay. The systems were characterized using Raman/SERS spectroscopy, reinforced through spectroscopic imaging of the multiplex bioassays with specific objectives:

(1)   to prepare suitable-sized gold nanoparticles (AuNPs) as the "hotspot" of SERS ,

(2)   to synthesise various surface-functionalized copolymer microbeads with unique Raman signatures by dispersion polymerisation, namely, poly(styrene-*co*-acrylic acid), poly(4-methylstyrene-*co*-acrylic acid), poly(4-tetrabutylstyrene-*co*-acrylic acid) and poly(glycidyl methacrylate-*co*-acrylic acid),

(3)   to produce the SAMs of Raman-active molecules, e. g. 4-aminothiophenol (4-ATP), 4-mercaptobenzoic acid (4-MBA), and 3-mercaptopropionic acid (3-MPA), on AuNPs and characterize their SERS signatures,

(4)   to synthesise dual encoder system comprising of two Raman microbeads and SERS tags, and their positive readout by Raman spectrums and high-resolution multiplex imaging.

(5)   to evaluate the efficiency and feasibility of microbead-based Raman/SERS immunoassays for Immunoglobulin (IgG) detection through Raman spectroscopy and imaging.

1.3   Thesis Outline

This thesis is written in a publication-based format. The following chapter descriptions provide a short summary of the thesis. **Chapter 1** introduces the background of the project and current research gaps of applying Raman and surface enhanced Raman scattering for multiplex detection. This is followed by the aim and objectives of this study together with an outline of the thesis. **Chapter 2** outlines a comprehensive literature review related to this project. This includes an introduction to Raman scattering, surface enhanced Raman scattering, SERS immunoassays. Furthermore, SERS immunoassays and Raman bioimaging were reviewed in substantial detail in this section. In **Chapter 3**, surface functionalized copolymer microbeads with narrow size distribution and unique Raman signatures were synthesised using modified

dispersion polymerisation, namely, poly(Sty-AA), poly(4tBS-AA), poly(4MS-AA) and poly(GMA-AA). The obtained microbeads were characterised and evaluated for their potential applications as the support in Raman coding bioassays. **Chapter 4** shows Raman imaging being successfully performed of two Raman encoded polymer microbeads of poly(Sty-AA) and poly(4tBS-AA) conjugated to a SERS nanotag (4-ATP on the surface of AuNPs). The result promises a substantial increase in the current combinatorial library for label free multiplexing in bioassays. Various characterisation from UV-vis spectrophotometer, titration, TEM, SEM, Raman spectrometer and Raman mapping reinforced their importance as the Raman/SERS dual coding supports in bead-based bioassays. In **Chapter 5**, a practical demonstration of a multiplex IgG immunoassay system based on carboxylated Raman encoded polymer microbeads and SERS nanotags is shown. The immunoassays were performed by mixing antibody conjugated polymer microbeads and antigen SERS reporters together. Due to the specific recognition of antibody and antigen, SERS nanotags attaching onto the surface of their specific antibody polymer microbeads could be positively verified from both Raman imaging and spectroscopic analysis. **Chapter 6** summarizes the key results and draws the conclusion, and also discusses future perspectives, developments and their application in biomedical imaging.

References

1.   Kendall, C.; Isabelle, M.; Bazant-Hegemark, F.; Hutchings, J.; Orr, L.; Babrah, J.; Baker, R.; Stone, N., Vibrational spectroscopy: a clinical tool for cancer diagnostics. *Analyst* **2009,** *134* (6), 1029-1045.

2.   Hanlon, E.; Manoharan, R.; Koo, T. W.; Shafer, K.; Motz, J.; Fitzmaurice, M.; Kramer, J.; Itzkan, I.; Dasari, R.; Feld, M., Prospects for in vivo Raman spectroscopy. *Physics in Medicine & Biology* **2000,** *45* (2), R1.

3.   Jess, P. R.; Mazilu, M.; Dholakia, K.; Riches, A. C.; Herrington, C. S., Optical detection and grading of lung neoplasia by Raman microspectroscopy. *International Journal of Cancer* **2009,** *124* (2), 376-380.

4.   Jess, P. R.; Smith, D. D.; Mazilu, M.; Dholakia, K.; Riches, A. C.; Herrington, C. S., Early detection of cervical neoplasia by Raman spectroscopy. *International Journal of Cancer* **2007,** *121* (12), 2723-2728.

5.   Canetta, E.; Mazilu, M.; De Luca, A. C.; Carruthers, A. E.; Dholakia, K.; Neilson, S.; Sargeant, H.; Briscoe, T.; Herrington, C. S.; Riches, A. C., Modulated Raman spectroscopy for enhanced identification of bladder tumor cells in urine samples. *Journal of Biomedical Optics* **2011,** *16* (3), 037002.

6.   Fleischmann, M.; Hendra, P. J.; McQuillan, A. J., Raman spectra of pyridine adsorbed at a silver electrode. *Chemical Physics Letters* **1974,** *26* (2), 163-166.

7.   Ni, J.; Lipert, R. J.; Dawson, G. B.; Porter, M. D., Immunoassay readout method using extrinsic Raman labels adsorbed on immunogold colloids. *Analytical Chemistry* **1999,** *71* (21), 4903-4908.

8.   Qian, X.; Peng, X.; Ansari, D., QQ Yin-Goen, GZ Chen, DM Shin, L. Yang, AN Young, MD Wang, SM Nie. *Nat. Biotechnol* **2008,** *26*, 83.

9.   Maiti, K. K.; Dinish, U.; Samanta, A.; Vendrell, M.; Soh, K.-S.; Park, S.-J.; Olivo, M.; Chang, Y.-T., Multiplex targeted in vivo cancer detection using sensitive near-infrared SERS nanotags. *Nano Today* **2012,** *7* (2), 85-93.

10.   Vendrell, M.; Maiti, K. K.; Dhaliwal, K.; Chang, Y.-T., Surface-enhanced Raman scattering in cancer detection and imaging. *Trends in Biotechnology* **2013,** *31* (4), 249-257.

11.   Bantz, K. C.; Meyer, A. F.; Wittenberg, N. J.; Im, H.; Kurtuluş, Ö.; Lee, S. H.; Lindquist, N. C.; Oh, S.-H.; Haynes, C. L., Recent progress in SERS biosensing. *Physical Chemistry Chemical Physics* **2011,** *13* (24), 11551-11567.

12.   Singer, J. M.; Plotz, C. M., The latex fixation test: I. Application to the serologic diagnosis of rheumatoid arthritis. *The American Journal of Medicine* **1956,** *21* (6), 888-892.

13.   Lee, H.-L.; Weng, Y.-P.; Ku, W.-Y.; Huang, L. L., A nanobead based sandwich immunoassay. *Journal of the Taiwan Institute of Chemical Engineers* **2012,** *43* (1), 9-14.

14.   Blais, D. R.; Alvarez-Puebla, R. A.; Bravo-Vasquez, J. P.; Fenniri, H.; Pezacki, J. P., Multiplex pathogen detection based on spatially addressable microarrays of barcoded resins. *Biotechnology Journal* **2008,** *3* (7), 948-953.

15.   Fenniri, H.; Terreau, O.; Chun, S.; Oh, S. J.; Finney, W. F.; Morris, M. D., Classification of spectroscopically encoded resins by Raman mapping and infrared hyperspectral imaging. *Journal of Combinatorial Chemistry* **2006,** *8* (2), 192-198.

Chapter 2 : Recent Advances in Surface Enhanced Raman Scattering for Bioanalysis

Umar Azhar[1], Zeyad Alwahabi[1], Sheng Dai[1, 2]*

[1]School of Chemical Engineering, the University of Adelaide, Adelaide SA 5005 Australia

[2]School of Engineering, Newcastle University, Newcastle upon Tyne NE1 7RU United Kingdom

* Corresponding author: sheng.dai@ncl.ac.uk

ABSTRACT

Diseases as noxious as cancer are shadowed by the requisite for therapeutic treatment with side effects inflicted after incurring costly surgeries and medicines. To curtail these drawbacks recent times has been stressed upon to undertake extensive research and technological advancements in biomolecular assays for early and high throughput diagnostics. The advancements particularly need to meet the stringent errands such as minimal sample, high sensitivity, rapid diagnosis, multiplexing and label free. In this context, Raman spectroscopy initially established its viability as a powerful analytical tool with no sample preparation, however, botched to progress due to its inherently weak sensitivity. The advent of surface enhanced Raman scattering (SERS) augmented Raman spectroscopy with enhanced sensitivity, making it once again a frontline contender for bioassay characterization and a bio-imaging modality. Technologies using SERS have experienced significant growth in immunoassay leading its way into clinical translation. This has led to oodles of advances for synthesis of SERS probes and SERS based immunoassays. Here, it is intended to provide a classifiable understanding of SERS probes and SERS based immunoassay along with its consolidated bio-imaging applications related to cancer detection.

2.1. Introduction

The "Raman effect" is an inelastic scattering of light. It can be used as a non-destructive vibrational approach for identifying molecular fingerprinting. Raman scattering is intrinsically weak, however the same phenomenon observed on a roughened metal surface gives rise to an ultrahigh sensitivity called the "surface enhanced Raman scattering (SERS)". SERS is an enhanced version of the "Raman effect". Carrying the advantages of Raman scattering complimented by nanotechnology, SERS has found wide utility in science, engineering and biomedical analysis. Particularly, last few decades have seen an enormous increase in the recognition of biological molecules with imaging of cells and tissues. Rather than accept single-dimensional forms of information, users now demand multidimensional and multiplexed assessment of analyst samples. High sensitivity with the need for little or no sample preparation makes Raman and its enhanced version SERS a highly attractive analytical technique, particularly in the field of bio-imaging that provides motivation for continuing advances in its supporting technology and utilization. This review presents an introduction to Raman scattering, SERS, and current tools employed in Raman/SERS imaging with specific emphasis on demonstrated utility in immunoassay research for complex bioanalysis. History, principles, and leading edge of Raman scattering over traditional optical techniques is covered in Section 1. This is followed by explanation of surface enhanced Raman scattering, its history, pros & cons, and fundamental mechanisms in Section 2. Section 3 is focused on SERS immunoassays, lying out a clear and concise understanding of the different methodologies used by different researches in a more set pattern. Section 4 is used to target specific applications of SERS based immunoassays in cancer bio-imaging (in-vivo and in-vitro) performed on a cellular basis and in tissues. In the last section, future challenges with respect to improvements in SERS nanotags components (signal consistency, toxicology and multiplexing) and futuristic insight into clinical application of SERS based immunoassays are presented.

2.2. Raman Scattering and Surface Enhanced Raman Scattering

2.2.1 Raman Scattering

It is a non-destructive method that allows characterizing the composition and the structure of a sample through study of the molecular vibrations using inelastic scattering of monochromatic light source. In 1923, Adolf Smerkal was the first to experience the inelastic scattering of light [1]. However, it was not till 1928 that it was reported and experimentally narrated by C.V Raman. He used ordinary sunlight and narrow band photographic filters to observe this inelastic scattering of light. The outcome illustrated that incident light is scattered in two ways by subject molecules, firstly, the scattered radiation having the same wavelength as the incident beam and secondly, the scattered radiation with a degraded frequency. This steered to the foundation of the well-known phenomenon to date, called the "Raman effect" and led to the award of a noble prize to Sir C.V Raman in 1930 [2]. In between 1930 and 1934, Czechoslovak physicist George Placzek theoretically elaborated the "Raman effect" [3]. Experiments were conducted using mercury arc as the principal light source, with photographic detectors succeeded by spectrophotometric detectors. In the years ensuing its discovery, Raman spectroscopy was used to provide the first catalogue of molecular vibrational fingerprints. However, due to the intrinsically weak sensitivity and lack of technological advancement, huge efforts were obligatory to obtain Raman spectrum. To increase the sensitivity of Raman scattering, large volumes of highly concentrated samples were prepared and used. Therefore, the use of Raman spectroscopy dwindled especially when commercial IR spectrophotometers developed in the 1940s. In 1960, Raman spectroscopy again came into the lime light with the advent of laser. This monochromatic light source simplified the detection instrument along with the enriched sensitivity of the technique. This rejuvenated Raman spectroscopy as a valuable analytical technique.
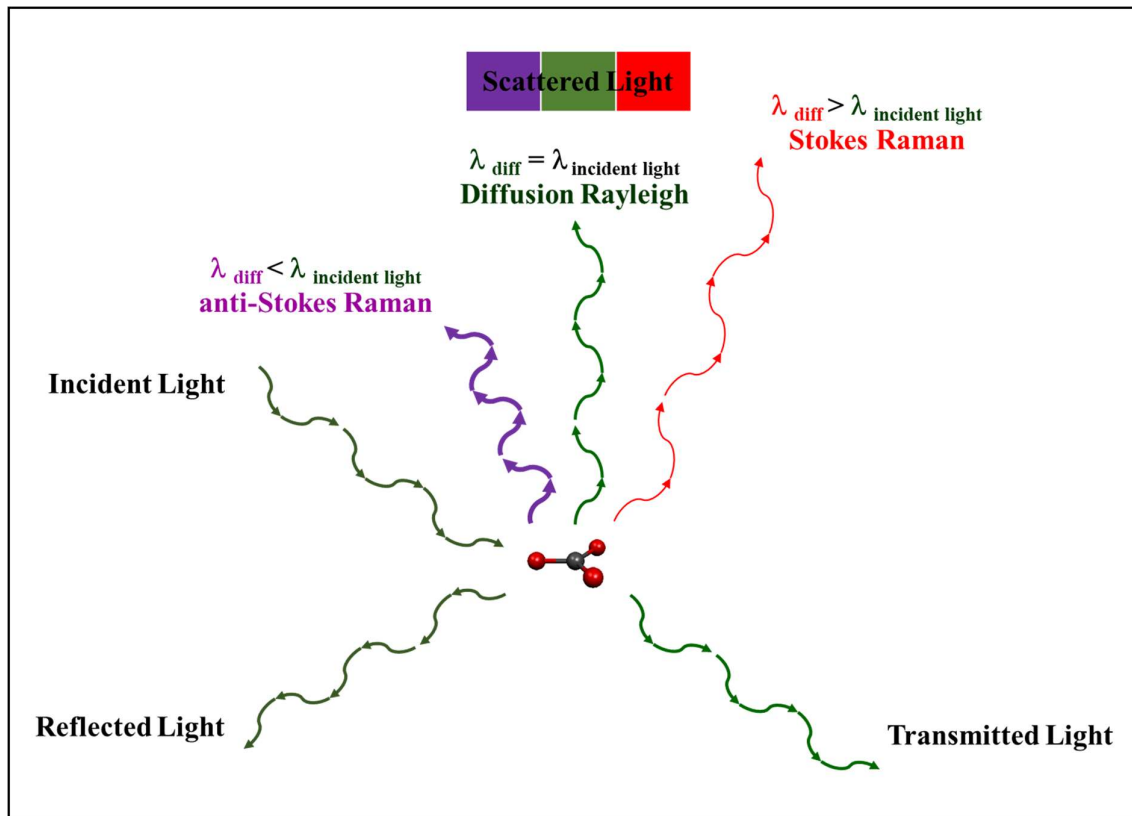
Figure 2-1. Interaction of light with matter resulting in reflection, transmittance and scattering of incident light. The difference between the frequencies ($\nu = 1/\lambda$) of the incident light and the scattered light corresponds to the frequency of the vibration $\nu_{scattered} = \nu_{incident\ light} \pm \nu_{vibration}$ '+' anti-Stokes; '-' Stokes.

Light falling on an object can be transmitted, reflected, absorbed or scattered. Raman effect investigates the scattering of light (Figure 2-1). A change in wavelength of the scattered light ensues, as compared to the incident light. This change occurs via the energy exchange taking place due to the molecular vibrations in the sample. Therefore, the delta in wavelength between the incident and scattered light is directly dependent on the molecular structure of the material. There are two different possibilities for light scattering:

a.	Rayleigh scattering: The light which is scattered with no change in its wavelength in comparison to the incident light is called elastic or Rayleigh scattering. It was discovered and

named after Lord Rayleigh [4]. Therefore, this happens when the scattered photon and incident photon have the same energy. Approximately every 1 out of 10,000 photons scatter without change of energy.

b.   Raman scattering: A small portion of the scattered light does change its wavelength in the process and such scattering is known as the "Raman effect" or inelastic scattering. Approximately every 1 out of 100 000 000 photons scatter with a change of energy. There are further two types of inelastic scattering. Stokes: energy of the scattered photon is weaker than the incident photon and anti-Stokes: energy of the scattered photon is greater than the incident photon. Raman scattering is suitable for most organic and inorganic materials with added advantages when compared to other spectroscopic techniques: (1) High specificity (2) No sample preparation needed (3) Non-destructive (4) Raman signals are not interfered by water (5) Can be used with solids and liquids (6) Results acquired within seconds (7) Analysis possible through glass or a polymer (8) Remote analysis through use of optical fibres (9) A very small sample required for analysis (< 1 μm in diameter). However, it also has the disadvantages such as (1) intrinsically very weak sensitivity, which necessitates a highly sensitive and optimized instrumentation (2) cannot be used for metals or alloys (3) strong heat energy from laser source can damage the sample or induce fluorescence from samples or impurities. These disadvantages can easily overlay and hide Raman spectrum.

2.2.2 Surface Enhanced Raman Scattering

The term "*surface enhanced Raman scattering (SERS)*" implies that it provides the same information that traditional Raman does, simply with a greatly enhanced Raman signatures. This enhancement is achieved by adsorbing sample molecules on a roughened metal surface. In 1973, the SERS was first observed by Martin Fleischmann, Patrick J. Hendra and A. James McQuillan from pyridine adsorbed on electrochemically roughened silver at the University of Southampton [5]. Here, due to the roughened metal surface it was detected that the incident

photons (~1 in 10 million) were inelastically scattered with Raman peak intensities enhanced by several folds. Therefore, SERS is a surface-sensitive "Raman effect" enhancement technique, that facilitated overcoming the biggest drawback of Raman scattering of being intrinsically weak, which usually required highly sensitive and optimized instrumentation. Nowadays, SERS of analyte molecules is recorded by adsorption on rough metal surfaces or nanostructures such as plasmonic-magnetic silica nanotubes [6]. The enhancement factor can be as much as 10^{10} to 10^{11}, which means the technique is able to detect single molecules [7-10].

The number of vibrational modes in any spectroscopic technique is governed by the selection rule (mutual exclusion rule). Generally, SERS spectra are similar to the Raman spectra for the same sample. However, in some cases additional peaks may appear and disappear in SERS spectra as compared to the Raman spectra for the same sample. This is complimented to the change in centre of symmetry of the Raman molecule after physical adsorption or chemical binding to metal surface [11,12]. On the contrary, the orientation of adsorption can also be determined by the new modes observed in the SERS spectrum [13].

SERS-based platforms have several advantages as compared to other spectroscopic techniques. These include: no photo bleaching [14], narrow Raman peak widths (Table 2-1) [15-17], multiplex analysis using a single laser line, low auto fluorescence NIR laser, and superlative for biological samples as SERS spectra has no interference from water [18].

In 1977, the SERS amplification of the Raman scattering intensities was first attributed to the electro-magnetic (EM) field enhancements by Jeanmaire and Van Duyne [19], and simultaneously to the chemical enhancements by Albrecht and Creighton [20]. Among them, the electro-magnetic field enhancement is more practically dominant in explaining SERS [21-23].

Table 2-1. Comparison of SERS tags with quantum dots and conventional fluorescent dyes.

Properties	SERS Tags	Quantum Dots	Conventional Dyes
Physical Principle	Raman scattering	Fluorescence emission	Electronic absorption/fluorescence emission
Core Component	Au and Ag based NPs or rough surfaces	PbS, CdSe and CdTe based NPs, etc.	Organic or organic-metallic compounds
Size	~5-50 nm	<10 nm	~1 nm
Bandwidth	Less than 2 nm	~30–50 nm	more than 50 nm
Structural Information	Fingerprint	No fingerprint	No fingerprint
Multiplexing Capacity	~10–100	~3–10	~1–3
Photostability	Anti-photo bleaching	Decay under strong laser	Decay under weak excitation
Toxicity	Not toxic	Toxic	Toxic

2.2.2.1 Electromagnetic Enhancement

Electromagnetic force is a physical interaction occurring between electrically charged particles, which includes both electric and magnetic forces traveling perpendicular to each other as one elemental phenomenon [24]. EM enhancements are assumed to be the major contributors to SERS, arises from the electromagnetic wave mechanics which bounds electrons in orbits to form atoms. The behaviour constituting the movement of these electrons around the nuclei of the atom determine the plasmonic properties. The excitation of these plasmonic oscillations by a matched frequency gives rise to constructive interferences thus enhancing the local strength of an EM field. Rufus Ritchie, of Oak Ridge National Laboratory's Health Sciences Research Division, predicted the existence of the surface plasmon [25]. The plasmonic oscillations occur at two metric scales, namely:

a.   Surface Plasmon Polaritons (SPP): These oscillations occur at macroscopic level, involving the interface between metal-air, thus making use of surface oscillations around the metal called "surface plasmons" and the EM waves in the air called "polaritons". SPPs can be easily guided by the surface plane as they propagate along the metal surface plane and dielectric interface (Figure 2-2) [26-28].
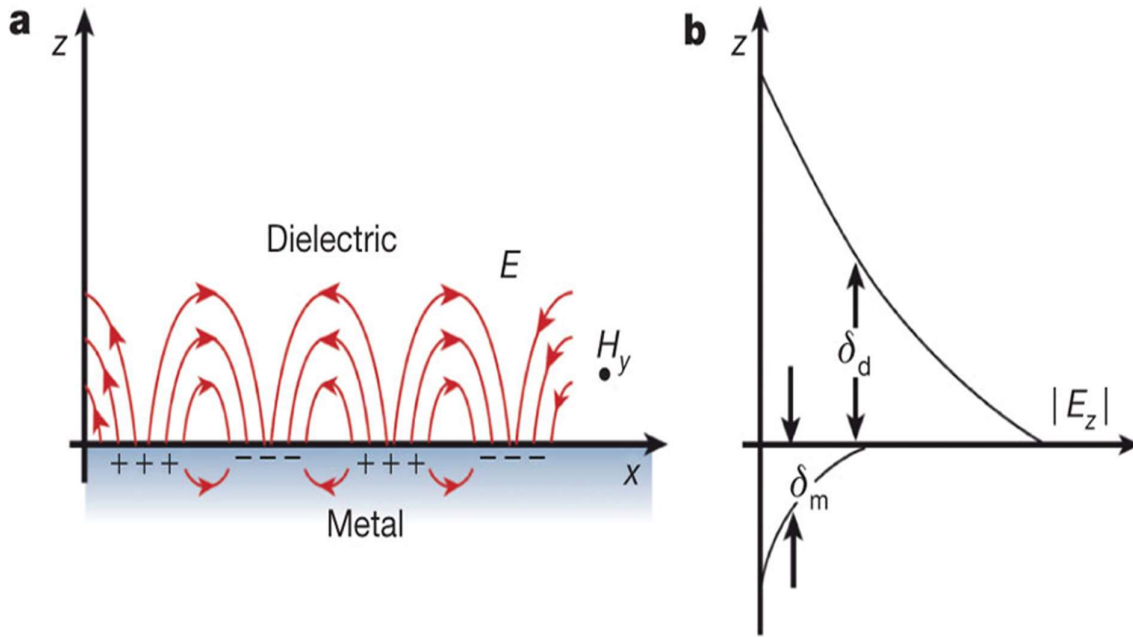
Figure 2-2. (a). SPs at the interface between a metal and a dielectric material have a combined electromagnetic wave and surface charge character. They are transverse magnetic in character (magnetic field H_y is in the y direction), and the generation of surface charge requires an electric field normal to the surface. (b). This combined character also leads to the field component perpendicular to the surface being enhanced near the surface and decaying exponentially with distance away from it. (Reprinted with permission from ref [26]. Copyright 2003 Nature).

b.   Localized surface plasmons (LSP): These oscillations occur at nanoscale level, generated by local oscillations of electron cloud around the metal nanostructure. The electrons oscillate to and forth due to the attractive and repulsive forces existing due the incident field and the positive nucleus.
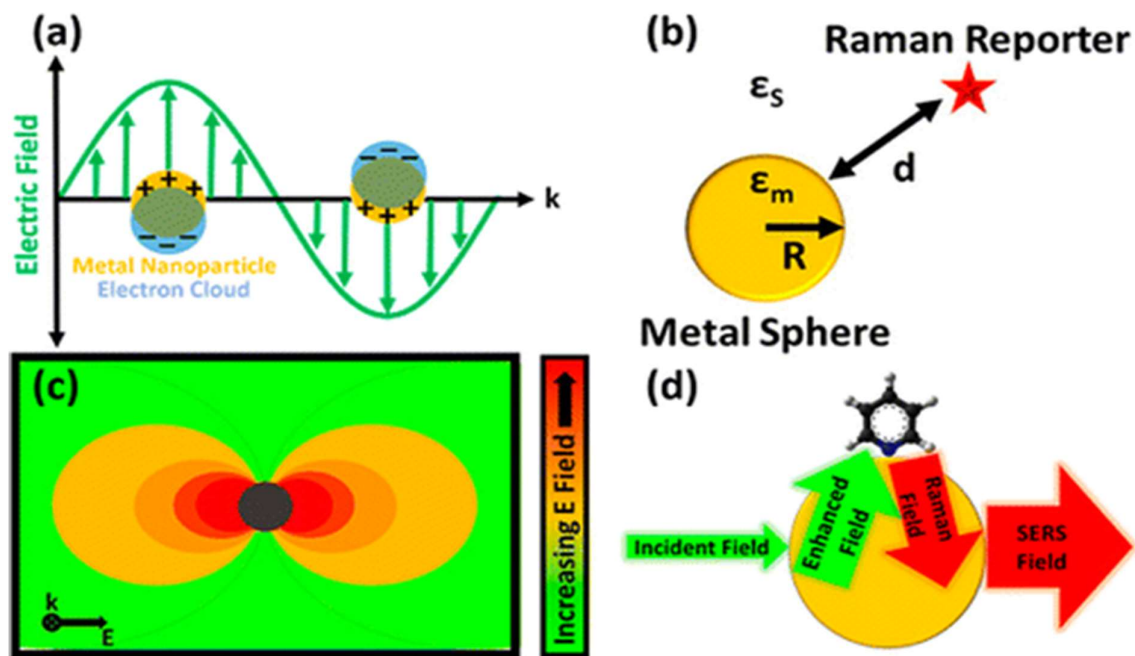
Figure 2-3. (a) Illustration of the oscillating electron cloud, which moves in opposite direction of the electric field vector, for a nanoparticle smaller than the wavelength of light. (b). Depiction of the parameters used in eq 1 of the main text. (c) Emitted dipole field of a metallic nanoparticle under light excitation. (d) EM enhancement of both the incident field and the scattered field. (Reprinted with permission from ref. [29]. Copyright 2015 American Chemical Society).

Generally, EM enhancement is estimated based on electrostatic dipole radiation (Figure 2-3). The phenomenon occurs due to oscillations of electrons around a nanoparticle. These oscillations are induced when the wavelength of the incident light is close or slightly greater than the size of the particle. This causes dielectric field of the particle to enhance, which in turn is used by the nearby molecule (Raman reporter) which further returns the vibrational enhancement to the nanoparticle for more enhancement. This overall EM enhancement (G_{SERS}) can be expressed in the form of fourth power law [23,30,31], as follows:

$$G_{SERS} \approx \left|\frac{E_{loc}}{E_0}\right| = \left|\frac{\varepsilon_m - \varepsilon_s}{\varepsilon_m + 2\varepsilon_s}\right|^4 \left(\frac{R}{R+d}\right)^{12} \tag{1}$$

where,

   E_{loc} = amplitude of the local field,

   E_0 = amplitude of the incident field,

   ε_m = permittivity of the metal sphere,

   ε_s = permittivity of the surroundings.

   R = radius of the metal nanostructure

   d = distance between the Raman reporter and metal nanostructure

EM enhancement is equally applicable to any Raman reporter molecule thus irrespective of the chemical structure but highly dependent on the distance (d) from the metal nanoparticle. Significant contribution of "d" is experienced for particle sizes ranging from 20-200 nm. As metal nanoparticles become larger the plasmonic oscillations are complexed (quadruple, octuplet etc.) leading to constructive and destructive interferences overlapping instantaneously. This leads to wider plasmonic band widths and decreased EM enhancements. Gold and silver nanoparticles in the range of 40-60 nm diameter have the highest enhancement factors. Therefore, the above equation provides two ways of interpretation for maximized SERS signal. Firstly, when the incident light and scattered field from the Raman reporter are in resonance with the metal localized surface plasmons:

$$E_{loc} = E_0 \tag{2}$$

However, experimental results are quite in contradiction to the above. In case of single particles, maximum SERS signal is observed when plasmon resonance is between the laser line and Raman bands of the reporter. Similarly, for colloidal metal nanoparticles SERS signal is maximized when the plasmon resonance is blue shifted with respect to the laser line with less overlap with the Raman bands of the reporter [33,34]. Second condition for the maximized EM enhancement to occur is when the metal has a negative real permittivity value (ε_m) equal to $2\varepsilon_s$:

$$\varepsilon_m = 2\varepsilon_s \rightarrow zero \tag{3}$$

Johnson and Christy [35] or Palik [36] are the leading researchers for referring calculations based on permittivity with respect to EM enhancements. At optical wavelengths, best metals that support LSPR frequencies with low absorbance are copper, silver, and gold [37-40].

The shape of the metal nanoparticles also has a major effect on the EM enhancement. As compared to nanospheres, anisotropic nanostructures offer wider tuneable range for LSPR wavelengths (red and NIR region). Again, even without making a significant size increase, shapes like cubes and triangles offer higher enhancement factor up to 10^{10} at the edges or vertices, which is 7-16 times greater than nanospheres [41-51]. At a distance greater than 0.5 nm from the edge, the enhancement factor drops back to the same value as for nanospheres (Figure 2-4) [52]. This happens as regions with higher curvatures or smaller effective radii have field strengths with a greater dependence on length (Equation 1). Therefore, such shapes are able to detect up to single molecules with intrinsic enhancement factor as high as 10^{14} -10^{15}, if they are adsorbed near the edges [53-55]. Recently, studies are fixated on fundamentals of blinking SERS, [56-60] "hot spots", [61-65] and active sites for chemical enhancement [57,66].
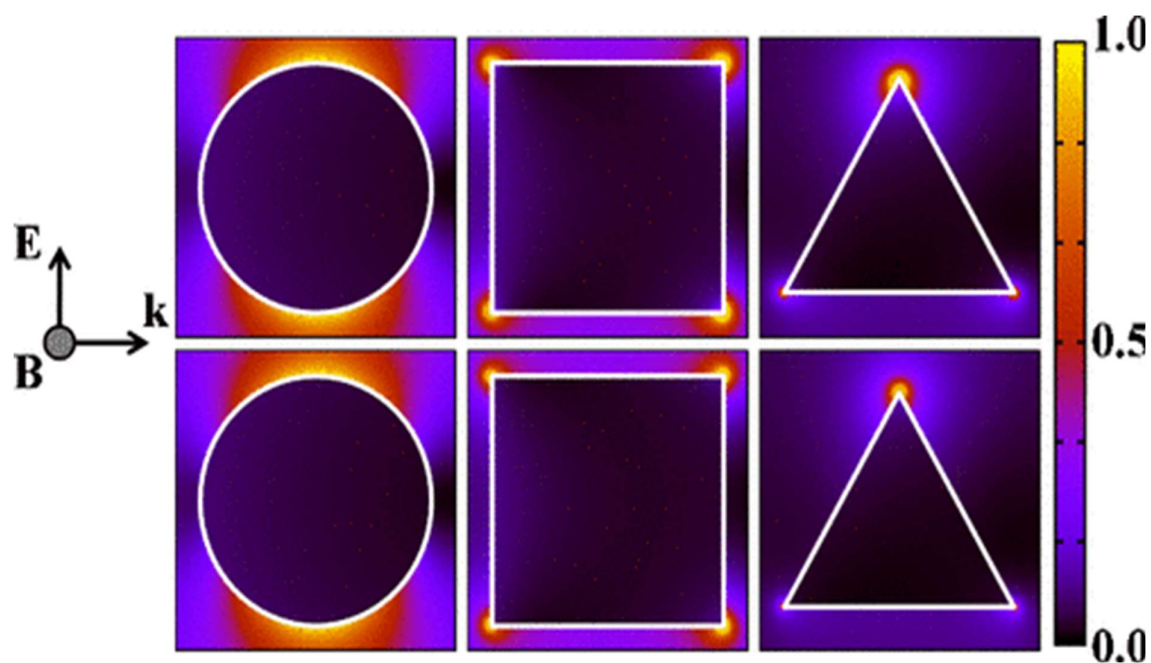
Figure 2-4. Normalized |E|2 intensity profiles at the LSPR energies in and around (left) cylindrical, (middle) square, and (right) triangular Au nanowires with diameters or side lengths of 50 nm. Both (top) local and (bottom) nonlocal calculations are shown. The polarization and direction of incident light is indicated; the nanowires are outlined in white. (Reprinted with permission from ref [36]. Copyright 2010 American Physical Society).

2.2.2.2 Chemical Enhancement (CE)

With the amount of Raman enhancement observed with SERS, researchers were not fully able to explain the phenomenon only through EM mechanism. Therefore, additional CE mechanism is also proposed to support the enhancement factor by certain orders of magnitude [67-69]. The CE enhancement relies on the charge transfer between the chemisorbed molecules (analyte or Raman reporter) and the metal surface [70]. Thus, CE enhancement should only be expected to occur if the analyte is adsorbed directly or is forming a covalent or ionic bond. Hence, this charge transfer intermediates provide greater Raman scattering cross sections. Moreover, the CE is initiated when in close proximity to the metal surface (angstrom scale) and requires much

more energy for excitation to occur usually in the UV range. However, if the LUMO and HOMO of the analyte falls symmetrically with the Fermi level of the metal surface, the excitation energy can be reduced to fall in the infrared to visible light range (Figure 2-5) [71-75]. It may be noted that in case of EM enhancement, the enhancement factor is dependent on the metal surface physical properties like size, shape and metal type etc., but for CE the enhancement factor is dependent on the chemical properties of the analyte.
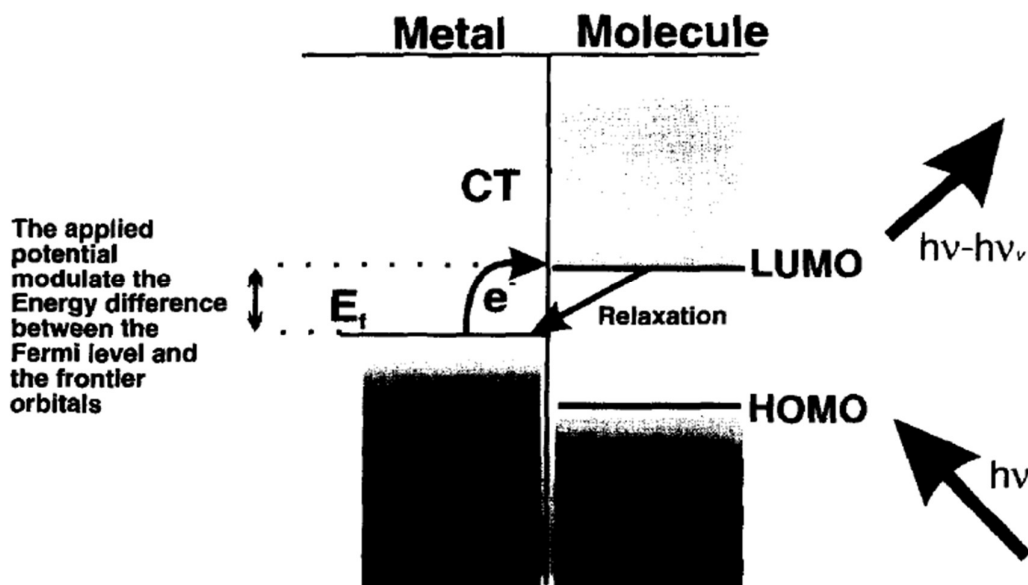
Figure 2-5. For adsorbed molecules containing empty low energy π' orbitals, an electron is transferred from the metal's Fermi level to the LUMO. This process is in resonance with the energy of the incident photon (hυ). The energy of the Fermi level can be modulated by the applied potential; the energy of the Fermi level either increases or decreases as a negative or positive potential, respectively, is applied. (Reprinted with permission from ref [75]. Copyright 1997 Elsevier B.V.)

The comparison between EM and CE mechanisms can be summarised in Table 2-2 [75]

Table 2-2. Comparison between electromagnetic and chemical mechanisms.

	Electromagnetic Mechanism	Chemical Mechanism
Dependence	EM enhancement emphasizes the role of the nanosubstrate providing the long-range electromagnetic fields, which depends on the nanosubstrate's physical properties (such as material type, size, and shape) [76]	However, CE is achieved by changing the scattering cross section of the analytes attached on a metal surface; thus, the extent of enhancement is determined by the chemical features of the analytes themselves [77]
Origin	Enhancement of the local electric field due to the coupling of the incident photon with the metal's surface plasmons	Resonance process involving the incident light and the CT band of the metal-molecule complex. (Resonance Raman-like process) [78-81]
Roughness	Large scale roughness (about 10-200 nm)	Atomic scale roughness (active sites)
Distance dependence	Long range. Important even for species several nm away from the surface, but decays with distance	Short range. Important only for species adsorbed directly onto the surface
Potential dependence	The enhancement factor does not depend on the applied potential; intensity changes in the potential profile are due to the variation of the surface coverage with potential	The CT band can be tuned by the applied potential; therefore, the enhancement factor is potential dependent
Excitation wavelength dependence	The enhancement factor depends on the metal dielectric constant, which is wavelength dependent. E_{max} does not shift for different incident photon energies	The resonance condition depends on the excitation wavelength. The potential at which the SER intensity maximizes (E_{max}) is different for different incident photon energies
Enhancement Range	10^{6-9}	$10^2 - 10^3$ [71,82]

2.2.2.3 Effective Enhancement Factor

The summation of the electromagnetic and chemical enhancements gives the total enhancement called the effective enhancement factor (EEF). The most accepted mathematical relationships to quantify EEF for nanoparticles are discussed here. Initially in 1997, Nie [83] and Kneipp [84] both reported single molecule detection of crystal violet in aqueous colloidal silver solution. The reported enhancement factor was 10^{14}-10^{15} times the normal Raman signal without colloidal metal solution [74,85,86]. These findings laid the foundation for the modern SERS tag detection. In 2002, Kneipp proposed a mathematical relationship for the calculation of SERS Stokes power [70,87,88]:

$$P^{SERS}(\upsilon_S) = N\sigma_{ads}^R |A(\upsilon_L)|^2 |A(\upsilon_S)|^2 I(\upsilon_L) \tag{4}$$

Where,

$I(\upsilon_L)$ = excitation laser intensity,

σ_{ads}^R = Raman cross section of the adsorbed molecule,

N = number of molecules that undergo the SERS process,

$A(\upsilon_L)$ & $A(\upsilon_S)$ = laser and Raman scattering field enhancement factor.

This deduction was based on single molecule SERS signal and this equation, helps determine SERS enhancement based on factors like, nanosubstrate, molecules attached and their number. Later in 2007, Le Ru et al. [89] elaborated on the issue of the multiple definitions of the enhancement factor in depth. The most effective calculation for EEF presented till date, is a product of electromagnetic and chemical enhancement (EEF = EM × CE),

$$EEF = \frac{I_{SERS}/N_{surface}}{I_{NRS}/N_{bulk}} \tag{5}$$

Where,

I_{SERS} & I_{NRS} = SERS and normal Raman spectroscopy (NRS) intensities,

$N_{surface}$ & N_{bulk} = Number of molecules contributing under SERS and NRS condition.

The above equation has been used by various researchers for estimating the enhancement factor. However, these reported results are neither comparable nor consistent due to varying experimental conditions. In light of these findings in 2013, Van Duyne group suggested three conditions to be considered before calculating EEF [90]. These are clear definition of how the EEF is determined, all reporter molecules within the excitation area contribute evenly to the EEF, and to utilize a commonly available Raman reporter with well-defined spectra and surface chemistry. More recent studies have further elaborated on the misconceptions and significant EM mechanisms contributing to the EEF [91].

2.3 SERS Immunoassays

Immunoassay is a biochemical test for early stage disease detection, through highly specific binding of antibodies-antigens. While, SERS can detect analytes at a single-molecule level, with high sensitivity. This high specificity and high sensitivity is captured in SERS-based immunoassay, which has gained unusual attention in development of biosensors. This type of assay consists of two major structural parts, together capturing the target analyte: (1) SERS tags/probes: used to specifically bind to the target analyte attached to the immune substrate and provide SERS spectrum (2) Immune substrate: used to provide a stable platform to specifically bind and immobilize the target analyte.

2.3.1 SERS Tags/Probes

It is a nanoprobe that consists of a core metal nanoparticle, which has Raman active molecules attached to it. A SERS tag generally consists of four main components for *in-vivo* or *in-vitro* applications.

2.3.1.1 Nanostructured Metal

Nanostructured metal is the building block of the SERS tags. As already elaborated the metal nanoparticles act as an amplifier for the EM enhancement factor. In bioanalysis the most desirable outcomes that are expected to be achieved from metal nanoparticles are intense field enhancement, and NIR plasmon resonance. This helps in using nanoparticles in biological samples, to avoid their burning out at shorter wavelengths and high energy of incident laser excitation.

The overall EEF (EM & CE) is dependent on the following properties of the metal nanoparticles: size, size distribution, shape, chemical composition and their surface chemistry. The size and chemical composition of the metal nanoparticles helps determine the SPR which can be complimented through shape. The surface chemistry helps determining in conjugation strength and selectivity of the metal nanoparticle with the analyte. The most known metal nanoparticles used are gold, silver and copper. Although copper, silver and gold are most commonly explored and used SERS metal substrates with SPR in the visible to IR range, recently aluminium has found utility in the UV range [92,93]. Aluminium also shows large EEF in the IR range which is surprising and not effusively understood as yet.

Since SERS EEF is highly dependent on the size and shape of the metal nanoparticles. Keeping the size constant, the EEF can still be increased with truncated shapes creating "hot spots" or gaps. Nevertheless, spherical shapes are preferred for ease of uniform distribution of the SERS signals across metal nanoparticles with favourable pharmacokinetics in bioanalysis [94]. In case of spherical metal nanoparticles, the size solely dictates the incident laser wavelength and absorption wavelength responsible to generate inelastic scattering [95,96]. The larger the spherical nanoparticle, the more the SPR shifts towards the IR range. However, the ideal size and/or thickness of the nanosubstrate is highly dependent on the wavelength of the incident laser [97]. Metal nanoparticles which are very large in size than the incident laser wavelength induce

multipole transitions, which are non-radiative and cause decrease in the overall SERS EEF. Similarly, metal nanoparticles which are very small in size than the incident laser wavelength fail to even create dipole transitions, hence no electrical conductance or plasmonic oscillations of electrons [98]. Mostly, gold nanoparticles are used for bioanalysis, as it is non-toxic and chemically inert. This has been clinically demonstrated, where gold nanoparticles were administered *in-vivo* to human being for cancer detection [99,100]. On the other hand, silver nanoparticles are less preferred due to problems like oxidation and toxicity [101-103]. Silver colloids are generally synthesised by reduction of silver nitrate using the Lee and Meisel method [104], while gold colloids by reduction of chloroauric acid using the Turkevich method [105,106]. In both these methods, citrate ions are used to keep the particles electrostatically stable in the solution. The SERS intensity is based on the frequency matching of the incident laser and the resonance of the metal nanospheres. In biomedical applications low power NIR lasers are preferred to avoid sample damage. Therefore, the resonance frequency of the nanosphere needs to match up with the NIR incident laser. This necessitates the size of the nanospheres to be increased, in order to use a laser with higher wavelength (red-shift or a bathochromic shift) for plasmonic oscillations to occur. Based on factors like aggregated and non-aggregated, colloidal platforms have been used and categorized as follows:

1) Non-Aggregated

Metal nanocolloids have been extensively used as a non-aggregated platform for SERS. The non-aggregated platform allows ease of pharmacokinetics. However, depending upon the size and shape, the synthesis processes and architectural designs have been varied in order to meet the desired EEF and biomedical application to use NIR excitation.

a)   Isotropic: This includes the gold and silver nanospheres with shape uniformity in all orientations and controlled size. These nanospheres allows ease of pharmacokinetics as well as homogeneity of enhanced signals across the surface of SERS tag. In order to use colloids

without the need to increase the number of nanoparticles with aggregation or agglomeration researchers have adopted the following two approaches:

Unmodified. The maximum sizes of Au and Ag nanospheres synthesized with controlled uniform size distribution allows SPR in between 400-600 nm [107,108]. Silver nanospheres offer 10-100 times greater enhancement factor than gold as less plasmonic damping is experienced in Ag due to d-s band gap in the UV region [109]. However due to cytotoxicity and short-term stability Ag are less preferred than Au in biomedical applications. These nanoparticles are useful for homogeneity of SERS signal across the entire surface but restricted by use of NIR lasers for detection due to controlled synthesis of large uniform spheres. Moreover, increasing the size of the nanospheres causes damping effects hence lowering the enhancement factor. The optimal size range is estimated to be 30-100 nm [88].

Modified. (Architectural Designing) In order to overcome the limitations of nanospheres with respect to controlled synthesis of large monodispersed nanospheres with SPR in the NIR range, architectural designs have been reported. These designs allow SPR in NIR range while maintaining pharmacokinetics and SERS signal homogeneity across the surface of the SERS tag. These also offer increased SPR in NIR with reduced size compared to nanospheres. Few such types of architecturally designed metal substrates are: hollow gold nanoshells (HGN) [110-112], nanocages [113,114], nanomatryoshkas [115-118]

Hollow gold nanoshells (HGNs) localize the surface electromagnetic fields through pinholes in the hollow particle structures [119]. The inner and outer shells of the HGN's induce the overall SPR, which can be tuned between visible to NIR by reducing the shell wall thickness [120-123]. The HGN have also shown limit of detection (LOD) from 1-10 pg/ml which is 100-1000 times greater than any ELISA [111]. Nanocages have been engineered for use as SERS tags with SPR in the NIR range, and as photothermal (PT) transducers for destroying cancer cells [124], as carriers for controlling drug release [125], and as contrast agents for optical imaging [126]. Recent

research to achieve quantitative analysis of SERS tags with consistency and reproducibility has made headway with the nanomatryoshkas model [115-118]. The model constituents of the core-Raman reporter-shell. Here, Raman reporter is enclosed between the metal nanoparticle (core) and the protective coating (shell). The Raman reporter is adsorbed on the core surface with no competing molecules and with protection from external environment provided by the shell. Therefore it is used as the internal standard (IS) [127]. The shell is usually made of the same or different metal nanoparticles as the core. The shell surface is used stand alone for the target capturing molecule. This model offers uniformity of SERS signals with standard deviation of less than 1.2% between samples.

b   Anisotropic: To make use of the same size range of metal nanoparticles researchers proposed innovations in shape that is use of anisotropic metal nanoparticles. Anisotropic shapes made use of the "hotspot" with sharp bends and tips [128-131]. This helps shift the SPR to NIR range and possible to use laser wavelength in the NIR region for bioanalysis. Typical examples of anisotropic shapes are: nanocubes [132-135], nanorods [130,136-138], nanotriangles [42,139,140], nanopolyhedrons [141], nanostars [142-144], nanourchins [145,146], nanoflowers [147-149], and others.

2) Aggregated

The use of aggregation or agglomeration is referred for intense field enhancement and NIR plasmon resonance, through creation of "hot spots" [72,74,150,151]. This could lead to achieve enhancement factors up to the order of 10^{10}, sufficient enough for single-molecule detection [152-155]. However, the lack of control on uniformity of aggregation of metal nanoparticles across the SERS substrate, causes inconsistencies in field intensities and reproducibility. Therefore, to achieve reproducible results the need to fabricate homogeneous nanoaggregates structures is required. This can happen through precisely controlling the shape and size of the aggregates. Broadly based on aggregation, NP's aggregates are divided into two categories for better apprehension:

a)   Clusters: Metal nanoparticles cluster is mostly formed through aggregation induced by addition of salts, thereby letting the attractive van der Waals potentials between particles to dominate the system (Figure 2-6A) [156,157]. This aggregation process is controlled through precise addition of salts or polymers. The polymers quench the process by forming a coating on the metal nanoparticles aggregates. This coating of polymer also acts as a protective shell to improve the biological and chemical stability for instance, Tan et al. [157] used polyvinylpyrrolidone (PVP) (Figure 2-6B) and Braun et al. [158] used PVP or polyvinylpyrrolidone–poly(acrylic acid) (PVPA) followed by polyethylene glycol (PEG)-thiol to achieve the same goal (Figure 2-6C). Metal nanoparticles can also be aggregated to form clusters through use of Raman reporters [159] (Figure 2-6D). In this case the citrate ions which electrostatically provide stability to the colloidal solution are replaced by the more affine Raman reporters. This reduces the electrostatic repulsive forces between the nanoparticles allowing aggregation, thus forming clusters [160,161]. This aggregation process is controlled through regulating the pH of NP's colloid [162].
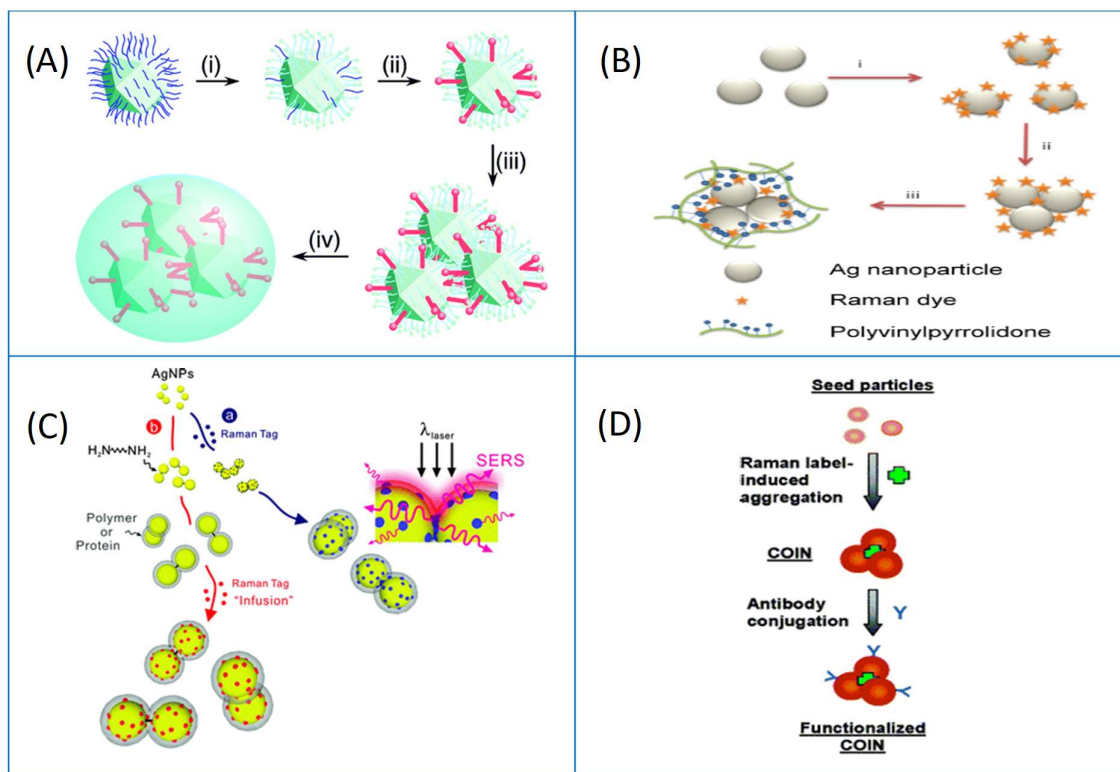
Figure 2-6. (A) Preparation of silica-coated, dye-tagged, silver nano-particles. (Reprinted with permission from ref [156]. Copyright 2008 Langmuir). (B). Preparation of PVP-coated, dye-tagged Ag nanoparticles. (Reprinted with permission from ref. [157]. Copyright 2009 IOPscience Nanotechnology). (C). Synthesis of SERS nanocapsule. (Reprinted with permission from ref. [158]. Copyright 2009 Journal of Physical Chemistry C). (D). Schematic illustration of COIN synthesis and COIN structure, showing particle enlargement, cluster formation, and antibody conjugation. (Reprinted with permission from ref. [159]. Copyright 2005 Nano Letters).

b) Support Assisted Cluster's: In this technique silica and polymer microbeads are used as support materials to provide a platform for growth of metal nanoparticles either through direct adsorption or *in-situ* growth. These nanoclusters offer high packaging densities with reproducible "hot spots" [163-165] (Figure 2-7). In *in-situ* synthesis, the support bead is functionalized with 3-mercaptopropyltrimethoxysilane (MPTMS) or treated with sulfuric acid, which enables the support bead to adsorb noble metal salts, and *in situ*-synthesis of the metal

NP's. This allows NP's compact distribution on the bead's surface and high reproducibility of SERS signals. The amount and size of the nanoparticles clusters on the support can be attuned by varying the concentration of metal salts and the reaction time [166]. In direct adsorption, the pre-synthesised metal nanoparticles are mixed with the support material for bonding through covalent or electrostatic forces [167].
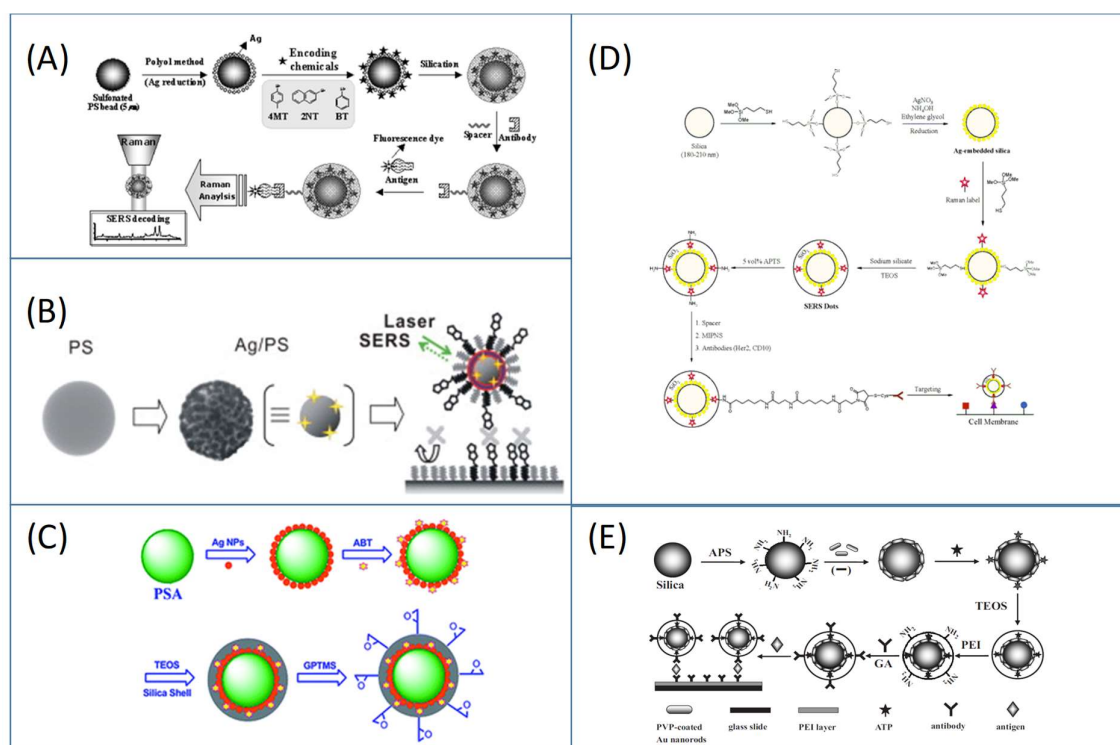
Figure 2-7. (A). Schematic illustration of SERS-encoded bead synthesis and bio-application. (Reprinted with permission from ref [163] Copyright 2007 American Chemical Society). (B). Scheme for fabrication of Ag-coated polystyrene (PS) bead usable as a template of biosensor operating via surface-enhanced Raman scattering; the last cartoon illustrates the interaction of biotinylated beads with other biotinylated substrates by the mediation of streptavidin molecules, labelled as "X." (Reprinted with permission from ref [164] Copyright 2008 Journal of Colloid and Interface Science). (C). Scheme for preparation of PSA@Ag-NPs@silica microspheres as SERS labels. (Reprinted with permission from ref [165] Copyright 2011 Journal of Materials Chemistry). (D). Schematic illustration of SERS dots synthesis and targeting of

cellular cancer markers. (Reprinted with permission from ref [168] Copyright 2006 Analytical Chemistry) (E). Schematic illustration of SiO2@GNRs@SiO2 (SERS tags) synthesis and targeting antigen using a sandwich assay. (Reprinted with permission from ref [167] Copyright 2008 Advanced Functional Materials)

2.3.1.2 Organic Raman Reporters

These can be classified into: Ready-Made and Tailor-Made. Raman reporters use the LSPR to enhance their chemical fingerprints and act as the detection label. The desirable properties for the Raman reporter to increase the total EEF and reduce noise signals from adsorption of potential contaminants are: (1) Large Raman cross section (2) High sensitivity (3) Absorption maxima in the NIR range (4) Absorption maxima overlapping with the incident laser source to invoke surface-enhanced resonance Raman scattering called SERRS nanoprobes (EEF = 10-100 times) [169,170] (5) High surface binding affinity through functional groups like sulphur and nitrogen especially in case of silver and gold nanoparticles (6) Dense formation of reporters on metal nanoparticles [70,87,88] (7) Few distinct characteristic peaks to accommodate more reporters within the spectral window for avoid overlapping and facilitate multiplexing. In addition, a strong adsorption of the Raman reporters with the ligands is highly desirable. This can be achieved through attractive electrostatic forces, for example, between negatively charged citrate-coated gold nanoparticles and positively charged diethylthiatricarbocyanine (DTTC) [171-173].

1) Ready Made

Some commonly used, and naturally available strong SERS reporters are chromophores such as Malachite green, Cyanine dyes, R6G, Crystal violet, and Nile blue. Example of ready-made Raman reporters along with their SERS attributes is summarized in Table 2-3 [174].

Table 2-3. Typical Raman reporters used for SERS tag preparation

Type	Example	Linking mode	Advantages	Disadvantages
nitrogen-containing cationic dye	crystal violet rhodamine B rhodamine 6G nile blue	electrostatic force N–Au(Ag) interaction	cheap large Raman cross section ready for SERRS	weak affinity to metal weak signal stability hard for further tag surface coating
sulfur-containing dyes	3,3′-diethylthiadicarbocyanine iodide malachite green isothiocyanate tetramethylrhodamine-5-isothiocyanate rhodamine-5-(and-6)-isothiocyanate	S–Au(Ag) interaction	large Raman cross section strong binding affinity to metal suitable for further tag coating and modification ready for SERRS	expensive limited types hard to form SAM
thio-small molecules	4-aminothiophenol 4-methylbenzenethiol 2-naphthalenethiol benzenethiol	S–Au(Ag) interaction	cheap strong binding affinity to metal few Raman peaks is beneficial for multiplexing	small Raman cross section not ready for SERRS

Recently, Raman reporters known as self-assembled monolayers (SAM) have been introduced [123,175-177]. These bifunctional Raman reporters perform two functions. They form a high-density

layer on the metal nanoparticles through the high affinity thiol group, and maintain electrostatic stability through the negatively charged carboxylic group. Therefore, high density coating of Raman reporters on NPs without inducing severe aggregation is achieved. The SAM-coating offers numerous advantages: (1) Greater surface area for higher SERS intensities (2) Uniform orientation offering reproducibility (3) Dense adsorption, defying co-adsorption of undesired molecules, and (4) Co-adsorption of different Raman reporter molecules on the same metal nanoparticles facilitating multi-encoded SERS tags for multiplexing.

2) Tailor Made

Use of the readily available reporters is extensive as listed above. Whereas, tailor made reporters can be modified to increase the EEF, integrity and overall capabilities of SERS tags. Recently, some novel reporters have been developed and have shown better results in terms of SERS signal intensity and stability better than ready-made strong Raman reporters like malachite green isothiocyanate (MGITC) and crystal violet [178,179]. These Raman reporters are synthesised by keeping triphenylmethine as parent structure with an anchor group of lipoic acid [180-182]. The triphenylmethine provides the strong SERS enhanced signals while the lipoic acid offers improved stability through bidentate thiol binding to the metal nanoparticles. This group also produced two new NIR Raman reporter molecules, Cy7LA, Cy7.5LA to partner with tricarbcyanine as parent structure called CyNAMLA-381 with dithiol anchoring group. This dye has offered 12 times more sensitivity than most popular ready-made dye 3,3′-diethylthiatricarbocyanine (DTTC). The use of this dye for ultrasensitive multiplex in-vivo detection has been illustrated by sensing cancer in a living mouse [182]. In 2015, a new dye named 2-thienyl-substituted chalcogenopyrylium (CP) has been synthesised [183,184]. These dyes have strong resonant signals in the NIR range (785 – 1280 nm) with pico to attomolar limits of detection (LOD). They also show high affinity for gold surfaces due to the presence of 2-thienyl

groups attached to the 2- and 6- positions of the dye. These results endorse the significance of designing and screening novel Raman reporters to achieve high sensitivity and specificity.

2.3.1.3 Protective Surface Coatings

Bioanalysis demands SERS tags to be highly stable in a strong ionic environment. The SERS tags which are stabilized electrostatically only, are subject to easy aggregation, precipitation, disassociation and contamination by competing proteins in a biological sample. Therefore, protective coating is beneficial, and also introduces surface functional groups for further analyte bioconjugation. This necessitates the use of protective fillers/coatings for SERS tags, which are bare and especially for not so densely populated with Raman reporters to improve their biocompatibility and stability. These protective coatings in SERS tag also enables researcher to quantify the number of SERS nanoparticles [185-187]. Based on the materials used for the protective surface coating for SERS tags, it can be divided into two categories:

1) Biomolecule Coatings

Two types of biological fillers and/or coatings are well known and used.

a)   Bovine   serum   albumin   (BSA):   Bovine   serum   albumin (also   known as BSA or "Fraction V") is a serum albumin protein derived from cows. BSA is the most widely used biomolecule SERS tag coating [188]. In 2006, SERS tags referred as Composite Organic-Inorganic Nanoparticles (COIN) were encapsulated using BSA (Figure 2-8). It forms a weak filling based on adsorption on the surface of the metal nanoparticles. Further, cross linked encapsulation was achieved by adding glutaraldehyde [189]. The sample is treated with glycine or sodium borohydride to remove the extra aldehyde functional groups. This also removes the surface amino groups from the BSA, leaving the surface with negatively charged carboxylic groups. These carboxylic groups are further bio conjugated to antibodies through EDC chemistry.
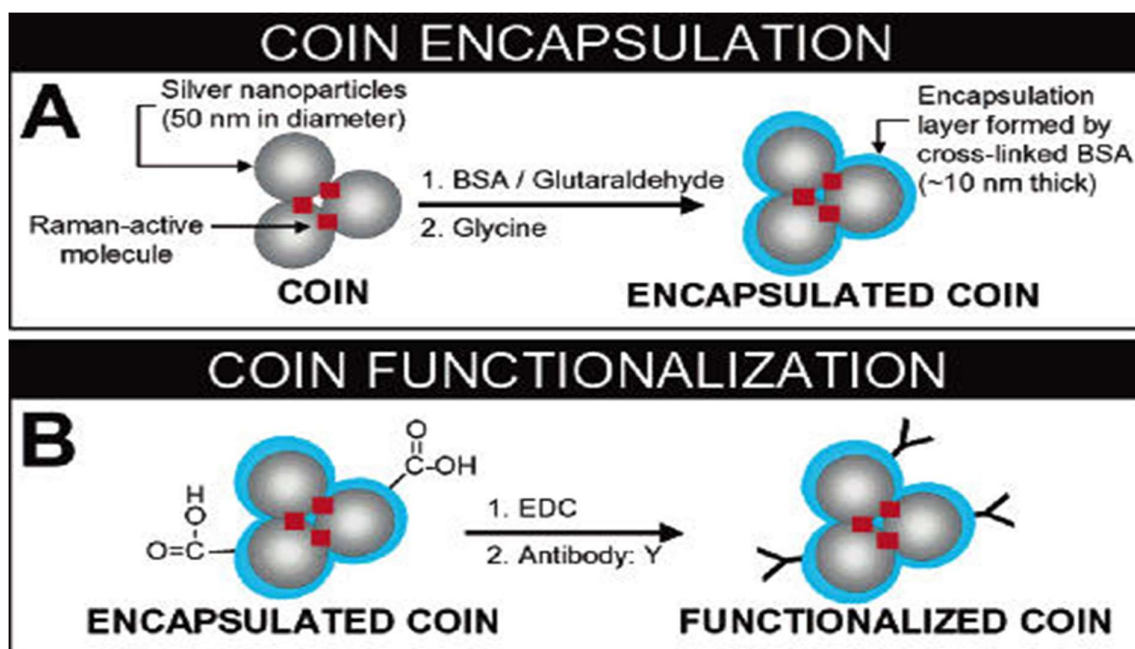
Figure 2-8. COIN encapsulation and functionalization method. (A). Schematic illustration of COIN encapsulation procedure. Bovine serum albumin (BSA) is coated to the COIN surface and cross-linked by glutaraldehyde. The extra aldehyde functional groups on the COIN surface are removed by glycine and sodium borohydride treatment. (B). Schematic illustration of COIN functionalization procedure. Carboxylic acid groups on the surface of the BSA encapsulation layer are activated by EDC and reacted with amines groups in the antibody. (Reprinted with permission from ref [189]. Copyright 2007 Nano Letters).

In 2008, the use of denatured BSA (*d*BSA) is reported with gold nanoflowers (AuNF) and rhodamine B as the Raman reporter [148]. The *d*BSA provided stability to the AuNF coated RhB SERS tag via its 35 thiol groups from 35 cysteine residues (Figure 2-9).
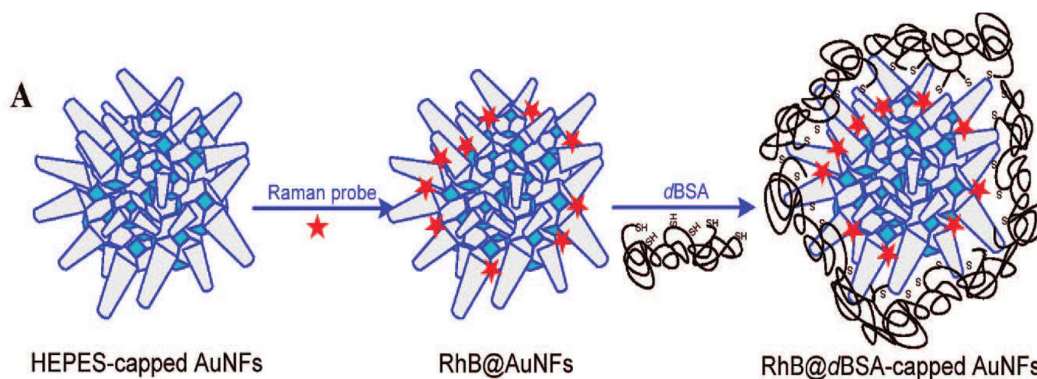
Figure 2-9. Preparation and design of dBSA-capped SERS tags. (Reprinted with permission from ref [148]. Copyright 2008 ACS Nano).

b)   Liposome Coating: Another biomolecule with promising application as SERS tag coating. It has ability to self-assemble onto metal nanoparticles with inherent biocompatibility. The use of immunoliposomes (ILs) with QD'S for *in-vivo* tumour imaging, therapeutics and drug delivery has also shown good targeting properties [190,191].
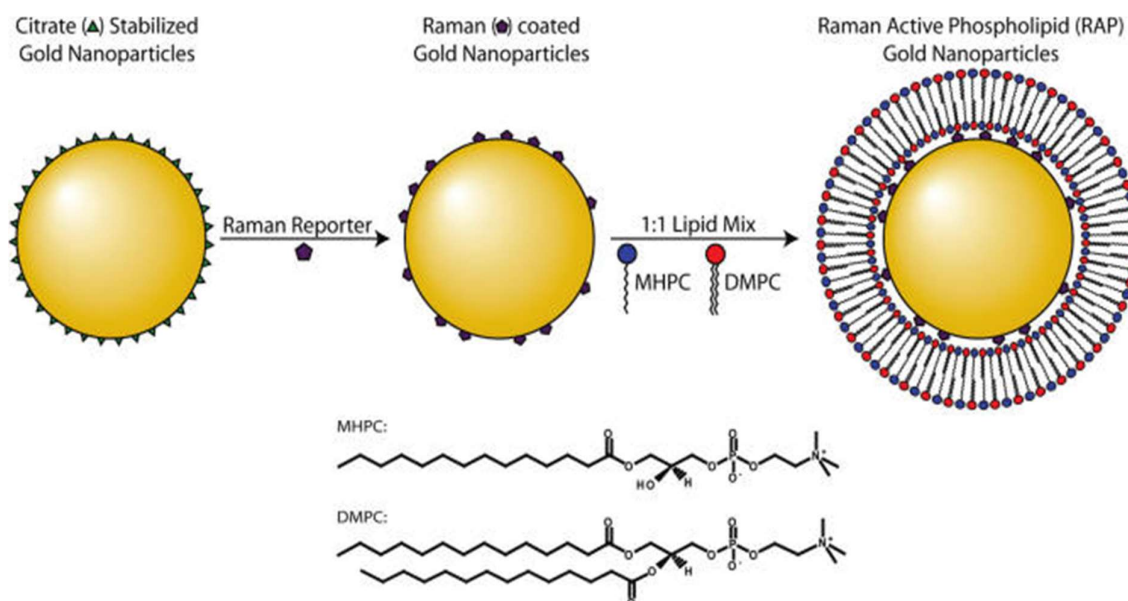
Figure 2-10. Scheme for synthesis of Raman-Active Phospholipid Gold Nanoparticles (Reprinted with permission from ref [192]. Copyright 2010 Bioconjugate Chemistry).

Tam et al. in 2010, translated these viable properties of liposomes into SERS tag coating. Colloidal gold nanoparticles of 60 nm with adsorbed Raman molecules were encapsulated by non-thiol phospholipid coating [192]. In 2011 Walker's group, encapsulated gold nanoparticles of 60 nm with lipids like DOPC, sphingomyclin and cholesterol. The lipid coating showed stability for weeks and versatility was also demonstrated by the incorporation of three different Raman reporters – MGITC, L-tryptophan and rhodamine by three different strategies [193]. In 2012 Natalie's group, also coated Raman active colloidal gold nanoparticles (60 nm) with phospholipid. These porphyrin−lipid stabilized AuNPs are also successfully used in cellular imaging (Figure 2-10) [194]. All these novel lipid-based SERS probe provides a viable alternate to the PEGylation and silica coating strategies due to its better reproducibility and stability.

2) Polymeric Coatings: PEG is an ideal polymer protective coating for the SERS tag. Some of the advantages are (Figure 2-11) [195-200]: (1) Non-toxic (2) Shell thickness can be adjusted (3) Highly hydrophilic offering weak affinity to interference molecules leading to prolonged lifetime *in-vivo* (4) Excellent *in-vivo* biodistribution and pharmacokinetic properties (5) Strong binding to metal nanoparticles due to distal thiol functional groups (6) High stability in strong ionic and pH media like biological and chemical environment (7) The second external functional group of PEG (e.g. carboxyl or amine) can be used to bioconjugate capturing agent like the peptide or antibody.
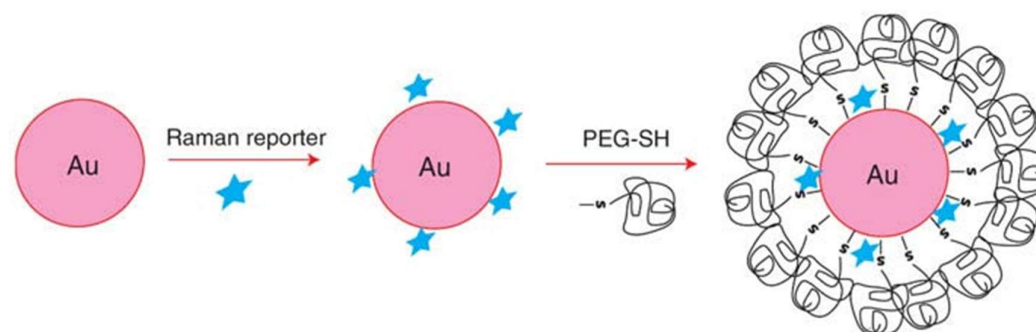
Figure 2-11. Design, preparation and properties of pegylated gold nanoparticles for in vivo tumor targeting and spectroscopic detection. (a) Preparation and schematic structures of the

original gold colloid, a particle encoded with a Raman reporter, and a particle stabilized with a layer of thiol-polyethyleneglycol (thiol-PEG). Approximately $1.4–1.5 \times 10^4$ reporter molecules (e.g., malachite green) are adsorbed on each 60-nm gold particle, which is further stabilized with 3.0×10^4 thiol-PEG molecules. (Reprinted with permission from ref [195]. Copyright 2010 Nature biotechnology).

Other commonly used polymers for their biocompatibility, biodegradability, and complexation with metal ions are PVP [157], chitosan [201,202], and polymers produced by reversible addition–fragmentation chain transfer (RAFT) [203]. Recently, a new polymeric coating with uniform thickness using amphiphilic di-block copolymer, polystyrene-block-poly(acrylic acid) (PS_{154}-b-PAA_{60}), has been reported through thermodynamically controlled process [204].

3) Silica Coatings: Silica encapsulation of the metal nanoparticle with the Raman reporter is another attractive protective coating method. In 2003 two groups simultaneously reported methods for silica encapsulation by hydrolysis of sodium silicate [205,206]. The metal nanoparticles along with the adsorbed Raman reporter is treated with a silane like 3-aminopropyltrimethoxysilane (APTMS) or mercaptotrimethoxysilane (MPTMS). The silanes one terminal group amine/thiol facilitates attachment to the metal nanoparticle. The other terminal group trimethoxysilane is used to make the metal nanoparticle surface vitrophilic. Later the solution is reacted with sodium silicate, which easily forms a layer of thin glass shell with the aid of trimethoxysilane (Figure 2-12 A). The only drawback with this glass coating was the SERS signal was suppressed due to silica interference. In 2009, Brady et al, via the same method used nanoclusters in order to increase the SERS signals from within the silica coated shells (Figure 2-12 B) [207]. This led to advantages like ultrathin silica layer, with a drawback such as tedious pre-treatment steps like dialysis, ion exchange and time consuming [208].
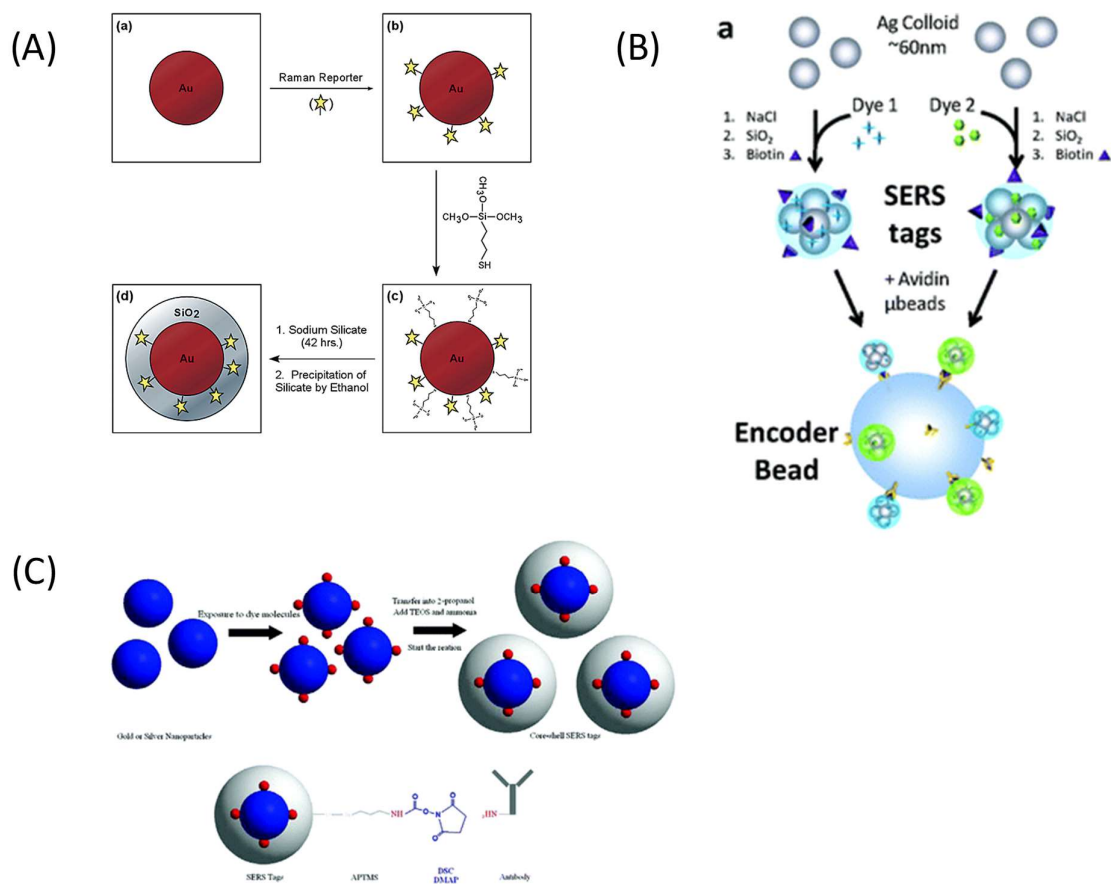
Figure 2-12. (A). Schematic illustration of the core-shell nanoparticle structure and the procedure for preparing silica-coated SERS-active gold colloids. (Reprinted with permission from ref [204] Copyright 2003 Analytical Chemistry). (B). Schematic of the process for generating encoder bead assemblies from SERS nanoparticle spectral tags. (Reprinted with permission from ref [207]. Copyright 2009 Analytical Chemistry). (C). Schematic illustration of the preparation of the core-shell SERS tags. (Reprinted with permission from ref [209]. Copyright 2010 Analytical Chemistry).

In 2010, Liu et al demonstrated a simple and fast method without any pre-treatment steps like dialysis, ion exchange etc. This method involved creating silica sols by adding ammonia and tetraethyl orthosilicate (TEOS) consecutively (Figure 2-12 C). The drawback in this ammonia catalysed hydrolysis of TEOS is that only strongly adsorbed Raman reporters like

isothiocyanate or multidentate thiol are feasible [209]. In 2009, Schlucker's group integrated the Raman reporter (4-MBA) and silica shell into a single functional group [210]. The gold/silver nanoshells were covered with SAM of 4-MBA. The surface charge of the SAM was used further to coat with a polyelectrolye (PAH-polyallylamine hydrochloride). The PAH facilitated adsorption of PVP, which made the surface vitrophilic and thus growth of silica shell using ammonia/2 propanol and TEOS by Stober method was achieved. In 2011, Huang et. al used a similar method with poly (acrylic acid) and then adsorbed APTMS or MPTMS to make the surface vitrophilic [119]. Then again using Stober method silica shell was deposited on the particle surface. In 2010, Schutz et al reported a fast and simple method of silica encapsulation, free from surface charge of the Raman reporter [176]. This method suggests covalently merging Raman reporter (4-MBA) and silica precursor (APTMS) as a single unit.

The advantages of silica coatings are (1) Biofunctionalization, accomplished by reaction of silica shell surface with aminopropyl which creates amine groups for conjugation with antibodies by forming amide bonds [211] (2) Silica coating offers high stability in biological and chemical environment [212] (3) It provides good water solubility and low nonspecific binding. On the other hand, its disadvantages include: (1) The use of silica is limited for creating the coating. This happens due to the high affinity of silica as compared to the Raman reporters. This allows the displacement of the Raman reporters resulting in low SERS signals. Therefore, only few Raman reporters with strong binding to the metal nanoparticles surface through isothiocyanate or thiols are preferred with silica coatings [14] (2) Functionalization of silica shell with amine groups creates positively charged surface that have a high affinity toward negatively charged cell membranes [213]. This causes the SERS tag to show reduced binding specificity as compared to bio functionalized PEG-coated SERS tags.

2.3.1.4 Attachment of Target Capturing Molecules

The next step is to attach the capture molecule to the SERS tag in order to guide and target the specific biological analyte. The capture molecules can be classified as, antibodies, aptamers or small molecule ligands. These capturing molecules can bind to the SERS tags through three functionalized routes that is indirectly either through the Raman reporter, the protective coating ligand or directly to the metal nanoparticle surface (Figure 2-13). Generally, the SERS tags are functionalized using sulfhydryl groups as thiols have high affinity for metal nanoparticles and easily form SAM. In case of the thiolated aptamers they easily replace the original surface ligands like citrate ions on the surface of the metal nanoparticles [214,215]. Stable covalent bonds can also be formed by SERS tags with OPSS-PEG-NHS (orthopyridyldisulfide-polyethyleneglycol- N-hydroxysuccinimide) and functional carboxylic groups on the original surface ligand to attach the antibodies. The antibodies can be attached through the EDC/NHS crosslinking chemistry to the Raman reporter or the protective coating. The carboxylic functional groups on the Raman reporter or the protective coating ligand is reacted with the amine groups on the antibody to form stable amide bonds. In case of small molecules ligands like biotin modified SERS tags can be used to target streptavidin tagged biomolecules.
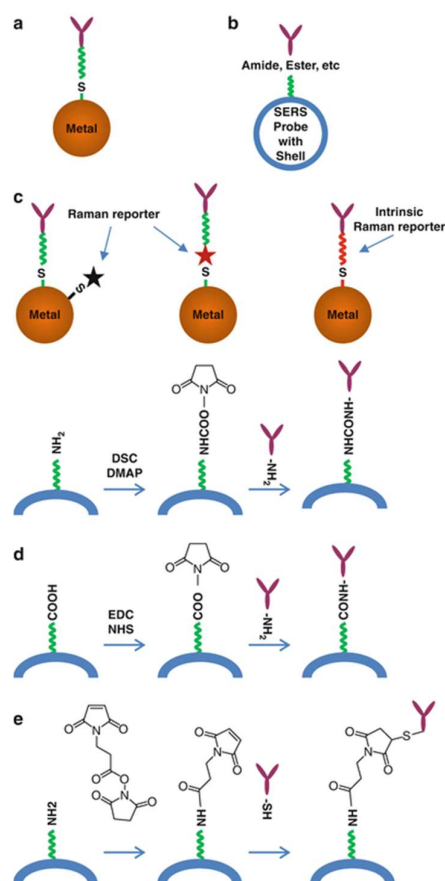
Figure 2-13. Various methods of bio-conjugation. (a) Direct immobilization of the linker molecule to the metal surface, (b) composite formation of the metal/biocompatible shell hybrids, (c) examples of direct immobilization to metal surface [216-218], (d) examples of active ester utilization [219,220], and (e) an example of maleimide-based bio-conjugation [168]. (Reprinted with permission from ref [221]. Copyright 2012 Raman Spectroscopy for Nanomaterials Characterization).

It is pertinent to mention here that in trying to accommodate this capturing molecule on the SERS tag the competition for surface space on the metal nanoparticle between the original surface ligand, Raman reporter and protective coating should be carefully administered. Original surface ligands like the citrate ions in case of synthesis of metal nanoparticles provide colloidal stability through electrostatic repulsion forces to avoid aggregation. Maximizing the

number of Raman reporters increases the SERS signal for better signal to noise ratio however, requires displacing the original surface ligands which leads to aggregation [222]. Similarly, the protective coating is vital for biocompatibility and to avoid biofouling. In case, the protective coating is not overlapping the SAM, placing the protective coating on the metal nanoparticle surface will require displacing the original surface ligand and/or the Raman reporter. This in turn will not only open venues for metal nanoparticles aggregation but also reduce the SERS signals. Therefore, a balanced ratio is important for maintaining metal nanoparticles stability, good SERS signals and to avoid biofouling. In this regard few noteworthy studies have been performed. In 2007, Qian et al. found that for each 60 nm colloidal gold nanoparticle the optimum ratios of Raman reporter (e.g., malachite green) and protective coating (thiol-polyethylene glycol) molecules is approximately 1.4-1.5 x 10^4 and 3 x 10^4 respectively [171]. In 2009, Schlucker group reported silica encapsulation of SAM (4-MBA) on the metal nanoparticle (Au or Ag) integrated as a single functional unit [223]. This was achieved through using polyelectrolyte (MPTMS) coating on the SAM which makes the Au or Ag surface vitrophilic. This MPTMS aids growing silica shell on top of the SAM by a modified Stober method [224]. So, this method allows silica protective layer growth on top of the SAM, thus eliminating the surface space on the metal nanoparticle competition between the protective coating with the original surface ligands and the Raman report. It also uses small Raman reporter, molecules having less spectral band facilitating multiplexing capabilities. The only drawback in this approach is to be mindful to have the complete monolayer SAM coverage, to overcome the weak SERS signals arising from small cross-sectional area and silica thickness covering the Raman reporter.

Another important factor for creating SERS tags is that the Raman reporters and protective coating ligands have a greater affinity for the metal nanoparticles, than the original surface ligands. This helps in easy displacement of the original surface ligands with the Raman reporter

and protective coating ligand. This is especially important when metal nanoparticles have original surface ligands like quaternary ammonium compounds or polymers [225,226], which are not only strongly adsorbed on the metal nanoparticles surface [227] but are also toxic to the cells [228,229]. In these cases, large amounts of Raman reporters and PEG will be needed to overcome the strong adsorption/affinity of original surface ligands [230-232].

Dialysis to gradually displace cetyltrimethylammonium bromide (CTAB) layers on gold nanorods, allowing more binding surface for thiolated polymers (PEG) and Raman-active molecules has been reported [138]. In 2014, Mehtala et al. suggested using excessive amounts of PEG with Raman reporters already attached to the metal nanoparticles via multidentate thiol groups or to convert strong original surface ligand like CTAB with weak original surface ligands like citrate ions [233]. This method provides displacement of the original surface ligand by protective coating ligand, while maintaining highly stable binding of Raman reporter.

2.3.2 Immune Substrate

Immune substrate is the platform, which helps capture the target analyte and becomes the base for the SERS nanoprobe . This substrate can be categorized as follows:

2.3.2.1 Immobilized Solid Support

These type of substrates includes fixed platforms, for the analysis and can be further categorized as follows based on the deposition techniques employed:

1) Self Assembled Deposition

In 1995, Natan's group proposed building fixed SERS monolayers on polymer coated substrates [234]. Colloidal metal nanoparticles are bound to the functionalized polymer coated substrate through cyanide (CN), amine (NH$_2$), and thiols (-SH) in a uniform architecture (Figure 2-14 A). This process yielded macroscopic surfaces for high EEF and reproducibility. This method produced less than 10% variation in results achieved from different substrates produced with monolayer of 12 nm Ag nanoparticles. In 2001, this study was further improved

by Maxwell et al. through introducing monodispersed Ag nanoparticles of size ranges 30-50, 50-80, 80-100 and > 100 nm deposited on polycarbonate membrane (Figure 2-14 B) [235]. The use of monodisperse colloids suggested better packing density and tuning of the incident laser excitation to SPR producing hot spots, thus increasing the overall EEF. In 2005, Hala's group continued to provide improvements in the EEF based on uniformity of SERS substrates that is distribution of colloidal particles (Au = 50 nm) forming the monolayers (Figure 2-14 C) [236]. A layer of ~ 4 nm thickness was achieved by encapsulating colloidal nanoparticles with ligands (CTAB) or an inorganic shell layer. This ligand binding not only allows uniform particle spacing of 10 nm, but also the electrostatic repulsion between particles prevented random distribution during monolayer formation. In 2010, shell isolated nanoparticle enhanced Raman scattering (SHINERS) were introduced (Figure 2-14 D) [208]. Here, AuNP's (55 nm) were encapsulated by an inorganic shell layer of an optically transparent material like silica or aluminum with shell thickness of 2 nm. A monolayer of nanoparticles is spread as 'smart dust' over the surface that is to be probed facilitating in-situ deposition of SERS tags and allows the nanoparticles to conform to different contours of analyte-based substrates. This provided uniform particles distribution and avoiding aggregation plus preventing particles from contamination. The drawback is the distance between the analyte and AuNP is increased due to silica or aluminium coating, which prevents achieving maximum EEF.

Alongside the above studies to assemble monodispersed spherical metal nanoparticles researchers have used Langmuir-Blodgett method for the organization of substrates [237,238]. In 2003 Tao et al. used PVP coated silver nanowires (d = 50 nm & l = 2-3 µm) arranged in 2-D array on a glass slide ('logs in a river") [239]. This arrangement showed results highly supporting reproducibility with EEF up to 10^9.
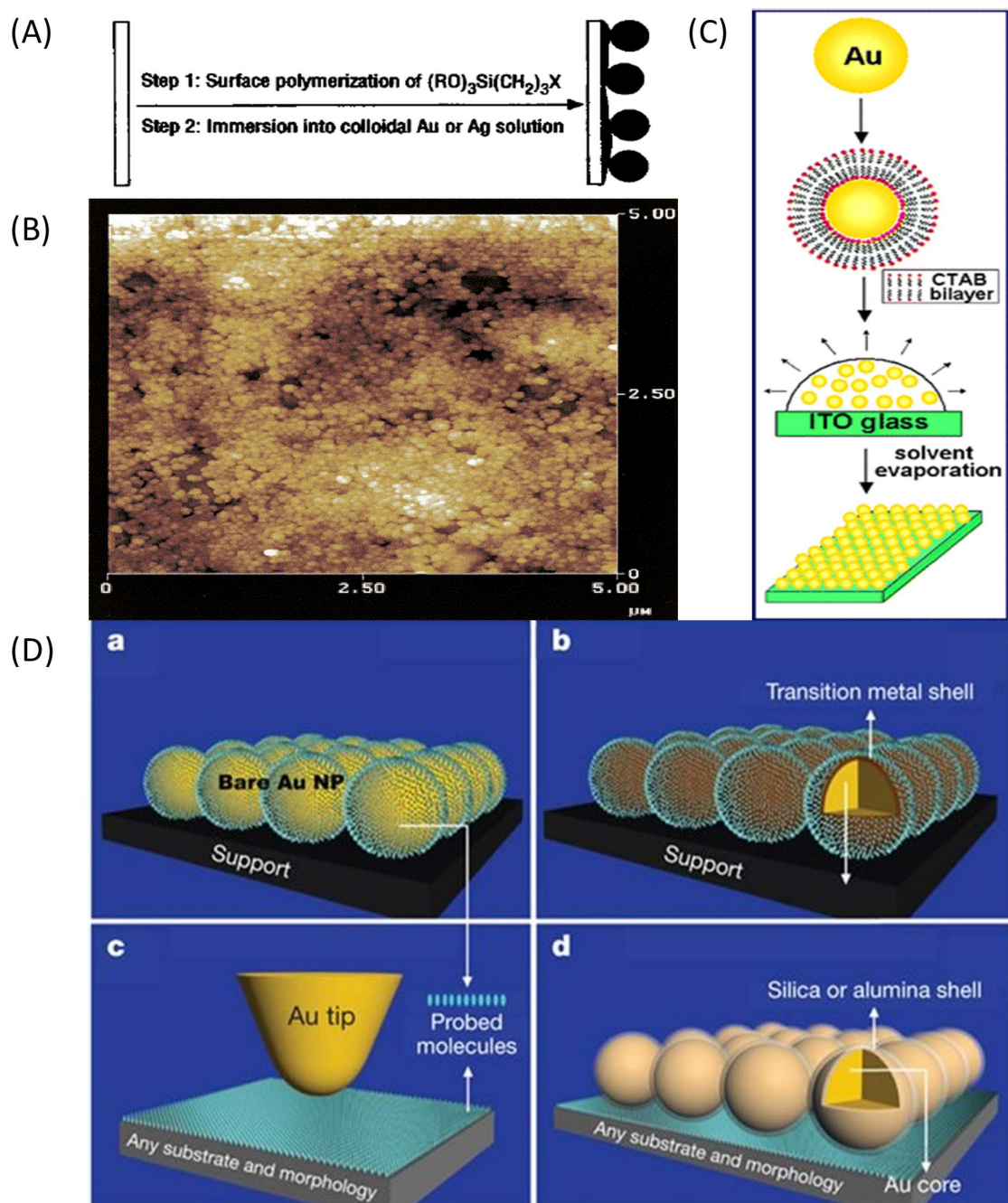
Figure 2-14. (A). Assembly strategy for Au and Ag colloid monolayers; X = CN, NH$_2$, 2-pyridyl, P(C$_6$H$_5$)$_2$, or SH; R = CH$_3$ or CH$_2$CH$_3$. (Reprinted with permission from ref [234]. Copyright 1995 Science). (B). Tapping-mode AFM image of a nanostructured thin film prepared from 50- to 80-nm Ag colloidal particles. (Reprinted with permission from ref [235]. Copyright 2001 Chemistry of Materials). (C). Schematic illustration of the fabrication of sub10

nm gap AuNP arrays. (Reprinted with permission from ref [236]. Copyright 20005 American Chemical Society). (D). Working principles of shell-isolated nanoparticle-enhanced Raman scattering (SHINERS) in comparison with other SERS substrates. (a). Bare Au nanoparticles. (b). Au core–transition metal shell nanoparticles. (c). Tip-enhanced Raman spectroscopy (TERS). (d). SHINERS: shell isolated mode. (Reprinted with permission from ref [208]. Copyright 2010 Nature Publishing Group).

2) Lithographic and Template Techniques

Lithography and template techniques allow high accuracy in fabricating uniformly distributed metallic nanoparticles substrates with precise control sanctioning spectral reproducibility. This allows tailored production of substrates for particular application as well as mass production for reproducibility on commercial scale. Ultrahigh sensitivity for single molecule detection is also possible through precisely controlled creation of "hot spots" and gaps. These structurally uniform nanosubstrates also allow homogenous SERS signal intensities. A few lithographic and template techniques are, Nanowire templating, [240,241] On-wire lithography, [242,243] Nanosphere lithography, [244-246] Electron beam lithography, [247-249] and Nanotransfer techniques [249]. Use of templates to synthesis bundles of metal nanowires has been demonstrated for creation of hot spot and subsequently enhanced SERS [240,241].

In 2006, Moskovits et al. used sacrificial templates of porous aluminium oxide (PAO) with hexagonal arrays, to fabricate bundles of Ag nanowires. This method is capable of producing closely packed bundles of nanowires with micrometer spacing. In 2009, Mirkin et al. introduced a technique called on-wire lithography (OWL) to further reduce the distance between the nanowires up to nanometers (~2 nm) [250]. This allowed SERS enhancement factors of 10^8 [251].

A technique called nanosphere lithography (NSL) or colloidal lithography (CL) is used to grow 2-D and 3-D periodic arrays of metallic nanostructures on a solid platform (glass slide) to develop a uniform SERS substrate [252-254]. A monolayer of micro-nano silica or polystyrene spheres is allowed to self-assemble by spin or drop coating on a solid platform (glass slide). A metal is deposited through vapour or electro deposition to mask on top of the silica or polystyrene beads (Figure 2-15). Based on the shape and size of the silica or polystyrene spheres in conjunction with specific deposition technique and conditions, three types of metal nanostructures can be formulated:

a. "Film Over Nanospheres" (FON) prepared by vapour deposition of 100-200 nm metal layer on top of the silica or polystyrene spheres [255,256].

b. Chemically etched away silica or polystyrene spheres gives a periodic array of nanostructured triangles on the solid platform [257].

c. Electrochemical deposition of metal followed by removal of silica or polystyrene spheres, e.g. nanoislands, nanoholes or nanovoids [258].

The several advantages of NSL or CL are: (1) Simple and inexpensive [254] (2) The shape, size and spacing of the nanostructures can be controlled by the size of silica or polystyrene spheres and the thickness of deposited metal, [259,260] (3) Provides high density of SERS-active sites with large defect-free regions of 10-100 μm with EEF of 10^6–10^8, as well as excellent spectral reproducibility. Overall, this facile nanofabrication technique is highly effective for generating SERS substrates to perform fundamental studies on trace analysis and detection of single molecule.
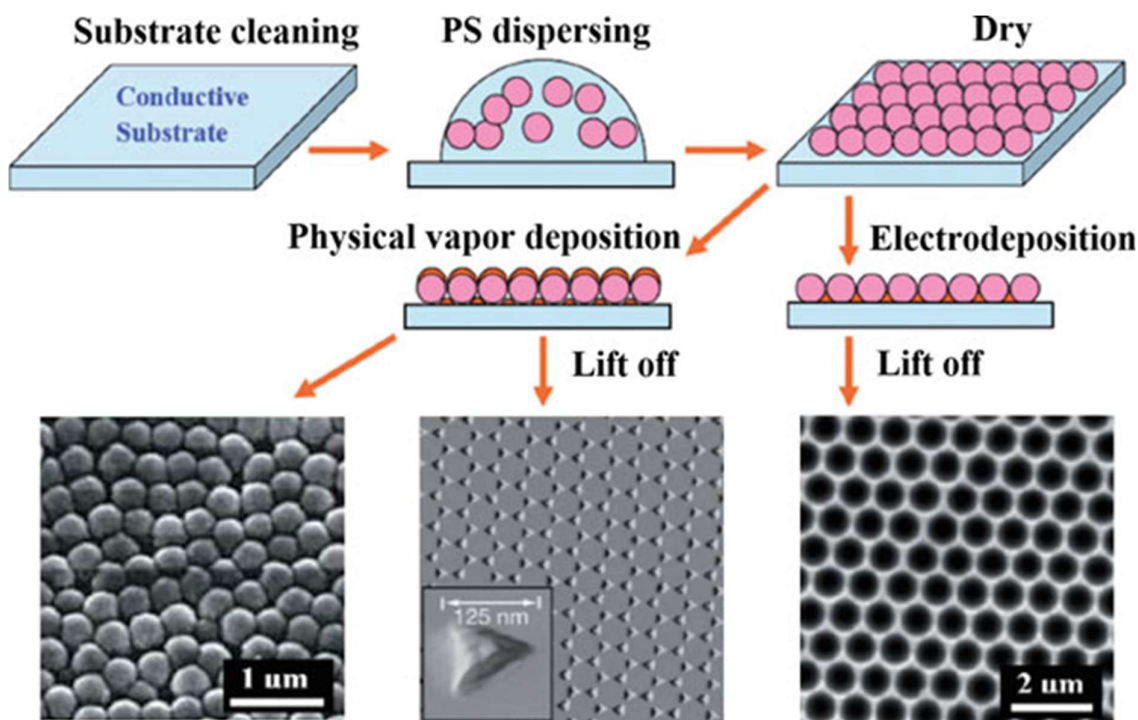
Figure 2-15. Schematic diagram of template methods using nanosphere lithography to fabricate ordered nanostructured SERS-active substrates, redrawn according to the published works of Van Duyne's group and Bartlett's group (Reprinted with permission from ref [261]. Copyright 2008 The Royal Society of Chemistry).

Electron beam lithography (EBL) and ion beam lithography (IBL) can be treated as a technological step forward as compared to NSL. This technique uses electron or ion beam to allow great control and precision in generating desired shapes and spacing between metal nanostructures for SERS substrates [262,263]. Silica wafer is initially coated with a photo resist material like poly (methyl methacrylate) (PMMA) layer, followed by chemical etching. Thereafter EBL uses two different strategies to fabricate the SERS active metal nanostructured substrate as shown in Figure 2-16. The first strategy involves electron beam exposure according to the intended shape and structure of the metal nanostructures, then removal of the remaining photoresist trailed by vapour deposition of metal. The second strategy involves vapour deposition of metal trailed by removal of the remaining photo resist coated with the metal. The

first strategy enables whole silica wafer covered with metal with imprinted nanostructure while, the second strategy enables array of nanostructures patterns with gaps of bare silica exposed [264-267]. Recently, in 2015 Tabatabaei et al. fabricated metallic nanoholes arrays with a high nanohole density by EBL and tested as molecular SERS sensors [268]. The best SERS EEF from Au nanodisks and nanoholes fabricated by EBL are reported as 4 x 10^5 and 1 x 10^3, respectively [269]. EBL in conjunction with other methods can produce dimer gaps smaller than 1 nm like electromigration and angled evaporation techniques [270,271]. These methods provide practical insights into the SERS enhancement plausible to classical electrodynamics and quantum mechanics. However, in comparison to template techniques, EBL and IBL methods are generally costly, and require extensive preparation times with the need for a specialized equipment.
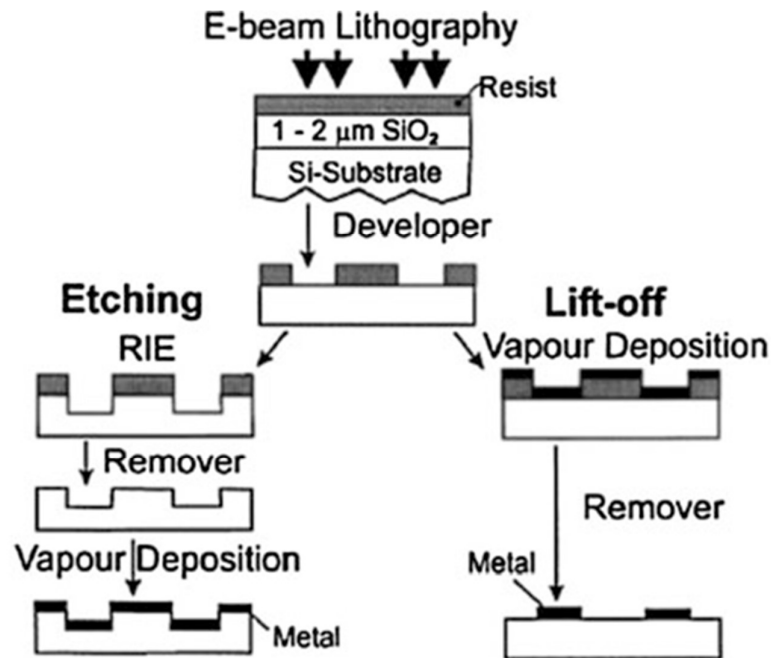
Figure 2-16. Schemes of etching and lift-off methods of substrate fabrication by e-beam lithography on oxidised silicon substrates (Reprinted with permission from ref [263]. Copyright 1998 Elsevier S.A.).

2.3.2.2 Colloidal Substrates (Suspension)

In this type of SERS immune substrate, microbeads are dispersed in a liquid solution. These microbeads include silica beads, polymer beads, magnetic beads etc. Few advantages of such suspension array are: (1) Faster immune reactions between capture and target analyte due to reduced diffusion distance. (2) Higher multiplexing ability by use of multiple microbeads with different capture analyte. (3) Probable use of magnetic beads for more enrichment of the nanoprobes. Colloidal substrates can be magnetic and nonmagnetic, these substrates are discussed with related examples as follows:

1) Nonmagnetic Substrate

The most commonly used non-magnetic substrates include silica spheres [272], polymer spheres [273], metal nanoparticles [274], photonic crystal beads [275]. These substrates are modified to attach the capturing analyte, which subsequently, would bind to the target analyte and SERS probe. Lijuan et al. demonstrated use of functionalized polystyrene microbeads as an immune substrate. Antibodies were attached to the immune substrate for specific binding of the target antigen based SERS probe. [273] Yan et al. also exhibited SERS-based detection technique built on Au@Ag NS's. Here, the metal nano-particles were used as the SERS immune substrate as well as the signal amplifier to detect chloramphenicol. [274] Photonic crystals (PC) beads [276], spherical colloidal crystal clusters [275], and 3-D silver nanoshells silica photonic crystal beads [276] (Ag-SPCBs) have also been used as an efficient immune substrate, as well as encoding element in bioassay to enhance multiplexing capabilities. Similarly, platforms like 'lab on bubble' where buoyant silica bubble microspheres have been used as the SERS immune substrate. [272] Furthermore, some studies have utilized SERS nanoparticles deposition [277] and self –assembly as a source of signal amplification for high sensitivity for quantitative analysis. The concept of using SERS based microbeads immunoassay with flow cytometer has been

demonstrated for detection of leukemia and lymphoma cells using SERS encoded nanoprobes [278]. This has future applications for disease diagnosis.

2) Magnetic Substrate

The most commonly used magnetic substrates are Fe_3O_4 [279] and Fe_2O_3 [280]. The advantages of using magnetic SERS immune substrate are: (1) High surface-to-volume ratio (2) Ease of fabrication (3) Low toxicity (4) Ease of bio-conjugation due to rich functional groups on their surface (5) Easy, rapid and repetitive washing using a magnet. Magnetic beads depending upon the utility that is either used as an immune substrate or SERS immune substrate plus SERS enhancement, are usually coated with a protective layer of silica, metal or polymer. These coatings offer further improved stability, biocompatibility and bio-conjugation. Wang et al. [281], Xiao et al. [282] and Xiong et al. [283] has used magnet assisted, and magnetic nanoclusters SERS based immunoassay, respectively. Shenfei et al. [284], has demonstrated use of silica-coated magnetic beads in SERS based immunoassay, respectively. [285] Li et al. fabricated composite magnetic beads [Fe_3O_4@polymethacrylic acid (PMAA)-SS-FA] to capture circulating tumor cells (HeLa cells) [286]. Magnetic beads have also been used with encapsulation with metal nanoparticles to be used as an immune substrate and signal amplification platform. The most popular model is the Fe_3O_4@Au. [287] Recently, $MnFe_2O_4$@Ag has been used as a magnetic substrate in a SERS bioassay for the single-cell detection of Staphylococcus aureus. [288]

2.4. SERS Immunoassay: Bio-Imaging for Cancer Detection

The first line of defence mechanism in a human body is its immune system, against infectious foreign bodies. This immune system generates antibodies (IgG) to neutralize the target pathogens. The realization and detection of these antibodies from the human body fluid (e.g. blood, urine, ascites, and saliva) is a vital indication of disease at early stages. Therefore, capturing these biomarkers, helps identify disease at its earliest possible stage and take

remedial actions for successful treatment. These biomarkers are usually captured by their counterpart specific antibodies. The usual methods of immunoassay diagnosis include, ELISA, Chemiluminescence, Colorimetry, Fluorescence, SPR etc.

Here progress of SERS based immunoassay will be discussed with respect to bio-imaging for cancer detection (*in-vitro* & *in-vivo*). Traditional approaches for cancer detection are, X-ray, computer tomography, endoscopy, ultrasonography and pathological section etc. These diagnostic tools rely on cancer detection in later stages, where deformity is the cause of detection [289-293], through surgically dissected tissue samples (biopsy). Therefore, for early stage cancer detection biomarkers secreted by the tumour cells into the body fluids (blood, urine, ascites and saliva etc.) need to be identified. Till date the most common biomarkers related to cancers include [294-299], proteins (e.g., receptors, cancer antigens), microRNAs (miRNAs), circulating DNA, and CTCs. Out of these biomarkers' species, proteins are the most well studied. Typical protein biomarkers include: Carcinoembryonic antigen (CEA), Alpha-fetoprotein (AFP), Human epidermal growth factor receptor 2 (HER2), vascular endothelial growth factor (VEGF), Prostate-specific antigen (PSA), tumor suppressor p53, and epidermal growth factor receptor (EGFR). A petite amount of body fluids is required in case of SERS-based immunoassays [276,300-310], this allows repetitive examinations for prognosis to regulate therapeutic strategies in time.

2.4.1 SERS Imaging of cancerous cells and tissues

SERS based imaging primarily focuses on visualization for therapeutics of targeted area in cells and tissues. Recently, SERS based immunoassay has progressed towards high resolution imaging due to technology advancements in diagnostic equipment's. The imaging relies on recognition of biomarkers by immuno-functionalized SERS nanoprobes and/or substrates to form an immunocomplex either *in-vitro* or *in-vivo*.

2.4.1.1 *In-vitro* - Cells

Numerous SERS based imaging has been performed outside of human body to demonstrate practical application of capturing cancerous cells and tissues. In bioanalytical applications in *in-vitro*, cell cultures are commonly used as models to mimic *in-vivo* tissues.

SERS bimetallic nanoprobes based on Au_{core}/Ag_{shell} and rhodamine 6G (R6G) as the SERS probe molecule have been conjugated to anti-mouse IgG through ortho-pyridyldisulfide-polyethylene glycol-N-succinimidyl propionate (OPSS-PEG-NHS). These were used to capture and image the presence of cancer biomarker phospholipase $C\gamma1(PLC\gamma1)$ (biomarker protein is overexpressed in some human hyper proliferative tissues, including breast carcinoma, colorectal carcinoma, familial adenomatous polyposis, and highly metastatic colorectal tumour cell lines) in live cells HEK293 (Figure 2-17 A). [311] In 2009, SERS nanoprobes based on hollow Au nanospheres (HGNs) and crystal violet as the SERS reporter molecules, were conjugated to anti-rabbit IgG through dihydrolipoic acid (DHLA). These were used to capture and image the presence of breast cancer biomarker in MCF7 live cells (Figure 2-17 B) [312]. SERS nanoprobes based on Au nanorods and Au nanostars have been used in SERS imaging applications, providing a larger surface area, stronger scattering and nanospheres, exhibiting plasmon bands in the near infrared range, which is more beneficial for bioassays. [313] SERS encoded magnetic nanoparticles (NPs) have also been used for detection, targeting and separation of cancer cells. These M-SERS dots consist of a magnetic core coated by silica shell prepared by thermal deposition and reverse microemulsion, respectively. As the SERS substrate, silver NPs were introduced on the surface of these silica-coated magnetic NPs. Overall, these M-SERS dots were again coated with silica for stability. These M-SERS dots successfully demonstrated detection and targeting of breast-cancer cells (SKBR3) and floating leukemia cells (SP2/O). These targeted cancerous cells embedded with M-SERS dots were further separated by applying an external magnetic field. The M-SERS dots were able to

produce "hot spots" with 1000 times greater enhancement factor [314]. In 2011, a combinatorial chemistry approach was used to report novel cyanine reporters with high-intensity Raman peaks with NIR excitation. [315] A lipoic acid-containing NIR-active tricarbocyanine library (CyNAMLA) was prepared for SERS signals after chemisorption on AuNPs. These CyNAMLA compounds exhibited strong SERS signals, and particularly, CyNAMLA-381 with exceptional signal stability and 12 times fold higher sensitivity as compared to standard DTTC. CyNAMLA-381 was further successfully applied to the preparation of ultrasensitive SERS probes for *in-vitro* cancer imaging and *in-vivo* spectral analysis, by conjugating CyNAMLA-381–AuNPs to scFv anti-HER2 tumour antibodies (Figure 2-17 C).

Multiplexing through SERS nanoprobes have also been introduced for cancer cell detection. SERS nanoprobes based on AuNPs encoded with two different SERS reporter molecules based on triphenylmethine and cyanine compunds (Cy3LA and Cy5LA), chemisorbed via lipoic acid (LA) linker were conjugated to anti-EGFR and anti-HER2 have been used to recognize and image different types of cancer cells (OSCC and SKBR-3, respectively) under co-culture conditions (Figure 2-17 D). [179]
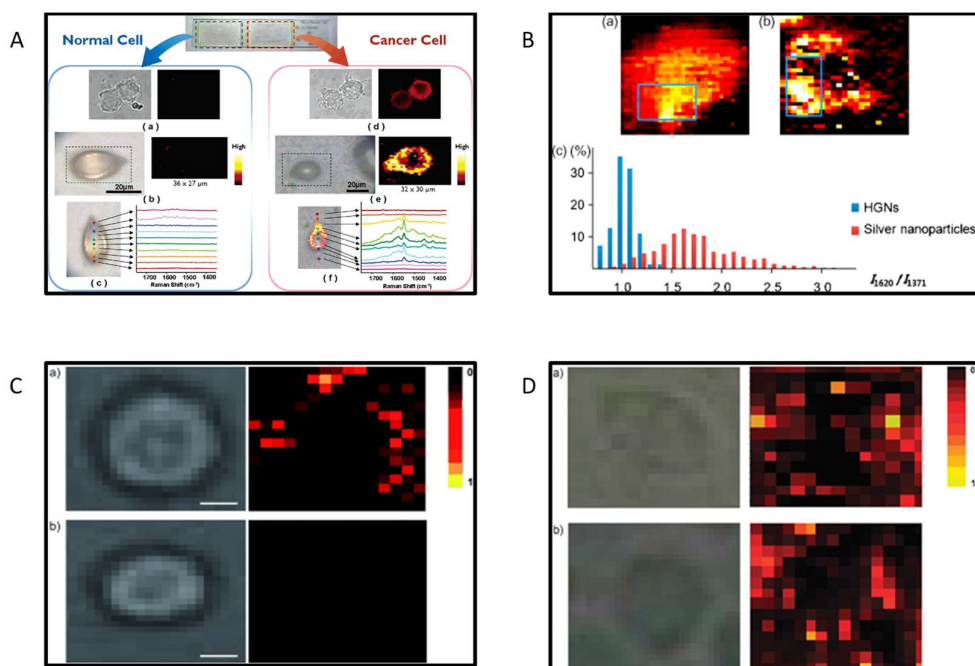
Figure 2-17. (A). Fluorescence and SERS images of normal HEK293 cells and PLCç1-expressing HEK293 cells. (Reprinted with permission from ref [311]. Copyright 2007 Analytical Chemistry). (B). SERS mapping images of HER2-expressing MCF7 cells using (a). HGNs and (b). silver nanoparticles. (c). Comparison of the histograms for intensity ratios (I1620/I1371) of HGNs and silver nanoparticles. (Reprinted with permission from ref [312]. Copyright 2009 Elsevier B.V.). (C). Bright-field and SERS mapping images of cells treated with CyNAMLA-381 nanotags: a). SKBR-3 and b). MDA-MB231 cells. (Reprinted with permission from ref [315]. Copyright 2011 Angewandte Chemie International Edition). (D). Bright field and SERS mapping images of: (a). B2LA anti-EGFR nanotag-treated OSCC cells (b). Cy3LAanti-HER2 nanotag-treated SKBR-3 cells. (Reprinted with permission from ref [179]. Copyright 2011 Chemical Communications).

Malini Olivo et al. prepared an organometallic-nanoparticle (OM-NP) conjugate, using an osmium metal carbonyl as a Raman reporter to develop the SERS nanotag. These OM-NP conjugates can be readily functionalized with suitable binding ligands, displaying excellent

aqueous dispersibility and storage stability. In live-cell imaging, the CO stretching vibration signal between 400-1800 cm^{-1} region, is well-separated from other molecular vibrational modes of the cell between 1800–2100 cm^{-1} region of the Raman spectrum (Figure 2-18 A). Furthermore, for the SERS imaging of live-cells, the OM-NP were conjugated with an antibody to capture epidermal growth factor receptors (anti-EGFR). [316]

SERS nanoprobes based on PMA coated Au nanostars (AuNS@PMA$_{TAMRA}$) encoded with five different SERS reporter molecules {Benzenethiol (BT), 1-naphthalenethiol (1-NaT), 2-naphthalenethiol (2-NaT), 4-methylbenzenethiol (4-MBT), and biphenyl-4-thiol (4-BPT)}, conjugated via thiol groups have been used to image five different types of breast cancer cells (HCC1395, SK-BR3, MDA.MB.231, CAMAI & MCF-7) in quintuple cell coculture (Figure 2-18 B). [317] Similarly, SERS nanoprobes based on polydopamine-encapsulated Au nanorods (AuNRs) embedded with p-MBA as the SERS reporter molecules, conjugated to anti-EpCAM (antibodies) have been used to capture, image and photothermal ablation of tumour cells DU145 derived from human prostate cancer (Figure 2-18 C). [318]
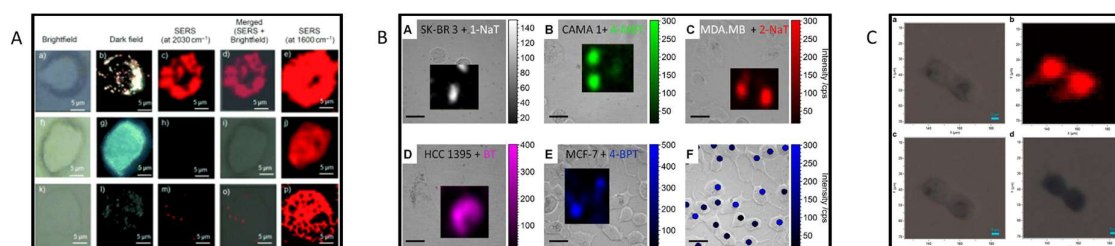
Figure 2-18. (A). Bright-field, dark-field, and SERS mapping images of (a–e). OSCC cells, (f–j). SKOV cells treated with OM-NP(PEG)-L conjugates, and (k–p). OSCC cells treated with anti-EGFR prior to incubation with OM-NP-(PEG)-L conjugate. (Reprinted with permission from ref [316]. Copyright 2012 Angewandte Chemie). **(B).** (A−E) Correlated transmitted light and SERS images of breast cancer cells corresponding to the cell-RaR combination C1. (F) Statistical SERS measurements by single-point SERS mapping of cells marked with 4-BPT tags allow fast analysis for high cell detection efficiency. (Reprinted with permission from ref

[317]. Copyright 2016 Chemistry of Materials). **(C).** (a) Bright field images of DU145 cell. (b) SERS images of DU145 cells. (c) Bright field images of DU145 cell after SERS imaging and trypan blue staining. (d) Bright field images of DU145 cell after photothermal therapy and trypan blue staining. (Reprinted with permission from ref [318]. Copyright 2017 Analytical and Bioanalytical Chemistry).

A few recent examples of SERS imaging in cancer cells include:

- A new shell-based spectroscopic platform, namely Mechanical Trap Surface Enhanced Raman Spectroscopy (MTSERS) for 3-D microscopic imaging of cell membrane of the MDA-MB-231 breast cancer cell. [319]

- The simultaneous imaging of multiple intracellular microRNAs (miRNAs - miR-21 and miR-203) were successfully detected in living MCF-7 cells. [320]

- Folate-targeted SERS nanoprobe for selective imaging and diagnosis of FR-cancer cells (folate receptor) based on click coupling strategy. [321]

- Synthesis of a gadolinium-gold composite nanoparticle (Gd-Au NPs), for imaging of EGFR expression levels in three human cancer cell lines (S18, A431 and A549) were measured. [322]

- A bio-orthogonal Raman reporter-embedded Au-core and polydopamine-shell nanoprobe (Au@PBAT@PDA) for live cancer cell imaging. [323]

2.4.1.2 *In-vitro* - Tissues

Diagnosis of surgically incisional tissues samples collected from patients as a result of abnormal growth, is of high importance in order to determine whether the tissue is benign or cancerous and at what stage the cancer is existing.

Recently, progress in SERS imaging for tissues has gained significant attention. In 2008, Woo et al. performed the first quantitative analysis of multiple protein expressions (CD34, Sca-1,

and SP-C) in tissue using dual mode labelling - SERS and fluorescence. They used fluorescent surface-enhanced Raman spectroscopic dots (F-SERS dots), composed of silver nanoparticle-embedded silica nanospheres, organic Raman tagging materials (mercaptotoluene, benzenethiol, and naphthalenethiol), and fluorescent dyes (fluorescein isothiocyanate and Alexa Fluor 647). The proteins were simultaneously expressed in bronchioalveolar stem cells (BASCs) in the murine lung (Figure 2-19 A), where these multifunctional F-SERS dots were successfully captured, tracked and imaged. [324] In 2009, Water soluble SAM-based SERS nanotags were used to image the localization of PSA in prostate cancer tissues from patients undergoing prostatectomy (Figure 2-19 B). [325] In 2011, Affibody-conjugated Au–silica NPs were used as Epidermal Growth Factor Receptor (EGFR) targeting and imaging agents for colon cancer (A431 tumour).[326] Recently in 2017, a new technique called Raman-encoded molecular imaging (REMI) has been performed. In this technique, targeted nanoparticles are applied on excised tissues to enable rapid visualization of a multiplexed panel of cell biomarkers at surgical margin surfaces (Figure 2-19 C). In this clinical study 57 fresh specimens were imaged to simultaneously quantify the expression of four biomarkers HER2, ER, EGFR, and CD44 (human breast tissues). [327]
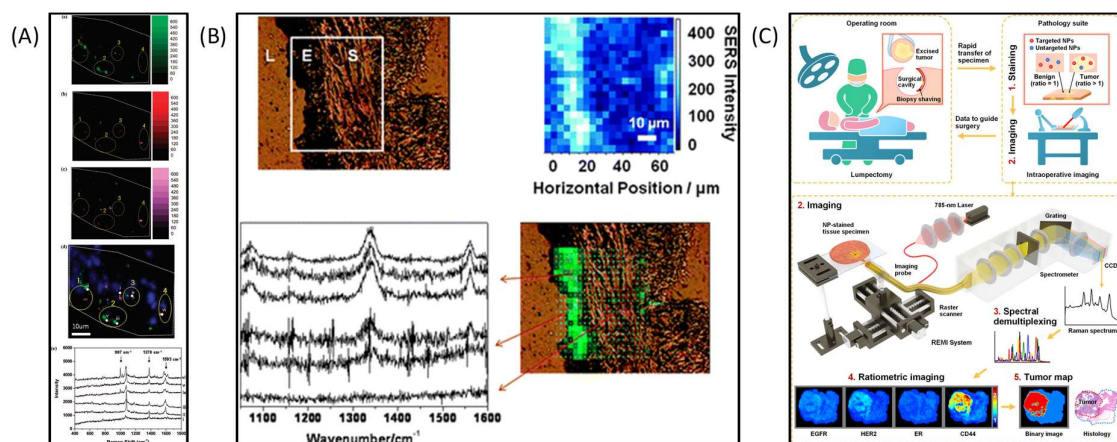
Figure 2-19. (A). SERS intensity mapping of BADJ: (a) Maps produced using baseline-corrected intensities of the 1593 cm^{-1} MT band corresponded to the CD34 protein. (b) The 997 cm^{-1} BT band corresponded to the Sca-1 protein. (c) The 1378 cm^{-1} NT band corresponded to SP-C protein. (d) The overlaid images of all three maps with nuclear staining images for the illustration of protein cellular distribution. (e) Representative Raman spectra at several points indicated by white dots. (i) NT signal, (ii) MT signal, (iii) NT and MT signals, (iv) BT and NT signals, (v) BT and MT signals, and (vi) BT, NT, and MT signals. (Reprinted with permission from ref [324]. Copyright 2008 Analytical chemistry). **(B).** Top: bright field microscope image of a prostate tissue section. The grid shows the locations at which Raman spectra were acquired in a point mapping experiment. The false-colour SERS image shows that the characteristic signal of the SERS-labelled antibody is observed selectively in the epithelium. (Reprinted with permission from ref [325]. Copyright 2009 Physical Chemistry). **(C).** REMI for intraoperative guidance of lumpectomy. Each specimen is topically stained with a mixture of SERS NPs (step 1), followed by spectroscopic imaging of the surgical margin surface (step 2). The acquired SERS spectra are demultiplexed to determine the ratio of the targeted vs. untargeted NPs (step 3), which enables the quantification of various biomarker targets (step 4). REMI images of the individual biomarkers are combined to detect the presence of residual tumours at the surgical

margin surfaces of the specimens (step 5). (Reprinted with permission from ref [327]. Copyright 2017 Cancer Research).

In 2012, a highly specific and sensitive methodology using 4-MBA labelled Au/Ag core-shell nanoparticles combined with a SERS imaging technique has been used for rapid analysis of LMP1 expression in nasopharyngeal cancer tissue (Figure 2-20 A) [328]. In 2011, Au nanostars have been used to image the abundance of the tumour suppressor p63 in benign prostate biopsies. [329] Similarly in 2014, small silica-coated clusters of gold nanoparticles as SERS-labels in conjunction with chimeric protein A/G, were used for co-localization of antibodies (p63 and PSA) on non-neoplastic prostate tissue FFPE specimens [330]. Here, two different Raman reports, namely 4-MBA (p63) and 4-NTB (PSA) were used to produce two false colored SERS images. In 2013, endoscopy imaging using fibre optic-based Raman spectroscopy was developed for multiplexed functional information during routine endoscopy by detection of tumour targeting SERS nanoparticles. Excised human tissue sample, were used to show detection up to 326-fM concentrations with unmixed 10 variations of colocalized SERS nanoparticles (Figure 2-20 B) [301]. These studies mark a promising future of SERS imaging in immunohistochemistry staining.
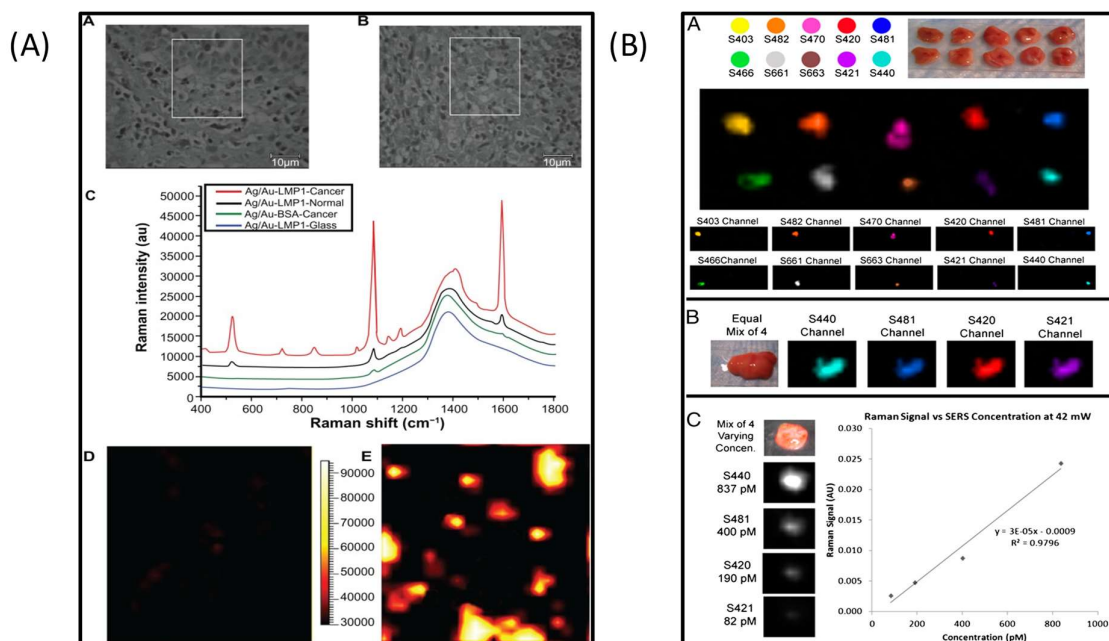
Figure 2-20. (A). (A) and (B) Bright field images of a region from examples of normal and cancerous nasopharyngeal tissue sections, respectively; (C) representative spectra obtained from latent membrane protein 1 surface-enhanced Raman scattering probes in cancerous nasopharyngeal tissue (red), normal nasopharyngeal tissue (blue) and glass (black), as well as nontargeted surface-enhanced Raman scattering probes in cancerous nasopharyngeal tissue (green); (D) and (E) surface-enhanced Raman scattering images of normal tissue and cancerous tissue, respectively. (Reprinted with permission from ref [328]. Copyright 2012 International Journal of Nanomedicine). **(B).** Demonstration of multiplexing on human tissue at 42 mW. (A) Ten unique flavors of SERS nanoparticles spatially separated onto 10 separate pieces of fresh human colon tissue. (B) Demonstration of colocalized multiplexing, where 4 SERS flavors were equally mixed and applied on a single piece of human colon tissue. (C) Mixture of 4 SERS nanoparticle flavors, each at varying concentrations, was combined and applied to a single piece of human colon tissue. (Reprinted with permission from ref [301]. Copyright 2013 Proceedings of the National Academy of Sciences).

2.4.1.3 *In vivo* imaging

Quantification of Raman signals is of vital importance for in-vivo SERS imaging. SERS has a limited penetration depth of few millimetres for *in-vivo* imaging, which can be increased to few centimetres by using SERS tags with NIR spectral properties. SERS imaging has been usually under explored due to the limited availability of near-infrared Raman reporters.

In 2008, one of the pioneering studies for in-vivo SERS nanotags for biomarker detection in human cancer cells and xenograft tumour models in live animals (mouse) was reported. Here, the detection was performed by use of PEGylated gold nanoparticles conjugated with single-chain variable fragment (ScFv) as the capture antibody and diethylthiatricarbocyanine (DTTC) as the Raman reporter. These SERS nanotags were established to have emission in the near infrared (NIR), brighter than quantum dots and successfully used to detect overexpressed EGFR (Figure 2-21 A) [195]. This study carried out spectral analysis only, however laid down the foundation for subsequent *in-vivo* Raman imaging.

One of the first examples of *in-vivo* tissues molecular imaging using SERS was performed by S.S Gambhir et al. in 2008 (Figure 2-21 B) [331]. The successfully designed PEGylated and nonPEGylated SERS-nanoparticles (Nanoplex Biotags - Oxonica), were imaged with maximized Raman signal, with NIR excitation and emission profiles which are ideal for minimizing light absorption by the liver tissue (tumour) in live mice. In a similar work Raman microscope was used to evaluate tumour targeting and localization of single walled carbon nanotubes (SWNTs) in mice. Raman images were acquired for tumour targeting RGD-SWNTs intravenously (Figure 2-21 C) [331].
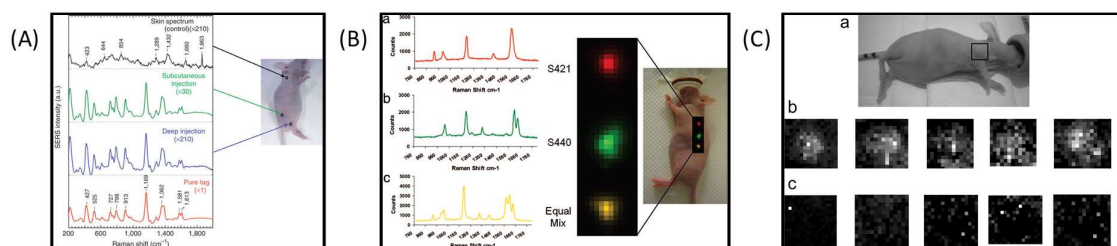
Figure 2-21. (A). Injection sites and laser beam positions are indicated by circles on the animal. A healthy nude mouse received 50 μl of the SERS nanoparticles tags (1 nM). The subcutaneous spectrum was obtained in 3 s, the muscular spectrum in 21 s, and the control spectrum also in 21 s. The reference spectrum (red) was obtained from the SERS nanoparticles in PBS solution in 0.1 s. The spectral intensities are adjusted for comparison by a factor (× 1, × 30 or × 210). The Raman reporter molecule is malachite green, with spectral signatures at 427, 525, 727, 798, 913, 1,169, 1,362, 1,581 and 1,613 cm^{-1}. Excitation wavelength, 785 nm; laser power, 20 mW. (Reprinted with permission from ref [195]. Copyright 2008 Nature Biotechnology). **(B).** Evaluation of multiplexing experiment. (a) Raman spectrum acquired from first s.c. injection of S421 SERS nanoparticles (red). (b) Raman spectrum acquired from second s.c. injection of S440 SERS nanoparticles (green). (c) Raman spectrum acquired from the third s.c. injection of an equal mix of S421 and S440 (yellow). (Reprinted with permission from ref [331]. Copyright 2008 Proceedings of the National Academy of Sciences). **(C).** Raster-scan images of tumor area (750 μm steps) using Raman spectroscopy in conjunction with SWNTs. (a), Digital photograph of tumor bearing mouse depicting tumor area scanned with Raman spectroscopy (black box). (b), Panel of tumor maps from mouse receiving RGD nanotubes at various time points post injection starting from left to right with 2, 8, 24, 48, and 72 h. (c), Panel of tumor maps from mouse receiving plain nanotubes at various time points post injection starting from left to right with 2, 8, 24, 48, and 72 h. (Reprinted with permission from ref [331]. Copyright 2008 Nano Letters).

Above mentioned studies have been followed by further research and development. The same research group of S.S Gambhir et al. demonstrated spectral readout of 10 different SERS nanotags, subcutaneously injected in a live mouse. This was followed by intravenous injection of five more spectrally unique SERS nanotags. These five SERS nanotags accumulated in the liver, and were successfully identified using false coloured Raman imaging (Figure 2-22 A) [187]. Likewise, Raman imaging of SERS NPs in a live zebrafish embryo has been studied. These SERS nanoprobes were injected to understand biocompatibility and biodistribution of nanostructures on a live subject. The SERS nanoprobes were constructed using gold nanoparticles (AuNPs) of two different sizes (diameter 25 & 40 nm), and two Raman reporters (mercaptobenzoic acid, MBA, and mercaptopyridine, MPY). The SERS NPs were microinjected into zebrafish at the one-cell stage to monitor the embryo development. The intricate physiological and pathological processes in embryo development were successfully monitored. This study has also set the stage for an *in-vivo* multiplex SERS imaging (Figure 2-22 B) [332].
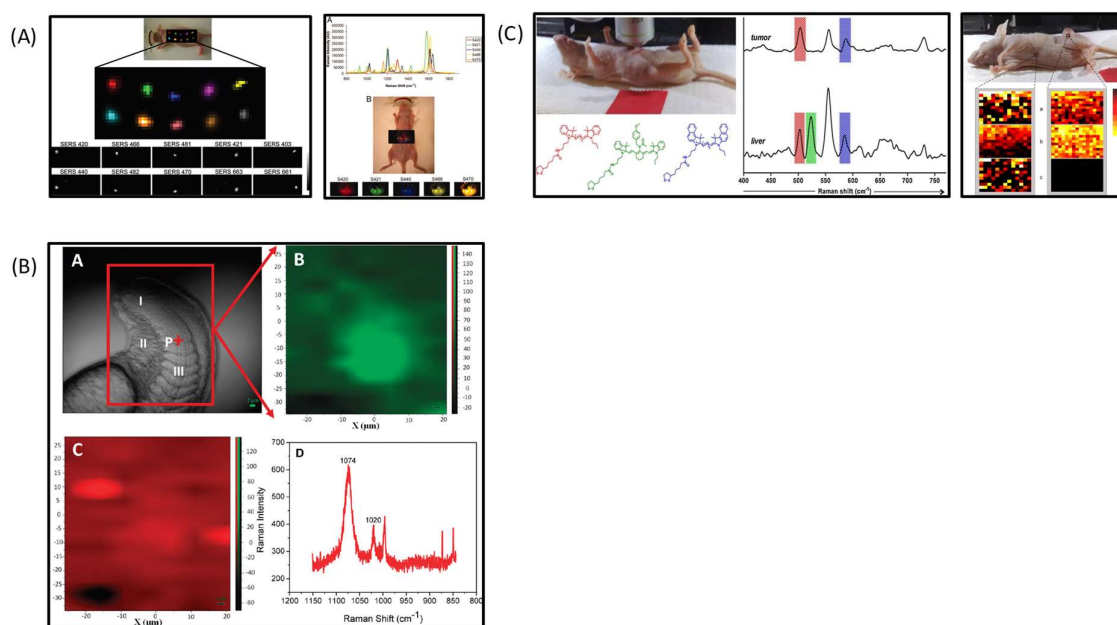
Figure 2-22. (A-1). Evaluation of multiplexing 10 different SERS nanoparticles in vivo. Raman map of 10 different SERS particles injected s.c. in a nude mouse. **(A-2)**. Demonstration

of deep-tissue multiplexed imaging 24 h after i.v. injection of five unique SERS nanoparticle batches simultaneously. (A) Graph depicting five unique Raman spectra, each associated with its own SERS batch. (B) Raman image of liver overlaid on digital photo of mouse, showing accumulation of all five SERS batches accumulating in the liver after 24 h post i.v. injection. (Reprinted with permission from ref [187]. Copyright 2009 Proceedings of the National Academy of Sciences). **(B).** Raman mapping of two SERS NPs in the posterior region of zebrafish embryo: (A) optical image of the zebrafish embryo and the markers highlight representative areas: (I) presomitic mesoderim, (II) blood island, (III) somite. (B) SERS intensity map of the CC vibration band from SERS NPs-1 at 1078 cm^1 and (C) SERS intensity map of ring breathing vibration band from SERS NPs-2 at 1020 cm^{-1}. (D) Typical SERS spectrum collected from the point marked by P as shown in panel A. (Reprinted with permission from ref [332]. Copyright 2010 ACS Nano). **(C-1)**. In vivo detection of HER2-positive tumors with scFv-conjugated CyNAMLA-381 SERS nanotags: SERS spectrum of pure nanotags (blue), and SERS signals of the tumor location (red) and an upper dorsal area (black). **(C-2).** Multiplex SERS mapping images: Left column from liver site and right column form tumor site (a: mapping corresponding to peak 523 cm^{-1} for CyNAMLA-381; b: mapping corresponding to peak 503 cm^{-1} for Cy7LA, and c: mapping corresponding to peak 586 cm^{-1} for Cy7.5LA). (Reprinted with permission from ref [333]. Copyright 2012 Nano Today).

The first real demonstration of *in-vivo* cancer imaging of multiplex targeted detection using ultrasensitive SERS nanotags in the NIR range has also been demonstrated (Figure 2-22 C) [333]. Three new NIR Raman reporter molecules, Cy7LA, Cy7.5LA and CyNAMLA-381 were used to construct SERS nanotags for multiplexing analysis.

In order to gain more accurate cancer diagnostics with respect to localization, metabolism and bio-distribution, multimodal probes have been used to confirm abnormalities through single

probe utilized in different imaging modalities. In 2011, a bimodal contrast agent, consisting of MRI-active superparamagnetic iron oxide nanoparticles coated with dextran (DTTC), stably complexed with gold nanostructures (AuMN-DTTC) was successfully used for two *in-vivo* imaging modalities - magnetic resonance imaging (MRI) and Raman spectroscopy in a living mice (Figure 2-23 A) [334]. Similarly, Positron-emission tomography is a nuclear medicine functional imaging technique that is used to observe metabolic and bio-distribution processes in the body. A PET-SERS probe has been prepared using radiolabelling AuNP's with Cu, to observe the natural bio-distribution of SERS probe via different administration routes (intravenous & intrarectal) (Figure 2-23 B) [335]. The study suggested rectal injection with minimal systemic distribution and toxicity, thus supporting the clinical translation of Raman spectroscopy as an endoscopic imaging tool.
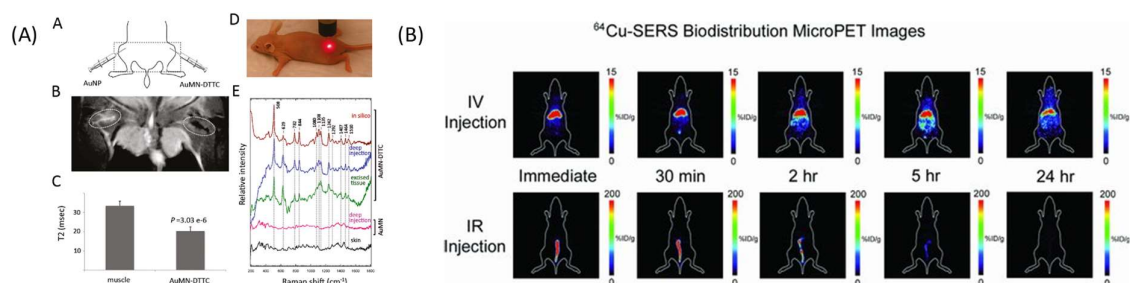
Figure 2-23. (A). MRI and Raman spectroscopy in vivo. (A). A schematic of the probe injection setup. (B). In vivo T2-weighted MR image of a mouse injected intramuscularly (i.m.) with AuMN-DTTC and the control probe, AuNP. (C). Calculated T2 values based on multiecho T2-weighted MRI. (D). Demonstration of the Raman spectroscopy experimental setup. (E). In vivo Raman spectra of a mouse injected i.m. with AuMN-DTTC and the control probe, AuMN. The in vivo Raman spectrum of muscle injected with AuMN-DTTC has a clear SERS signature, which is indistinguishable from that obtained ex vivo and in silico and is absent in skin tissue and in muscle injected with the control probe. (Reprinted with permission from ref [334]. Copyright 2010 ACS Nano). **(B).** MicroPET images of the accumulation of ^{64}Cu–SERS nanoparticles post IV injection (top panel) versus post IR injection (bottom panel). The images

represent a coronal slice of a single mouse taken at various time points; immediately, 30 min, 2 h, 5 h, and 24 h after either IV or IR injection. (Reprinted with permission from ref [335]. Copyright 2011 Small).

Co-functionalized gold nanorods (GNRs) with near-infrared (NIR) fluorescence and surface enhanced Raman scattering (SERS) have been used for optical imaging in a live mice. GNRs were synthesised by conventional seed mediated method and coated with PEG and DTTC. This PEG-DTTC-GNRs nanotag was used for dual bio-imaging based on NIR fluorescence and SERS. The experimental results have also shown the effective application of nanoparticles in animals without toxicity (Figure 2-24 A) [336]. In 2012, to further establish the high sensitivity with minimal detectable volume (few femtomolar) required by SERS for *in-vivo* imaging, a multimodal probe study was performed [337]. Here, quantitative data from three different molecular imaging modalities namely, MRI, photoacoustic and SERS was compared. The signals from all the three probes were highly co-related and quantified, obtained from a resected brain tumour of a mice (Figure 2-24 B). The SERS imaging showed highest sensitivity with lowest concentration of up to picomolar range, which makes it more viable for *in-vivo* imaging due to minimal injection of toxic material for molecular diagnostic [338,339].
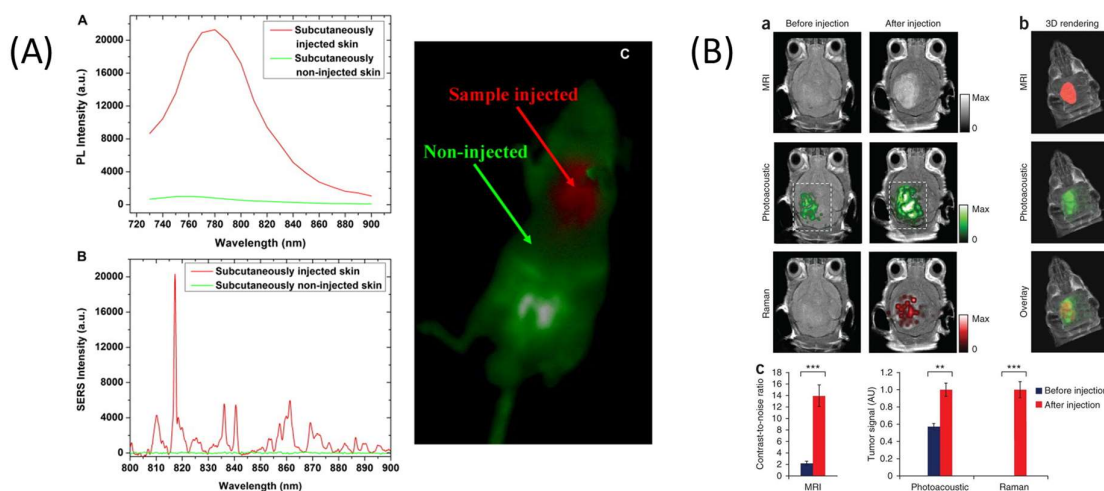
Figure 2-24. (A). NIR fluorescence and SERS imaging of a nude mouse subcutaneously injected with PEG-DTTC-GNRs (639 nm) 3 h after the injection. (A) NIR fluorescence spectra of the subcutaneously injected and non-injected skin, with fluorescence peak wavelengths of 780 nm and 760 nm, respectively. (B) NIR SERS spectra from the subcutaneously injected and non-injected skin (integrated time: 40,000 ms). (C) NIR fluorescence imaging of the treated mouse. (exposure time: 5000 ms). (Reprinted with permission from ref [336]. Copyright 2011 Biomaterials). **(B).** (a) Two-dimensional axial MRI, photoacoustic and Raman images. The post-injection images of all three modalities showed clear tumor visualization (b) A three-dimensional (3D) rendering of magnetic resonance images with the tumor segmented (red; top), an overlay of the three-dimensional photoacoustic images (green) over the MRI (middle) and an overlay of MRI, the segmented tumor and the photoacoustic images (bottom) showing good colocalization of the photoacoustic signal with the tumor. (c) Quantification of the signals in the tumor showing a significant increase in the MRI, photoacoustic and Raman signals. (Reprinted with permission from ref [337]. Copyright 2012 Nature Medicine).

Further study has also demonstrated use of Raman spectroscopy probe system that could overcome many of the disadvantages of current intra-operative methods [340]. Here 59 axillary lymph nodes, 43 negative and 16 positive from 58 patients undergoing breast surgery were

mapped using Raman micro-spectroscopy. These maps were then used to model the effect of using a Raman spectroscopic probe by selecting 5 and 10 probe points across the mapped images and evaluating the impact on disease detection. This work together with other examples, like the development of carbon nanotube-tipped endoscopes [341], highlights the important role that SERS technologies will play in the next generation of molecular imaging tools for cancer diagnostics and surgery guidance. Current efforts in *in-vivo* imaging are directed towards exploiting its multiplex capabilities to track multiple SERS nanotags in small-animal models [187,333], as well as in merging SERS technologies with other imaging modalities to augment the potential of molecular imaging. Also, using Raman spectroscopy probe systems for intra-operative assessment would allow for post-operative diagnosis.

2.5. Conclusion and Future Challenges

2.5.1. Conclusion

The initial discovery of "Raman Effect" in 1939 enabled scientists to chemically fingerprint materials based on inelastic scattering of light without the irony of sample preparation. The "Raman Effect" being inherently weak thereafter saw slow progression. In 1960 with the invention of laser, this spectroscopy technique saw revival. Furthermore, in 1977 with coincidental occurrence of enormous enhancement of "Raman Effect" called SERS phenomena saw an interest till date. In 1997 single molecule detection was reported using SERS, while in 2008 *in-vivo* use has been demonstrated. These results established the foundation for use of SERS tags in biomedical applications both *in-vitro* and *in-vivo*.

It has been about 77 years from discovery of "Raman Effect" and 40 years from SERS. SERS tags has experienced an explosion with respect to literature, and research with technology advancements. These advancements have enabled SERS to establish its mark in inter-disciplinary research and analysis. As with any discovery there is always a room for

improvement, similarly with respect to SERS tags the writers forecast increased utility of SERS, if issues like cytotoxicity, homogenous SERS signal distribution with consistency, use of nanosubstrate's for ease of secretion from human body etc. are addressed. In depth understanding, implementation of surface chemistry, physical interactions between SERS constituents (metal nanoparticles, Raman reporter, targeting (functional) molecules and protective coatings) can lead to clinical use through improved stability, reproducibility, strong affinity for target molecule, bio-imaging and multiplexed capability.

Therefore, SERS tags need to be studied from three perspectives:

- Individual constituents in terms of synthesis, physical and chemical properties.

- Conjugation and related changes in symmetry and responses.

- Establish universally accepted Raman and SERS theoretical and mathematical relationship.

The numerous advantages of SERS over other spectroscopic techniques has marked it as a desirable research area. This has led to vast progress and research which will soon find its way into the practical world of clinical applications with far more promising break throughs desirable for early disease diagnosis and remedies.

In view of the above, SERS based immunoassays have also shown leaps of progress with respect to spectroscopic characterization and imaging vis-à-vis *in-vitro* and *in-vivo*. These assays have deeply explored into single cellular hyperspectral imaging as well as cancerous tissues. Few of the significant advantages over traditional imaging modalities are: small sample volumes (~microliters), low detection limits (~femtomolar), high resolution and label-free detection. The limitation of SERS detection is its poor quantitative detection, which is primarily due to the skirmish between reproducibility and sensitivity. The integration of SERS based immunoassays with other imaging modalities as well as intraoperative imaging is a big shift towards its clinical transition. Few of the advances made and may require further

progression in SERS nanotags are: (1) SERS nanotags with LSPR in the near infrared (NIR) region. NIR is preferred due to low energy and higher wavelength. These attributes help avoid biodegradation of the sample and deep-tissue penetration (up to 5 mm) for better diagnosis (2) In-*vivo* multiplex SERS imaging, which again re-directs to the need for NIR active SERS nanotags with multiple distinct peaks.

Although SERS nanotags' have numerous advantages over the traditional techniques like fluorescent and QD's, however, clinical transition still requires more clearance efficiency. In many ways, the ongoing development and integration of SERS based immunoassays with other imaging modalities as well as intraoperative imaging is a big shift towards its clinical transition and promising use as a technique that can complement other clinical imaging/sensing tools in the near future.

2.5.2. Future Challenges

SERS tags have proven its wide application in optical spectroscopy analysis and imaging. The core requirements of any diagnostic technique are ultrahigh sensitivity and specificity. This further translates into reproducibility and multiplexing capabilities. There is always room for improvement, few areas that we have identified, which would be viable for research and bear high impact on SERS tags future success are briefly discussed here.

High sensitivity is desirable, this can be achieved by closely matching the LSPR frequency of the nanoparticles to the incident laser frequency. Another factor that can contribute to enhance sensitivity is by keeping interparticle distance between the nanoparticles less 10 nm. Moreover, uniformity in shape, size and arrangement of the nanoparticles over the substrate can ensure maximized signal with good reproducibility. The deviation in EEF should be less than 20% to affirm reproducibility.

2.5.2.1 SERS Tag Signal Consistency

Ultrahigh sensitivity of SERS tags for analysis and imaging is limited to the successful generation of "hot spots", "hot gaps" etc. as discussed in section 2.2. Therefore, this ultrahigh sensitivity is restricted to small cross section on the analyte surface, hence the probability of detection is also low. These limitations pose more challenges to the synthesis processes of SERS tag and technological advancements. However, in comparison to the synthesis optimization, technological advancements have far more progressed. Scientists in the field of programming, electronics and optical engineering have provided far reached solutions to improve the signal to noise ratio (SNR) and ability of the instrument to extract the desired results. This infers the need for more in-depth research for SERS mechanisms, theoretically and practically for better interpretation in synthesis procedures. This should in turn offer controlled synthesis of ultrahigh sensitive SERS tags with more consistency and probability. The uniformity of enhancement across the SERS tags is more important for quantitative analysis rather qualitative [342-345]. The uniformity of SERS signals dictates the need for a uniform shape and size of the substrate. Therefore, synthesis of uniform substrates with high enhancement factors is the suggested future direction [346,347]. Recent research to achieve quantitative analysis of SERS tags with consistency and reproducibility has made headway with the nanomatryoshkas model [115-118]. The model constituents of the core-Raman reporter-shell. Here, Raman reporter is enclosed between the metal nanoparticle (core) and the protective coating (shell). The Raman reporter is adsorbed on the core surface with no competing molecules and with protection from external environment provided by the shell. Therefore, it is used as the internal standard (IS) [127]. The shell is usually made of the same or different metal nanoparticles as the core. The shell surface is used stand alone for the target capturing molecule. This model offers uniformity of SERS signals with standard deviation of less than 1.2% between samples.

2.5.2.2 Toxicology

Like any other spectroscopy technique, toxicology which accompanies the use of metal nanoparticles is of major concern when used *in-vivo*. As discussed, gold and silver nanosubstrates are widely used for SERS tags. AuNP's are preferred over AgNP's for use inside human body. Silver is prone to oxidation, making it not suitable for biocompatibility due to genotoxicity and cytotoxicity [101-103,348]. AgNP's are also plasmonically less active in the NIR region making them again not suitable for biomedical applications. Largely gold is chemically inert and nontoxic. Clinical trials for cancer detection using gold nanoparticle with high dosages than required have been carried out safely for computed tomography (CT) scans [99,100]. However, care should be taken when using ultra small AuNP's as they have the ability to bind to the B-form DNA and be transported into the cell through endocytosis causing cytotoxicity. Moreover, AuNPs about 30–100 nm diameter that are commonly used as SERS substrates cause no noticeable toxicity at concentrations up to 100 mM [349]. By and large, it is always advisable to use lowest possible concentrations of AuNP's. This is only possible through optimization of SERS signals in NIR region with combination of surface-enhanced resonant Raman scattering (SERRS). The cytotoxicity of metal nanoparticles is controllable through use of functionalized biocompatible protective coating [338,339]. In 2011, Thakor et al. investigated biocompatibility of PEGylated AuNP's in human cells [350]. HeLa (human cervical cancer cells) or HepG2 (human liver cancer cells) were used to establish no cytotoxicity with PEGylated AuNP's. Only under prolonged exposure of 48 hrs and high concentrations of 1000 AuNP's per cell depicted minimal amount of cytotoxicity credited to increase in cellular oxidative stress. In 2011, Thakor et al. also demonstrated use of silica-coating to stabilize the SERS tag, as well as to reduce the toxicity of AuNPs. This favours Raman-silica-gold-nanoparticles (R-Si-Au-NPs) for *in-vivo* applications [350]. The effects of interaction between nanoparticles and cells at the molecular level still needs to be tacit.

References

(1)   Smekal, A. Zur quantentheorie der dispersion. *Naturwissenschaften* **1923,** *11* (43), 873.

(2)   Raman, C. V.; Krishnan, K. S. A new type of secondary radiation. *Nature* **1928,** *121*, 501.

(3)   Placzek, G. *Rayleigh-streuung und Raman-effekt*; Akad. Verlag-Ges., 1934.

(4)   Rayleigh, J. W. S. B. *On the Light from the Sky: Its Polarization and Colour*, 1870.

(5)   Fleischmann, M.; Hendra, P. J.; McQuillan, A. Raman spectra of pyridine adsorbed at a silver electrode. *Chemical Physics Letters* **1974,** *26* (2), 163.

(6)   Xu, X.; Li, H.; Hasan, D.; Ruoff, R. S.; Wang, A. X.; Fan, D. Near-field enhanced plasmonic-magnetic bifunctional nanotubes for single cell bioanalysis. *Advanced Functional Materials* **2013,** *23* (35), 4332.

(7)   Le Ru, E.; Blackie, E.; Meyer, M.; Etchegoin, P. G. Surface enhanced Raman scattering enhancement factors: a comprehensive study. *The Journal of Physical Chemistry C* **2007,** *111* (37), 13794.

(8)   Blackie, E. J.; Ru, E. C. L.; Etchegoin, P. G. Single-molecule surface-enhanced Raman spectroscopy of nonresonant molecules. *Journal of the American Chemical Society* **2009,** *131* (40), 14466.

(9)   Le Ru, E. C.; Meyer, M.; Etchegoin, P. Proof of single-molecule sensitivity in surface enhanced Raman scattering (SERS) by means of a two-analyte technique. *The Journal of Physical Chemistry B* **2006,** *110* (4), 1944.

(10)   Nie, S.; Emory, S. R. Probing single molecules and single nanoparticles by surface-enhanced Raman scattering. *Science* **1997,** *275* (5303), 1102.

(11)   Moskovits, M.; Suh, J. Surface selection rules for surface-enhanced Raman spectroscopy: calculations and application to the surface-enhanced Raman spectrum of phthalazine on silver. *The Journal of Physical Chemistry* **1984,** *88* (23), 5526.

(12)   Smith, E.; Dent, G. *Modern Raman spectroscopy: a practical approach*; John Wiley & Sons, 2013.

(13)   Brolo, A.; Jiang, Z.; Irish, D. The orientation of 2, 2′-bipyridine adsorbed at a SERS-active Au (111) electrode surface. *Journal of Electroanalytical Chemistry* **2003,** *547* (2), 163.

(14)   Doering, W. E.; Nie, S. Spectroscopic tags using dye-embedded nanoparticles and surface-enhanced Raman scattering. *Analytical Chemistry* **2003,** *75* (22), 6171.

(15)   McCreery, R. L. *Raman spectroscopy for chemical analysis*; John Wiley & Sons, 2005.

(16)   Schlücker, S. SERS microscopy: nanoparticle probes and biomedical applications. *ChemPhysChem* **2009,** *10* (9-10), 1344.

(17)   Bantz, K. C.; Meyer, A. F.; Wittenberg, N. J.; Im, H.; Kurtuluş, Ö.; Lee, S. H.; Lindquist, N. C.; Oh, S.-H.; Haynes, C. L. Recent progress in SERS biosensing. *Physical Chemistry Chemical Physics* **2011,** *13* (24), 11551.

(18)   Aroca, R. F.; Ross, D. J.; Domingo, C. Surface-enhanced infrared spectroscopy. *Applied Spectroscopy* **2004,** *58*, 324A.

(19)   Jeanmaire, D. L.; Van Duyne, R. P. Surface Raman spectroelectrochemistry: Part I. Heterocyclic, aromatic, and aliphatic amines adsorbed on the anodized silver electrode. *Journal of Electroanalytical Chemistry and Interfacial Electrochemistry* **1977,** *84* (1), 1.

(20)   Albrecht, M. G.; Creighton, J. A. Anomalously intense Raman spectra of pyridine at a silver electrode. *Journal of the American Chemical Society* **1977,** *99* (15), 5215.

(21)   King, F. W.; Van Duyne, R. P.; Schatz, G. C. Theory of Raman scattering by molecules adsorbed on electrode surfaces. *The Journal of Chemical Physics* **1978,** *69* (10), 4472.

(22)   Moskovits, M. Surface roughness and the enhanced intensity of Raman scattering by molecules adsorbed on metals. *The Journal of Chemical Physics* **1978,** *69* (9), 4159.

(23)   Schatz, G. C.; Van Duyne, R. P. Electromagnetic mechanism of surface-enhanced spectroscopy. *Handbook of Vibrational Spectroscopy* **2002**.

(24)   Ulaby, F. T.; Michielssen, E.; Ravaioli, U.; Hayt, W.; Buck, J. Fundamentals of Applied Electromagnetics, ISBN: 978-0-13-213931-1. *Instructor* **2014,** *201409*.

(25)   Robertson, K. D. DNA methylation and human disease. *Nat Rev Genet* **2005,** *6* (8), 597.

(26)   Barnes, W. L.; Dereux, A.; Ebbesen, T. W. Surface plasmon subwavelength optics. *Nature* **2003,** *424* (6950), 824.

(27)   Willets, K. A.; Van Duyne, R. P. Localized Surface Plasmon Resonance Spectroscopy and Sensing. *Annual Review of Physical Chemistry* **2007,** *58* (1), 267.

(28)   Zayats, A. V.; Smolyaninov, I. I.; Maradudin, A. A. Nano-optics of surface plasmon polaritons. *Physics Reports* **2005,** *408* (3-4), 131.

(29)   Lane, L. A.; Qian, X.; Nie, S. SERS Nanoparticles in Medicine: From Label-Free Detection to Spectroscopic Tagging. *Chemical Reviews* **2015,** *115* (19), 10489.

(30)   Gersten, J.; Nitzan, A. Electromagnetic theory of enhanced Raman scattering by molecules adsorbed on rough surfaces. *The Journal of Chemical Physics* **1980,** *73* (7), 3023.

(31)   García-Vidal, F. J.; Pendry, J. Collective theory for surface enhanced Raman scattering. *Physical Review Letters* **1996,** *77* (6), 1163.

(32)   McFarland, A. D.; Young, M. A.; Dieringer, J. A.; Van Duyne, R. P. Wavelength-Scanned Surface-Enhanced Raman Excitation Spectroscopy. *The Journal of Physical Chemistry B* **2005,** *109* (22), 11279.

(33)   Sivapalan, S. T.; DeVetter, B. M.; Yang, T. K.; van Dijk, T.; Schulmerich, M. V.; Carney, P. S.; Bhargava, R.; Murphy, C. J. Off-Resonance Surface-Enhanced Raman Spectroscopy from Gold Nanorod Suspensions as a Function of Aspect Ratio: Not What We Thought. *ACS Nano* **2013,** *7* (3), 2099.

(34)   Li, M.; Kang, J. W.; Dasari, R. R.; Barman, I. Shedding Light on the Extinction-Enhancement Duality in Gold Nanostar-Enhanced Raman Spectroscopy. *Angewandte Chemie International Edition* **2014,** *53* (51), 14115.

(35)   Johnson, P. B.; Christy, R. W. Optical Constants of the Noble Metals. *Phys. Rev. B* **1972,** *6* (12), 4370.

(36)   Palik, E. D. In *Handbook of Optical Constants of Solids*; Elsevier BV, 1998, DOI:10.1016/b978-0-08-055630-7.50004-3 10.1016/b978-0-08-055630-7.50004-3.

(37)   Henglein, A. Physicochemical properties of small metal particles in solution: "microelectrode" reactions, chemisorption, composite metal particles, and the atom-to-metal transition. *The Journal of Physical Chemistry* **1993,** *97* (21), 5457.

(38)   Linnert, T.; Mulvaney, P.; Henglein, A. Surface chemistry of colloidal silver: surface plasmon damping by chemisorbed iodide, hydrosulfide (SH-), and phenylthiolate. *The Journal of Physical Chemistry* **1993,** *97* (3), 679.

(39)   Mulvaney, P. Surface Plasmon Spectroscopy of Nanosized Metal Particles. *Langmuir* **1996,** *12* (3), 788.

(40)   Kreibig, U.; Gartz, M.; Hilger, A. Mie resonances: Sensors for physical and chemical cluster interface properties. *Berichte der Bunsengesellschaft für Physikalische Chemie* **1997,** *101* (11), 1593.

(41)   Liz-Marzán, L. M. Tailoring Surface Plasmons through the Morphology and Assembly of Metal Nanoparticles. *Langmuir* **2006,** *22* (1), 32.

(42)   Jin, R. Photoinduced Conversion of Silver Nanospheres to Nanoprisms. *Science* **2001,** *294* (5548), 1901.

(43)   Murphy, C. J.; Jana, N. R. Controlling the Aspect Ratio of Inorganic Nanorods and Nanowires. *Adv. Mater.* **2002,** *14* (1), 80.

(44)   Shuford, K. L.; Ratner, M. A.; Schatz, G. C. Multipolar excitation in triangular nanoprisms. *The Journal of Chemical Physics* **2005,** *123* (11), 114713.

(45)   Millstone, J. E.; Hurst, S. J.; Métraux, G. S.; Cutler, J. I.; Mirkin, C. A. Colloidal Gold and Silver Triangular Nanoprisms. *Small* **2009,** *5* (6), 646.

(46)   Near, R. D.; Hayden, S. C.; Hunter, R. E.; Thackston, D.; El-Sayed, M. A. Rapid and Efficient Prediction of Optical Extinction Coefficients for Gold Nanospheres and Gold Nanorods. *J. Phys. Chem. C* **2013,** *117* (45), 23950.

(47)   Sönnichsen, C.; Franzl, T.; Wilk, T.; von Plessen, G.; Feldmann, J.; Wilson, O.; Mulvaney, P. Drastic Reduction of Plasmon Damping in Gold Nanorods. *Phys. Rev. Lett.* **2002,** *88* (7).

(48)   Munechika, K.; Smith, J. M.; Chen, Y.; Ginger, D. S. Plasmon Line Widths of Single Silver Nanoprisms as a Function of Particle Size and Plasmon Peak Position. *J. Phys. Chem. C* **2007,** *111* (51), 18906.

(49)   Le Ru, E. C.; Grand, J.; Sow, I.; Somerville, W. R. C.; Etchegoin, P. G.; Treguer-Delapierre, M.; Charron, G.; Félidj, N.; Lévi, G.; Aubard, J. A Scheme for Detecting Every Single Target Molecule with Surface-Enhanced Raman Spectroscopy. *Nano Letters* **2011,** *11* (11), 5013.

(50)   Xu, H.; Bjerneld, E. J.; Käll, M.; Börjesson, L. Spectroscopy of Single Hemoglobin Molecules by Surface Enhanced Raman Scattering. *Phys. Rev. Lett.* **1999,** *83* (21), 4357.

(51)   Xu, H.; Aizpurua, J.; Käll, M.; Apell, P. Electromagnetic contributions to single-molecule sensitivity in surface-enhanced Raman scattering. *Physical Review E* **2000,** *62* (3), 4318.

(52)   McMahon, J. M.; Gray, S. K.; Schatz, G. C. Calculating nonlocal optical properties of structures with arbitrary shape. *Phys. Rev. B* **2010,** *82* (3).

(53)   Hildebrandt, P.; Stockburger, M. Surface-enhanced resonance Raman spectroscopy of Rhodamine 6G adsorbed on colloidal silver. *The Journal of Physical Chemistry* **1984,** *88* (24), 5935.

(54)   Pettinger, B.; Krischer, K.; Ertl, G. Giant Raman scattering cross section for an adsorbed dye at Ag colloids associated with low EM field enhancement. *Chemical Physics Letters* **1988,** *151* (1), 151.

(55)   Kneipp, K.; Wang, Y.; Kneipp, H.; Perelman, L. T.; Itzkan, I.; Dasari, R. R.; Feld, M. S. Single molecule detection using surface-enhanced Raman scattering (SERS). *Physical Review Letters* **1997,** *78* (9), 1667.

(56)   Krug, J. T.; Wang, G. D.; Emory, S. R.; Nie, S. Efficient Raman enhancement and intermittent light emission observed in single gold nanocrystals. *Journal of the American Chemical Society* **1999,** *121* (39), 9208.

(57)   Doering, W. E.; Nie, S. Single-molecule and single-nanoparticle SERS: examining the roles of surface active sites and chemical enhancement. *The Journal of Physical Chemistry B* **2002,** *106* (2), 311.

(58)   Maruyama, Y.; Ishikawa, M.; Futamata, M. Thermal activation of blinking in SERS signal. *The Journal of Physical Chemistry B* **2004,** *108* (2), 673.

(59)   Emory, S. R.; Jensen, R. A.; Wenda, T.; Han, M.; Nie, S. Re-examining the origins of spectral blinking in single-molecule and single-nanoparticle SERS. *Faraday Discussions* **2006,** *132*, 249.

(60)   Lombardi, J. R.; Birke, R. L.; Haran, G. Single molecule SERS spectral blinking and vibronic coupling. *The Journal of Physical Chemistry C* **2011,** *115* (11), 4540.

(61)   Talley, C. E.; Jackson, J. B.; Oubre, C.; Grady, N. K.; Hollars, C. W.; Lane, S. M.; Huser, T. R.; Nordlander, P.; Halas, N. J. Surface-enhanced Raman scattering from

individual Au nanoparticles and nanoparticle dimer substrates. *Nano Letters* **2005,** *5* (8), 1569.

(62)   Le Ru, E.; Etchegoin, P.; Meyer, M. Enhancement factor distribution around a single surface-enhanced Raman scattering hot spot and its relation to single molecule detection. *The Journal of Chemical Physics* **2006,** *125* (20), 204701.

(63)   Camden, J. P.; Dieringer, J. A.; Wang, Y.; Masiello, D. J.; Marks, L. D.; Schatz, G. C.; Van Duyne, R. P. Probing the structure of single-molecule surface-enhanced Raman scattering hot spots. *Journal of the American Chemical Society* **2008,** *130* (38), 12616.

(64)   Le Ru, E.; Meyer, M.; Blackie, E.; Etchegoin, P. Advanced aspects of electromagnetic SERS enhancement factors at a hot spot. *Journal of Raman Spectroscopy* **2008,** *39* (9), 1127.

(65)   Chen, G.; Wang, Y.; Yang, M.; Xu, J.; Goh, S. J.; Pan, M.; Chen, H. Measuring ensemble-averaged surface-enhanced Raman scattering in the hotspots of colloidal nanoparticle dimers and trimers. *Journal of the American Chemical Society* **2010,** *132* (11), 3644.

(66)   Imura, K.; Okamoto, H.; Hossain, M. K.; Kitajima, M. Near-field imaging of surface-enhanced Raman active sites in aggregated gold nanoparticles. *Chemistry Letters* **2006,** *35* (1), 78.

(67)   Kambhampati, P.; Child, C. M.; Foster, M. C.; Campion, A. On the chemical mechanism of surface enhanced Raman scattering: Experiment and theory. *Journal of Chemical Physics* **1998,** *108* (12), 5013.

(68)   Kambhampati, P.; Child, C. M.; Campion, A. On the role of charge-transfer resonances in the chemical mechanism of surface-enhanced Raman scattering. *Journal of the Chemical Society-Faraday Transactions* **1996,** *92* (23), 4775.

(69)   Campion, A.; Ivanecky, J. E.; Child, C. M.; Foster, M. On the mechanism of chemical enhancement in surface-enhanced Raman-scattering. *Journal of the American Chemical Society* **1995,** *117* (47), 11807.

(70)   Kneipp, K.; Kneipp, H.; Itzkan, I.; Dasari, R. R.; Feld, M. S. Ultrasensitive chemical analysis by Raman spectroscopy. *Chemical Reviews* **1999,** *99* (10), 2957.

(71)   Jensen, L.; Aikens, C. M.; Schatz, G. C. Electronic structure methods for studying surface-enhanced Raman scattering. *Chemical Society Reviews* **2008,** *37* (5), 1061.

(72)   Ansari, D. O. *Raman-encoded nanoparticles for biomolecular detection and cancer diagnostics*; ProQuest, 2008.

(73)   Campion, A.; Kambhampati, P. Surface-enhanced Raman scattering. *Chemical Society Reviews* **1998,** *27* (4), 241.

(74)   Michaels, A. M.; Jiang, J.; Brus, L. Ag nanocrystal junctions as the site for surface-enhanced Raman scattering of single Rhodamine 6G molecules. *Journal of Physical Chemistry B* **2000,** *104* (50), 11965.

(75)   Brolo, A. G.; Irish, D. E.; Smith, B. D. Applications of surface enhanced Raman scattering to the study of metal-adsorbate interactions. *Journal of Molecular Structure* **1997,** *405* (1), 29.

(76)   Xie, W.; Qiu, P.; Mao, C. Bio-imaging, detection and analysis by using nanostructures as SERS substrates. *Journal of Materials Chemistry* **2011,** *21* (14), 5190.

(77)   Stiles, P. L.; Dieringer, J. A.; Shah, N. C.; Van Duyne, R. R. In *Annual Review of Analytical Chemistry*, 2008; Vol. 1.

(78)   Morton, S. M.; Ewusi-Annan, E.; Jensen, L. Controlling the non-resonant chemical mechanism of SERS using a molecular photoswitch. *Phys. Chem. Chem. Phys.* **2009,** *11* (34), 7424.

(79) Lombardi, J. R.; Birke, R. L. A Unified Approach to Surface-Enhanced Raman Spectroscopy. *J. Phys. Chem. C* **2008,** *112* (14), 5605.

(80) Kambhampati, P.; Child, C. M.; Foster, M. C.; Campion, A. On the chemical mechanism of surface enhanced Raman scattering: Experiment and theory. *The Journal of Chemical Physics* **1998,** *108* (12), 5013.

(81) Valley, N.; Greeneltch, N.; Van Duyne, R. P.; Schatz, G. C. A Look at the Origin and Magnitude of the Chemical Contribution to the Enhancement Mechanism of Surface-Enhanced Raman Spectroscopy (SERS): Theory and Experiment. *J. Phys. Chem. Lett.* **2013,** *4* (16), 2599.

(82) Morton, S. M.; Jensen, L. Understanding the Molecule−Surface Chemical Coupling in SERS. *J. Am. Chem. Soc.* **2009,** *131* (11), 4090.

(83) Nie, S. M.; Emery, S. R. Probing single molecules and single nanoparticles by surface-enhanced Raman scattering. *Science* **1997,** *275* (5303), 1102.

(84) Kneipp, K.; Wang, Y.; Kneipp, H.; Perelman, L. T.; Itzkan, I.; Dasari, R.; Feld, M. S. Single molecule detection using surface-enhanced Raman scattering (SERS). *Physical Review Letters* **1997,** *78* (9), 1667.

(85) Kneipp, K.; Kneipp, H.; Itzkan, I.; Dasari, R. R.; Feld, M. S. Surface-enhanced Raman scattering and biophysics. *Journal of Physics-Condensed Matter* **2002,** *14* (18), R597.

(86) Campion, A.; Kambhampati, P. Surface-enhanced Raman scattering. *Chem. Soc. Rev.* **1998,** *27* (4), 241.

(87) Kneipp, J.; Kneipp, H.; Rice, W. L.; Kneipp, K. Optical probes for biological applications based on surface-enhanced Raman scattering from indocyanine green on gold nanoparticles. *Analytical Chemistry* **2005,** *77* (8), 2381.

(88) Moskovits, M. Surface-enhanced Raman spectroscopy: a brief retrospective. *Journal of Raman Spectroscopy* **2005,** *36* (6-7), 485.

(89)   Le Ru, E. C.; Blackie, E.; Meyer, M.; Etchegoin, P. G. Surface Enhanced Raman Scattering Enhancement Factors: A Comprehensive Study. *J. Phys. Chem. C* **2007,** *111* (37), 13794.

(90)   Kleinman, S. L.; Frontiera, R. R.; Henry, A.-I.; Dieringer, J. A.; Van Duyne, R. P. Creating, characterizing, and controlling chemistry with SERS hot spots. *Phys. Chem. Chem. Phys.* **2013,** *15* (1), 21.

(91)   Moskovits, M. Persistent misconceptions regarding SERS. *Physical Chemistry Chemical Physics* **2013,** *15* (15), 5301.

(92)   Dörfer, T.; Schmitt, M.; Popp, J. Deep-UV surface-enhanced Raman scattering. *Journal of Raman Spectroscopy* **2007,** *38* (11), 1379.

(93)   Jha, S. K.; Ahmed, Z.; Agio, M.; Ekinci, Y.; Löffler, J. r. F. Deep-UV surface-enhanced resonance Raman scattering of adenine on aluminum nanoparticle arrays. *Journal of the American Chemical Society* **2012,** *134* (4), 1966.

(94)   Ayas, S.; Cinar, G.; Ozkan, A. D.; Soran, Z.; Ekiz, O.; Kocaay, D.; Tomak, A.; Toren, P.; Kaya, Y.; Tunc, I. Label-free nanometer-resolution imaging of biological architectures through surface enhanced raman scattering. *Scientific reports* **2013,** *3*.

(95)   Lu, H.; Zhang, H.; Yu, X.; Zeng, S.; Yong, K.-T.; Ho, H.-P. Seed-mediated plasmon-driven regrowth of silver nanodecahedrons (NDs). *Plasmonics* **2012,** *7* (1), 167.

(96)   Aroca, R. *Surface-enhanced vibrational spectroscopy*; John Wiley & Sons, 2006.

(97)   Bao, L. L.; Mahurin, S. M.; Liang, C. D.; Dai, S. Study of silver films over silica beads as a surface-enhanced Raman scattering (SERS) substrate for detection of benzoic acid. *Journal of Raman Spectroscopy* **2003,** *34* (5), 394.

(98)   Moskovits, M. In *Surface-Enhanced Raman Scattering*; Springer, 2006.

(99)   Cormode, D. P.; Roessl, E.; Thran, A.; Skajaa, T.; Gordon, R. E.; Schlomka, J.-P.; Fuster, V.; Fisher, E. A.; Mulder, W. J.; Proksa, R. Atherosclerotic plaque composition:

analysis with multicolor CT and targeted gold nanoparticles 1. *Radiology* **2010,** *256* (3), 774.

(100) Popovtzer, R.; Agrawal, A.; Kotov, N. A.; Popovtzer, A.; Balter, J.; Carey, T. E.; Kopelman, R. Targeted Gold Nanoparticles Enable Molecular CT Imaging of Cancer. *Nano Letters* **2008,** *8* (12), 4593.

(101) Ahamed, M.; Karns, M.; Goodson, M.; Rowe, J.; Hussain, S. M.; Schlager, J. J.; Hong, Y. DNA damage response to different surface chemistry of silver nanoparticles in mammalian cells. *Toxicology and Applied Pharmacology* **2008,** *233* (3), 404.

(102) Greulich, C.; Braun, D.; Peetsch, A.; Diendorf, J.; Siebers, B.; Epple, M.; Köller, M. The toxic effect of silver ions and silver nanoparticles towards bacteria and human cells occurs in the same concentration range. *RSC Advances* **2012,** *2* (17), 6981.

(103) Bondarenko, O.; Juganson, K.; Ivask, A.; Kasemets, K.; Mortimer, M.; Kahru, A. Toxicity of Ag, CuO and ZnO nanoparticles to selected environmentally relevant test organisms and mammalian cells in vitro: a critical review. *Archives of Toxicology* **2013,** *87* (7), 1181.

(104) Lee, P. C.; Meisel, D. Adsorption and surface-enhanced Raman of dyes on silver and gold sols. *The Journal of Physical Chemistry* **1982,** *86* (17), 3391.

(105) Turkevich, J.; Stevenson, P. C.; Hillier, J. The Formation of Colloidal Gold. *The Journal of Physical Chemistry* **1953,** *57* (7), 670.

(106) Frens, G. Controlled Nucleation for the Regulation of the Particle Size in Monodisperse Gold Suspensions. *Nat Phys Sci* **1973,** *241* (105), 20.

(107) Link, S.; El-Sayed, M. A. Spectral Properties and Relaxation Dynamics of Surface Plasmon Electronic Oscillations in Gold and Silver Nanodots and Nanorods. *The Journal of Physical Chemistry B* **1999,** *103* (40), 8410.

(108)   Evanoff, D. D.; Chumanov, G. Size-controlled synthesis of nanoparticles. 1. "Silver-only" aqueous suspensions via hydrogen reduction. *Journal of Physical Chemistry B* **2004,** *108* (37), 13948.

(109)   Abalde-Cela, S.; Aldeanueva-Potel, P.; Mateo-Mateo, C.; Rodriguez-Lorenzo, L.; Alvarez-Puebla, R. A.; Liz-Marzan, L. M. Surface-enhanced Raman scattering biomedical applications of plasmonic colloidal particles. *Journal of the Royal Society Interface* **2010,** *7*, S435.

(110)   Schwartzberg, A. M.; Oshiro, T. Y.; Zhang, J. Z.; Huser, T.; Talley, C. E. Improving nanoprobes using surface-enhanced Raman scattering from 30-nm hollow gold particles. *Analytical Chemistry* **2006,** *78* (13), 4732.

(111)   Chon, H.; Lee, S.; Son, S. W.; Oh, C. H.; Choo, J. Highly Sensitive Immunoassay of Lung Cancer Marker Carcinoembryonic Antigen Using Surface-Enhanced Raman Scattering of Hallow Gold Nanospheres. *Analytical Chemistry* **2009,** *81* (8), 3029.

(112)   Ochsenkuhn, M. A.; Jess, P. R. T.; Stoquert, H.; Dholakia, K.; Campbell, C. J. Nanoshells for Surface-Enhanced Raman Spectroscopy in Eukaryotic Cells: Cellular Response and Sensor Development. *ACS Nano* **2009,** *3* (11), 3613.

(113)   Rycenga, M.; Hou, K. K.; Cobley, C. M.; Schwartz, A. G.; Camargo, P. H. C.; Xia, Y. Probing the surface-enhanced Raman scattering properties of Au-Ag nanocages at two different excitation wavelengths. *Physical Chemistry Chemical Physics* **2009,** *11* (28), 5903.

(114)   Fang, J.; Lebedkin, S.; Yang, S.; Hahn, H. A new route for the synthesis of polyhedral gold mesocages and shape effect in single-particle surface-enhanced Raman spectroscopy. *Chemical Communications* **2011,** *47* (18), 5157.

(115) Lim, D.-K.; Jeon, K.-S.; Hwang, J.-H.; Kim, H.; Kwon, S.; Suh, Y. D.; Nam, J.-M. Highly uniform and reproducible surface-enhanced Raman scattering from DNA-tailorable nanoparticles with 1-nm interior gap. *Nature Nanotech* **2011,** *6* (7), 452.

(116) Song, J.; Duan, B.; Wang, C.; Zhou, J.; Pu, L.; Fang, Z.; Wang, P.; Lim, T. T.; Duan, H. SERS-Encoded Nanogapped Plasmonic Nanoparticles: Growth of Metallic Nanoshell by Templating Redox-Active Polymer Brushes. *J. Am. Chem. Soc.* **2014,** *136* (19), 6838.

(117) Feng, Y.; Wang, Y.; Wang, H.; Chen, T.; Tay, Y. Y.; Yao, L.; Yan, Q.; Li, S.; Chen, H. Engineering "Hot" Nanoparticles for Surface-Enhanced Raman Scattering by Embedding Reporter Molecules in Metal Layers. *Small* **2012,** *8* (2), 246.

(118) Gandra, N.; Singamaneni, S. Bilayered Raman-Intense Gold Nanostructures with Hidden Tags (BRIGHTs) for High-Resolution Bioimaging. *Advanced Materials* **2013,** *25* (7), 1022.

(119) Huang, J.; Kim, K. H.; Choi, N.; Chon, H.; Lee, S.; Choo, J. Preparation of Silica-Encapsulated Hollow Gold Nanosphere Tags Using Layer-by-Layer Method for Multiplex Surface-Enhanced Raman Scattering Detection. *Langmuir* **2011,** *27* (16), 10228.

(120) Jackson, J. B.; Halas, N. J. Surface-enhanced Raman scattering on tunable plasmonic nanoparticle substrates. *Proceedings of the National Academy of Sciences of the United States of America* **2004,** *101* (52), 17930.

(121) Loo, C.; Lin, A.; Hirsch, L.; Lee, M. H.; Barton, J.; Halas, N. J.; West, J.; Drezek, R. Nanoshell-enabled photonics-based imaging and therapy of cancer. *Technology in Cancer Research & Treatment* **2004,** *3* (1), 33.

(122) Gellner, M.; Kuestner, B.; Schluecker, S. Optical properties and SERS efficiency of tunable gold/silver nanoshells. *Vibrational Spectroscopy* **2009,** *50* (1), 43.

(123) Schwartzberg, A. M.; Olson, T. Y.; Talley, C. E.; Zhang, J. Z. Synthesis, characterization, and tunable optical properties of hollow gold nanospheres. *Journal of Physical Chemistry B* **2006,** *110* (40), 19935.

(124) Au, L.; Zheng, D.; Zhou, F.; Li, Z.-Y.; Li, X.; Xia, Y. A quantitative study on the photothermal effect of immuno gold nanocages targeted to breast cancer cells. *ACS Nano* **2008,** *2* (8), 1645.

(125) Yavuz, M. S.; Cheng, Y.; Chen, J.; Cobley, C. M.; Zhang, Q.; Rycenga, M.; Xie, J.; Kim, C.; Song, K. H.; Schwartz, A. G. Gold nanocages covered by smart polymers for controlled release with near-infrared light. *Nature Materials* **2009,** *8* (12), 935.

(126) Song, K. H.; Kim, C.; Cobley, C. M.; Xia, Y.; Wang, L. V. Near-infrared gold nanocages as a new class of tracers for photoacoustic sentinel lymph node mapping on a rat model. *Nano letters* **2008,** *9* (1), 183.

(127) Shen, W.; Lin, X.; Jiang, C.; Li, C.; Lin, H.; Huang, J.; Wang, S.; Liu, G.; Yan, X.; Zhong, Q.et al. Reliable Quantitative SERS Analysis Facilitated by Core-Shell Nanoparticles with Embedded Internal Standards. *Angewandte Chemie International Edition* **2015,** *54* (25), 7308.

(128) Liao, P. F. Lightning rod effect in surface enhanced Raman scattering. *The Journal of Chemical Physics* **1982,** *76* (1), 751.

(129) Mohamed, M. B.; Volkov, V.; Link, S.; El-Sayed, M. A. The `lightning' gold nanorods: fluorescence enhancement of over a million compared to the gold metal. *Chemical Physics Letters* **2000,** *317* (6), 517.

(130) Nikoobakht, B.; Wang, J.; El-Sayed, M. A. Surface-enhanced Raman scattering of molecules adsorbed on gold nanorods: off-surface plasmon resonance condition. *Chemical Physics Letters* **2002,** *366* (1-2), 17.

(131)   Hong, S.; Shuford, K. L.; Park, S. Shape Transformation of Gold Nanoplates and their Surface Plasmon Characterization: Triangular to Hexagonal Nanoplates. *Chemistry of Materials* **2011,** *23* (8), 2011.

(132)   Sherry, L. J.; Chang, S.-H.; Schatz, G. C.; Van Duyne, R. P.; Wiley, B. J.; Xia, Y. Localized Surface Plasmon Resonance Spectroscopy of Single Silver Nanocubes. *Nano Letters* **2005,** *5* (10), 2034.

(133)   Sun, Y. Shape-Controlled Synthesis of Gold and Silver Nanoparticles. *Science* **2002,** *298* (5601), 2176.

(134)   McLellan, J. M.; Li, Z.-Y.; Siekkinen, A. R.; Xia, Y. The SERS Activity of a Supported Ag Nanocube Strongly Depends on Its Orientation Relative to Laser Polarization. *Nano Letters* **2007,** *7* (4), 1013.

(135)   McLellan, J. M.; Siekkinen, A.; Chen, J.; Xia, Y. Comparison of the surface-enhanced Raman scattering on sharp and truncated silver nanocubes. *Chemical Physics Letters* **2006,** *427* (1-3), 122.

(136)   Orendorff, C. J.; Gearheart, L.; Jana, N. R.; Murphy, C. J. Aspect ratio dependence on surface enhanced Raman scattering using silver and gold nanorod substrates. *Phys. Chem. Chem. Phys.* **2006,** *8* (1), 165.

(137)   Huang, X.; El-Sayed, I. H.; Qian, W.; El-Sayed, M. A. Cancer Cells Assemble and Align Gold Nanorods Conjugated to Antibodies to Produce Highly Enhanced, Sharp, and Polarized Surface Raman Spectra: A Potential Cancer Diagnostic Marker. *Nano Letters* **2007,** *7* (6), 1591.

(138)   von Maltzahn, G.; Centrone, A.; Park, J.-H.; Ramanathan, R.; Sailor, M. J.; Hatton, T. A.; Bhatia, S. N. SERS-Coded Gold Nanorods as a Multifunctional Platform for Densely Multiplexed Near-Infrared Imaging and Photothermal Heating. *Adv. Mater.* **2009,** *21* (31), 3175.

(139) Ciou, S.-H.; Cao, Y.-W.; Huang, H.-C.; Su, D.-Y.; Huang, C.-L. SERS Enhancement Factors Studies of Silver Nanoprism and Spherical Nanoparticle Colloids in The Presence of Bromide Ions. *J. Phys. Chem. C* **2009,** *113* (22), 9520.

(140) Scarabelli, L.; Coronado-Puchau, M.; Giner-Casares, J. J.; Langer, J.; Liz-Marzán, L. M. Monodisperse Gold Nanotriangles: Size Control, Large-Scale Self-Assembly, and Performance in Surface-Enhanced Raman Scattering. *ACS Nano* **2014,** *8* (6), 5833.

(141) Wu, H.-L.; Tsai, H.-R.; Hung, Y.-T.; Lao, K.-U.; Liao, C.-W.; Chung, P.-J.; Huang, J.-S.; Chen, I. C.; Huang, M. H. A Comparative Study of Gold Nanocubes, Octahedra, and Rhombic Dodecahedra as Highly Sensitive SERS Substrates. *Inorganic Chemistry* **2011,** *50* (17), 8106.

(142) Khoury, C. G.; Vo-Dinh, T. Gold Nanostars For Surface-Enhanced Raman Scattering: Synthesis, Characterization and Optimization. *J. Phys. Chem. C* **2008,** *112* (48), 18849.

(143) Nalbant Esenturk, E.; Hight Walker, A. R. Surface-enhanced Raman scattering spectroscopy via gold nanostars. *J. Raman Spectrosc.* **2009,** *40* (1), 86.

(144) Barbosa, S.; Agrawal, A.; Rodríguez-Lorenzo, L.; Pastoriza-Santos, I.; Alvarez-Puebla, R. A.; Kornowski, A.; Weller, H.; Liz-Marzán, L. M. Tuning Size and Sensing Properties in Colloidal Gold Nanostars. *Langmuir* **2010,** *26* (18), 14943.

(145) Liu, Z.; Cheng, L.; Zhang, L.; Jing, C.; Shi, X.; Yang, Z.; Long, Y.; Fang, J. Large-area fabrication of highly reproducible surface enhanced Raman substrate via a facile double sided tape-assisted transfer approach using hollow Au–Ag alloy nanourchins. *Nanoscale* **2014,** *6* (5), 2567.

(146) Liu, Z.; Yang, Z.; Peng, B.; Cao, C.; Zhang, C.; You, H.; Xiong, Q.; Li, Z.; Fang, J. Highly Sensitive, Uniform, and Reproducible Surface-Enhanced Raman Spectroscopy from Hollow Au-Ag Alloy Nanourchins. *Adv. Mater.* **2014,** *26* (15), 2431.

(147) Jena, B. K.; Raj, C. R. Seedless, Surfactantless Room Temperature Synthesis of Single Crystalline Fluorescent Gold Nanoflowers with Pronounced SERS and Electrocatalytic Activity. *Chemistry of Materials* **2008,** *20* (11), 3546.

(148) Xie, J.; Zhang, Q.; Lee, J. Y.; Wang, D. I. C. The Synthesis of SERS-Active Gold Nanoflower Tags for In Vivo Applications. *ACS Nano* **2008,** *2* (12), 2473.

(149) Jiang, Y.; Wu, X.-J.; Li, Q.; Li, J.; Xu, D. Facile synthesis of gold nanoflowers with high surface-enhanced Raman scattering activity. *Nanotechnology* **2011,** *22* (38), 385601.

(150) Bosnick, K. A.; Jiang, J.; Brus, L. E. Fluctuations and local symmetry in single-molecule rhodamine 6G Raman scattering on silver nanocrystal aggregates. *Journal of Physical Chemistry B* **2002,** *106* (33), 8096.

(151) Halas, N. J.; Lal, S.; Chang, W.-S.; Link, S.; Nordlander, P. Plasmons in Strongly Coupled Metallic Nanostructures. *Chemical Reviews* **2011,** *111* (6), 3913.

(152) Driskell, J. D.; Lipert, R. J.; Porter, M. D. Labeled gold nanoparticles immobilized at smooth metallic substrates: Systematic investigation of surface plasmon resonance and surface-enhanced Raman scattering. *Journal of Physical Chemistry B* **2006,** *110* (35), 17444.

(153) Dieringer, J. A.; Lettan, R. B.; Scheidt, K. A.; Van Duyne, R. P. A Frequency Domain Existence Proof of Single-Molecule Surface-Enhanced Raman Spectroscopy. *J. Am. Chem. Soc.* **2007,** *129* (51), 16249.

(154) Bell, S. E. J.; McCourt, M. R. SERS enhancement by aggregated Au colloids: effect of particle size. *Phys. Chem. Chem. Phys.* **2009,** *11* (34), 7455.

(155) Kleinman, S. L.; Ringe, E.; Valley, N.; Wustholz, K. L.; Phillips, E.; Scheidt, K. A.; Schatz, G. C.; Van Duyne, R. P. Single-Molecule Surface-Enhanced Raman

Spectroscopy of Crystal Violet Isotopologues: Theory and Experiment. *J. Am. Chem. Soc.* **2011,** *133* (11), 4115.

(156) Brown, L. O.; Doorn, S. K. A controlled and reproducible pathway to dye-tagged, encapsulated silver nanoparticles as substrates for SERS multiplexing. *Langmuir* **2008,** *24* (6), 2277.

(157) Tan, X.; Wang, Z.; Yang, J.; Song, C.; Zhang, R.; Cui, Y. Polyvinylpyrrolidone- (PVP-) coated silver aggregates for high performance surface-enhanced Raman scattering in living cells. *Nanotechnology* **2009,** *20* (44).

(158) Braun, G. B.; Lee, S. J.; Laurence, T.; Fera, N.; Fabris, L.; Bazan, G. C.; Moskovits, M.; Reich, N. O. Generalized Approach to SERS-Active Nanomaterials via Controlled Nanoparticle Linking, Polymer Encapsulation, and Small-Molecule Infusion. *Journal of Physical Chemistry C* **2009,** *113* (31), 13622.

(159) Su, X.; Zhang, J.; Sun, L.; Koo, T. W.; Chan, S.; Sundararajan, N.; Yamakawa, M.; Berlin, A. A. Composite organic-inorganic nanoparticles (COINs) with chemically encoded optical signatures. *Nano Letters* **2005,** *5* (1), 49.

(160) Futamata, M.; Yu, Y.-Y.; Yanatori, T.; Kokubun, T. Closely Adjacent Ag Nanoparticles Formed by Cationic Dyes in Solution Generating Enormous SERS Enhancement. *Journal of Physical Chemistry C* **2010,** *114* (16), 7502.

(161) Tay, L.-L.; Huang, P.-J.; Tanha, J.; Ryan, S.; Wu, X.; Hulse, J.; Chau, L.-K. Silica encapsulated SERS nanoprobe conjugated to the bacteriophage tailspike protein for targeted detection of Salmonella. *Chemical Communications* **2012,** *48* (7), 1024.

(162) Huang, P.-J.; Chau, L.-K.; Yang, T.-S.; Tay, L.-L.; Lin, T.-T. Nanoaggregate- Embedded Beads as Novel Raman Labels for Biodetection. *Advanced Functional Materials* **2009,** *19* (2), 242.

(163) Jun, B.-H.; Kim, J.-H.; Park, H.; Kim, J.-S.; Yu, K.-N.; Lee, S.-M.; Choi, H.; Kwak, S.-Y.; Kim, Y.-K.; Jeong, D. H.et al. Surface-enhanced Raman spectroscopic-encoded beads for multiplex immunoassay. *Journal of Combinatorial Chemistry* **2007,** *9* (2), 237.

(164) Kim, K.; Lee, H. B.; Park, H. K.; Shin, K. S. Easy deposition of Ag onto polystyrene beads for developing surface-enhanced-Raman-scattering-based molecular sensors. *Journal of Colloid and Interface Science* **2008,** *318* (2), 195.

(165) Li, J.-M.; Ma, W.-F.; Wei, C.; Guo, J.; Hu, J.; Wang, C.-C. Poly(styrene-co-acrylic acid) core and silver nanoparticle/silica shell composite microspheres as high performance surface-enhanced Raman spectroscopy (SERS) substrate and molecular barcode label. *Journal of Materials Chemistry* **2011,** *21* (16), 5992.

(166) Kim, J.-H.; Kim, J.-S.; Choi, H.; Lee, S.-M.; Jun, B.-H.; Yu, K.-N.; Kuk, E.; Kim, Y.-K.; Jeong, D. H.; Cho, M.-H.et al. Nanoparticle probes with surface enhanced Raman spectroscopic tags for cellular cancer targeting. *Analytical Chemistry* **2006,** *78* (19), 6967.

(167) Wang, C.; Chen, Y.; Wang, T.; Ma, Z.; Su, Z. Monodispersed gold nanorod-embedded silica particles as novel Raman labels for biosensing. *Advanced Functional Materials* **2008,** *18* (2), 355.

(168) Kim, J.-H.; Kim, J.-S.; Choi, H.; Lee, S.-M.; Jun, B.-H.; Yu, K.-N.; Kuk, E.; Kim, Y.-K.; Jeong, D. H.; Cho, M.-H. Nanoparticle probes with surface enhanced Raman spectroscopic tags for cellular cancer targeting. *Analytical Chemistry* **2006,** *78* (19), 6967.

(169) McNay, G.; Eustace, D.; Smith, W. E.; Faulds, K.; Graham, D. Surface-Enhanced Raman Scattering (SERS) and Surface-Enhanced Resonance Raman Scattering (SERRS): A Review of Applications. *Applied Spectroscopy* **2011,** *65* (8), 825.

(170) Harmsen, S.; Huang, R.; Wall, M. A.; Karabeber, H.; Samii, J. M.; Spaliviero, M.; White, J. R.; Monette, S.; O'Connor, R.; Pitter, K. L. Surface-enhanced resonance Raman scattering nanostars for high-precision cancer imaging. *Science Translational Medicine* **2015,** *7* (271), 271ra7.

(171) Qian, X.; Peng, X.-H.; Ansari, D. O.; Yin-Goen, Q.; Chen, G. Z.; Shin, D. M.; Yang, L.; Young, A. N.; Wang, M. D.; Nie, S. In vivo tumor targeting and spectroscopic detection with surface-enhanced Raman nanoparticle tags. *Nat Biotechnol* **2007,** *26* (1), 83.

(172) Jiang, L.; Qian, J.; Cai, F.; He, S. Raman reporter-coated gold nanorods and their applications in multimodal optical imaging of cancer cells. *Anal Bioanal Chem* **2011,** *400* (9), 2793.

(173) Samanta, A.; Maiti, K. K.; Soh, K.-S.; Liao, X.; Vendrell, M.; Dinish, U. S.; Yun, S.-W.; Bhuvaneswari, R.; Kim, H.; Rautela, S.et al. Ultrasensitive Near-Infrared Raman Reporters for SERS-Based In Vivo Cancer Detection. *Angewandte Chemie International Edition* **2011,** *50* (27), 6089.

(174) Wang, Y.; Yan, B.; Chen, L. SERS tags: novel optical nanoprobes for bioanalysis. *Chemical Reviews* **2012,** *113* (3), 1391.

(175) Gellner, M.; Koempe, K.; Schluecker, S. Multiplexing with SERS labels using mixed SAMs of Raman reporter molecules. *Analytical and Bioanalytical Chemistry* **2009,** *394* (7), 1839.

(176) Schuetz, M.; Kuestner, B.; Bauer, M.; Schmuck, C.; Schluecker, S. Synthesis of Glass-Coated SERS Nanoparticle Probes via SAMs with Terminal SiO2 Precursors. *Small* **2010,** *6* (6), 733.

(177)   Jehn, C.; Kuestner, B.; Adam, P.; Marx, A.; Stroebel, P.; Schmuck, C.; Schluecker, S. Water soluble SERS labels comprising a SAM with dual spacers for controlled bioconjugation. *Physical Chemistry Chemical Physics* **2009,** *11* (34), 7499.

(178)   Maiti, K. K.; Dinish, U. S.; Fu, C. Y.; Lee, J.-J.; Soh, K.-S.; Yun, S.-W.; Bhuvaneswari, R.; Olivo, M.; Chang, Y.-T. Development of biocompatible SERS nanotag with increased stability by chemisorption of reporter molecule for in vivo cancer detection. *Biosensors and Bioelectronics* **2010,** *26* (2), 398.

(179)   Maiti, K. K.; Samanta, A.; Vendrell, M.; Soh, K.-S.; Olivo, M.; Chang, Y.-T. Multiplex cancer cell detection by SERS nanotags with cyanine and triphenylmethine Raman reporters. *Chemical Communications* **2011,** *47* (12), 3514.

(180)   Cho, S. J.; Ahn, Y.-H.; Maiti, K. K.; Dinish, U. S.; Fu, C. Y.; Thoniyot, P.; Olivo, M.; Chang, Y.-T. Combinatorial synthesis of a triphenylmethine library and their application in the development of Surface Enhanced Raman Scattering (SERS) probes. *Chemical Communications* **2010,** *46* (5), 722.

(181)   Samanta, A.; Maiti, K. K.; Soh, K.-S.; Liao, X.; Vendrell, M.; Dinish, U. S.; Yun, S.-W.; Bhuvaneswari, R.; Kim, H.; Rautela, S.et al. Ultrasensitive Near-Infrared Raman Reporters for SERS-Based In Vivo Cancer Detection. *Angewandte Chemie-International Edition* **2011,** *50* (27), 6089.

(182)   Maiti, K. K.; Dinish, U. S.; Samanta, A.; Vendrell, M.; Soh, K.-S.; Park, S.-J.; Olivo, M.; Chang, Y.-T. Multiplex targeted in vivo cancer detection using sensitive near-infrared SERS nanotags. *Nano Today* **2012,** *7* (2), 85.

(183)   Bedics, M. A.; Kearns, H.; Cox, J. M.; Mabbott, S.; Ali, F.; Shand, N. C.; Faulds, K.; Benedict, J. B.; Graham, D.; Detty, M. R. Extreme red shifted SERS nanotags. *Chem. Sci.* **2015,** *6* (4), 2302.

(184) Harmsen, S.; Bedics, M. A.; Wall, M. A.; Huang, R.; Detty, M. R.; Kircher, M. F. Rational design of a chalcogenopyrylium-based surface-enhanced resonance Raman scattering nanoprobe with attomolar sensitivity. *Nature Communications* **2015,** *6*, 6570.

(185) Chen, Y.; Vela, J.; Htoon, H.; Casson, J. L.; Werder, D. J.; Bussian, D. A.; Klimov, V. I.; Hollingsworth, J. A. "Giant" Multishell CdSe Nanocrystal Quantum Dots with Suppressed Blinking. *J. Am. Chem. Soc.* **2008,** *130* (15), 5026.

(186) Lane, L. A.; Smith, A. M.; Lian, T.; Nie, S. Compact and Blinking-Suppressed Quantum Dots for Single-Particle Tracking in Live Cells. *The Journal of Physical Chemistry B* **2014,** *118* (49), 14140.

(187) Zavaleta, C. L.; Smith, B. R.; Walton, I.; Doering, W.; Davis, G.; Shojaei, B.; Natan, M. J.; Gambhir, S. S. Multiplexed imaging of surface enhanced Raman scattering nanotags in living mice using noninvasive Raman spectroscopy. *Proceedings of the National Academy of Sciences* **2009,** *106* (32), 13511.

(188) Yue, J.; Liu, Z.; Cai, X.; Ding, X.; Chen, S.; Tao, K.; Zhao, T. Bull serum albumin coated Au@ Agnanorods as SERS probes for ultrasensitive osteosarcoma cell detection. *Talanta* **2016,** *150*, 503.

(189) Sun, L.; Sung, K.-B.; Dentinger, C.; Lutz, B.; Nguyen, L.; Zhang, J.; Qin, H.; Yamakawa, M.; Cao, M.; Lu, Y.et al. Composite organic-inorganic nanoparticles as Raman labels for tissue analysis. *Nano Letters* **2007,** *7* (2), 351.

(190) Weng, K. C.; Noble, C. O.; Papahadjopoulos-Sternberg, B.; Chen, F. F.; Drummond, D. C.; Kirpotin, D. B.; Wang, D.; Hom, Y. K.; Hann, B.; Park, J. W. Targeted tumor cell internalization and imaging of multifunctional quantum dot-conjugated immunoliposomes in vitro and in vivo. *Nano Letters* **2008,** *8* (9), 2851.

(191) Al-Jamal, W. T.; Al-Jamal, K. T.; Tian, B.; Cakebread, A.; Halket, J. M.; Kostarelos, K. Tumor targeting of functionalized quantum dot-liposome hybrids by intravenous administration. *Molecular Pharmaceutics* **2009,** *6* (2), 520.

(192) Tam, N. C. M.; Scott, B. M. T.; Voicu, D.; Wilson, B. C.; Zheng, G. Facile Synthesis of Raman Active Phospholipid Gold Nanoparticles. *Bioconjugate Chemistry* **2010,** *21* (12), 2178.

(193) Ip, S.; MacLaughlin, C. M.; Gunari, N.; Walker, G. C. Phospholipid Membrane Encapsulation of Nanoparticles for Surface-Enhanced Raman Scattering. *Langmuir* **2011,** *27* (11), 7024.

(194) Tam, N. C. M.; McVeigh, P. Z.; MacDonald, T. D.; Farhadi, A.; Wilson, B. C.; Zheng, G. Porphyrin-Lipid Stabilized Gold Nanoparticles for Surface Enhanced Raman Scattering Based Imaging. *Bioconjugate Chemistry* **2012,** *23* (9), 1726.

(195) Qian, X.; Peng, X.-H.; Ansari, D. O.; Yin-Goen, Q.; Chen, G. Z.; Shin, D. M.; Yang, L.; Young, A. N.; Wang, M. D.; Nie, S. In vivo tumor targeting and spectroscopic detection with surface-enhanced Raman nanoparticle tags. *Nature Biotechnology* **2008,** *26* (1), 83.

(196) Huang, Y.; Swarup, V. P.; Bishnoi, S. W. Rapid Raman Imaging of Stable, Functionalized Nanoshells in Mammalian Cell Cultures. *Nano Letters* **2009,** *9* (8), 2914.

(197) Nguyen, C. T.; Nguyen, J. T.; Rutledge, S.; Zhang, J.; Wang, C.; Walker, G. C. Detection of chronic lymphocytic leukemia cell surface markers using surface enhanced Raman scattering gold nanoparticles. *Cancer Letters* **2010,** *292* (1), 91.

(198) Martin, L. C.; Larmour, I. A.; Faulds, K.; Graham, D. Turning up the lights-fabrication of brighter SERRS nanotags. *Chemical Communications* **2010,** *46* (29), 5247.

(199) Wang, Y.; Schlücker, S. Rational design and synthesis of SERS labels. *The Analyst* **2013,** *138* (8), 2224.

(200) Jeon, S. I.; Lee, J. H.; Andrade, J. D.; De Gennes, P. G. Protein—surface interactions in the presence of polyethylene oxide. *Journal of Colloid and Interface Science* **1991,** *142* (1), 149.

(201) Xu, D.; Gu, J.; Wang, W.; Yu, X.; Xi, K.; Jia, X. Development of chitosan-coated gold nanoflowers as SERS-active probes. *Nanotechnology* **2010,** *21* (37).

(202) Potara, M.; Maniu, D.; Astilean, S. The synthesis of biocompatible and SERS-active gold nanoparticles using chitosan. *Nanotechnology* **2009,** *20* (31).

(203) Merican, Z.; Schiller, T. L.; Hawker, C. J.; Fredericks, P. M.; Blakey, I. Self-assembly and encoding of polymer-stabilized gold nanoparticles with surface-enhanced Raman reporter molecules. *Langmuir* **2007,** *23* (21), 10539.

(204) Yang, M.; Chen, T.; Lau, W. S.; Wang, Y.; Tang, Q.; Yang, Y.; Chen, H. Development of Polymer-Encapsulated Metal Nanopartictes as Surface-Enhanced Raman Scattering Probes. *Small* **2009,** *5* (2), 198.

(205) Doering, W. E.; Nie, S. M. Spectroscopic tags using dye-embedded nanoparticles and surface-enhanced Raman scattering. *Analytical Chemistry* **2003,** *75* (22), 6171.

(206) Mulvaney, S. P.; Musick, M. D.; Keating, C. D.; Natan, M. J. Glass-coated, analyte-tagged nanoparticles: A new tagging system based on detection with surface-enhanced Raman scattering. *Langmuir* **2003,** *19* (11), 4784.

(207) Brady, C. I.; Mack, N. H.; Brown, L. O.; Doorn, S. K. Self-Assembly Approach to Multiplexed Surface-Enhanced Raman Spectral-Encoder Beads. *Analytical Chemistry* **2009,** *81* (17), 7181.

(208) Li, J. F.; Huang, Y. F.; Ding, Y.; Yang, Z. L.; Li, S. B.; Zhou, X. S.; Fan, F. R.; Zhang, W.; Zhou, Z. Y.; Wu, D. Y.et al. Shell-isolated nanoparticle-enhanced Raman spectroscopy. *Nature* **2010,** *464* (7287), 392.

(209) Liu, X.; Knauer, M.; Ivleva, N. P.; Niessner, R.; Haisch, C. Synthesis of Core-Shell Surface-Enhanced Raman Tags for Bioimaging. *Analytical Chemistry* **2010,** *82* (1), 441.

(210) Kuestner, B.; Gellner, M.; Schuetz, M.; Schoeppler, F.; Marx, A.; Stroebel, P.; Adam, P.; Schmuck, C.; Schluecker, S. SERS Labels for Red Laser Excitation: Silica-Encapsulated SAMs on Tunable Gold/Silver Nanoshells. *Angewandte Chemie-International Edition* **2009,** *48* (11), 1950.

(211) Liu, X.; Knauer, M.; Ivleva, N. P.; Niessner, R.; Haisch, C. Synthesis of Core−Shell Surface-Enhanced Raman Tags for Bioimaging. *Analytical Chemistry* **2010,** *82* (1), 441.

(212) Mulvaney, S. P.; Musick, M. D.; Keating, C. D.; Natan, M. J. Glass-Coated, Analyte-Tagged Nanoparticles: A New Tagging System Based on Detection with Surface-Enhanced Raman Scattering. *Langmuir* **2003,** *19* (11), 4784.

(213) Chung, T.-H.; Wu, S.-H.; Yao, M.; Lu, C.-W.; Lin, Y.-S.; Hung, Y.; Mou, C.-Y.; Chen, Y.-C.; Huang, D.-M. The effect of surface charge on the uptake and biological function of mesoporous silica nanoparticles in 3T3-L1 cells and human mesenchymal stem cells. *Biomaterials* **2007,** *28* (19), 2959.

(214) Chiu, T.-C.; Huang, C.-C. Aptamer-Functionalized Nano-Biosensors. *Sensors* **2009,** *9* (12), 10356.

(215) Wang, G.; Wang, Y.; Chen, L.; Choo, J. Nanomaterial-assisted aptamers for optical sensing. *Biosensors & Bioelectronics* **2010,** *25* (8), 1859.

(216) Sun, L.; Yu, C.; Irudayaraj, J. Surface-enhanced Raman scattering based nonfluorescent probe for multiplex DNA detection. *Analytical Chemistry* **2007,** *79* (11), 3981.

(217) Grubisha, D. S.; Lipert, R. J.; Park, H.-Y.; Driskell, J.; Porter, M. D. Femtomolar detection of prostate-specific antigen: an immunoassay based on surface-enhanced Raman scattering and immunogold labels. *Analytical Chemistry* **2003,** *75* (21), 5936.

(218) Lyandres, O.; Shah, N. C.; Yonzon, C. R.; Walsh, J. T.; Glucksberg, M. R.; Van Duyne, R. P. Real-time glucose sensing by surface-enhanced Raman spectroscopy in bovine plasma facilitated by a mixed decanethiol/mercaptohexanol partition layer. *Analytical Chemistry* **2005,** *77* (19), 6134.

(219) Sun, L.; Sung, K.-B.; Dentinger, C.; Lutz, B.; Nguyen, L.; Zhang, J.; Qin, H.; Yamakawa, M.; Cao, M.; Lu, Y. Composite organic− inorganic nanoparticles as Raman labels for tissue analysis. *Nano Letters* **2007,** *7* (2), 351.

(220) Liu, X.; Knauer, M.; Ivleva, N. P.; Niessner, R.; Haisch, C. Synthesis of core− shell surface-enhanced Raman tags for bioimaging. *Analytical Chemistry* **2009,** *82* (1), 441.

(221) Jeong, D. H.; Kim, G.; Lee, Y.-S.; Jun, B.-H. In *Raman Spectroscopy for Nanomaterials Characterization*; Springer, 2012.

(222) Su, X.; Zhang, J.; Sun, L.; Koo, T.-W.; Chan, S.; Sundararajan, N.; Yamakawa, M.; Berlin, A. A. Composite Organic−Inorganic Nanoparticles (COINs) with Chemically Encoded Optical Signatures. *Nano Letters* **2005,** *5* (1), 49.

(223) Küstner, B.; Gellner, M.; Schütz, M.; Schöppler, F.; Marx, A.; Ströbel, P.; Adam, P.; Schmuck, C.; Schlücker, S. SERS Labels for Red Laser Excitation: Silica-Encapsulated SAMs on Tunable Gold/Silver Nanoshells. *Angewandte Chemie International Edition* **2009,** *48* (11), 1950.

(224) Stöber, W.; Fink, A.; Bohn, E. Controlled growth of monodisperse silica spheres in the micron size range. *Journal of Colloid and Interface Science* **1968,** *26* (1), 62.

(225) Personick, M. L.; Mirkin, C. A. Making Sense of the Mayhem behind Shape Control in the Synthesis of Gold Nanoparticles. *J. Am. Chem. Soc.* **2013,** *135* (49), 18238.

(226) Zheng, Y.; Zhong, X.; Li, Z.; Xia, Y. Successive, Seed-Mediated Growth for the Synthesis of Single-Crystal Gold Nanospheres with Uniform Diameters Controlled in the Range of 5–150 nm. *Particle & Particle Systems Characterization* **2014,** *31* (2), 266.

(227) Xia, X.; Yang, M.; Wang, Y.; Zheng, Y.; Li, Q.; Chen, J.; Xia, Y. Quantifying the Coverage Density of Poly(ethylene glycol) Chains on the Surface of Gold Nanostructures. *ACS Nano* **2012,** *6* (1), 512.

(228) Connor, E. E.; Mwamuka, J.; Gole, A.; Murphy, C. J.; Wyatt, M. D. Gold Nanoparticles Are Taken Up by Human Cells but Do Not Cause Acute Cytotoxicity. *Small* **2005,** *1* (3), 325.

(229) Murphy, C. J.; Gole, A. M.; Stone, J. W.; Sisco, P. N.; Alkilany, A. M.; Goldsmith, E. C.; Baxter, S. C. Gold Nanoparticles in Biology: Beyond Toxicity to Cellular Imaging. *Accounts of Chemical Research* **2008,** *41* (12), 1721.

(230) Kinnear, C.; Dietsch, H.; Clift, M. J. D.; Endes, C.; Rothen-Rutishauser, B.; Petri-Fink, A. Gold Nanorods: Controlling Their Surface Chemistry and Complete Detoxification by a Two-Step Place Exchange. *Angewandte Chemie* **2013,** *125* (7), 1988.

(231) Niidome, T.; Yamagata, M.; Okamoto, Y.; Akiyama, Y.; Takahashi, H.; Kawano, T.; Katayama, Y.; Niidome, Y. PEG-modified gold nanorods with a stealth character for in vivo applications. *Journal of Controlled Release* **2006,** *114* (3), 343.

(232) Huang, X.; Peng, X.; Wang, Y.; Wang, Y.; Shin, D. M.; El-Sayed, M. A.; Nie, S. A Reexamination of Active and Passive Tumor Targeting by Using Rod-Shaped Gold Nanocrystals and Covalently Conjugated Peptide Ligands. *ACS Nano* **2010,** *4* (10), 5887.

(233) Mehtala, J. G.; Zemlyanov, D. Y.; Max, J. P.; Kadasala, N.; Zhao, S.; Wei, A. Citrate-Stabilized Gold Nanorods. *Langmuir* **2014,** *30* (46), 13727.

(234) Freeman, R. G.; Grabar, K. C.; Allison, K. J.; Bright, R. M.; Davis, J. A.; Guthrie, A. P.; Hommer, M. B.; Jackson, M. A.; Smith, P. C.; Walter, D. G.et al. Self-Assembled Metal Colloid Monolayers: An Approach to SERS Substrates. *Science* **1995,** *267* (5204), 1629.

(235) Maxwell, D. J.; Emory, S. R.; Nie, S. Nanostructured Thin-Film Materials with Surface-Enhanced Optical Properties. *Chemistry of Materials* **2001,** *13* (3), 1082.

(236) Wang, H.; Levin, C. S.; Halas, N. J. Nanosphere Arrays with Controlled Sub-10-nm Gaps as Surface-Enhanced Raman Spectroscopy Substrates. *J. Am. Chem. Soc.* **2005,** *127* (43), 14992.

(237) Chung, S. W.; Markovich, G.; Heath, J. R. Fabrication and Alignment of Wires in Two Dimensions. *The Journal of Physical Chemistry B* **1998,** *102* (35), 6685.

(238) Kim, F.; Kwan, S.; Akana, J.; Yang, P. Langmuir−Blodgett Nanorod Assembly. *J. Am. Chem. Soc.* **2001,** *123* (18), 4360.

(239) Tao, A.; Kim, F.; Hess, C.; Goldberger, J.; He, R.; Sun, Y.; Xia, Y.; Yang, P. Langmuir−Blodgett Silver Nanowire Monolayers for Molecular Sensing Using Surface-Enhanced Raman Spectroscopy. *Nano Letters* **2003,** *3* (9), 1229.

(240) Yao, J. L.; Pan, G. P.; Xue, K. H.; Wu, D. Y.; Ren, B.; Sun, D. M.; Tang, J.; Xu, X.; Tian, Z. Q. A complementary study of surface-enhanced Raman scattering and metal nanorod arrays. *Pure and Applied Chemistry* **2000,** *72* (1-2).

(241) Lee, S. J.; Morrill, A. R.; Moskovits, M. Hot Spots in Silver Nanowire Bundles for Surface-Enhanced Raman Spectroscopy. *J. Am. Chem. Soc.* **2006,** *128* (7), 2200.

(242) Qin, L.; Zou, S.; Xue, C.; Atkinson, A.; Schatz, G. C.; Mirkin, C. A. Designing, fabricating, and imaging Raman hot spots. *Proceedings of the National Academy of Sciences* **2006,** *103* (36), 13300.

(243) Qin, L.; Banholzer, M. J.; Millstone, J. E.; Mirkin, C. A. Nanodisk Codes. *Nano Letters* **2007,** *7* (12), 3849.

(244) Dick, L. A.; McFarland, A. D.; Haynes, C. L.; Van Duyne, R. P. Metal Film over Nanosphere (MFON) Electrodes for Surface-Enhanced Raman Spectroscopy (SERS): Improvements in Surface Nanostructure Stability and Suppression of Irreversible Loss. *The Journal of Physical Chemistry B* **2002,** *106* (4), 853.

(245) Haes, A. J.; Haynes, C. L.; McFarland, A. D.; Schatz, G. C.; Van Duyne, R. P.; Zou, S. Plasmonic Materials for Surface-Enhanced Sensing and Spectroscopy. *MRS Bulletin.* **2005,** *30* (05), 368.

(246) Haynes, C. L.; McFarland, A. D.; Smith, M. T.; Hulteen, J. C.; Van Duyne, R. P. Angle-resolved nanosphere lithography: manipulation of nanoparticle size, shape, and interparticle spacing. *The Journal of Physical Chemistry B* **2002,** *106* (8), 1898.

(247) Fromm, D. P.; Sundaramurthy, A.; Kinkhabwala, A.; Schuck, P. J.; Kino, G. S.; Moerner, W. E. Exploring the chemical enhancement for surface-enhanced Raman scattering with Au bowtie nanoantennas. *The Journal of Chemical Physics* **2006,** *124* (6), 061101.

(248) Félidj, N.; Aubard, J.; Lévi, G.; Krenn, J. R.; Hohenau, A.; Schider, G.; Leitner, A.; Aussenegg, F. R. Optimized surface-enhanced Raman scattering on gold nanoparticle arrays. *Appl. Phys. Lett.* **2003,** *82* (18), 3095.

(249) Abu Hatab, N. A.; Oran, J. M.; Sepaniak, M. J. Surface-Enhanced Raman Spectroscopy Substrates Created via Electron Beam Lithography and Nanotransfer Printing. *ACS Nano* **2008,** *2* (2), 377.

(250) Banholzer, M. J.; Qin, L.; Millstone, J. E.; Osberg, K. D.; Mirkin, C. A. On-wire lithography: synthesis, encoding and biological applications. *Nat Protoc* **2009,** *4* (6), 838.

(251) Qin, L.; Jang, J.-W.; Huang, L.; Mirkin, C. A. Sub-5-nm Gaps Prepared by On-Wire Lithography: Correlating Gap Size with Electrical Transport. *Small* **2007,** *3* (1), 86.

(252) Hulteen, J. C.; Treichel, D. A.; Smith, M. T.; Duval, M. L.; Jensen, T. R.; Van Duyne, R. P. Nanosphere Lithography: Size-Tunable Silver Nanoparticle and Surface Cluster Arrays. *The Journal of Physical Chemistry B* **1999,** *103* (19), 3854.

(253) Hulteen, J. C. Nanosphere lithography: A materials general fabrication process for periodic particle array surfaces. *Journal of Vacuum Science & Technology A: Vacuum, Surfaces, and Films* **1995,** *13* (3), 1553.

(254) Zhang, J.; Li, Y.; Zhang, X.; Yang, B. Colloidal Self-Assembly Meets Nanofabrication: From Two-Dimensional Colloidal Crystals to Nanostructure Arrays. *Advanced Materials* **2010,** *22* (38), 4249.

(255) Baia, M.; Astilean, S.; Iliescu, T. In *Raman and SERS Investigations of Pharmaceuticals*; Springer, 2008.

(256) Baia, M.; Baia, L.; Astilean, S. Gold nanostructured films deposited on polystyrene colloidal crystal templates for surface-enhanced Raman spectroscopy. *Chemical physics letters* **2005,** *404* (1), 3.

(257) Hulteen, J. C.; Van Duyne, R. P. Nanosphere lithography: a materials general fabrication process for periodic particle array surfaces. *Journal of Vacuum Science & Technology A* **1995,** *13* (3), 1553.

(258) Abdelsalam, M. E.; Bartlett, P. N.; Baumberg, J. J.; Cintra, S.; Kelf, T. A.; Russell, A. E. Electrochemical SERS at a structured gold surface. *Electrochemistry Communications* **2005,** *7* (7), 740.

(259) Jensen, T. R.; Malinsky, M. D.; Haynes, C. L.; Van Duyne, R. P. Nanosphere lithography: tunable localized surface plasmon resonance spectra of silver nanoparticles. *The Journal of Physical Chemistry B* **2000,** *104* (45), 10549.

(260) Haynes, C. L.; Van Duyne, R. P. Nanosphere Lithography: A Versatile Nanofabrication Tool for Studies of Size-Dependent Nanoparticle Optics. *The Journal of Physical Chemistry B* **2001,** *105* (24), 5599.

(261) Wu, D.-Y.; Li, J.-F.; Ren, B.; Tian, Z.-Q. Electrochemical surface-enhanced Raman spectroscopy of nanostructures. *Chemical Society Reviews* **2008,** *37* (5), 1025.

(262) Atay, T.; Song, J.-H.; Nurmikko, A. V. Strongly Interacting Plasmon Nanoparticle Pairs: From Dipole−Dipole Interaction to Conductively Coupled Regime. *Nano Letters* **2004,** *4* (9), 1627.

(263) Kahl, M.; Voges, E.; Kostrewa, S.; Viets, C.; Hill, W. Periodically structured metallic substrates for SERS. *Sensors and Actuators B: Chemical* **1998,** *51* (1), 285.

(264) Gunnarsson, L.; Bjerneld, E. J.; Xu, H.; Petronis, S.; Kasemo, B.; Käll, M. Interparticle coupling effects in nanofabricated substrates for surface-enhanced Raman scattering. *Appl. Phys. Lett.* **2001,** *78* (6), 802.

(265) Jain, P. K.; Huang, W.; El-Sayed, M. A. On the Universal Scaling Behavior of the Distance Decay of Plasmon Coupling in Metal Nanoparticle Pairs: A Plasmon Ruler Equation. *Nano Letters* **2007,** *7* (7), 2080.

(266) Lee, K.; Irudayaraj, J. Correct spectral conversion between surface-enhanced Raman and plasmon resonance scattering from nanoparticle dimers for single-molecule detection. *Small* **2013,** *9* (7), 1106.

(267) Chirumamilla, M.; Toma, A.; Gopalakrishnan, A.; Das, G.; Zaccaria, R. P.; Krahne, R.; Rondanina, E.; Leoncini, M.; Liberale, C.; De Angelis, F.et al. 3D Nanostar Dimers

with a Sub-10-nm Gap for Single-/Few-Molecule Surface-Enhanced Raman Scattering. *Adv. Mater.* **2014,** *26* (15), 2353.

(268) Tabatabaei, M.; Najiminaini, M.; Davieau, K.; Kaminska, B.; Singh, M. R.; Carson, J. J.; Lagugné-Labarthet, F. Tunable 3D plasmonic cavity nanosensors for surface-enhanced Raman spectroscopy with sub-femtomolar limit of detection. *ACS Photonics* **2015,** *2* (6), 752.

(269) Yu, Q.; Guan, P.; Qin, D.; Golden, G.; Wallace, P. M. Inverted size-dependence of surface-enhanced Raman scattering on gold nanohole and nanodisk arrays. *Nano letters* **2008,** *8* (7), 1923.

(270) Ward, D. R.; Grady, N. K.; Levin, C. S.; Halas, N. J.; Wu, Y.; Nordlander, P.; Natelson, D. Electromigrated Nanoscale Gaps for Surface-Enhanced Raman Spectroscopy. *Nano Letters* **2007,** *7* (5), 1396.

(271) Theiss, J.; Pavaskar, P.; Echternach, P. M.; Muller, R. E.; Cronin, S. B. Plasmonic Nanoparticle Arrays with Nanometer Separation for High-Performance SERS Substrates. *Nano Letters* **2010,** *10* (8), 2749.

(272) Schmit, V.; Martoglio, R.; Carron, K. Lab-on-a-bubble surface enhanced Raman indirect immunoassay for cholera. *Analytical Chemistry* **2012,** *84* (9), 4233.

(273) Wei, L.; Jin, B.; Dai, S. Polymer microbead-based surface enhanced Raman scattering immunoassays. *The Journal of Physical Chemistry C* **2012,** *116* (32), 17174.

(274) Yan, W.; Yang, L.; Zhuang, H.; Wu, H.; Zhang, J. Engineered "hot" core–shell nanostructures for patterned detection of chloramphenicol. *Biosensors and Bioelectronics* **2016,** *78*, 67.

(275) Zheng, F.; Cheng, Y.; Wang, J.; Lu, J.; Zhang, B.; Zhao, Y.; Gu, Z. Aptamer-Functionalized Barcode Particles for the Capture and Detection of Multiple Types of Circulating Tumor Cells. *Advanced Materials* **2014,** *26* (43), 7333.

(276) Liu, B.; Zhao, X.; Jiang, W.; Fu, D.; Gu, Z. Multiplex bioassays encoded by photonic crystal beads and SERS nanotags. *Nanoscale* **2016,** *8* (40), 17465.

(277) Lee, J. H.; Xu, P. F.; Domaille, D. W.; Choi, C.; Jin, S.; Cha, J. N. M13 bacteriophage as materials for amplified surface enhanced Raman scattering protein sensing. *Advanced Functional Materials* **2014,** *24* (14), 2079.

(278) Dye-Labeled, S.-E. R. S. Au Nanoparticles for Triplexed Detection of Leukemia and Lymphoma Cells and SERS Flow Cytometry MacLaughlin. *Christina M*, 1908.

(279) Tai, Y.; Wang, L.; Yan, G.; Gao, J. m.; Yu, H.; Zhang, L. Recent research progress on the preparation and application of magnetic nanospheres. *Polymer International* **2011,** *60* (7), 976.

(280) Iranifam, M. Analytical applications of chemiluminescence-detection systems assisted by magnetic microparticles and nanoparticles. *TrAC Trends in Analytical Chemistry* **2013,** *51*, 51.

(281) Wang, R.; Chon, H.; Lee, S.; Cheng, Z.; Hong, S. H.; Yoon, Y. H.; Choo, J. Highly sensitive detection of hormone estradiol E2 using surface-enhanced Raman scattering based immunoassays for the clinical diagnosis of precocious puberty. *ACS Applied Materials & Interfaces* **2016,** *8* (17), 10665.

(282) Xiao, R.; Wang, C.; Zhu, A.; Long, F. Single functional magnetic-bead as universal biosensing platform for trace analyte detection using SERS-nanobioprobe. *Biosensors and Bioelectronics* **2016,** *79*, 661.

(283) Xiong, K.; Wei, W.; Jin, Y.; Wang, S.; Zhao, D.; Wang, S.; Gao, X.; Qiao, C.; Yue, H.; Ma, G. Biomimetic Immuno-Magnetosomes for High-Performance Enrichment of Circulating Tumor Cells. *Advanced Materials* **2016,** *28* (36), 7929.

(284) Zong, S.; Wang, Z.; Zhang, R.; Wang, C.; Xu, S.; Cui, Y. A multiplex and straightforward aqueous phase immunoassay protocol through the combination of

SERS-fluorescence dual mode nanoprobes and magnetic nanobeads. *Biosensors and Bioelectronics* **2013,** *41*, 745.

(285) Li, C.; Ma, C.; Wang, F.; Xi, Z.; Wang, Z.; Deng, Y.; He, N. Preparation and biomedical applications of core–shell silica/magnetic nanoparticle composites. *Journal of Nanoscience and Nanotechnology* **2012,** *12* (4), 2964.

(286) Li, D.; Zhang, Y.; Li, R.; Guo, J.; Wang, C.; Tang, C. Selective Capture and Quick Detection of Targeting Cells with SERS-Coding Microsphere Suspension Chip. *Small* **2015,** *11* (18), 2200.

(287) Baniukevic, J.; Boyaci, I. H.; Bozkurt, A. G.; Tamer, U.; Ramanavicius, A.; Ramanaviciene, A. Magnetic gold nanoparticles in SERS-based sandwich immunoassay for antigen detection by well oriented antibodies. *Biosensors and Bioelectronics* **2013,** *43*, 281.

(288) Wang, J.; Wu, X.; Wang, C.; Shao, N.; Dong, P.; Xiao, R.; Wang, S. Magnetically assisted surface-enhanced Raman spectroscopy for the detection of Staphylococcus aureus based on aptamer recognition. *ACS Applied Materials & Interfaces* **2015,** *7* (37), 20919.

(289) Ahmed, F. E. Sample preparation and fractionation for proteome analysis and cancer biomarker discovery by mass spectrometry. *Journal of Separation Science* **2009,** *32* (5-6), 771.

(290) Haga, H.; Patel, T. Molecular diagnosis of intrahepatic cholangiocarcinoma. *Journal of Hepato-Biliary-Pancreatic Sciences* **2015,** *22* (2), 114.

(291) Gavelli, G.; Giampalma, E. Sensitivity and specificity of chest x-ray screening for lung cancer. *Cancer* **2000,** *89* (S11), 2453.

(292) Ang Tl, K.; Gotoda, T. Diagnosis and endoscopic resection of early gastric cancer. *Singapore Med J* **2010,** *51* (2), 93.

(293) Smith, R. A.; Cokkinides, V.; Brawley, O. W. Cancer screening in the United States, 2009: a review of current American Cancer Society guidelines and issues in cancer screening. *CA: A Cancer Journal for Clinicians* **2009,** *59* (1), 27.

(294) Paterlini-Brechot, P.; Benali, N. L. Circulating tumor cells (CTC) detection: clinical impact and future directions. *Cancer Letters* **2007,** *253* (2), 180.

(295) Schwarzenbach, H.; Hoon, D. S.; Pantel, K. Cell-free nucleic acids as biomarkers in cancer patients. *Nature Reviews Cancer* **2011,** *11* (6), 426.

(296) Srinivas, P. R.; Kramer, B. S.; Srivastava, S. Trends in biomarker research for cancer detection. *The Lancet Oncology* **2001,** *2* (11), 698.

(297) Zaenker, P.; Ziman, M. R. Serologic autoantibodies as diagnostic cancer biomarkers—a review. *Cancer Epidemiology and Prevention Biomarkers* **2013**.

(298) Stearns, V.; Yamauchi, H.; Hayes, D. F. Circulating tumor markers in breast cancer: accepted utilities and novel prospects. *Breast Cancer Research and Treatment* **1998,** *52* (1-3), 239.

(299) Zhang, A.-h.; Sun, H.; Yan, G.-l.; Han, Y.; Wang, X.-j. Serum proteomics in biomedical research: a systematic review. *Applied Biochemistry and Biotechnology* **2013,** *170* (4), 774.

(300) Lee, M.; Lee, K.; Kim, K. H.; Oh, K. W.; Choo, J. SERS-based immunoassay using a gold array-embedded gradient microfluidic chip. *Lab on a Chip* **2012,** *12* (19), 3720.

(301) Zavaleta, C. L.; Garai, E.; Liu, J. T.; Sensarn, S.; Mandella, M. J.; Van de Sompel, D.; Friedland, S.; Van Dam, J.; Contag, C. H.; Gambhir, S. S. A Raman-based endoscopic strategy for multiplexed molecular imaging. *Proceedings of the National Academy of Sciences* **2013,** *110* (25), E2288.

(302) Granger, J. H.; Granger, M. C.; Firpo, M. A.; Mulvihill, S. J.; Porter, M. D. Toward development of a surface-enhanced Raman scattering (SERS)-based cancer diagnostic immunoassay panel. *Analyst* **2013,** *138* (2), 410.

(303) Lee, M.; Lee, S.; Lee, J.-h.; Lim, H.-w.; Seong, G. H.; Lee, E. K.; Chang, S.-I.; Oh, C. H.; Choo, J. Highly reproducible immunoassay of cancer markers on a gold-patterned microarray chip using surface-enhanced Raman scattering imaging. *Biosensors and Bioelectronics* **2011,** *26* (5), 2135.

(304) Worsley, G.; Attree, S.; Noble, J.; Horgan, A. Rapid duplex immunoassay for wound biomarkers at the point-of-care. *Biosensors and Bioelectronics* **2012,** *34* (1), 215.

(305) Ko, J.; Lee, S.; Lee, E. K.; Chang, S.-I.; Chen, L.; Yoon, S.-Y.; Choo, J. SERS-based immunoassay of tumor marker VEGF using DNA aptamers and silica-encapsulated hollow gold nanospheres. *Physical Chemistry Chemical Physics* **2013,** *15* (15), 5379.

(306) Nguyen, A. H.; Lee, J.; Choi, H. I.; Kwak, H. S.; Sim, S. J. Fabrication of Plasmon length-based surface enhanced Raman scattering for multiplex detection on microfluidic device. *Biosensors and Bioelectronics* **2015,** *70*, 358.

(307) Ye, S.; Zhai, X.; Wu, Y.; Kuang, S. Dual-primer self-generation SERS signal amplification assay for PDGF-BB using label-free aptamer. *Biosensors and Bioelectronics* **2016,** *79*, 130.

(308) He, Y.; Wang, Y.; Yang, X.; Xie, S.; Yuan, R.; Chai, Y. Metal Organic Frameworks Combining CoFe2O4 Magnetic Nanoparticles as Highly Efficient SERS Sensing Platform for Ultrasensitive Detection of N-Terminal Pro-Brain Natriuretic Peptide. *ACS Applied Materials & Interfaces* **2016,** *8* (12), 7683.

(309) Lin, Y.; Xu, G.; Wei, F.; Zhang, A.; Yang, J.; Hu, Q. Detection of CEA in human serum using surface-enhanced Raman spectroscopy coupled with antibody-modified Au and

γ-Fe 2 O 3@ Au nanoparticles. *Journal of Pharmaceutical and Biomedical Analysis* **2016,** *121*, 135.

(310) Cao, C.; Zhang, J.; Wen, X.; Dodson, S. L.; Dao, N. T.; Wong, L. M.; Wang, S.; Li, S.; Phan, A. T. a.; Xiong, Q. Metamaterials-based label-free nanosensor for conformation and affinity biosensing. *ACS Nano* **2013,** *7* (9), 7583.

(311) Lee, S.; Kim, S.; Choo, J.; Shin, S. Y.; Lee, Y. H.; Choi, H. Y.; Ha, S.; Kang, K.; Oh, C. H. Biological imaging of HEK293 cells expressing PLCγ1 using surface-enhanced Raman microscopy. *Analytical Chemistry* **2007,** *79* (3), 916.

(312) Lee, S.; Chon, H.; Lee, M.; Choo, J.; Shin, S. Y.; Lee, Y. H.; Son, S. W.; Oh, C. H. Surface-enhanced Raman scattering imaging of HER2 cancer markers overexpressed in single MCF7 cells using antibody conjugated hollow gold nanospheres. *Biosensors and Bioelectronics* **2009,** *24* (7), 2260.

(313) Park, H.; Lee, S.; Chen, L.; Lee, E. K.; Shin, S. Y.; Lee, Y. H.; Son, S. W.; Oh, C. H.; Song, J. M.; Kang, S. H. SERS imaging of HER2-overexpressed MCF7 cells using antibody-conjugated gold nanorods. *Physical Chemistry Chemical Physics* **2009,** *11* (34), 7444.

(314) Jun, B. H.; Noh, M. S.; Kim, J.; Kim, G.; Kang, H.; Kim, M. S.; Seo, Y. T.; Baek, J.; Kim, J. H.; Park, J. Multifunctional Silver-Embedded Magnetic Nanoparticles as SERS Nanoprobes and Their Applications. *Small* **2010,** *6* (1), 119.

(315) Samanta, A.; Maiti, K. K.; Soh, K. S.; Liao, X.; Vendrell, M.; Dinish, U.; Yun, S. W.; Bhuvaneswari, R.; Kim, H.; Rautela, S. Ultrasensitive Near-Infrared Raman Reporters for SERS-Based In Vivo Cancer Detection. *Angewandte Chemie International Edition* **2011,** *50* (27), 6089.

(316) Kong, K. V.; Lam, Z.; Goh, W. D.; Leong, W. K.; Olivo, M. Metal Carbonyl–Gold Nanoparticle Conjugates for Live-Cell SERS Imaging. *Angewandte Chemie* **2012,** *124* (39), 9934.

(317) Jimenez de Aberasturi, D.; Serrano-Montes, A. B.; Langer, J.; Henriksen-Lacey, M.; Parak, W. J.; Liz-Marzán, L. M. Surface enhanced raman scattering encoded gold nanostars for multiplexed cell discrimination. *Chemistry of Materials* **2016,** *28* (18), 6779.

(318) Sun, C.; Gao, M.; Zhang, X. Surface-enhanced Raman scattering (SERS) imaging-guided real-time photothermal ablation of target cancer cells using polydopamine-encapsulated gold nanorods as multifunctional agents. *Analytical and Bioanalytical Chemistry* **2017**, 1.

(319) Jin, Q.; Li, M.; Polat, B.; Paidi, S. K.; Dai, A.; Zhang, A.; Pagaduan, J. V.; Barman, I.; Gracias, D. H. Mechanical Trap Surface-Enhanced Raman Spectroscopy for Three-Dimensional Surface Molecular Imaging of Single Live Cells. *Angewandte Chemie* **2017,** *129* (14), 3880.

(320) Ye, S.; Li, X.; Wang, M.; Tang, B. Fluorescence and SERS Imaging for the Simultaneous Absolute Quantification of Multiple miRNAs in Living Cells. *Analytical Chemistry* **2017,** *89* (9), 5124.

(321) Liu, R.; Zhao, J.; Han, G.; Zhao, T.; Zhang, R.; Liu, B.; Liu, Z.; Zhang, C.; Yang, L.; Zhang, Z. Click-Functionalized SERS Nanoprobes with Improved Labeling Efficiency and Capability for Cancer Cell Imaging. *ACS Applied Materials & Interfaces* **2017**.

(322) Xiao, L.; Tian, X.; Harihar, S.; Li, Q.; Li, L.; Welch, D. R.; Zhou, A. Gd 2 O 3-doped silica@ Au nanoparticles for in vitro imaging cancer biomarkers using surface-enhanced Raman scattering. *Spectrochimica Acta Part A: Molecular and Biomolecular Spectroscopy* **2017,** *181*, 218.

(323) Zhang, L.; Zhang, R.; Gao, M.; Zhang, X. Facile synthesis of thiol and alkynyl contained SERS reporter molecular and its usage in assembly of polydopamine protected bioorthogonal SERS tag for live cell imaging. *Talanta* **2016,** *158*, 315.

(324) Woo, M.-A.; Lee, S.-M.; Kim, G.; Baek, J.; Noh, M. S.; Kim, J. E.; Park, S. J.; Minai-Tehrani, A.; Park, S.-C.; Seo, Y. T. Multiplex immunoassay using fluorescent-surface enhanced Raman spectroscopic dots for the detection of bronchioalveolar stem cells in murine lung. *Analytical chemistry* **2008,** *81* (3), 1008.

(325) Jehn, C.; Küstner, B.; Adam, P.; Marx, A.; Ströbel, P.; Schmuck, C.; Schlücker, S. Water soluble SERS labels comprising a SAM with dual spacers for controlled bioconjugation. *Physical Chemistry Chemical Physics* **2009,** *11* (34), 7499.

(326) Jokerst, J. V.; Miao, Z.; Zavaleta, C.; Cheng, Z.; Gambhir, S. S. Affibody-functionalized gold–silica nanoparticles for Raman molecular imaging of the epidermal growth factor receptor. *Small* **2011,** *7* (5), 625.

(327) Reder, N. P.; Kang, S.; Glaser, A. K.; Yang, Q.; Wall, M. A.; Javid, S. H.; Dintzis, S. M.; Liu, J. T. Raman-Encoded Molecular Imaging with Topically Applied SERS Nanoparticles for Intraoperative Guidance of Lumpectomy. *Cancer Research* **2017,** *77* (16), 4506.

(328) Chen, Y.; Zheng, X.; Chen, G.; He, C.; Zhu, W.; Feng, S.; Xi, G.; Chen, R.; Lan, F.; Zeng, H. Immunoassay for LMP1 in nasopharyngeal tissue based on surface-enhanced Raman scattering. *International Journal of Nanomedicine* **2012,** *7*, 73.

(329) Schütz, M.; Steinigeweg, D.; Salehi, M.; Kömpe, K.; Schlücker, S. Hydrophilically stabilized gold nanostars as SERS labels for tissue imaging of the tumor suppressor p63 by immuno-SERS microscopy. *Chemical Communications* **2011,** *47* (14), 4216.

(330)   Salehi, M.; Schneider, L.; Ströbel, P.; Marx, A.; Packeisen, J.; Schlücker, S. Two-color

SERS microscopy for protein co-localization in prostate tissue with primary antibody–

protein A/G–gold nanocluster conjugates. *Nanoscale* **2014,** *6* (4), 2361.

(331)   Keren, S.; Zavaleta, C.; Cheng, Z.; de La Zerda, A.; Gheysens, O.; Gambhir, S.

Noninvasive molecular imaging of small living subjects using Raman spectroscopy.

Proceedings of the National Academy of Sciences **2008,** *105* (15), 5844.

(332)   Wang, Y.; Seebald, J. L.; Szeto, D. P.; Irudayaraj, J. Biocompatibility and

biodistribution of surface-enhanced Raman scattering nanoprobes in zebrafish

embryos: in vivo and multiplex imaging. *ACS Nano* **2010,** *4* (7), 4039.

(333)   Maiti, K. K.; Dinish, U.; Samanta, A.; Vendrell, M.; Soh, K.-S.; Park, S.-J.; Olivo, M.;

Chang, Y.-T. Multiplex targeted in vivo cancer detection using sensitive near-infrared

SERS nanotags. *Nano Today* **2012,** *7* (2), 85.

(334)   Yigit, M. V.; Zhu, L.; Ifediba, M. A.; Zhang, Y.; Carr, K.; Moore, A.; Medarova, Z.

Noninvasive MRI-SERS imaging in living mice using an innately bimodal

nanomaterial. *ACS Nano* **2010,** *5* (2), 1056.

(335)   Zavaleta, C. L.; Hartman, K. B.; Miao, Z.; James, M. L.; Kempen, P.; Thakor, A. S.;

Nielsen, C. H.; Sinclair, R.; Cheng, Z.; Gambhir, S. S. Preclinical evaluation of Raman

nanoparticle biodistribution for their potential use in clinical endoscopy imaging. *Small*

2011, *7* (15), 2232.

(336)   Qian, J.; Jiang, L.; Cai, F.; Wang, D.; He, S. Fluorescence-surface enhanced Raman

scattering co-functionalized gold nanorods as near-infrared probes for purely optical in

vivo imaging. *Biomaterials* **2011,** *32* (6), 1601.

(337)   Kircher, M. F.; De La Zerda, A.; Jokerst, J. V.; Zavaleta, C. L.; Kempen, P. J.; Mittra,

E.; Pitter, K.; Huang, R.; Campos, C.; Habte, F. A brain tumor molecular imaging

strategy using a new triple-modality MRI-photoacoustic-Raman nanoparticle. *Nature Medicine* **2012,** *18* (5), 829.

(338) Wang, Z.; Zong, S.; Yang, J.; Song, C.; Li, J.; Cui, Y. One-step functionalized gold nanorods as intracellular probe with improved SERS performance and reduced cytotoxicity. *Biosensors and Bioelectronics* **2010,** *26* (1), 241.

(339) Boca, S. C.; Astilean, S. Detoxification of gold nanorods by conjugation with thiolated poly (ethylene glycol) and their assessment as SERS-active carriers of Raman tags. *Nanotechnology* **2010,** *21* (23), 235601.

(340) Horsnell, J. D.; Smith, J. A.; Sattlecker, M.; Sammon, A.; Christie-Brown, J.; Kendall, C.; Stone, N. Raman spectroscopy–a potential new method for the intra-operative assessment of axillary lymph nodes. *The Surgeon* **2012,** *10* (3), 123.

(341) Niu, J. J.; Schrlau, M. G.; Friedman, G.; Gogotsi, Y. Carbon Nanotube-Tipped Endoscope for In Situ Intracellular Surface-Enhanced Raman Spectroscopy. *Small* **2011,** *7* (4), 540.

(342) Dinish, U. S.; Yaw, F. C.; Agarwal, A.; Olivo, M. Development of highly reproducible nanogap SERS substrates: Comparative performance analysis and its application for glucose sensing. *Biosensors and Bioelectronics* **2011,** *26* (5), 1987.

(343) Pazos-Pérez, N.; Ni, W.; Schweikart, A.; Alvarez-Puebla, R. A.; Fery, A.; Liz-Marzán, L. M. Highly uniform SERS substrates formed by wrinkle-confined drying of gold colloids. *Chemical Science* **2010,** *1* (2), 174.

(344) De Luca, A. C.; Reader-Harris, P.; Mazilu, M.; Mariggiò, S.; Corda, D.; Di Falco, A. Reproducible Surface-Enhanced Raman Quantification of Biomarkers in Multicomponent Mixtures. *ACS Nano* **2014,** *8* (3), 2575.

(345) Lin, X.-M.; Cui, Y.; Xu, Y.-H.; Ren, B.; Tian, Z.-Q. Surface-enhanced Raman spectroscopy: substrate-related issues. *Anal Bioanal Chem* **2009,** *394* (7), 1729.

(346) Shafer-Peltier, K. E.; Haynes, C. L.; Glucksberg, M. R.; Van Duyne, R. P. Toward a Glucose Biosensor Based on Surface-Enhanced Raman Scattering. *J. Am. Chem. Soc.* **2003,** *125* (2), 588.

(347) Biggs, K. B.; Camden, J. P.; Anker, J. N.; Duyne, R. P. V. Surface-Enhanced Raman Spectroscopy of Benzenethiol Adsorbed from the Gas Phase onto Silver Film over Nanosphere Surfaces: Determination of the Sticking Probability and Detection Limit Time †. *J. Phys. Chem. A* **2009,** *113* (16), 4581.

(348) AshaRani, P.; Low Kah Mun, G.; Hande, M. P.; Valiyaveettil, S. Cytotoxicity and genotoxicity of silver nanoparticles in human cells. *ACS Nano* **2008,** *3* (2), 279.

(349) Jiang, W.; Kim, B. Y.; Rutka, J. T.; Chan, W. C. Nanoparticle-mediated cellular response is size-dependent. *Nature Nanotechnology* **2008,** *3* (3), 145.

(350) Thakor, A. S.; Paulmurugan, R.; Kempen, P.; Zavaleta, C.; Sinclair, R.; Massoud, T. F.; Gambhir, S. S. Oxidative Stress Mediates the Effects of Raman-Active Gold Nanoparticles in Human Cells. *Small* **2011,** *7* (1), 126.

Chapter 3   Identify Label-free Surface-functionalized Monodisperse Polymer Microbeads through Multiplex Raman Mapping

Umar Azhar[1], Zeyad Alwahabi[1] *, Sheng Dai[1, 2]*

[1]*School of Chemical Engineering, The University of Adelaide, Adelaide, SA 5005 Australia*

[2]*Department of Chemical Engineering, Brunel University London, Kingston Lane, Uxbridge, UB8 3PH, United Kingdom*

* Corresponding author

Email: sheng.dai@brunel.ac.uk; zeyad.alwahabi@adelaide.edu.au

TOC Figure
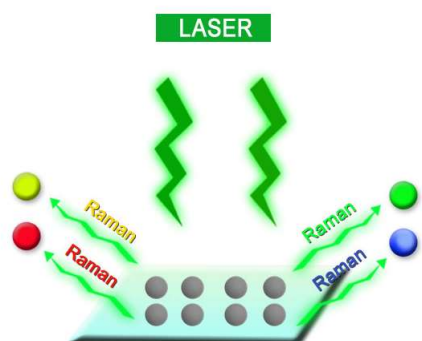
Abstract

Spectroscopic encoded polymer beads are widely used as the physical support in various bioanalysis, where complicated labelling is always required to achieve multiplex readout in a single incident. Spatially-resolved Raman Spectroscopy (SRRS) was applied to four different polymer microbeads prepared by dispersion polymerization. These beads are poly(styrene-co-acrylic acid), poly(4-tetrabutylstyrene-co-acrylic acid), poly(4-methylstyrene-co-acrylic acid) and poly(glycidyl methacrylate-co-acrylic acid), they possess unique Raman signature at four different wavenumbers, namely 1000, 1109, 1183 and 1259 cm^{-1}. It was found that these monodisperse microbeads (sizes of ~1.5 µm) can be well-dispersed in aqueous system, and more importantly, their surfaces contain carboxylic acid groups for further functionalisation. Using SRRS, it was found that these spectroscopic-encoded multiplex microbeads can be readout and distinguished simultaneously. The result signifies the ability of using characteristically unique Raman-encoded polymer beads as the ideal label-free support in multiplex suspension analysis to replace traditional spectroscopic encoded systems.

Keywords: Raman, label-free, monodisperse, microbeads, multiplex, spectroscopic-encoded.

3.1 Introduction

Simultaneous identification of multiple target analytes through multiplexed encoding techniques with high sensitivity is of vital importance in modern bioanalysis. Current bioassay research is focused on enhancing combinatorial chemistry and multiplexing diagnostics[1]. Practically, labelling is the prerequisite in encoding systems so as to be distinguished by various readout techniques such as mass spectrometry [2], high-resolution magic angle spinning [3], energy-dispersive X-ray spectroscopy [4], X-ray photoelectron spectroscopy [5], infrared [6] and fluorescence spectroscopy[7]. Since most the above techniques suffer from high costs, low reproducibility, slow kinetics, intensive labour and poor flexibility[8], fluorescence is nowadays the most popular readout approach in bioanalysis. Traditional fluorescent encoders like dyes or quantum dots are encumbered to multiplex due to various limitations like photo-bleaching, broad emission spectra, toxicity and surface property change after modification, and thus the development of new coding systems become more and more crucial.

Raman spectroscopy indicates the Raman active modes in a system helping to provide structural fingerprints of individual molecules. It is a non-destructive analytical technique, and the narrow spectral fingerprints can offer better multiplexing. Intrinsic Raman signals are weak, however, associated with recent advancement in hardware and software of analytical techniques, Raman spectroscopy has found popular usage in various molecular-level diagnostics [9-14].

Polymers have marked their profound use in our daily life, industries and biotechnology. The unique chain molecular structure, good biocompatibility and ability of being easily modified make them ideal contenders in various bio-research [15-18]. Among them, polymer beads has been widely used as the physical support in latex immunoassays [19]. Surface functionalized polymer beads covalently bonded with bio-ligands have been pragmatic as a diagnosis of rheumatoid and detection of human rotaviruses[20-22]. Moreover, polymer micro- or nano- beads have also been reported for establishing sandwich immunoassays as the support [23-24]. Since different

monomers have their distinct Raman fingerprints, polymer microbeads composing of various monomers will display distinguishable Raman spectra in their narrow vibrational bands. Due to free from labelling, the synthesis and screening of polymer sphericity in nano- or micro-scale with uniform distribution have attracted oodles of research in multiplex analysis [25-26]. The combination of polymer and Raman effectively subsides major drawbacks of other encoding systems like tedious work of synthesis, surface property and stability change after labelling, and limitations of labels in photo-bleaching, toxicity and spectral overlapping.

Our group performed spectroscopic study of Raman and surface enhanced Raman spectroscopy (SERS) encoding with a single polymer microbead together with fluorescence imaging and flow cytometer analysis [27]. It is crucial to control surface functional groups and particle size distributions of polymer microbeads for exploring further multiplex Raman imaging assays. This requires high resolution imaging through narrow spectral bands to use polymer microbeads as the support and multiplex encoders, where samples can be analysed by optical imaging with an overlapping chemically false coloured Raman spectroscopic mapping [24, 28]. The latter is promising as it helps to identify distributions of the heterogeneously mixed microbeads in lieu of labelling.

SRRS is an invaluable technique as it allows different polymer microbeads to be viewed, invisible and/or indistinguishable by standard optical microscopy. Therefore, the use of Raman as a readout method along with spectroscopically encoded label-free polymer microbeads can prove a major breakthrough offering advanced multiplex analysis [29].

In this study, multiple polymer microbeads with narrow particle size distributions and surface functional groups were synthesised. These microbeads showed distinguished Raman features, and can be easily readout from Raman spectra. As a result, it allowed individual beads to be simultaneously identified from a microbead mixture through the high-resolution multiplex

Raman mapping. A successful label-free multiplex microbead readout has been performed in a single laser incident through distinct Raman spectral bands with good repeatability.

3.2. Experimental

3.2.1 Materials

Styrene (Sty), 4-tert-butylstyrene (4tBS), glycidyl methacrylate (GMA), 4-methylstyrene (4MS), Triton X-305 (70 % in H_2O) and polyvinylpyrrolidone (PVP 360,000) were purchased from Sigma-Aldrich. Acrylic acid (AA) and 2, 2'-azo-bis (2-methylpropanitrile) (AIBN) was supplied by Acros Organics. Absolute ethanol was from Merck. Deionized water (DI water, 18.2 MΩ·cm^{-1}) was from an EASY pure II ultrapure water purification system. All chemicals were used as received without further purification.

3.2.2 Synthesis of copolymer microbeads

Two stage dispersion polymerization technique [30] was applied to synthesise a series of surface functionalized and monodisperse copolymer microbeads with distinct Raman signatures. The resulting copolymer microbeads were named as the P(Sty-co-AA) beads, P(4MS-co-AA) beads, P(4tBS-co-AA) beads and P(GMA-co-AA) beads. In the first stage, the monomer (6.0 g), initiator (0.24 g AIBN), stabiliser (0.27 g PVP), co-stabiliser (0.30 g 70 % Triton X-305) and solvent (34 g 95 % ethanol) were charged to a 250 mL three-neck flask equipped with a gas inlet/outlet, a condenser and a mechanical stirrer. The mixture was deoxygenated by nitrogen bubbling for 40 min at room temperature. The flask was then merged into a pre-heated 70 °C oil-bath and stirred mechanically at 100 rpm for 1 h. In the second stage, the preheated AA solution (2 wt. % AA to the total monomer feed in stage 1 was mixed with 16 g 95 % ethanol) was added to the reaction flask. The reaction was continued for another 24 h under stirring and nitrogen protection. After polymerisation, conversion was determined by a gravity

method. The synthesised microbeads were washed three times with 95 % ethanol and four times with DI water, and finally redispersed in DI water for storage.

3.2.3 Instrumentation

Particle sizes and size distributions of synthesised copolymer microbeads were analysed by a Malvern 2000 Mastersizer. Morphologies of microbeads were recorded using a Quanta 450 SEM (scanning electron microscope). The presence of surface AA functional groups was identified by pH and conductivity titrations at room temperature.

A LabRAM Horiba confocal Raman microscope equipped LabSpec 6 software was employed to monitor Raman spectra and microbeads mappings in solid states. Diluted microbead suspensions were dried on glass slides, and Raman spectra/mappings of these beads were captured under optimum measurement settings. A diode-pumped solid-state (DPSS) Nd: YAG (neodymium-doped yttrium aluminum garnet; $Nd:Y_3Al_5O_{12}$) laser of 532 nm with a maximum intensity of 25 mW was used for excitation. The laser spot size was primarily defined by the laser wavelength (λ) and microscope objective being used, and the laser spot diameter (spatial resolution) can be roughly estimated by the (0.61λ /NA) with NA the numerical aperture of microscope objective. On the other hand, Raman scattering intensity (sensitivity) is proportional to the λ^{-4}. Therefore, a low wavelength laser offers high spatial resolution and sensitivity, and 532 nm laser was selected to achieve high spatial resolution and sensitivity for Raman measurements. Based on a 0.90/100x objective, the spatial resolution was 361 nm, which ~24% smaller than the typical bead's diameter.

Raman spectra were collected using an acquisition time of 5 s and an accumulation time of 3 s, and the SWIFT^{TM} ultra-fast Raman imaging mode in LabSpec 6 was used for Raman mapping with an acquisition time of 1 s and step size of ≤ 0.1 micron. SWIFT mapping can only be used for single window spectrum acquisition with a single accumulation. The

integrated Raman intensity (approx. 10 to 20 cm^{-1} "filters") around the distinct dominant Raman shift peaks of various microbeads was captured for generating the Raman false colour images.

3.3. Results and Discussion

3.3.1 Synthesis and characterization of polymer microbeads

Dispersion polymerization is an attractive method for preparing polymer beads with their diameters in the range of 1-15 μm [30]. The one-stage dispersion polymerization by simply mixing all reactants together followed by heating to a suitable polymerization temperature often leads to microbeads with exceptionally narrow size distribution due to its unique nucleation mechanism. However, preparation of monodisperse functionalized copolymer microbeads by dispersion copolymerization is more desirable for various end-use applications. The presence of co-monomers always disturbs the nucleation mechanism and broadens size distribution in the one-stage dispersion polymerization. In practical, delayed addition of functional co-monomers after the completion of nucleation stage can minimize broadening of microbead size distributions. Therefore, the two-stage dispersion polymerization was chosen to synthesise monodisperse copolymer microbeads with surface functional groups and unique Raman signatures.
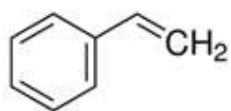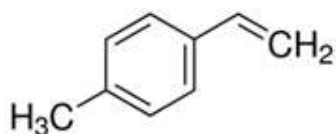
Styrene (Sty)   **4-tert-Butylstyrene (4tBS)**
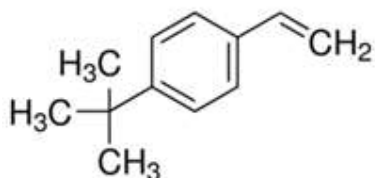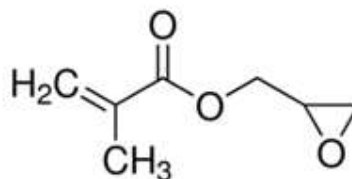
4-Methylstyrene (4MS)   **Glycidyl methacrylate (GMA)**

Scheme 1. Chemical structures of the monomers being used for various microbead synthesis.

SEM images of the copolymer microbeads prepared by two-stage dispersion polymerization are shown in Figure 3-1 with relevant monomer chemical structures in Scheme 1. From SEM images, it can be clearly observed the uniform size distributions of four different polymer beads with an average size of approximate 1.5 μm. Most importantly, these beads can be well-dispersed in water or ethanol for a few months without aggregation, which renders the synthesised beads to be stable enough for diverse analytical applications.
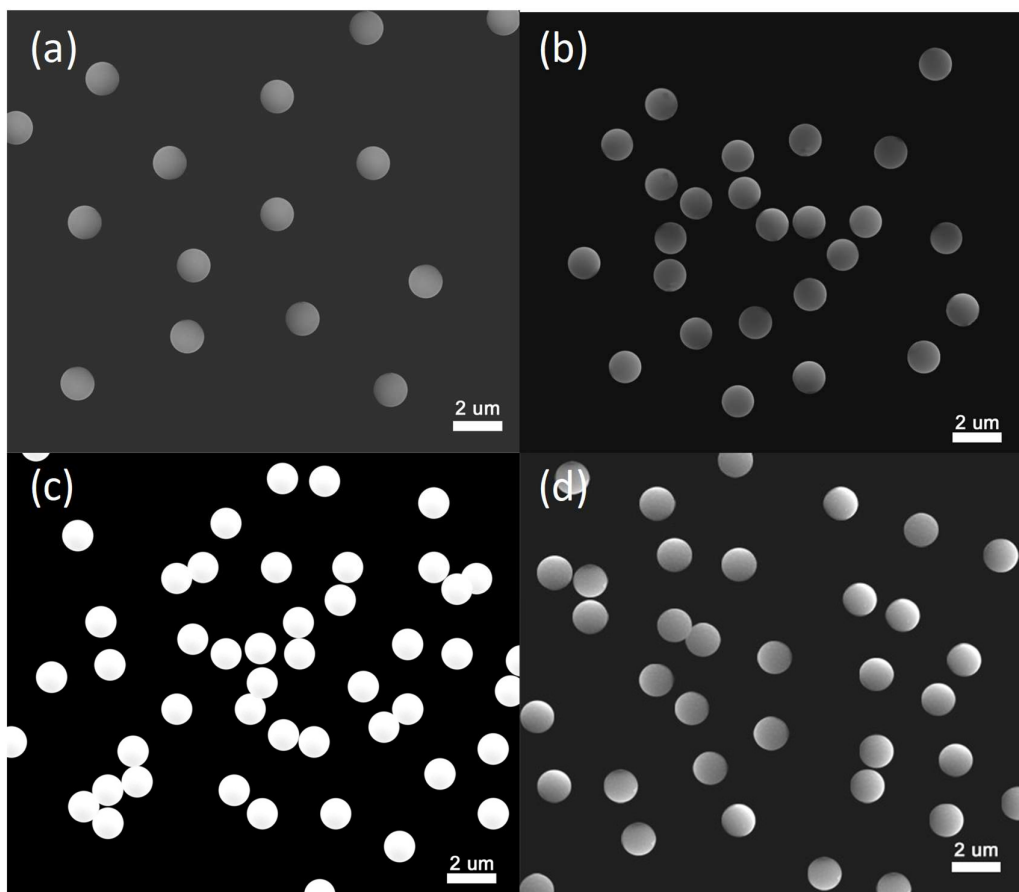
Figure 3-1. SEM images of the synthesised copolymers microbeads. (a) P(Sty-co-AA), (b) P(4tBS-co-AA), (c) P(4MS-co-AA) and (d) P(GMA-co-AA).

Mastersizer was further used to study the particle sizes and size distributions of polymer microbeads as shown in Figure 3-2. All synthesised polymer beads show narrow distributions with their average sizes of ~1.45 μm. The results from Mastersizer are identical to that from SEM, and the slight change in the apparent particle sizes from Mastersizer measurements is attributed to the formation of surface hydration layers, which enhances microbead stability in water.
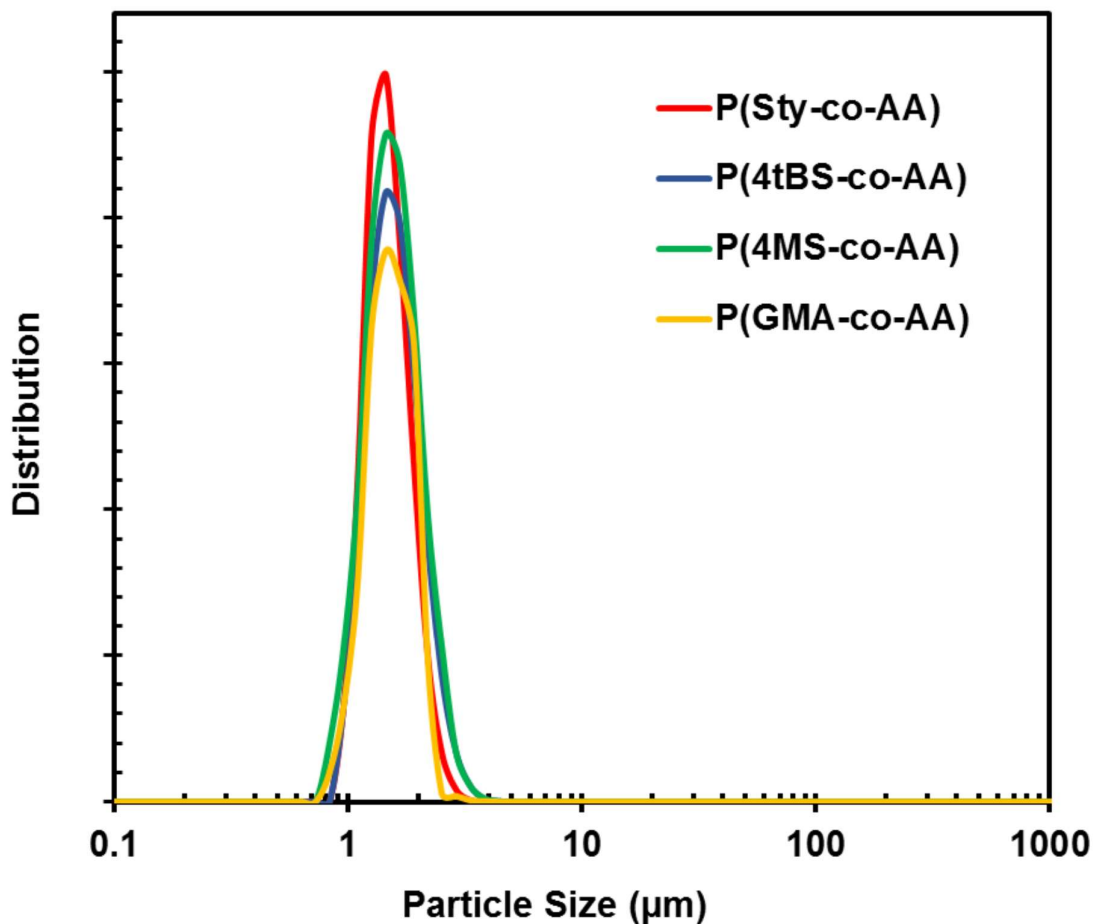
Figure 3-2. Sizes and size distributions of P(Sty-co-AA), P(4tBS-co-AA), P(4MS-co-AA) and P(GMA-co-AA) microbeads in water as measured by Mastersizer.

The presence of carboxylic acid groups on microbead surfaces was examined by potentiometric/conductometric titrations at room temperature (Figure 3-3). In pH titration curve, the presence of buffering range indicates the presence of weak acidic/basic groups on bead surface. In the conductometric titration curve, NaOH consumption between the two transition points can be used to quantify the amount of functional AA on microbead surface. For all microbeads, approximate 3 % of feed AA are located on surfaces. The presence of surface carboxylic acid not only increases microbead stability but also render their possibility for further surface modification.
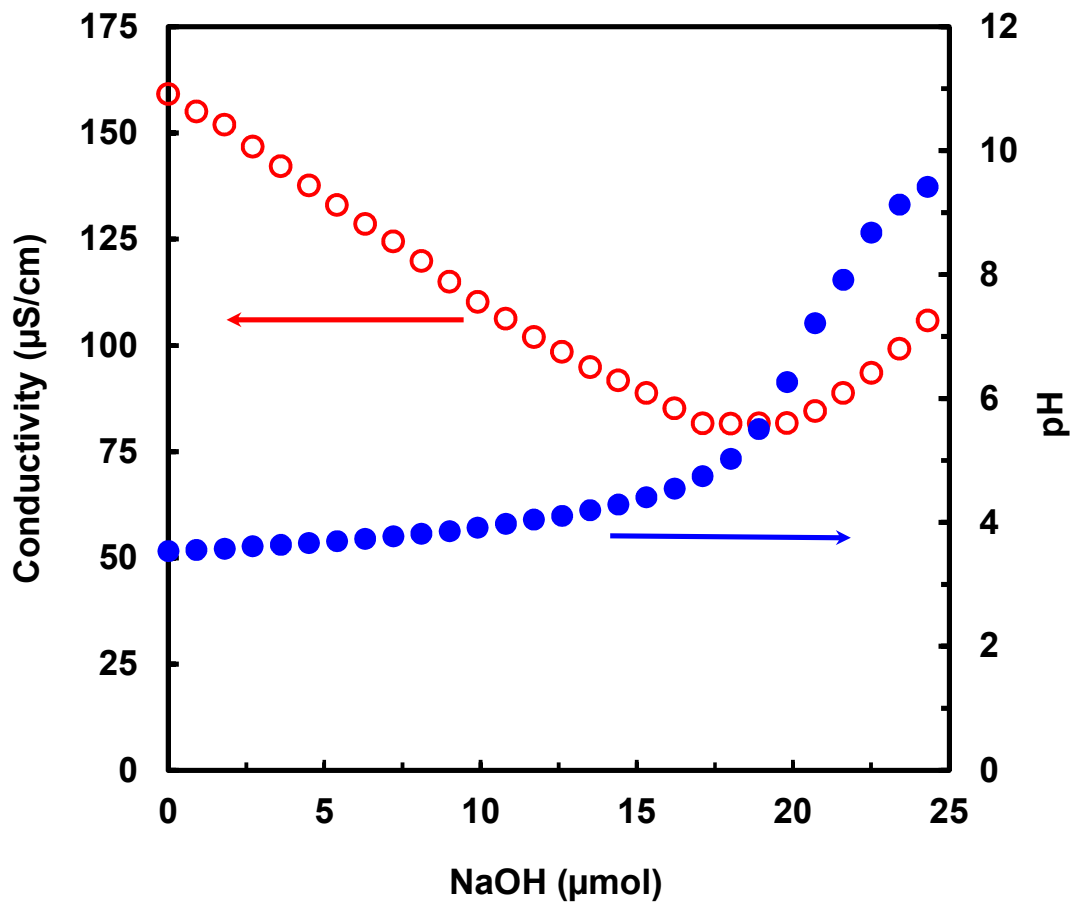
Figure 3-3. Potentiometric and conductometric titrations of P(Sty-co-AA) microbeads using standard NaOH at room temperature.

Given that the main purpose is to prepare monodisperse microbeads with distinct Raman signatures, Raman spectra of these microbeads were collected from the centre of individual beads from 400 to 1800 cm^{-1} with 100X, acquisition time of 5 s, accumulation time of 3 s and a confocal hole of 200. The distinct Raman shifts of these beads and detailed Raman vibrational peak assignments are summarized in Table 3-1.

Table 3-1. Comparison on the Raman vibrational bands of four copolymer microbeads.

Microbeads	Raman Shift (cm^{-1})	Intensity	Peak Assignment
P(Sty-co-AA)	1603	s	$\alpha+\beta$
	1584	m	$\alpha+\beta$
	1449	m	$\alpha+\beta$, $\delta_s(CH_2)$
	1328	w	β
	1199	m	$\upsilon(CC)+\alpha$
	1182	m	$\alpha+\beta$
	1154	m	$\alpha+\beta$
	1030	s	$\alpha+\beta$
	1000	s	α
	904	w	γ
	794	m	α
	760	w	γ
	620	s	α
P(4tBS-co-AA)	1630	s	$\gamma(829+826)$
	1611	s	$\alpha+\beta$
	1462	w	$\delta_a(CH_3)$
	1446	s	$\delta_s(CH_2)$
	1420	w	-
	1402	w	-
	1318	w	-
	1297	w	-
	1267	w	$\upsilon_a(CC\ in\ t\text{-}Bu)+rk(CH_3)$
	1200	s	$\upsilon(CC)+\alpha$
	1190	s	$\upsilon_s(CC\ in\ t\text{-}Bu)+rk(CH_3),\ \upsilon(CC)+\alpha$
	1107	s	$\upsilon_a(CC)$
	920	m	$\upsilon_s(CC)+rk(CH_3)$
	842	w	γ
	786	s	α
	688	m	α
	640	s	α
P(4MS-co-AA)	1614	s	$\alpha+\beta$
	1578	w	$\alpha+\beta$
	1448	s	$\delta_a(CH_3)$, $\delta_s(CH_2)$
	1377	s	$\delta_s(CH_3)$
	1324	w	-
	1303	w	-
	1202	s	$\upsilon(CC)+\alpha$
	1183	s	$\alpha+\beta$
	1084	m	-
	827	s	α
	807	s	α
	642	s	α
	398	w	-
	321	m	ϕ
P(GMA-co-AA)	1259	s	-
	1448	s	-

s, strong; m, medium; w, weak; α, in-plane ring deformation; β, in-plane ring bending; γ, out-of-plane ring bending; υ, stretch; rk, rocking; C, carbon in ring; C', carbon in chain; δ_s, symmetric deformation; δ_a, asymmetric deformation; ϕ, out of the plane ring deformation.

In detail, the characteristic strong bands of poly(Sty-co-AA) microbeads at 620, 1000, 1030 and 1603 cm^{-1} are assigned as α, α, α+β and α+β respectively [31] (Figure 3-4A). The typical Raman spectra of P(4tBS-co-AA) beads show the strongest vibrational peaks located at 640, 786, 1107, 1190, 1200, 1446, 1611 and 1630 cm^{-1} assigned to the α, α, v_a(CC), v_s(CC in *t*-Bu)+rk(CH$_3$), v(CC)+α, $δ_s$(CH$_2$), α+β and γ(829+826) (Figure 3-4B). The most intensified Raman bands of P(4MS-co-AA) are at 642, 807, 827, 1183, 1202, 1377, 1448 and 1614 cm^{-1} assigned to α, α, α, α+β, v(CC)+α, $δ_s$(CH$_3$), $δ_a$(CH$_3$) and α+β respectively (Figure 3-4C). Similarly, the most intensified Raman bands of P(GMA-co-AA) centre at 1259 and 1448 cm^{-1} (Figure 3-4D) [32]. From the Raman results, it is evident that the unique Raman spectra of these microbeads, might make them to be easily readout from Raman mapping so as to be used as an ideal label-free support in multiplex analysis.
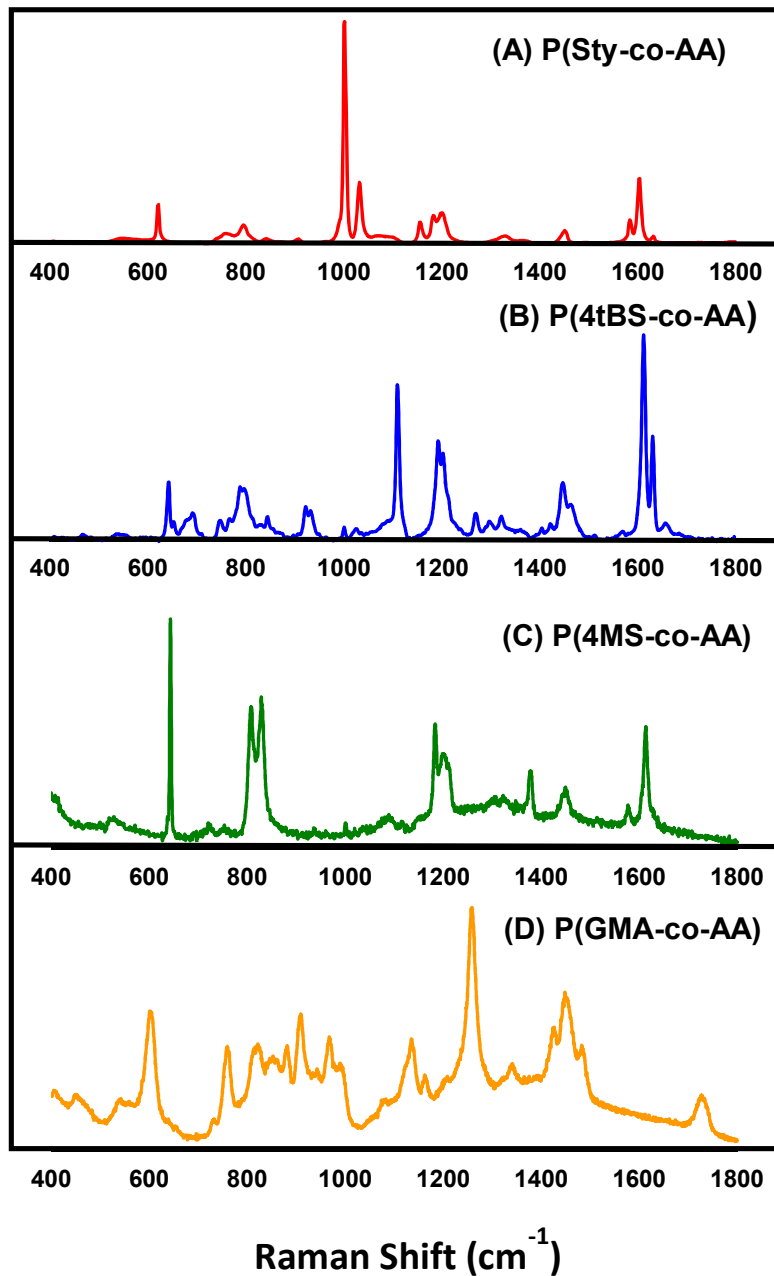
Figure 3-4. Raman spectra of polymer microbeads (A) P(Sty-co-AA), (B) P(4tBS-co-AA), (C) P(4MS-co-AA) and (D) P(GMA-co-AA).

3.3.2 Readout of microbeads from Raman mapping

Microbead mapping can be carried out using the peak identification technique with a single spectral window covering the fingerprint region of polymers from 975 to 1300 cm^{-1}. It was

found that using a medium resolution grating with 1800 groves per millimeter was sufficient to resolve the Raman features of the four different encoded microbeads. The increment between data points was 0.1 μm step size with an acquisition time was set to 1 s for better spatial resolution. The distinct peaks were marked between a cursor of 20 cm^{-1}. This permits ultra-fast mapping. The identification of the peaks at 1000, 1007, 1183 and 1259 cm^{-1} were used for mapping of P(Sty-co-AA), P(4tBS-co-AA), P(4MS-co-AA) and P(GMA-co-AA) separately (Figure 3-5). The brightness of the mapped beads is proportional to the intensity of the characteristic vibrational band in their relevant spectra. This is evident by the readout of these monodisperse beads under Raman mapping with identical bead sizes as SEM measurements. The successfully readout of various microbeads with different Raman signatures reinforces the broad applications of applying label-free spectroscopic-encoded beads for diverse applications to replace traditional fluorescence-labelled beads.
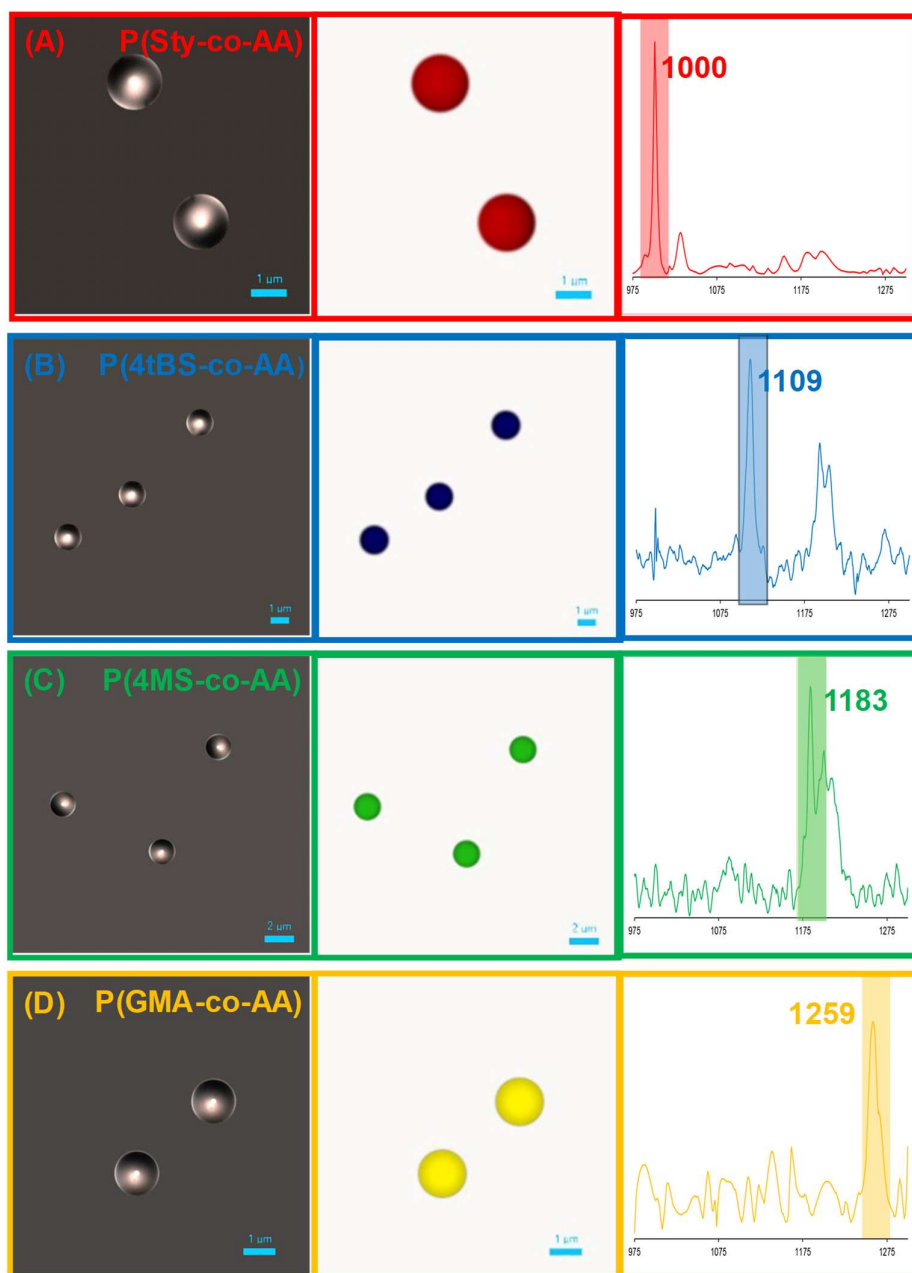
Figure 3-5. False coloured Raman mappings of individual polymer microbeads using the selected spectral region technique under the SWIFT mode: (A) P(Sty-co-AA), (B) P(4tBS-co-AA), (C) P(4MS-co-AA) and (D) P(GMA-co-AA).

3.3.3 Readout of microbead mixtures from Raman mapping using multivariate analysis technique

The narrow line-width of Raman spectra is critically important to identify peaks from multiple beads. Simultaneous detection of more than one type of microbeads in their mixture requires to use the multivariate analysis technique known as the Classical Least Squares (CLS) fitting. This supervised multivariate decomposition technique can also be used to identify the distribution of reference component spectra within a spectral array to create a profile/map based on component distribution. Therefore, within the same spectral window of 975 to 1300 cm^{-1}, Raman mapping of a mixture of the four polymer microbeads using CLS mapping was performed. 1800 gr/mm with 0.1-micron step size and an acquisition time of 1 s was used for better spatial resolution.
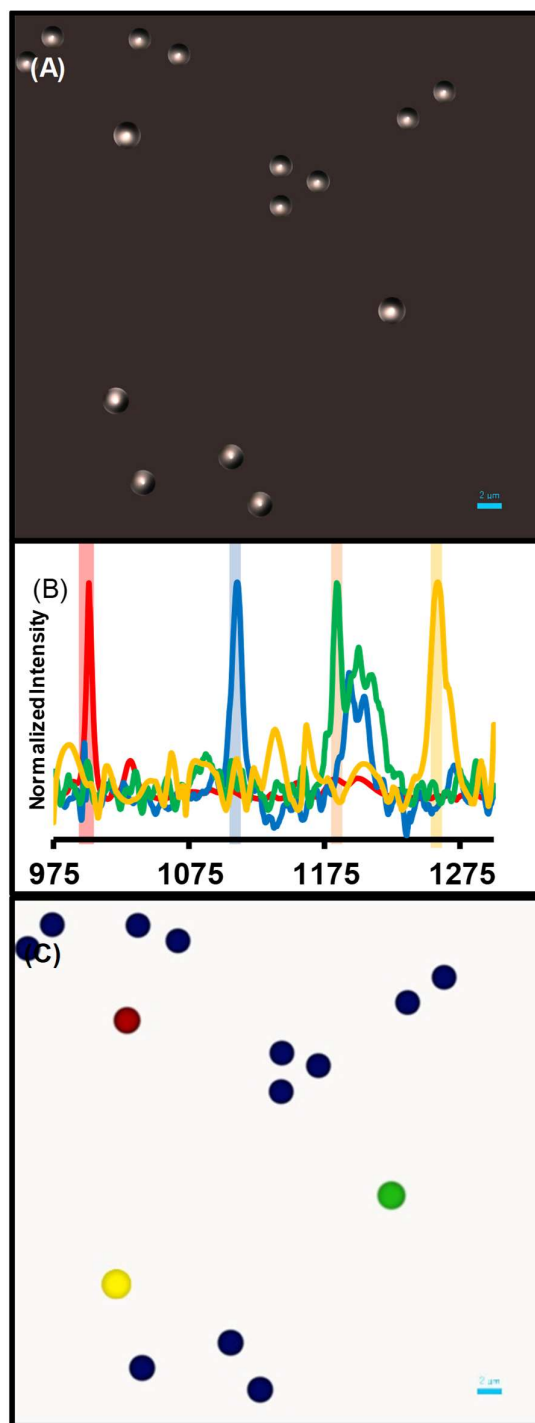
Figure 3-6. Communal (A) Optical image, (B) Raman spectra and (C) Raman mapping of a mixture of four polymer microbeads using the multivariate analysis technique with SWIFT mode: P(Sty-co-AA) in red colour, P(4tBS-co-AA) in blue colour, P(4MS-co-AA) in green colour and P(GMA-co-AA) in yellow colour.

From Figure 3-6A, monodisperse microbeads can be observed in the optical image, but this does not help identify individual beads from one another. Traditional approach to read these mixed beads is achieved by fluorescence labelling, but fluorescence labelling is associated with various limitations, such as changing surface property, photo-bleaching, and spectrum overlapping etc. Figure 3-6B reveal the typical Raman active bands of these polymer beads, which renders it possible to read beads in lieu of any labelling technique. Figure 3-6C indicates these microbeads can be clearly distinguished after being Raman mapped unambiguously. Most immortally, there is no Raman peak overlapping and thus significantly increase the sensitivity than fluorescence. It is noteworthy that the spatial resolution of polymer beads under the same experimental conditions depends on the intensity of their individual Raman bands. Therefore, the unequivocal mapping of microbeads with distinct Raman signatures (known as Raman-encoded microbeads) opens a venue for future simultaneous multiplex analysis.

3.4. Conclusion

Four monodisperse polymer microbeads with distinct Raman spectra were synthesised by two-stage disperse polymerization and systematically characterised using various analytical techniques. Besides their narrow particle size distributions, carboxylic acid function groups are presented on bead surfaces, which renders it possible for future surface modification or conjugation. These microbeads show distinguished Raman spectra, and thus are easily identifiable from Raman measurements. Due to unique Raman signatures and narrow Raman features of these microbeads, individual bead can be simultaneously identified from bead mixtures through high spatial resolution multiplex Raman mapping. Our study illustrates the promising application of these label-free and Raman-encoded microbeads as the support in modern bio-sensing and bio-imaging for ease and quick analysis of complex systems.

Acknowledgement

References

1.   Czarnik, A. W., Encoding methods for combinatorial chemistry. *Current Opinion in Chemical Biology* **1997,** *1* (1), 60-66.

2.   Brummel, C. L.; Lee, I.; Zhou, Y.; Benkovic, S. J.; Winograd, N., A mass spectrometric solution to the address problem of combinatorial libraries. *Science* **1994,** *264* (5157), 399-402.

3.   Xu, J.; Szakal, C. W.; Martin, S. E.; Peterson, B. R.; Wucher, A.; Winograd, N., Molecule-specific imaging with mass spectrometry and a buckminsterfullerene probe: application to characterizing solid-phase synthesized combinatorial libraries. *Journal of the American Chemical Society* **2004,** *126* (12), 3902-3909.

4.   Neilly, J.; Hochlowski, J., Elemental analysis of individual combinatorial chemistry library members by energy-dispersive X-ray spectroscopy. *Applied Spectroscopy* **1999,** *53* (1), 74-81.

5.   Yoo, S.-e.; Gong, Y.-D.; Seo, J.-s.; Sung, M. M.; Lee, S. S.; Kim, Y., X-ray photoelectron spectroscopy analysis of solid-phase reactions using 3-brominated Wang resin. *Journal of Combinatorial Chemistry* **1999,** *1* (3), 177-180.

6.   Yan, B.; Yan, H., Combination of single bead FTIR and chemometrics in combinatorial chemistry: Application of the multivariate calibration method in monitoring solid-phase organic synthesis. *Journal of Combinatorial Chemistry* **2001,** *3* (1), 78-84.

7.   Scott, R. H.; Balasubramanian, S., Properties of fluorophores on solid phase resins; implications for screening, encoding and reaction monitoring. *Bioorganic & Medicinal Chemistry Letters* **1997,** *7* (12), 1567-1572.

8.   Birtwell, S.; Morgan, H., Microparticle encoding technologies for high-throughput multiplexed suspension assays. *Integrative Biology* **2009,** *1* (5-6), 345-362.

9.   Hashimoto, M.; Araki, T.; Kawata, S., Molecular vibration imaging in the fingerprint region by use of coherent anti-Stokes Raman scattering microscopy with a collinear configuration. *Optics Letters* **2000,** *25* (24), 1768-1770.

10.   Adar, F.; Lee, E.; Mamedov, S.; Whitley, A., Raman imaging: Defining the spatial resolution of the technology. *Spectroscopy* **2006**.

11.   Fenniri, H.; Terreau, O.; Chun, S.; Oh, S. J.; Finney, W. F.; Morris, M. D., Classification of spectroscopically encoded resins by Raman mapping and infrared hyperspectral imaging. *Journal of Combinatorial Chemistry* **2006,** *8* (2), 192-198.

12.   Raez, J.; Blais, D. R.; Zhang, Y.; Alvarez-Puebla, R. A.; Bravo-Vasquez, J. P.; Pezacki, J. P.; Fenniri, H., Spectroscopically encoded microspheres for antigen biosensing. *Langmuir* **2007,** *23* (12), 6482-6485.

13.   Lai, Y.; Sun, S.; He, T.; Schlücker, S.; Wang, Y., Raman-encoded microbeads for spectral multiplexing with sers detection. *RSC Advances* **2015,** *5* (18), 13762-13767.

14.   Bravo-Vasquez, J. P.; Alvarez-Puebla, R. A.; Fenniri, H., Self-encoded polymer beads for microarray technologies. *Sensors and Actuators B: Chemical* **2007,** *125* (2), 357-359.

15.   Kage, D.; Fischer, L.; Hoffmann, K.; Thiele, T.; Schedler, U.; Resch-Genger, U., Close spectroscopic look at dye-stained polymer microbeads. *The Journal of Physical Chemistry C* **2018,** *122* (24), 12782-12791.

16.   Kroneková, Z.; Pelach, M.; Mazancová, P.; Uhelská, L.; Treľová, D.; Rázga, F.; Némethová, V.; Szalai, S.; Chorvát, D.; McGarrigle, J. J., Structural changes in alginate-based microspheres exposed to in vivo environment as revealed by confocal Raman microscopy. *Scientific Reports* **2018,** *8* (1), 1637.

17.   Ghosal, S.; Chen, M.; Wagner, J.; Wang, Z.-M.; Wall, S., Molecular identification of polymers and anthropogenic particles extracted from oceanic water and fish stomach–A Raman micro-spectroscopy study. *Environmental Pollution* **2018,** *233*, 1113-1124.

18.   Kang, H.; Jeong, S.; Koh, Y.; Cha, M. G.; Yang, J.-K.; Kyeong, S.; Kim, J.; Kwak, S.-Y.; Chang, H.-J.; Lee, H., Direct identification of on-bead peptides using surface-enhanced

Raman spectroscopic barcoding system for high-throughput bioanalysis. *Scientific Reports* **2015,** *5*, 10144.

19. Wang, Z.; Zong, S.; Wu, L.; Zhu, D.; Cui, Y., SERS-activated platforms for immunoassay: probes, encoding methods, and applications. *Chemical Reviews* **2017,** *117* (12), 7910-7963.

20. Singer, J. M.; Plotz, C. M., The latex fixation test: I. Application to the serologic diagnosis of rheumatoid arthritis. *The American Journal of Medicine* **1956,** *21* (6), 888-892.

21. Hughes, J. H.; Tuomari, A.; Mann, D.; Hamparian, V., Latex immunoassay for rapid detection of rotavirus. *Journal of Clinical Microbiology* **1984,** *20* (3), 441-447.

22. Prokopov, N. I.; Gritskova, I. A.; Cherkasov, V. R.; Chalykh, A. E. e., Synthesis of monodisperse functional polymeric microspheres for immunoassay. *Russian Chemical Reviews* **1996,** *65* (2), 167-180.

23. Lee, H.-L.; Weng, Y.-P.; Ku, W.-Y.; Huang, L. L., A nanobead based sandwich immunoassay. *Journal of the Taiwan Institute of Chemical Engineers* **2012,** *43* (1), 9-14.

24. Blais, D. R.; Alvarez-Puebla, R. A.; Bravo-Vasquez, J. P.; Fenniri, H.; Pezacki, J. P., Multiplex pathogen detection based on spatially addressable microarrays of barcoded resins. *Biotechnology Journal* **2008,** *3* (7), 948-953.

25. Xu, W.; Wu, F.; Jiao, Y.; Liu, M., A general micromechanical framework of effective moduli for the design of nonspherical nano-and micro-particle reinforced composites with interface properties. *Materials & Design* **2017,** *127*, 162-172.

26. Yu, B.; Chang, Z.; Zhang, Y.; Wang, C., Preparation and formation mechanism of size-controlled lignin based microsphere by reverse phase polymerization. *Materials Chemistry and Physics* **2018,** *203*, 97-105.

27. Wei, L.; Jin, B.; Dai, S., Polymer microbead-based surface enhanced Raman scattering immunoassays. *The Journal of Physical Chemistry C* **2012,** *116* (32), 17174-17181.

28.   Fitzgerald, J. E.; Zhu, J.; Bravo-Vasquez, J. P.; Fenniri, H., Cross-reactive, self-encoded polymer film arrays for sensor applications. *RSC Advances* **2016,** *6* (86), 82616-82624.

29.   Schlücker, S., Surface-Enhanced raman spectroscopy: Concepts and chemical applications. *Angewandte Chemie International Edition* **2014,** *53* (19), 4756-4795.

30.   Song, J.-S.; Chagal, L.; Winnik, M. A., Monodisperse micrometer-size carboxyl-functionalized polystyrene particles obtained by two-stage dispersion polymerization. *Macromolecules* **2006,** *39* (17), 5729-5737.

31.   Liang, C.; Krimm, S., Infrared spectra of high polymers. VI. Polystyrene. *Journal of Polymer Science* **1958,** *27* (115), 241-254.

32.   Fenniri, H.; Chun, S.; Ding, L.; Zyrianov, Y.; Hallenga, K., Preparation, physical properties, on-bead binding assay and spectroscopic reliability of 25 barcoded polystyrene-poly (ethylene glycol) graft copolymers. *Journal of the American Chemical Society* **2003,** *125* (35), 10546-10560.

Chapter 4   Synthesis and Spectroscopic Study of Dual-encoded Microbeads by Raman Scattering and Surface Enhanced Raman Scattering

Umar Azhar[1], Zeyad Alwahabi,[1]* Sheng Dai[1,2]*

[1] School of Chemical Engineering, the University of Adelaide, Adelaide, SA 5005, Australia

[2] Department of Chemical Engineering, Brunel University London, Uxbridge, UB8 3PH,

United Kingdom

Corresponding author:
sheng.dai@brunel.ac.uk; zeyad.alwahabi@adelaide.edu.au

ABSTRACT

The unique Raman spectra of various polymers render the polymer microbeads to be an attractive choice in Raman-based multiplex analysis and simultaneous biomolecular recognition as encoded supports. The combination of Raman microbeads with highly sensitive surface enhanced Raman scattering (SERS) codes will be able to significantly enhance the combinatory library for bioanalysis. However, there is lack study on the preparation and spectroscopic analysis of microbeads with both Raman and SERS signatures. This study established a robust synthesis protocol and spectral analysis of the microbeads with bi-codes viz., Raman and SERS. Surface functionalized monodisperse microbeads of polystyrene and poly(4-tetrabutylstyrene) were conjugated with the amine groups of 4-aminthiophenol, followed by the adsorption of gold nanoparticles (AuNP) on microbead surfaces. The thiol functional group of 4-aminthiophenol is able to form the self-assembled monolayers (SAM) with AuNPs. The resulting microbeads are dual (Raman and SERS) encoded as evident from the Raman spectroscopic and imaging analysis. The synthesis and spectroscopic analysis of the Raman and SERS dual-encoded systems suggest the potential expansion of multiplex library in suspension bioassays.

Keywords: Raman, SERS, microbeads, dual-encoding, dispersion polymerization, conjugation, Raman imaging

4.1 Introduction

Rapid simultaneous identification of multiple target analytes (typically biomolecules) with high sensitivity is of vital importance in modern bioanalysis [1-3]. For complex diseases, this helps in time apposite therapeutic treatment, curtailing the disease from spreading, limiting the side effects of long-term medications and/or surgeries. Existing diagnostic technologies for this purpose include ELISA (enzyme-linked immunosorbant assay) [4-5], printed microarrays [6-7], and serological tests. However, these methods suffer from drawbacks such as reproducibility, slow kinetics, intensive labor, poor flexibility and high costs [8]. Therefore, alternatives such as "encoding strategies based on polymer beads" are studied to subdue the limitation[9]. The polymer microbeads can either be self-encoded as proposed by Fenniri's group [10-11], or an external unique identifier such as molecular fluorophore markers [12-13], dyes [14], photonic crystals [15] or semiconductor quantum dots [16-17] can be conjugated to the beads. However, the use of these identifiers is usually impeded by issues like photobleaching, broad emission spectra, toxicity and surface modifications.

The co-accidental invention of surface enhanced Raman spectroscopy (SERS – an enhanced version of Raman spectroscopy) [18-20] opens up new avenues to overcome impediments of the aforementioned conventional encoding methods, offering high sensitivity, narrow emission spectra and photostability [21-23]. SERS has been reported to detect up to a single molecule with an effective enhancement factor of 10^{14-15} or more [24-25]. Moreover, the SERS phenomena uses a single laser source to induce localized surface plasmonic resonance (LSPR) in metal colloidal solutions conjugated with organic compounds to amplify their Raman signatures, collectively called "SERS tags". The SERS tag is usually accompanied by a protective coating of silica, which provides stability and enables further chemical modifications for bio-conjugation, but this layer also hinders the SERS intensity [26-28]. Recently, the spectroscopic analysis of these SERS tags, along with Raman encoded microbeads (BCR's - bar coded resins), has also been

investigated for application in in-vitro sandwich immunoassay [29-30]. More recently, to demonstrate the viability for multiplexing, spectroscopic imaging (31 different codes) using SERS tags has also been demonstrated. Here SERS images of polystyrene (PS) beads encoded by five different silica-encapsulated SAM-based SERS labels were used [31]. Nevertheless, these studies are limited to the analysis of spectrum and/or imaging using single labels that is SERS tag, only [32].

In this study, a more distinctive strategy is proposed for synthesis and multiplexing, by use of bi-labels without silica coating - Raman and SERS tag. Monodisperse microbeads (polystyrene and poly(4-tetrabutylstyrene)) were synthesized based on approaches reported earlier [29] and encoded by SERS label, followed by adsorption of AuNPs. Polymer microbeads acts as the solid support in this Raman and SERS dual encoded system [26, 33-34]. Three spatially distinct Raman peaks were used from the two polymer microbeads and SERS tags, respectively. These assisted in efficacious Raman/SERS imaging of PS and P4tBS microbeads encoded with a distinguishable single SERS tag corroborating the multiplexing capability of this approach. This marks the enhanced capability for multiplexing through aid of using one microbead to conjugate with different biomarkers or vice versa. This method also eliminates the tedious synthesis process and drawback of the silica protective coating. Synthesis and analysis of such encoding technique will help enhance the combinatory library for multiplexing in bioassays.

4.2 Experimental

4.2.1 Chemicals. Gold (III) chloride trihydrate ($HAuCl_4 \cdot 3H_2O$), 4-aminothiophenol (4-ATP), styrene, 4-tertbutylstyrene and polyvinylpyrrolidone (PVP 360000) were purchased from Sigma-Aldrich. Acrylic acid (AA), N-(3-dimethylaminopropyl)-N′-ethylcarbodiimide hydrochloride (EDC) and N-hydroxysuccinimide (NHS) were supplied by Acros. Tri-sodium

citrate dehydrate (Na$_3$Ct) was obtained from Prolabo. Deionized water (DI water, 18.2 MΩ·cm^{-1}) was obtained from an EASY pure II ultrapure water purification system.

4.2.2 Synthesis of Surface Functionalized Microbeads. Monodisperse PS and P4tBS microbeads with surface carboxyl functional groups were synthesised by the two-stage dispersion polymerisation technique [31]. In the first stage, the monomer (6.0 g styrene or 4-tertbutylstyrene), initiator (0.24 g AIBN), stabiliser (0.27 g PVP 360000), co-stabiliser (0.30 g 70 % Triton X-305) and 34 g 95 % ethanol were charged to a 250 mL three neck flask. The mixture was deoxygenated by nitrogen bubbling for 40 minutes at room temperature. The flask was merged into a pre-heated 70 °C oil bath and stirred mechanically at 100 rpm for one hour. In the second stage, the preheated co-monomer AA solution (2 wt % AA to the monomer, was mixed with 16 g 95 % ethanol) was added to the reaction flask. The reaction was continued for another 24 hours. After polymerisation, the conversion was determined by a gravity method. The obtained microbeads were washed three times with 95 % ethanol and four times with DI water. Finally, the microbeads were redispersed in DI water.

4.2.3 Preparation of AuNPs. A reduction of gold (III) chloride trihydrate using sodium citrate was used to prepare gold nanoparticles [35]. 50 mL of 10^{-3} M HAuCl$_4$·3H$_2$O were brought to the boil, followed by rapidly adding 1 wt% sodium citrate with a mixing molar ratio of 1:2. After continuously stirring at boiling temperature for 20 min, a red-colour gold colloidal solution was obtained.

4.2.4 Conjugation of SERS-tag to Microbead. SERS-tag molecule of 4-aminothiophenol was conjugated to PS or P4tBS microbeads by EDC/NHS chemistry. In detail, microbeads were first activated using EDC/NHS and then reacted with 4-ATP. 50 μL (5.25 mg per 50 μL) of PS–COOH or P4tBS-COOH was re-dispersed in 12 mL of HEPES buffer (pH 5.8) under stirring. 0.9427 mL of NHS (5.7545 mg in a 50 mL HEPES buffer) and 1.4153 mL of EDC (9.858 mg in a 50 mL HEPES buffer) were added into the microbead suspension and stirred

for 2 hours to allow NHS to react with the carboxyl groups. The microbeads were then washed to remove excess NHS/EDC and re-dispersed in HEPES. Subsequently, 1.4153 mL of 4-ATP (6.2595 mg in 50 mL ethanol) was added to the surface-activated microbead suspensions separately, whilst being stirred for 24 hrs. Finally, 200 µL AuNPs were added to form self-assembly monolayers with 4-ATP. The resulting SERS-tag labelled microbeads were washed and re-dispersed in water.

4.2.5 Instrumentation. Characterization of microbeads was performed using Malvern Mastersizer 2000, Zetasizer Nano S Dynamic Light Scattering System (DLS) and SEM Quanta 450 for particle size distribution, zeta potential and image analysis. The UV−vis absorption spectra of AuNPs, PS@SAM-AuNP and P4tBS@SAM-AuNP were recorded using a Shimadzu UV-1601 UV−vis spectrophotometer. Transmission electron micrographs of AuNPs were taken using a Phillips CM200 Transmission Electron Microscope (TEM) operating at an accelerating voltage of 160 kV. A Thermo Nicolet 6700 FTIR spectrometer with OMNIC software was used to record the FT-IR spectra of the microbeads. A LabRAM Horiba Raman microscope equipped with LabSpec 6 software was employed to measure the Raman spectrums and imaging of solid samples such as polymer microbeads, PS@SAM-AuNP and P4tBS@SAM-AuNP. 785 nm LASER line from a He–Ne source was used for excitation of the Raman spectrums and imaging with the monochromator comprising of 1800 grooves per mm grating. The Raman spectra were collected using an acquisition time of 5 seconds and an accumulation time of 3 seconds. The SWIFT mode in LabSpec 6 was used for Raman imaging with an acquisition time of 1 second and a step size of ≤ 0.1 micron. The integrated Raman intensity (approximately 10 to 20 cm^{-1} "filters") around the dominant Raman shift of the corresponding Raman solid substrate and the SERS-tag molecule were captured for generating the Raman false color images.

4.3 Results and Discussion

4.3.1 Gold Nanoparticles. AuNPs with a LSPR at 525 nm and an average diameter of around 20 nm (Figure 4-1) were synthesized. The presence of plenty citrate ions on nanoparticle surfaces keeps gold colloidal solution stable at room temperature, and these AuNPs have been reported to be able to from self-assembly monolayers with various thiol compounds (known as SERS-reporter) [36].
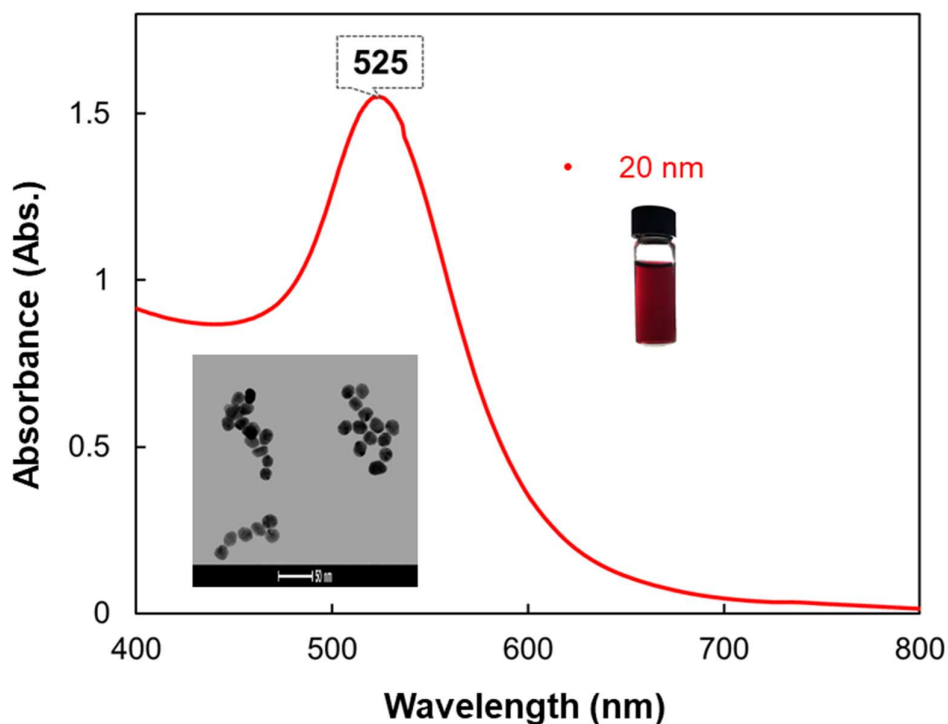
Figure 4-1. UV-vis adsorption spectrum of gold nanoparticles. The insets are the TEM image and the physical appearance of synthesized nanoparticles.

4.3.2 Polymer Microbeads. Polymer microbeads of PS and P4tBS were prepared by dispersion polymerization. SEM images show their narrow size distributions with an approximate diameter of 1.5 µm (Figures 4-2A & 4-2B). The particle size distributions of these microbeads were further examined by the Mastersizer, and it also reveals narrow distribution of these microbeads with median particle size of 1.45 micron (Figure 4-2C). Both SEM and

particle size results are closed to each other indicate the weak surface solvation of both polymer microbeads.
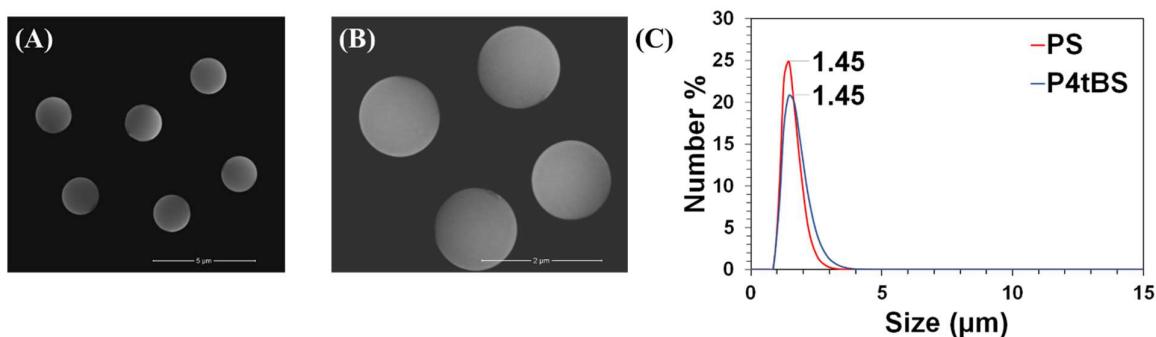
Figure 4-2. SEM images of (A) PS and (B) P4tBS microbeads. (C) the particle size distributions of both microbeads from Mastersizer measurement.

The presence of carboxylic acid group is vital for further conjugation, and the concentrations of COOH groups on the surfaces of both microbeads were examined by potentiometric/conductometric titrations (Figure 4-3). In the conductometric titration curves, the NaOH consumption between the two transition points can be used to quantify the amount of functional AA on microbead surface. For both microbeads, approximately 3 % of feed AA are located on their surfaces, rendering their possibility for further surface modification [37].
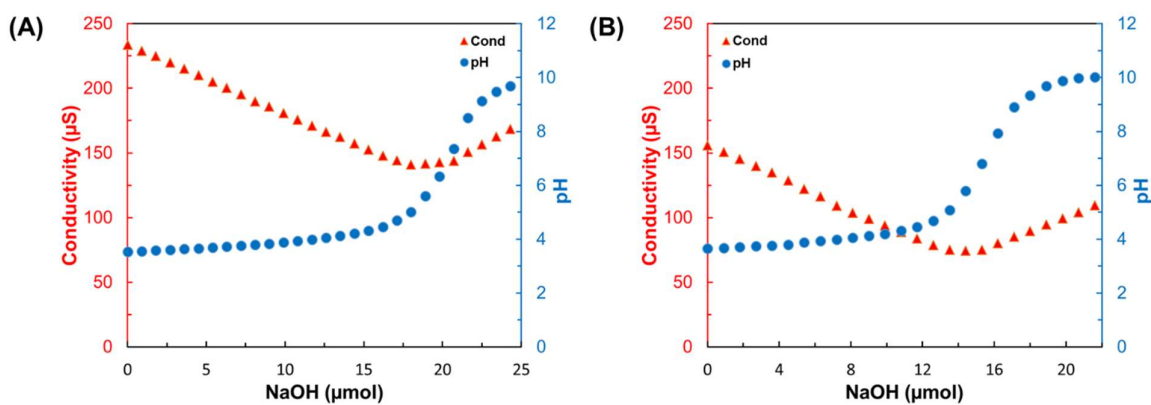
Figure 4-3. Potentiometric and conductometric titrations of (A) P(Sty-co-AA) and (B) P(4tBS-co-AA) microbeads using NaOH at room temperature.

The FTIR spectra of PS and P4tBS microbeads are shown in Figures 4-4. The pattern of the out-of-plane (oop) C–H bending bands in the region 900–675 cm^{-1} is characteristic of the aromatic substitution pattern, being intense at 697 and 757 cm^{-1}, assigned to υ_{11} (B2) and υ_{10B} (B2) bands respectively [38-41]. As FTIR spectroscopy is sensitive to hetero-nuclear functional group vibrations and polar bonds, carboxyl groups functionalized on the surface of the microbeads have a representation with a peak at 1655 cm^{-1} for PS microbeads and 1687 cm^{-1} for P4tBS microbeads [42]. The FTIR was also collected after EDC/NHS modification. It was evident of the conversion COOH to active O-acylisourea and O-acylisourea intermediates due to the omission of peaks at 1655 and 1687 cm^{-1} in the FTIR. The O-acylisourea and O-acylisourea intermediates will be able to conjugate 4-ATP to the surface of microbeads.
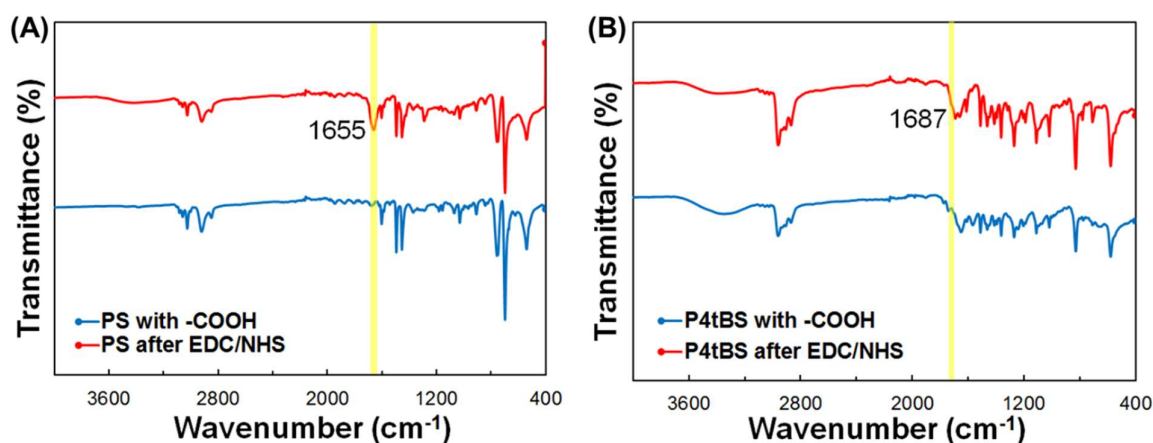
Figure 4-4. FTIR spectra of (A) polystyrene microbeads before and after EDC/NHS reaction and (B) poly (4-tetrabutylstyrene) microbeads before and after EDC/NHS reaction.

4-ATP is chosen as a model SERS-tag in this study, which has a ($-NH_2$) and a $-SH$ group. The amino group is able to attach to the above surface functionalized microbeads via EDC chemistry and the $-SH$ group can interact with AuNP to form SAM. The SAM on gold surface has been intensively studied [43-46], and it has been well-established that AuNPs prefer to interact with $-SH$ group. Thus, polymer microbeads with surface conjugated 4-ATP further allows

AuNP to self-assemble on the surface via Au−S bonds and provides SERS signatures besides Raman signals of microbeads.

The comparison on the Raman spectra is shown in Figure 4-5. The typical Raman spectrum of PS beads show distinct vibrational peaks located at 1002 cm^{-1}, which is assigned to a υ1 symmetrical ring and another peak related to the υ18A vibrations located at 1033 cm^{-1} [47]. Similarly, the typical Raman spectra of P4tBS beads shows distinct vibrational peaks located at 1109 cm^{-1} (strong) and 1611 cm^{-1} (very strong). Carboxyl groups before and after EDC/NHS conjugation on the surface of polymer microbeads cannot be observed in the Raman spectra, as Raman is more sensitive to homo-nuclear molecular and non-polar bonds. The Raman spectrum of 4-ATP as depicted in Figure 4-5 reveals two strong Raman peaks at 474 cm^{-1} and 1086 cm^{-1}, which correspond to the vibrational modes of γCCC and υCS, respectively [48-50]. The 4-ATP conjugation to microbeads cannot be evident from both FTIR and Raman spectra due to their small amount. However, small sized aromatic molecules with uniform orientation on AuNP surface can enable its own SERS signatures. After the formation of SAM of 4-ATP with AuNPs, the enhanced 4-ATP peaks at 474, 1086 and 1598 cm^{-1} can be clearly observed besides the PS & P4tBS peaks at 1002 and 1109 cm^{-1}, owing to the LSPR of AuNPs.
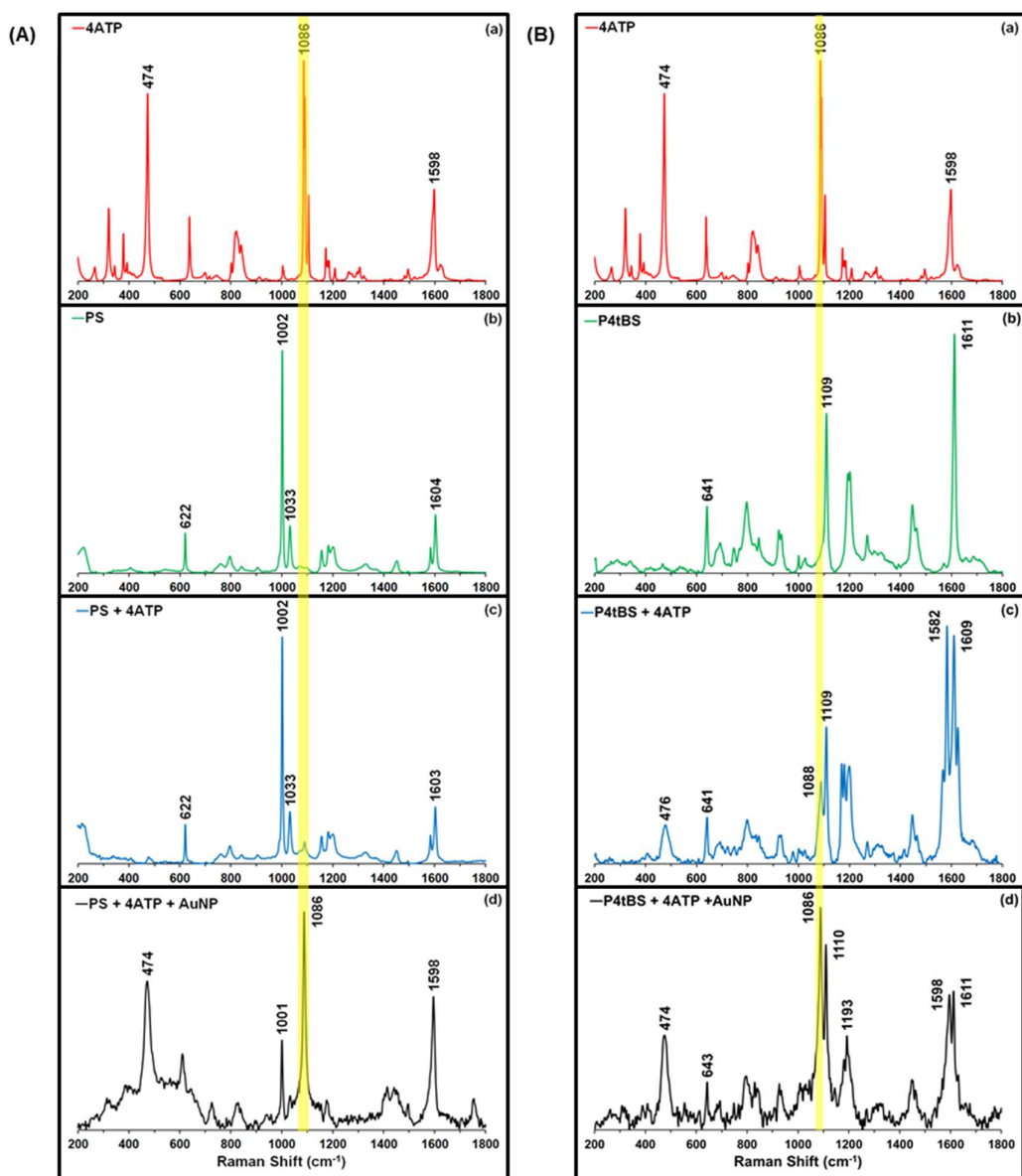
Figure 4-5. (A) Raman spectra of bulk 4-ATP (curve a), polystyrene microbeads (curve b), polystyrene microbeads after EDC/NHS conjugation with 4-ATP (curve c) and AuNP/4-ATP/PS (curve d). (B) Raman spectra of bulk 4-ATP (curve a), poly(4-tetrabutylstyrene) microbeads (curve b), poly(4-tetrabutylstyrene) microbeads after EDC/NHS conjugation with 4-ATP (curve c) and AuNP/4-ATP/P4tBS (curve d).

Functionalized microbeads can be further identified by a Raman optical microscopy with 100X magnification and then characterized by false-color Raman imaging. Figure 4-6

shows the imaging results obtained for two microbead mapping of PS and P4tBS. The false-color Raman image of the microbeads is achieved by integrating the Raman peak intensities between 997 and 1007 cm^{-1} for PS and 1104 and 1114 cm^{-1} for P4tBS, with a SWIFT mapping mode using a single spectral window between 950 and 1250 cm^{-1}, with a step size of 0.1 um and an integration time of 1 second. It was found that both optical and Raman false-color images show excellent overlapping correspondence and, more importantly, a homogenous distribution of the Raman signal across all microbeads. The normalized Raman spectrum of the microbeads is shown in Figure 4-6C, exhibiting the distinct peaks used for identification. In addition, there is no difference in the Raman images of both microbeads before and after EDC/NHS modification.
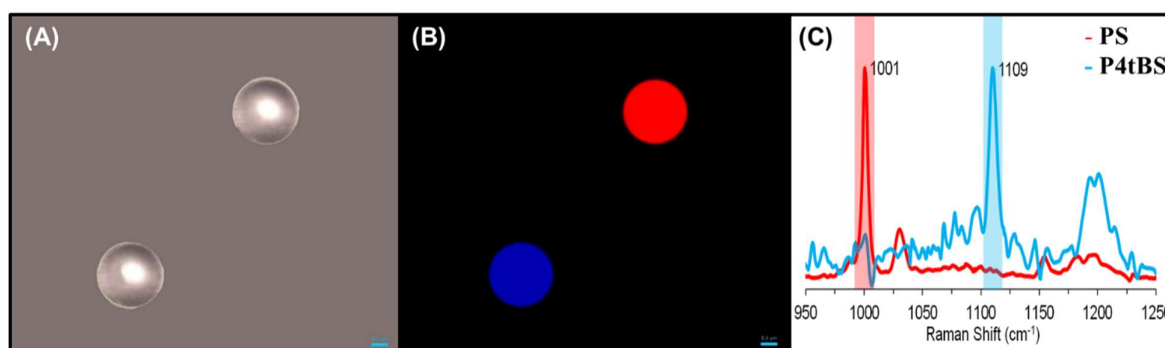
Figure 4-6. (A) An optical image, (B) false colour Raman imaging and (C) Raman spectra (C) a PS microbead and a P4tBS microbead.

4.3.3 Spectra and Images of Polymer Microbeads with Raman and SERS Dual Codes
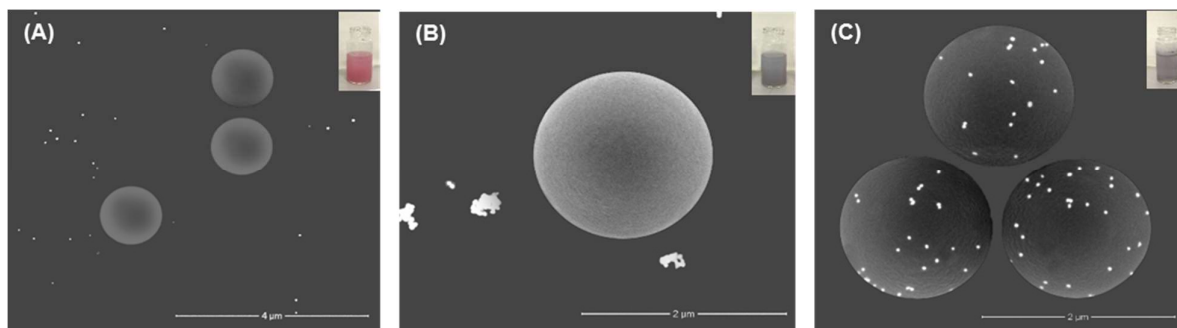
Figure 4-7. SEM images of (A) PS microbeads physically mixed with AuNP, (B) PS microbeads physically mixed with AuNP and free 4-ATP; (C) PS microbeads with 4-ATP being conjugated on surface physically mixed with AuNP. Insets are the colours of various suspensions.

4-ATP plays an important role to introduce AuNP and SERS to microbeads. In the absence of 4-ATP, weak AuNPs and microbeads interaction is observed in Figure 4-7A due to the electrostatic repulsion of these particles. In the condition of adding free 4-ATP to the mixture of microbeads and AuNPs, 4-ATP will form SAM with AuNPs, but they are not attached to microbead surface (Figure 4-7B). The attachment of 4-ATP on microbead surface is able to introduce AuNPs on microbead surface with random distribution and less aggregation (Figure 4-7C). Obviously, our approach is able to introduce AuNP as well as SERS signals to microbead surface in a controlled manner.
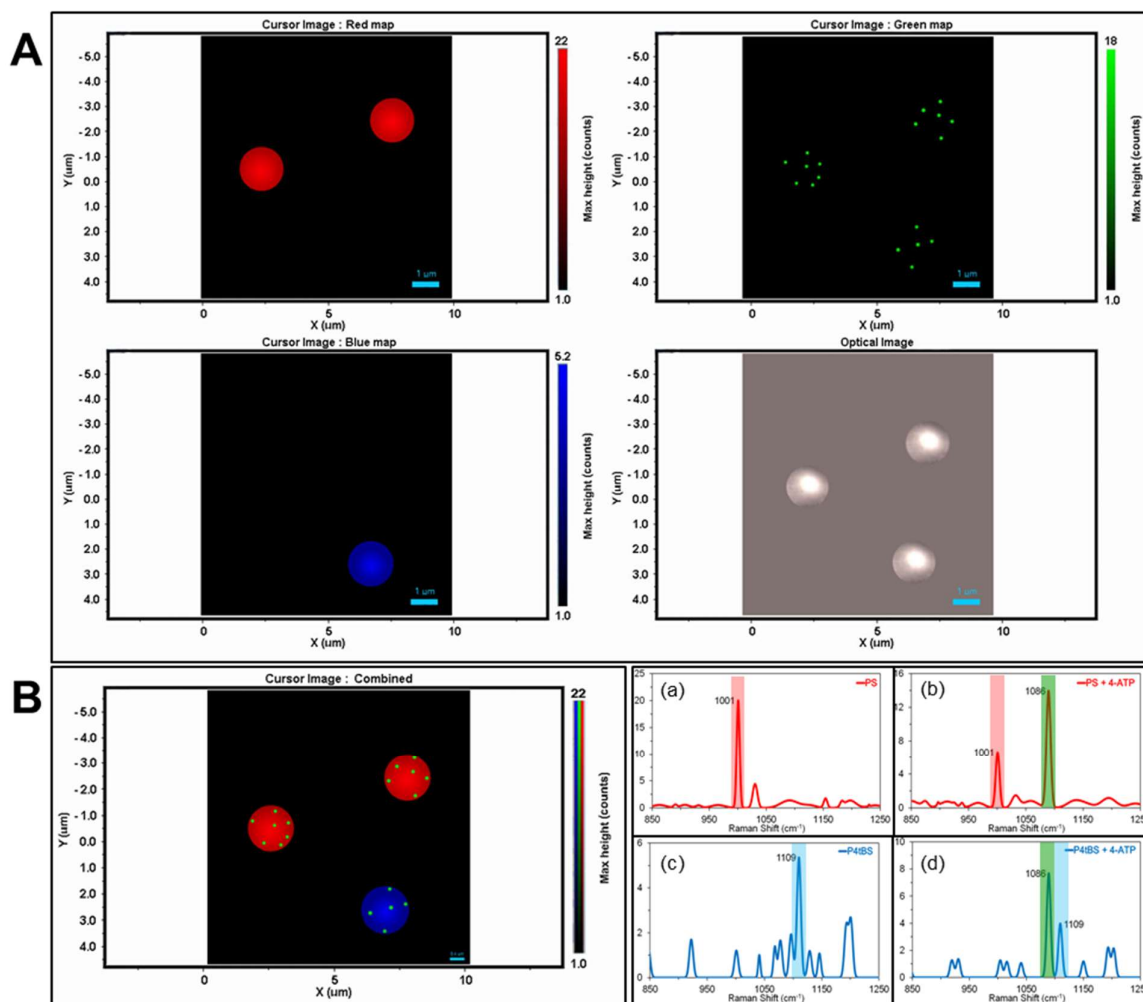
Figure 4-8. (A) Optical and false-coloured spectroscopic images of mixed PS microbeads (red), P4tBS microbeads (blue) and 4-ATP SERS tag (green). (B) Overlaying spectroscopic image of PS, P4tBS and 4-ATP SERS-tag with corresponding Gaussian deconvoluted Raman spectra of (a) PS, (b) PS + 4-ATP, (c) P4tBS, and (d) P4tBS + 4-ATP.

This study aims to report the preparation and spectroscopic imaging of dual Raman and SERS encoded microbeads. In Figure 4-8, a mixture of AuNP-modified microbeads is analyzed by optical and Raman mapping. The false-colored Raman images of PS and P4tBS are achieved by integrating the intensities between 995 and 1005 cm^{-1}, 1103 and 1113 cm^{-1}. The SERS images of 4-ATP@AuNPs is achieved by integrating the

intensities between 1075 and 1095 cm^{-1}. It was found that the false-color Raman mapping is able to distinguish these two microbeads rather than optical images. Homogenous distributions of Raman signals across all microbeads demonstrate the possibility of application these microbeads in single bead multiplex detection with good reproducibility and sensitivity. In addition, the Raman mapping of SERS-tag (4-ATP) shows random distribution of SERS-tag on polymer microbead surfaces. As such, Raman mapping of microbeads exhibiting the characteristic peak of the PS, P4tBS and 4-ATP stretching vibration at 1000.42 cm^{-1}, 1108.68 cm^{-1} and 1086 cm^{-1}. By selecting and deselecting distinct peaks of the two polymer microbeads and SERS-tag, these microbeads can be clearly depicted. Raman imaging clearly reveals the successful introduction of SERS signals to corresponding two microbeads. This approach is able to produce dual Raman and SERS encoded microbeads, which can expand based on different polymers and SERS tags for multiplexing in future immunoassays. The detailed protocol is described in Scheme 1.
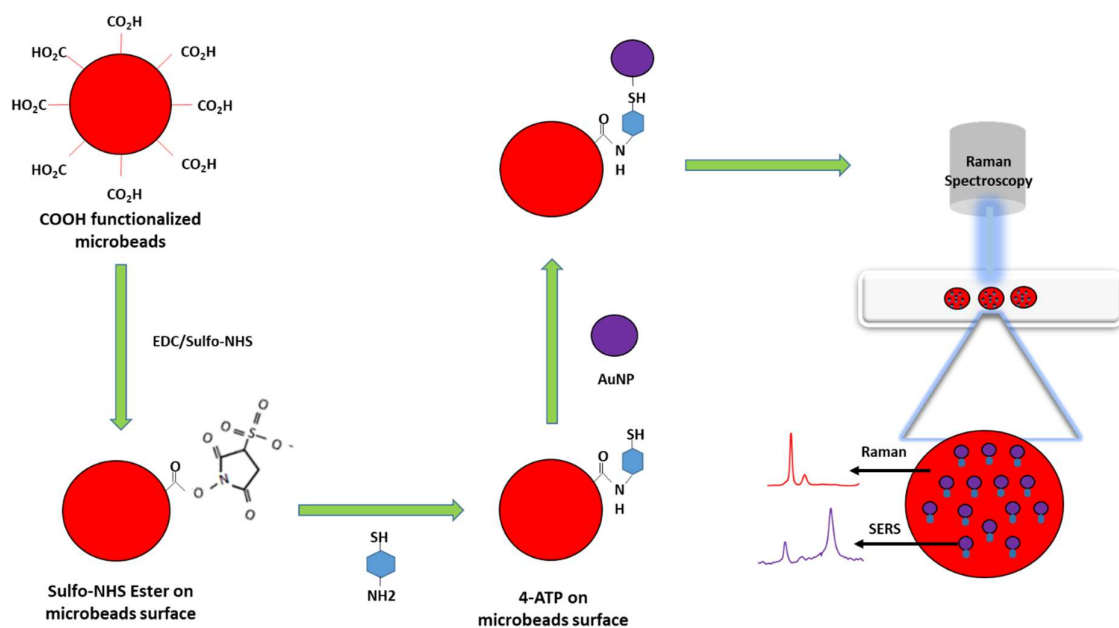
Scheme 1. Schematic description on the preparation of dual-encoded microbeads of Raman and SERS.

4.4 Conclusion

Two monodisperse microbeads were conjugated to a SERS tag, and positively characterized by Raman spectroscopy and imaging analysis. The carboxylic surface functionalized polymer microbeads were attached to the amine groups of the reporting molecules (4-ATP), while the thiol groups of 4-ATP were used to form the self-assembled layers of AuNP's. This synthesised dual encoder system comprising of two Raman microbeads and SERS tags, showed unique characteristic peaks at different wave numbers. This eased the readout of Raman and SERS tags simultaneously, by Raman spectrums and high-resolution multiplex imaging. Here, we successfully demonstrated synthesis, Raman spectroscopic and imaging analysis of bi-labels – Raman and SERS tags. This study promises a substantial increase in the current combinatorial library for label free multiplexing in bioassays.

References

1. Ng, P.; Tan, J. J.; Ooi, H. S.; Lee, Y. L.; Chiu, K. P.; Fullwood, M. J.; Srinivasan, K. G.; Perbost, C.; Du, L.; Sung, W.-K., Multiplex Sequencing of Paired-End Ditags (Ms-Pet): A Strategy for the Ultra-High-Throughput Analysis of Transcriptomes and Genomes. *Nucleic Acids Research* **2006**, *34*, e84-e84.

2. Boja, E.; Hiltke, T.; Rivers, R.; Kinsinger, C.; Rahbar, A.; Mesri, M.; Rodriguez, H., Evolution of Clinical Proteomics and Its Role in Medicine. *Journal of Proteome Research* **2010**, *10*, 66-84.

3. Lam, K. S.; Lebl, M.; Krchnák, V., The "One-Bead-One-Compound" Combinatorial Library Method. *Chemical Reviews* **1997**, *97*, 411-448.

4. Gearheart, L. A.; Ploehn, H. J.; Murphy, C. J., Oligonucleotide Adsorption to Gold Nanoparticles: A Surface-Enhanced Raman Spectroscopy Study of Intrinsically Bent DNA. *The Journal of Physical Chemistry B* **2001**, *105*, 12609-12615.

5. Gunnarsson, L.; Bjerneld, E. J.; Xu, H.; Petronis, S.; Kasemo, B.; Käll, M., Interparticle Coupling Effects in Nanofabricated Substrates for Surface-Enhanced Raman Scattering. *Appl. Phys. Lett.* **2001**, *78*, 802.

6. Miklos, G. L. G.; Maleszka, R., Microarray Reality Checks in the Context of a Complex Disease. *Nature Biotechnology* **2004**, *22*, 615-621.

7. Canales, R. D.; Luo, Y.; Willey, J. C.; Austermiller, B.; Barbacioru, C. C.; Boysen, C.; Hunkapiller, K.; Jensen, R. V.; Knight, C. R.; Lee, K. Y., Evaluation of DNA Microarray Results with Quantitative Gene Expression Platforms. *Nature Biotechnology* **2006**, *24*, 1115-1122.

8. Birtwell, S.; Morgan, H., Microparticle Encoding Technologies for High-Throughput Multiplexed Suspension Assays. *Integrative Biology* **2009**, *1*, 345-362.

9. Battersby, B. J.; Trau, M., Optically Encoded Particles and Their Applications in Multiplexed Biomedical Assays. *Australian Journal of Chemistry* **2007**, *60*, 343-353.

10. Fenniri, H.; Terreau, O.; Chun, S.; Oh, S. J.; Finney, W. F.; Morris, M. D., Classification of Spectroscopically Encoded Resins by Raman Mapping and Infrared Hyperspectral Imaging. *Journal of Combinatorial Chemistry* **2006**, *8*, 192-198.

11. Raez, J.; Blais, D. R.; Zhang, Y.; Alvarez-Puebla, R. A.; Bravo-Vasquez, J. P.; Pezacki, J.P.; Fenniri, H., Spectroscopically Encoded Microspheres for Antigen Biosensing. *Langmuir* **2007**, *23*, 6482-6485.

12. De Silva, A. P.; James, M. R.; McKinney, B. O.; Pears, D. A.; Weir, S. M., Molecular Computational Elements Encode Large Populations of Small Objects. *Nature Materials* **2006**, *5*, 787-789.

13. Battersby, B. J.; Bryant, D.; Meutermans, W.; Matthews, D.; Smythe, M. L.; Trau, M., Toward Larger Chemical Libraries: Encoding with Fluorescent Colloids in Combinatorial Chemistry. *Journal of the American Chemical Society* **2000**, *122*, 2138-2139.

14. Zhao, X.-W.; Liu, Z.-B.; Yang, H.; Nagai, K.; Zhao, Y.-H.; Gu, Z.-Z., Uniformly Colorized Beads for Multiplex Immunoassay. *Chemistry of Materials* **2006**, *18*, 2443-2449.

15. Cunin, F.; Schmedake, T. A.; Link, J. R.; Li, Y. Y.; Koh, J.; Bhatia, S. N.; Sailor, M. J., Biomolecular Screening with Encoded Porous-Silicon Photonic Crystals. *Nature Materials* **2002**, *1*, 39-41.

16.   Zhao, Y.; Shum, H. C.; Chen, H.; Adams, L. L.; Gu, Z.; Weitz, D. A., Microfluidic Generation of Multifunctional Quantum Dot Barcode Particles. *Journal of the American Chemical Society* **2011**, *133*, 8790-8793.

17.   Han, M.; Gao, X.; Su, J. Z.; Nie, S., Quantum-Dot-Tagged Microbeads for Multiplexed Optical Coding of Biomolecules. *Nature Biotechnology* **2001**, *19*, 631-635.

18.   Schlücker, S., Sers Microscopy: Nanoparticle Probes and Biomedical Applications. *ChemPhysChem* **2009**, *10*, 1344-1354.

19.   Raman, C. V.; Krishnan, K. S., A New Type of Secondary Radiation. *Nature* **1928**, *121*, 501-502.

20.   Fleischmann, M.; Hendra, P. J.; McQuillan, A., Raman Spectra of Pyridine Adsorbed at a Silver Electrode. *Chemical Physics Letters* **1974**, *26*, 163-166.

21.   Qu, H.; Lai, Y.; Niu, D.; Sun, S., Surface-Enhanced Raman Scattering from Magneto-Metal Nanoparticle Assemblies. *Analytica Chimica Acta* **2013**, *763*, 38-42.

22.   Schlücker, S., Surface-Enhanced Raman Spectroscopy: Concepts and Chemical Applications. *Angewandte Chemie International Edition* **2014**, *53*, 4756-4795.

23.   Lai, Y.; Wang, J.; He, T.; Sun, S., Improved Surface Enhanced Raman Scattering for Nanostructured Silver on Porous Silicon for Ultrasensitive Determination of 2, 4, 6-Trinitrotoluene. *Analytical Letters* **2014**, *47*, 833-842.

24.   Nie, S.; Emory, S. R., Probing Single Molecules and Single Nanoparticles by Surface-Enhanced Raman Scattering. *Science* **1997**, *275*, 1102-1106.

25.   Le Ru, E. C.; Meyer, M.; Etchegoin, P., Proof of Single-Molecule Sensitivity in Surface Enhanced Raman Scattering (Sers) by Means of a Two-Analyte Technique. *The Journal of Physical Chemistry B* **2006**, *110*, 1944-1948.

26. Jun, B.-H.; Kim, J.-H.; Park, H.; Kim, J.-S.; Yu, K.-N.; Lee, S.-M.; Choi, H.; Kwak, S.-Y.; Kim, Y.-K.; Jeong, D. H., Surface-Enhanced Raman Spectroscopic-Encoded Beads for Multiplex Immunoassay. *Journal of Combinatorial Chemistry* **2007**, *9*, 237-244.

27. Schütz, M.; Küstner, B.; Bauer, M.; Schmuck, C.; Schlücker, S., Synthesis of Glass-Coated SERS Nanoparticle Probes via SAMS with Terminal SiO_2 Precursors. *Small* **2010**, *6*, 733- 737.

28. Schütz, M.; Salehi, M.; Schlücker, S., Direct Silica Encapsulation of Self-Assembled-Monolayer-Based Surface-Enhanced Raman Scattering Labels with Complete Surface Coverage of Raman Reporters by Noncovalently Bound Silane Precursors. *Chemistry– An Asian Journal* **2014**, *9*, 2219-2224.

29. Wei, L.; Jin, B.; Dai, S., Polymer Microbead-Based Surface Enhanced Raman Scattering Immunoassays. *The Journal of Physical Chemistry C* **2012**, *116*, 17174-17181.

30. Xu, Y.; Wang, H.; Chen, B.; Liu, H.; Zhao, Y., Emerging Barcode Particles for Multiplex Bioassays. *Science China Materials* **2018**, 1-36.

31. Lai, Y.; Sun, S.; He, T.; Schlücker, S.; Wang, Y., Raman-Encoded Microbeads for Spectral Multiplexing with Sers Detection. *RSC Advances* **2015**, *5*, 13762-13767.

32. Wang, Z.; Zong, S.; Wu, L.; Zhu, D.; Cui, Y., SERS-Activated Platforms for Immunoassay: Probes, Encoding Methods, and Applications. *Chemical Reviews* **2017**, *117*, 7910-7963.

33.   McCabe, A. F.; Eliasson, C.; Prasath, R. A.; Hernandez-Santana, A.; Stevenson, L.; Apple, I.; Cormack, P. A.; Graham, D.; Smith, W. E.; Corish, P., Serrs Labelled Beads for Multiplex Detection. *Faraday Discussions* **2006**, *132*, 303-308.

34.   Abdelrahman, A. I.; Ornatsky, O.; Bandura, D.; Baranov, V.; Kinach, R.; Dai, S.; Thickett, S. C.; Tanner, S.; Winnik, M. A., Metal-Containing Polystyrene Beads as Standards for Mass Cytometry. *Journal of Analytical Atomic Spectrometry* **2010**, *25*, 260-268.

35.   Turkevich, J.; Stevenson, P. C.; Hillier, J., A Study of the Nucleation and Growth Processes in the Synthesis of Colloidal Gold. *Discussions of the Faraday Society* **1951**, *11*, 55-75.

36.   Ni, J.; Lipert, R. J.; Dawson, G. B.; Porter, M. D., Immunoassay Readout Method Using Extrinsic Raman Labels Adsorbed on Immunogold Colloids. *Analytical Chemistry* **1999**, *71*, 4903-4908.

37.   Abdelrahman, A. I.; Dai, S.; Thickett, S. C.; Ornatsky, O.; Bandura, D.; Baranov, V.; Winnik, M. A., Lanthanide-Containing Polymer Microspheres by Multiple-Stage Dispersion Polymerization for Highly Multiplexed Bioassays. *Journal of the American Chemical Society* **2009**, *131*, 15276-15283.

38.   Torres, F. J.; Civalleri, B.; Pisani, C.; Musto, P.; Albunia, A. R.; Guerra, G., Normal Vibrational Analysis of a Trans-Planar Syndiotactic Polystyrene Chain. *The Journal of Physical Chemistry B* **2007**, *111*, 6327-6335.

39.   Torres, F. J.; Civalleri, B.; Meyer, A.; Musto, P.; Albunia, A. R.; Rizzo, P.; Guerra, G., Normal Vibrational Analysis of the Syndiotactic Polystyrene S (2/1) 2 Helix. *The Journal of Physical Chemistry B* **2009**, *113*, 5059-5071.

40.   Liang, C.; Krimm, S., Infrared Spectra of High Polymers: Part Ix. Polyethylene Terephthalate. *Journal of Molecular Spectroscopy* **1959**, *3*, 554-574.

41.   Chen, G.; Liu, S.; Chen, S.; Qi, Z., Ftir Spectra, Thermal Properties, and Dispersibility of a Polystyrene/Montmorillonite Nanocomposite. *Macromolecular Chemistry and Physics* **2001**, *202*, 1189-1193.

42.   Roghani-Mamaqani, H.; Haddadi-Asl, V.; Khezri, K.; Salami-Kalajahi, M., Polystyrene-Grafted Graphene Nanoplatelets with Various Graft Densities by Atom Transfer Radical Polymerization from the Edge Carboxyl Groups. *RSC Advances* **2014**, *4*, 24439-24452.

43.   Weisbecker, C. S.; Merritt, M. V.; Whitesides, G. M., Molecular Self-Assembly of Aliphatic Thiols on Gold Colloids. *Langmuir* **1996**, *12*, 3763-3772.

44.   Garg, N.; Carrasquillo-Molina, E.; Lee, T. R., Self-Assembled Monolayers Composed of Aromatic Thiols on Gold: Structural Characterization and Thermal Stability in Solution. *Langmuir* **2002**, *18*, 2717-2726.

45.   Barriet, D.; Yam, C. M.; Shmakova, O. E.; Jamison, A. C.; Lee, T. R., 4-Mercaptophenylboronic Acid Sams on Gold: Comparison with Sams Derived from Thiophenol, 4-Mercaptophenol, and 4-Mercaptobenzoic Acid. *Langmuir* **2007**, *23*, 8866- 8875.

46.   Vercelli, B.; Zotti, G.; Berlin, A., Star-Shaped and Linear Terthiophene-Thiol Self-Assembled Monolayers as Scaffolds for Gold Nanoparticles. *Chemistry of Materials* **2007**, *19*, 443-452.

47.   Liang, C.; Krimm, S., Infrared Spectra of High Polymers. Vi. Polystyrene. *Journal of Polymer Science* **1958**, *27*, 241-254.

48. Osawa, M.; Matsuda, N.; Yoshii, K.; Uchida, I., Charge Transfer Resonance Raman Process in Surface-Enhanced Raman Scattering from P-Aminothiophenol Adsorbed on Silver: Herzberg-Teller Contribution. *The Journal of Physical Chemistry* **1994**, *98*, 12702-12707.

49. Ye, J.; Hutchison, J. A.; Uji-i, H.; Hofkens, J.; Lagae, L.; Maes, G.; Borghs, G.; Van Dorpe, P., Excitation Wavelength Dependent Surface Enhanced Raman Scattering of 4-Aminothiophenol on Gold Nanorings. *Nanoscale* **2012**, *4*, 1606-1611.

50. Kim, K.; Shin, D.; Lee, H. B.; Shin, K. S., Surface-Enhanced Raman Scattering of 4-Aminobenzenethiol on Gold: The Concept of Threshold Energy in Charge Transfer Enhancement. *Chemical Communications* **2011**, *47*, 2020-2022.

Chapter 5   Sensitive Multiplex Imaging for Raman/SERS-Dual Encoded Bioassays

Umar Azhar[1], Zeyad Alwahabi[1], Sheng Dai[1,2]*

[1]School of Chemical Engineering, the University of Adelaide, Adelaide SA 5005 Australia

[2]School of Engineering, Newcastle University, Newcastle upon Tyne NE1 7RU United Kingdom
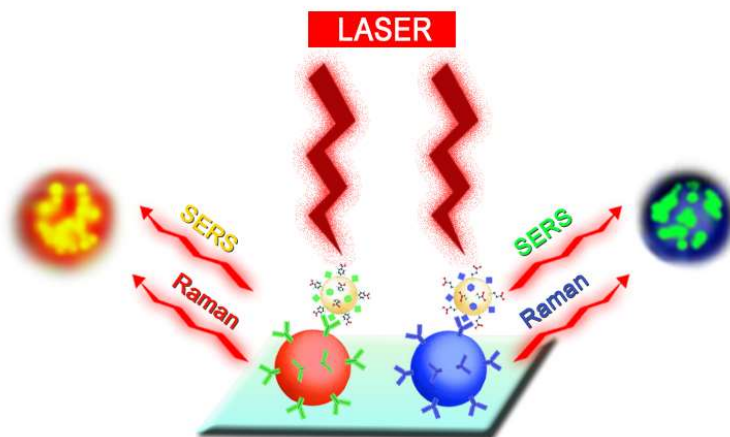
* Corresponding author: sheng.dai@ncl.ac.uk

Abstract

Suspension microsphere immunoassays are rapidly gaining recognition in multiplex bioassays. Accurate detection of multiple analytes from a single sample is critical in modern bioanalysis, which always requires complex encoding systems. In this study, a Raman and surface enhanced Raman scattering (SERS) dual coding system was developed as a model multiplex immunoassay for Raman mapping. The developed homogeneous immunoassays include two functional Raman-encoded polymer microbeads, two gold nanoparticle (AuNPs) and its self-assembled SERS-encoded reporters. The two microbeads, polystyrene and poly(4-tetrabutylstyrene) act as the immune solid support, whereas the IgG modified SERS nanotags (4-mercaptobenzoic acid and 3-mercaptopropionic acid) are used as the SERS reporters. Such Raman/SERS-based immunoassays are able to selectively identify the specific antibody-antigen interaction under a single laser illumination. Due to the presence of SERS, the detection limit can be significantly improved. As a result, it might hold great promise in future biomedical analysis.

5.1. Introduction

Cancer is one of the most malignant diseases of modern era, still lacking a cure. Accurate diagnosis of such diseases at the earliest stage is vital to curtail the side effects of surgical procedures, subsequently followed by costly treatment. Typically, infectious or immune-system-related diseases generate various antigens as the first sign of abnormality in organism. The most representative method for analyses of such disease biomarkers is immunoassays, realized by the immune recognition between antigens (IgG's) and relevant specific antibodies. In clinical applications, diseases as complex as cancer always necessitate multiplex diagnostics that is to simultaneously analyse multiple analytes from a single sample. Hence, high sensitivity and high throughput are the desired features of the development of multiplex immunoassays. According to the signal readout schemes, immunoassays for IgG's can be divided into several categories, including enzyme-linked immunosorbent assays (ELISA),[1-3] chemiluminescence,[4-5] colorimetric,[6-7] fluorescence,[8-9] surface plasmon resonance (SPR),[10-11] and surface-enhanced Raman scattering (SERS),[12-13] etc. Traditional biological detection strategies like ELISA and fluorescence are popularly used in clinical applications, but they suffer from some shortcomings, such as high background noise, high spectral overlap, low sensitivity and photobleaching. Amongst these technologies, SERS-based immunoassays have found profound applications in the detection of IgG's. SERS has shown great promise in biomolecular analysis, as it only requires a little amount of body fluids (e.g., blood, urine, ascites, and saliva) allowing repetitive and timely examinations without any anatomic form of tissues. SERS-based immunoassays achieve low limit of detection (LOD), large dynamic range and high sensitivity due to the enhanced Raman signals offered by Raman reporter molecules adsorbed on noble metal nanoparticles.[14-16] Also, the full width at half wavelength (FWHW) of a Raman peak is much narrower than that of fluorescence dyes. Therefore, the interference caused by

overlapping broad emission spectra will be greatly decreased between different SERS encoding elements, which makes it an efficient encoding element in multiplex bioassays.

To date, SERS-based immunoassays have been well-employed in biochemical and biomedical applications for the detection of various biological targets, such as proteins,[17-19] nucleic acids,[20-21] virus,[22] cells,[23-24] and toxins.[25] This type of biomolecular recognition uses an immuno-functionalized SERS nanoprobe to recognize target analytes. In a typical SERS encrypting method, distinct emission signatures can be obtained by selecting different Raman reporters or their combinations.[26] As such, series of SERS tags has been developed for multiplex bioassays.[27-35] Nevertheless, the encoding capacity of SERS tags is still limited. Therefore, to fulfil the requirements of high sensitivity and large dynamic detection range, the combined advantages of SERS tags with other encoding elements is intriguing for the development of new multiplex bioassays.

Among the different SERS-based immunoassays techniques, the bead-based SERS immunoassay has gained exponential recognition in recent years. As compared to the well-established bead-based fluorescence/SER immunoassay, the bead-based Raman/SERS immunoassay has shown obvious advantages such as fluorescence label-free, narrow vibration spectra, high sensitivity and single excitation wavelength, in turn offering higher multiplexing capability. Recent spectroscopic studies by Raez et al. and Wei et al. have shown use of Raman or IR encoded polymer beads not only as a platform for immune support but also as a second reporter.[36-37]

Here, Raman imaging is presented for a novel dual encoded multiplex bioassay system based on Raman encoded polymeric microbeads and SERS encoded nanotags. As illustrated in Figure 5-1, the SERS-encoded nanotags were prepared by the self-assembly of functional SERS-active molecules to gold nanoparticle (AuNP) surfaces, and the SERS-encoded reporters were obtained from SERS-encoded nanotags and antigens. On the other hand, the capture antibodies

were immobilized onto Raman-encoded polymer microbeads. In an immunocomplex mixture of functionalized SERS reporters and Raman microbeads, Raman imaging's at different vibration Raman bands allowed accurately identify these analytes. Our results showed the ability of applying Raman imaging for multiplex bioanalysis with high sensitivity and high specificity. It holds great promise for future applications in multiplexing, high throughput screening and detection of complex human diseases.
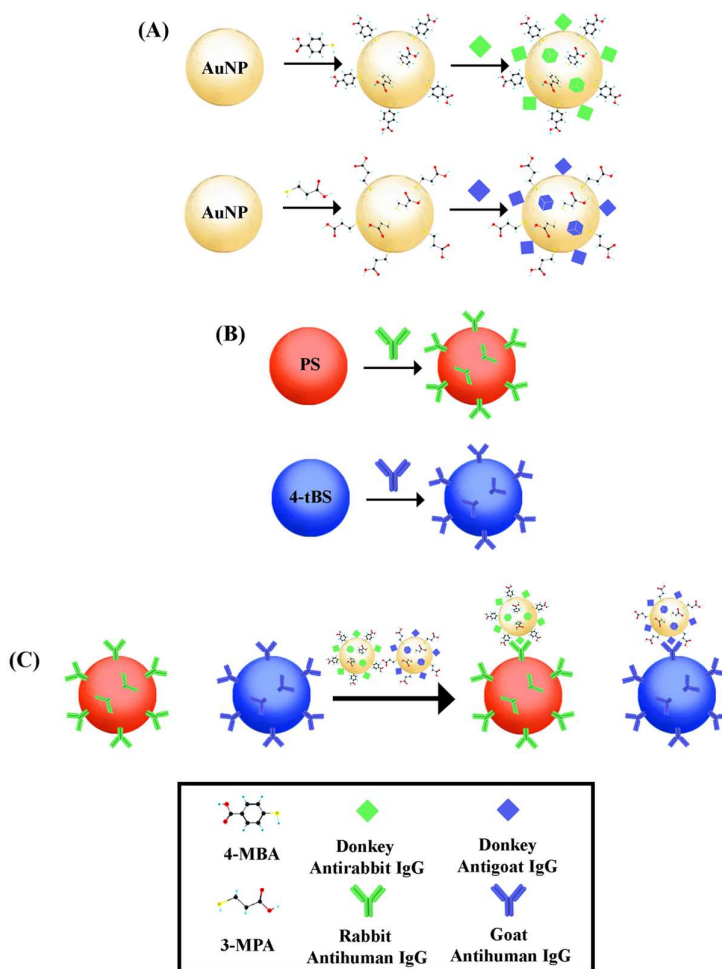
Figure 5-1. Schematic description on the preparation of SERS-encoded reporters (A), Raman-encoded microbeads (B) and resulting multiplex immunoassays (C).

5.2. Materials and Methods

5.2.1 Materials

Gold (III) chloride trihydrate (HAuCl$_4$·3H$_2$O), 4-mercaptobenzoic acid (4-MBA), 3-mercaptopropionic acid (3-MPA), styrene, 4-tertbutylstyrene, polyvinylpyrrolidone (PVP 360000) and bovine serum albumin (BSA) were purchased from Sigma-Aldrich. Acrylic acid (AA), 2,2'-Azobis(2-methylpropionitrile) (AIBN), N-(3-dimethylaminopropyl)-N'-ethylcarbodiimide hydrochloride (EDC) and N-hydroxysuccinimide (NHS) were supplied by Acros organics. Tri-sodium citrate dehydrate (Na$_3$Ct) was obtained from Prolabo. AffiniPure donkey antirabbit IgG, AffiniPure donkey antigoat IgG, AffiniPure rabbit antihuman IgG, AffiniPure goat antihuman IgG were obtained from Jackson ImmunoResearch (PA). Hydroxylamine (1M), phosphate-buffered saline (PBS, 0.01 M sodium phosphate, 0.25 M NaCl, pH 7.6), block solution (50 mM Tris, 0.14 M NaCl, 1% BSA, pH 8) and wash solution (50 mM Tris, 0.14 M NaCl, 0.05% Tween 20, pH 8) were prepared in-house. Deionized water (DI water, 18.2 MΩ·cm^{-1}) was obtained from an EASY pure II ultrapure water purification system.

5.2.2 Preparation of Raman-encoded microbeads

Monodisperse poly (styrene-*co*-AA) and poly (4-tetrabutlystyrene-*co*-AA) beads were synthesized following a two stage dispersion polymerization process.[38] In the first stage, the monomer (6.0 g styrene or 4-tertbutylstyrene), initiator (0.24 g AIBN), stabiliser (0.27 g PVP 360000), co-stabiliser (0.30 g 70 % Triton X-305) and 34 g 95 % ethanol were charged to a 250 ml three neck flask. The mixture was deoxygenated by nitrogen bubbling for 40 minutes at room temperature. The flask was merged into a pre-heated 70 ºC oil bath and stirred mechanically at 100 rpm for one hour. In the second stage, the preheated co-monomer AA solution (2 wt % of AA to the feed monomer was mixed with 16 g 95 % ethanol) was added to the reaction flask. The reaction was continued for a further 24 hours. To purify polymer

microbeads, the synthesised microbeads were washed three times with 95 % ethanol and four times with DI water to remove any reaction residual. Finally, the washed microbeads were redispersed in DI water. The solids contents of the microbead suspensions were obtained by gravity approach.

The functional carboxylic groups on microbead surface were used to conjugate antibodies by EDC/NHS chemistry. In a typical experiment, this was achieved by mixing 100 µl of 1.9 wt % purified microbeads (PS or P4tBS) and 100 µl of EDC/NHS/PBS (20 mg of EDC and 30 mg of NHS in 1 ml of phosphate buffer saline pH 7.4) were mixed for 15 min at room temperature, followed by the addition of 10 µg of model antibodies (e.g., donkey anti-rabbit IgG for PS and donkey anti-goat IgG for P4tBS). Incubate the mixture solution at room temperature for 2 hours with gentle rotation and then quenched using 1 M hydroxylamine. Washing the antibody-conjugated microbeads with phosphate buffer (0.01 M sodium phosphate, 0.25 M NaCl, pH 7.6) three times and blocked using 1 ml block solution (50 mM Tris, 0.14 M NaCl, 1 % BSA, pH 8) for 30 min at room temperature. Finally, washing microbeads four times using wash solution (50 mM Tris, 0.14 M NaCl, 0.05 % Tween 20, pH 8), and redisperse the antibody-conjugated microbeads in 100 µl DI water.

5.2.3 Preparation of SERS-encoded nanotags and SERS-encoded reporters

Reduction of gold (III) chloride trihydrate using sodium citrate was used to prepare the gold nanoparticles.[39] Briefly, 50 ml of 10^{-3} M $HAuCl_4 \cdot 3H_2O$ was brought to a boil, followed by rapidly adding 1 wt % sodium citrate with a mixing molar ratio of 1:2.[37] After continuously stirring at the boiling temperature, a red gold colloidal solution was obtained.

The SERS-encoded nanotags were prepared by the formation of different self-assembled monolayers (SAM) of functional thiols on AuNP surfaces. Here, the solutions of 4-MBA or 3-MPA (2.5 µl, 10^{-3} M), were added separately to 1 ml of the above AuNP suspensions, under vigorous stirring for 2 min at room temperature, and the mixture solutions turned purple. The

resulting SERS nanotags were washed three times by operating centrifugation (8000 rmp) and redispersion cycles, and finally redispersed in 100 µl DI water. Hereafter, two different sets of antigens (rabbit anti-human IgG and goat anti-human IgG) were separately coupled to perform SERS-encoded nanotags via ionic and hydrophobic interactions.[40] 5 mg antigens in phosphate buffer were separately charged to these 100 µl SERS-encoded nanotag suspensions under gentle rotation at room temperature for 2 hours. Then, 100 µl of 10 % BSA solution was added to the mixtures and rotated for another 30 min. Followed by three-time washing using DI water, the final antigen coupled SERS-encoded nanotags (i.e. SERS-encoded reporters) were redispersed in 100 µl DI water and stored at 4 °C.

5.2.4 Multiplex Immunoassays

50 µl of the two antibody-conjugated Raman-encoded microbeads solutions were separately mixed with the two antigen-conjugated SERS-encoded reporters, simultaneously. The four mixtures were incubated for 1 hour under gentle rotation at room temperature. After washing several times using DI water, they were redispersed in 50 µl DI water. The resulting immunocomplexes were subjected to Raman spectroscopic and Raman imaging analysis.

5.2.5 Equipment

The images of polymer microbeads and gold nanoparticles were performed by using Scanning Electron Microscopy (SEM - Quanta 450) and Transmission Electron Microscope (TEM - Phillips CM200). The UV−vis absorption spectra were recorded using a Shimadzu UV-1601, UV−vis spectrophotometer. A LabRAM Horiba Raman Microscope equipped with LabSpec 6 software was employed to measure Raman spectra and image polymer microbeads, SERS reporters and immunocomplexes. The 785 nm Xtra II diode laser from Toptica was used for Raman imaging with the monochromator comprising of 600 grooves per mm grating. The Raman spectrums were collected using an acquisition time of 5 seconds and an accumulation time of 3 seconds. The SWIFT mode in LabSpec 6 was used for Raman imaging with an

acquisition time of 1 second and a step size of ≤ 0.1 micron. The peak and CLS mode in the Raman microscope were used to generate the Raman false colour images to establish selective binding in the immunoassays.

5.3. Results and Discussion

5.3.1 Raman-encoded microbeads

Raman-encoded polymer microbeads were used as the immune solid support in the immunoassay system.[41-43] Dispersion polymerization was used for the synthesis of monodisperse polymer microbeads with an average size of approximately 1.5 μm (Figure 5-2), where a small amount of AA was introduced as the comonomer to generate carboxylic groups on the surface of microbeads. It has been established that under such experimental conditions (2 wt % of AA to the feed monomer with PVP 360000 stabiliser) using potentiometric and conductometric titrations that the quantity of carboxyl groups on the surface of synthesised polymer microbeads is approximate 11 % of the feed –COOH group from AA.[38] These functional groups not only promote microbead stability and narrow size distribution (CV < 1 %) but also allow further surface conjugation. The presence of carboxylic groups render the ability for the capture antibodies being immobilized on microbeads by covalent bonding via the EDC/NHS chemistry.
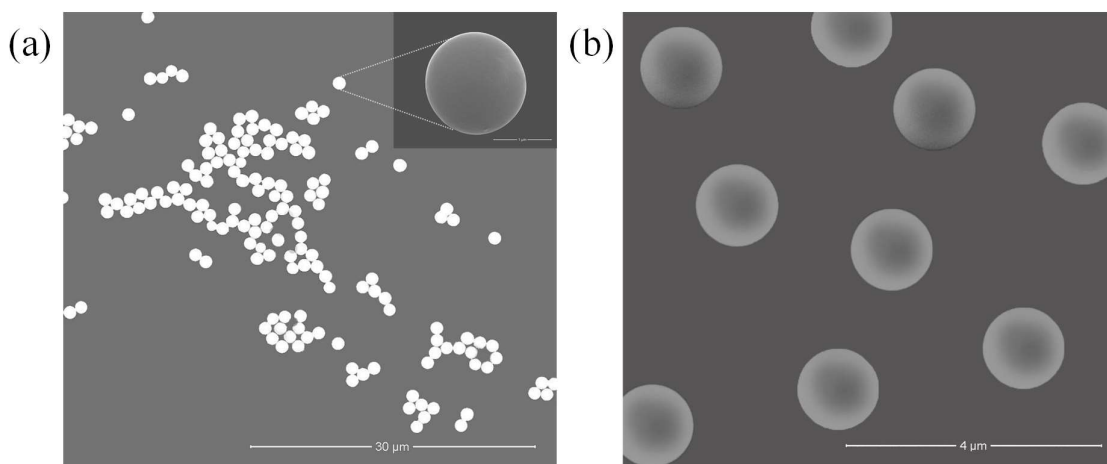
Figure 5-2. SEM images of monodisperse carboxylic functionalized PS (a) and P4tBS (b) microbeads.

Due to the presence of different monomers for the synthesis of polymer microbeads, various Raman spectral peaks will be visible, which render them to be suitable as the Raman coded support in bioanalysis. Since polymers are long chain molecules composed of huge amount of monomers connected to each other by covalent bonds, the Raman signals of polymer beads are strong. The Raman spectrum (Figure 5-3a) of PS beads shows a distinct vibrational peak centred at 1002 cm^{-1}(strong), which is assigned to the υ_1 symmetrical ring. Another peak related to the υ_{18A} vibration is located at the Raman shift of 1032 cm^{-1} (medium).[44] Similarly, the Raman spectrum of P4tBS beads shows distinct vibrational peaks located at 1109 cm^{-1} (strong) and 1611 cm^{-1} (very strong) (Figure 5-3b). Although carboxyl groups are functionalized on the surface of polymer microbeads, no Raman spectral representation for carboxyl group before and after EDC/NHS conjugation is evident, as Raman is sensitive to homo-nuclear molecular and non-polar bonds.
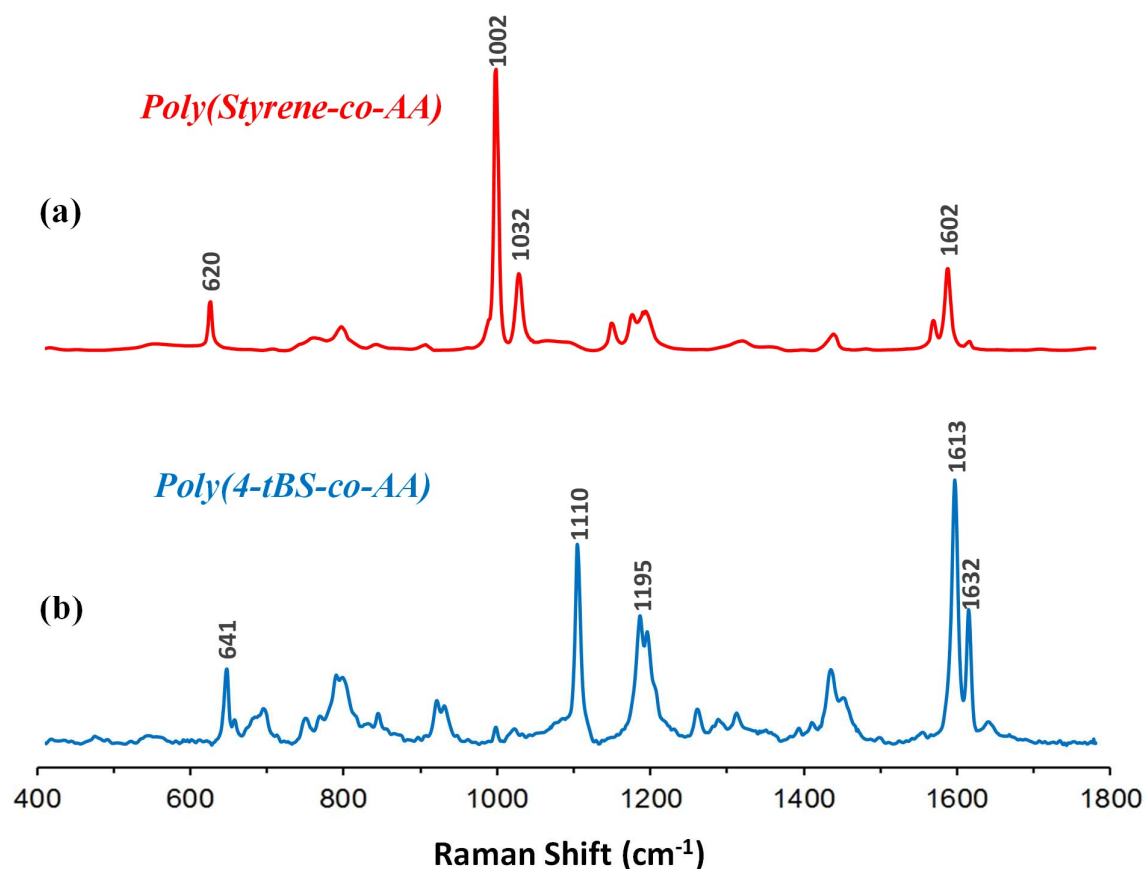
Figure 5-3. Raman spectra of the two Raman-encoded polymer microbeads. The most distinctive characteristic Raman shifts for each microbeads are marked.

5.3.2 SERS-encoded nanotags and SERS-encoded reporters

The detail of the SERS-encoded reporters is illustrated in Figure 5-1, where these SERS-encoded nanotags act as the SERS-codes in the reporters for immunoassay analysis after introduction of IgG. To prepare the SERS-encoded nanotags, we synthesized red colored AuNP solution using a feed molar ratio of 1:2 between $HAuCl_4.3H_2O$ and Na_3Ct. This ensures presence of sufficient citrate ions on the surface of AuNPs, keeping the colloidal solution stable at room temperature for several months.

The localized surface plasmon resonance (LSPR) of AuNPs were characterized by an UV-vis spectrophotometer, while the morphology being examined by TEM. The characteristic

absorption peak is observed at 525 nm, with an average size of approximately 25 nm (Figure 5-4a). Further, 4-MBA and 3-MPA were separately mixed with AuNPs to form the SERS-encoded nanotags. Both 4-MBA and 3-MPA, used in this study have carboxylic group (-COOH) and thiol group (-SH). AuNPs has strong affinity to their thiol groups.[45] 4-MBA and 3-MPA form self-assembled monolayer (SAM) on the surface of AuNPs via the Au-S bond as well as hotspots. An inevitable aggregation takes place after the formation of the SAM of tag molecules and AuNPs, due to the increase in surface hydrophobicity.[46] This aggregation forms "hotspots" and facilitates stronger SERS signals. It is also noted that the absorption peak red shifts to 536 nm upon addition of 4-MBA and 3-MPA.[47] This further signifies AuNP aggregation in solution and successful formation of SAM's. A TEM image was used to identify formation of SAM on AuNPs (Figure 5-4b), where a thin layer of few nm is observed on the surface of the aggregated AuNPs.

Antibodies, rabbit anti-human and goat anti-human were then introduced to the 4-MBA and 3-MPA SERS-encoded nanotags to form two distinct SERS-encoded reporters. The hydrophilic characteristic of the antibodies helps in enhancing the stability of AuNPs in aqueous solution. The LSPR of SAM AuNPs before and after the antibody's conjugation was recorded. There is no red shift after conjugation, validating no further aggregation. After conjugation, 10 % BSA was used as blocking solution for SERS-encoded reporters, and any unbounded antigens or BSA were removed by centrifugation and redispersion washing cycles with water.

The Raman spectrums were analysed using a Raman confocal microscopy. The Raman spectrum of bulk 4-MBA and the SERS spectra of 4-MBA on AuNPs before and after antigens introduction is shown in Figure 5-4c. The characteristic vibrational modes include the $\upsilon(CC)$ ring-breathing modes at 1074 and 1583 cm^{-1} for 4-MBA Raman and SERS (with & without IgG), while other less intense modes at the $\delta(CH)$ (1132 and 1173 cm^{-1}) and $\upsilon_s(COO^-)$ (1375 cm^{-1}) are observed in SERS spectra, but are below the signal-to-noise for the Raman spectrum

of bulk 4-MBA.[48-50] Similarly, the Raman spectrum of bulk 3-MPA, SERS spectra of 3-MPA on AuNPs with and without, IgG are shown in Figure 5-4d. All spectra are dominated by three distinct peaks at 674, 867 and 1430 cm^{-1}, which are assigned to the $\upsilon(CS)_G$, $\delta(SH)$ and $\delta(CH_2)$ characteristic vibrational modes.[51] We also observed that the SERS of the antigens is ignorable for both the SERS-encoded reporters (Fig. 4c & d), which indicates no direct interaction between AuNPs and these antigens.
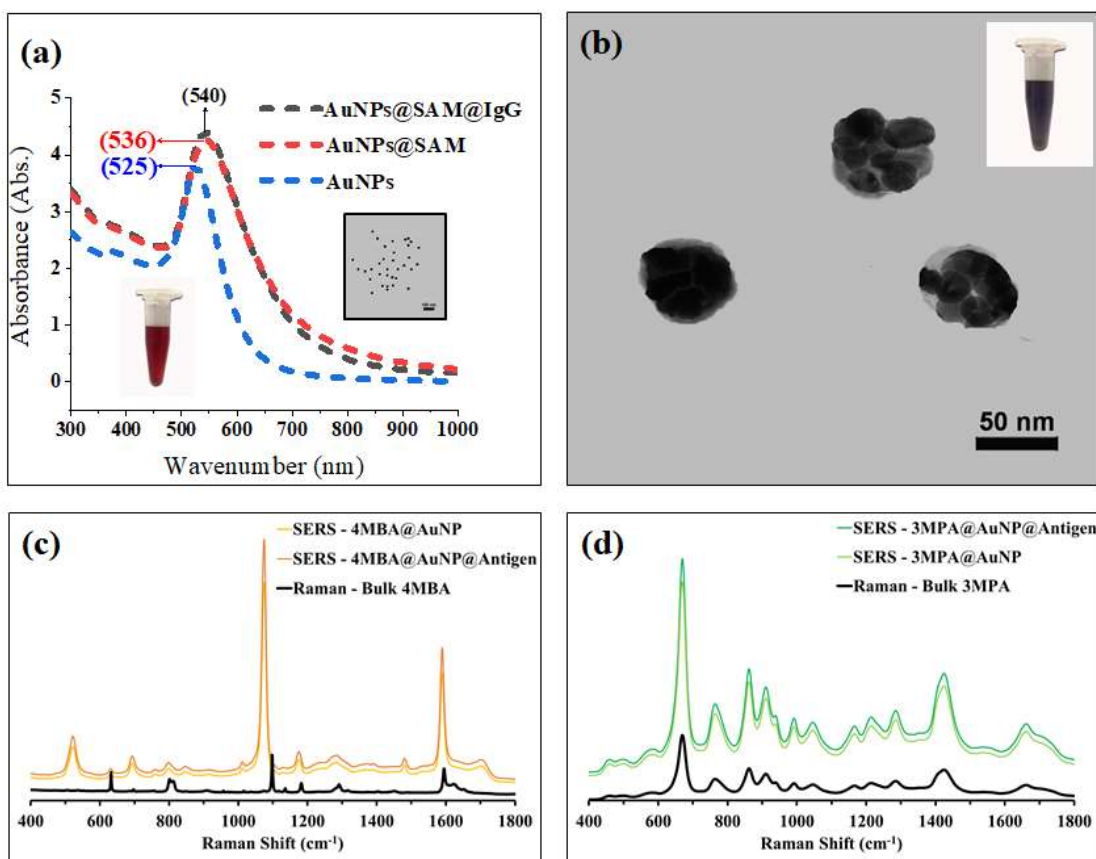
Figure 5-4. (a) TEM image (inset) and UV-vis absorption spectra of AuNP, UV-vis absorption spectra of AuNP@ SAM and AuNP@SAM@IgG. (b) TEM image of SERS nanotags, and (c & d) Raman spectra of SERS nanotags before and after antibody conjugation.

Since the most intensive peaks of 4-MBA and 3-MPA are separated with narrow bandwidths, the SERS signature can be easily distinguished, resulting in a straightforward SERS-encoded

nanotags. Moreover, as the Raman scattering cross-sections of the nanotags are much larger than ordinary molecules (4-MBA and 3-MPA), the intensities of Raman signals enhanced by AuNPs can reach a level of 10^6. That is much higher than background. The great increase in the signal-to-noise ratio is favourable for highly sensitive detection. In addition, the homologs of the Raman is beneficial for the high encoding capacity needed for high throughput analysis. The formed self-assembled gold colloid helps enhance the Raman signals of the 4-MBA and 3-MPA. Due to this enhancement effect of the SERS-encoded nanotags, it is possible to lower the concentration limit for IgG detection. The increase in the intensity of SERS signal to Raman signal is quantified by the effective enhancement factor (EEF). The EEF can be calculated using the following expression:

$$EEF = \frac{I_{SERS}\, N_{bulk}}{I_{bulk} N_{SERS}}$$

where I_{SERS} and I_{bulk} are the intensities of the same band for the SERS and bulk spectra, N_{bulk} is the number of molecules for a bulk samples, and N_{SERS} is the number of molecules in SERS.[52-53] Under the experimental condition, 2.5 μL 10^{-3} M of 4-MBA and 3-MPA was charged separately to 1 mL of 10^{-3} M AuNP aqueous solution to prepare the SAM. The calculated AuNP concentration is 3.12×10^{11} particles/mL with an average AuNP surface area of 1962.5 nm^2. The molar ratio for both 4-MBA and 3-MPA to AuNP is 1.92×10^3 or about 2.44 per nm^2 of AuNP surface. Using the band of 1074 cm^{-1} for 4-MBA, the EEF was calculated to be 1.08×10^6. Similarly, using the band of 674 cm^{-1} for 3-MPA, the EEF was calculated to be 1.25×10^7.

5.3.3 Multiplex assays

We aim to develop a novel bioassays for IgG detection using Raman-encoded microbeads and SERS-encoded reporters with details being shown in Figure 5-1. In this study, donkey anti-rabbit IgG, and donkey anti-goat IgG are considered model antibodies, while rabbit anti-human

IgG, and goat anti-human IgG are considered as model antigens. The PS and P4tBS microbeads were separately immobilized with donkey anti-rabbit and donkey anti-goat antibodies. On the other hand, rabbit anti-human IgG was fixed to the 4-MBA encoded SERS nanotag as the antigen of donkey anti-rabbit antibody, and the 3-MPA encoded SERS nanotag was decorated with the goat anti-human as the antigen of donkey anti-goat antibody. Due to the specific recognition between these paired antibodies and antigens, the SERS encoded nanotags should be used to report the matched antibody on microbead surfaces. In another words, in the presence of matched antibody-antigen pairs, both the code of Raman bands from the beads and the SERS signals from the nanotags can be read out simultaneously. Otherwise, only the Raman bands of the microbeads can be read in the presence of unmatched antibody-antigen pairs.

After mixing antibody-immobilized Raman microbeads and antigen-introduced SERS encoded reporters, the SEM images of these polymer microbeads were observed as shown in Figure 5-5. The SEM images clearly establishes bioconjugation of SERS-encoded reporters to Raman-encoded beads. However, in order to conclude the specific bio-recognition of antibodies conjugated Raman beads to its counterpart antigen conjugated SERS-encoded nanotags, we need to perform Raman spectrum and imaging analysis.
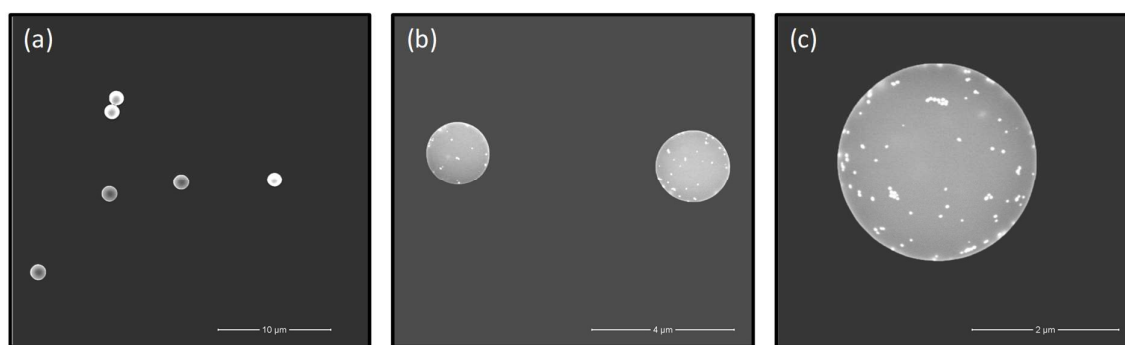
Figure 5-5. SEM images of polymer microbeads and the immunoassay. Low magnification image of the polymer microbeads (a), low magnification image of SERS-encoded reporters on the Raman-encoded beads surface. (b) and high magnification image of SERS-encoded reporters on the Raman-encoded beads surface.

The Raman and SERS spectra of the matched immunoassays are shown in Figure 5-6 (a & b). As mentioned earlier, the typical Raman spectrum of PS microbeads displays two strong vibrational bands at 1002 and 1032 cm^{-1}, whereas, the vibrational bands for 4-MBA SERS are located at 1074 and 1583 cm^{-1}. After the specific binding of the matched IgG functionalized microbeads (donkey anti-rabbit IgG) with AuNPs (rabbit anti-human IgG), both the Raman signals of PS microbeads and the SERS signals of 4-MBA can be observed. Similarly, the typical Raman spectrum of P4tBS microbeads displays two strong vibrational bands at 1110 and 1613 cm^{-1}, whereas, the vibrational bands of 4-MPA are located at 674 and 2576 cm^{-1}. Again, due to the specific binding of the matched IgG functionalized polymer microbeads (donkey anti-goat IgG) with AuNPs (goat anti-human IgG), both the Raman signals of P4tBS microbeads and the SERS signals of 3-MPA can be observed. In presence of unmatched antibody-antigen pairs, only the Raman signals of PS or P4tBS can be observed due to the lack of specific binding. These results demonstrate that SERS-reporters can selectively bind to microbeads through the specific matched antibody-antigen interaction, which indicates the system's high sensitivity and selectivity.

In addition, the Raman shifts are reproducible in our repeating experiments for polymer microbeads, SERS nanotags as well as the antibody coated polymer microbeads with the matched antigen coated AuNP@SERS reporters. However, the Raman intensity ratios of the polymer microbeads and SERS reporters are difficult to repeat since the effective enhancement factor of SERS is not a controlled parameter. The possible reasons might be attributed to the inhomogeneous distribution and orientation of the AuNPs@Raman reporters (4-MBA & 3-MPA) on the surface of the microbeads. However, the specific recognition of antibodies and antigens will be able to be examined by the Raman mapping technique.
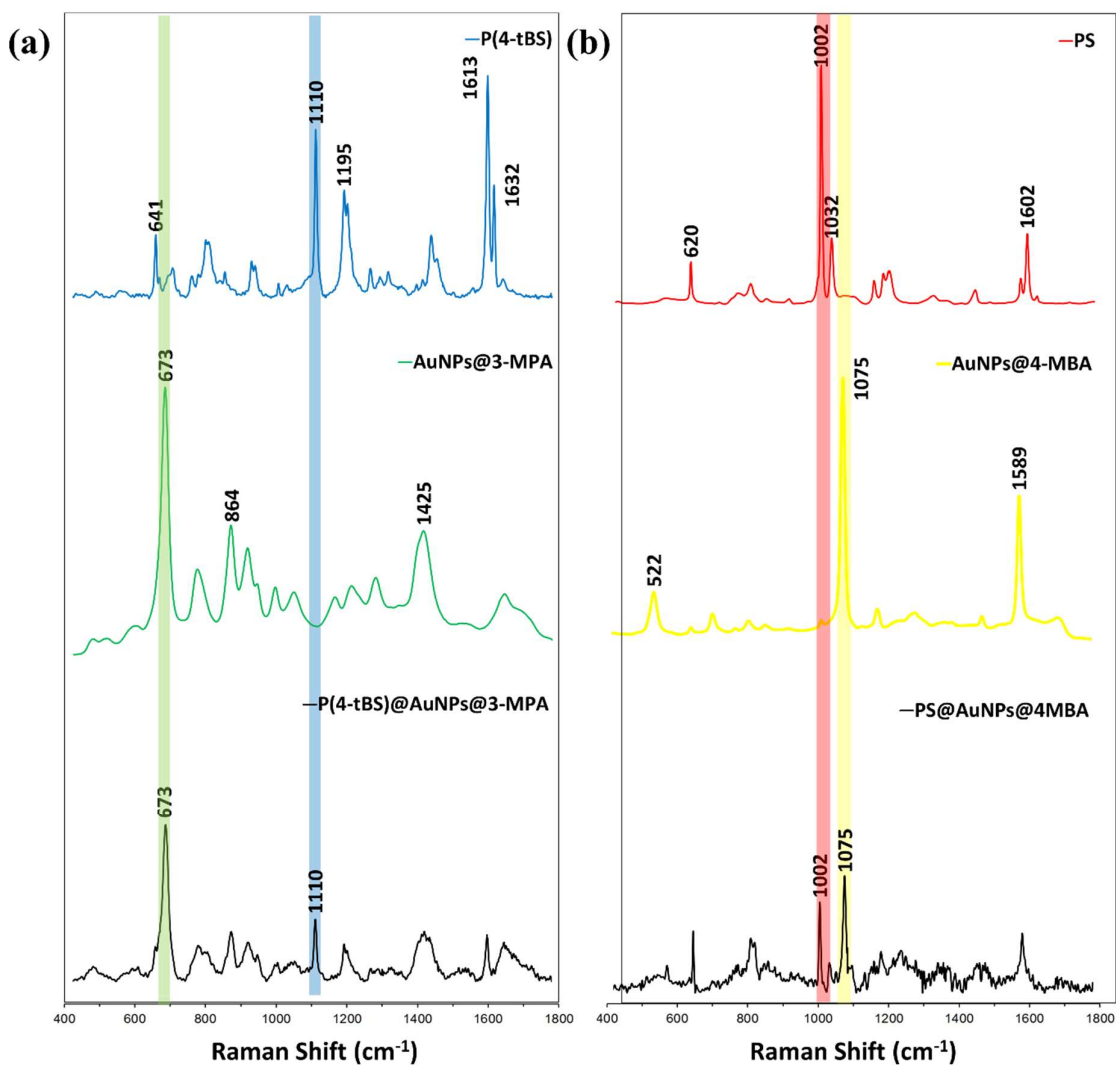
Figure 5-6. (a) Raman spectrum of P4tBS, AuNPs@3-MPA, and P4tBS bioconjugated to 3-MPA SERS nanotags via donkey antigoat IgG + goat antihuman IgG. (b) Raman spectrum of PS, AuNPs@4-MBA, and PS bioconjugated to 4-MBA SERS nanotags via donkey antirabbit IgG + rabbit antihuman IgG.

Raman imaging analysis was used to examine the above immunoassays. The aim is to explore the multiplexed immunocomplex through spectroscopic imaging of SERS nanotags on the Raman encoded microbeads. After mixing the two SERS-nanotag labelled antigens with the two Raman microbeads with immobilised antibodies, the Raman images can report the specific

interaction of antibodies and antigens. The false coloured Raman images are achieved based on the distinct spectral peaks of the dual -micro and -nano encoders, as well as using classical least squares (CLS) algorithm mode. Figure 5-7f shows optical images of the mixtures of two SERS-encoded reporters and two Raman-encoded polymer microbeads with surface antibody conjugation, and no immunoprecipitation or aggregation is observed, indicating the selective and specific interaction. This is important for Raman/SERS applications in multiplex analysis to ensure high reproducibility and reliability of measurements. By selecting and deselecting distinct signals of the two polymer microbeads and the two SERS nanotags, different Raman mapping images are depicted in Figure 5-7a-d. From that, we can distinguish the microbeads and SERS nanotags.

Raman imaging reveals that there is no cross-interaction of SERS nanotag signals. This is due to the matched IgG recognized by corresponding antigen labelled SERS nanotags. Therefore, the false coloured Raman imaging analysis further reinforces the Raman and SERS immunoassay results, that the interaction is highly selective and highly specific.
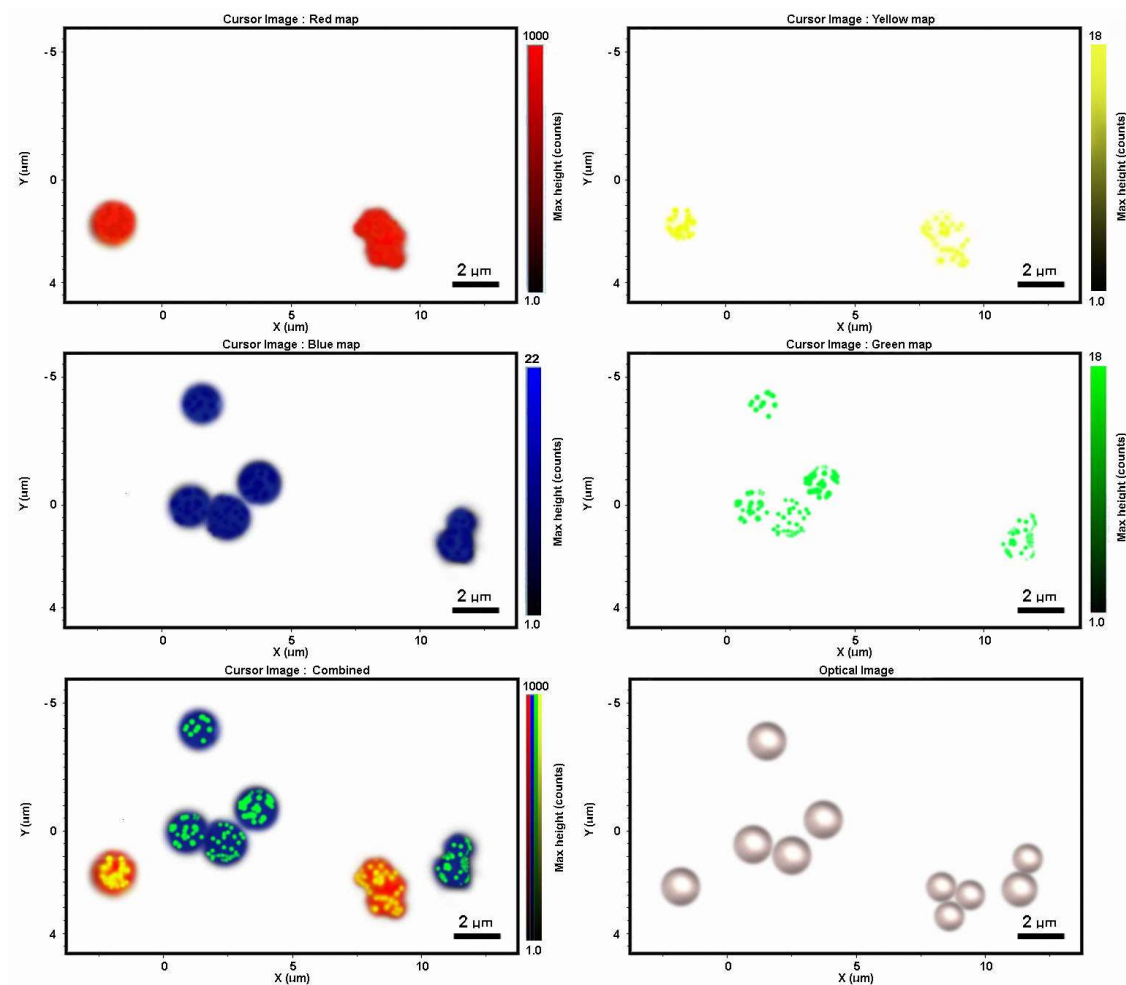
Figure 5-7. Raman imaging of the multiplex assays. (a-d) Raman images of PS microbeads (red), P4tBS microbeads (blue), 4-MBA SERS-nanotags (yellow) & 3-MPA SERS nanotags (green), (e-f) combined optical and false-coloured spectroscopic images of polymer microbeads PS and P4tBS with specific SERS nanotags.

As unabridged both Raman spectra and Raman imaging analysis indicate the specific recognition between antibodies and antigens. In clinical applications, fluorescence labels are popularly used for bioanalysis, but auto-fluorescence, photobleaching, and peak overlapping hinders its end-use applications. Our system combines the Raman signals of polymer microbeads (carrier) and SERS (reporter) signals for biomolecular diagnosis in lieu of these limitation. Various polymer microbeads can be easily synthesized, which gives rise to different

distinct Raman spectra. The formation of SAM on AuNP surface results in significant enhancement of reporter detection limits. The Raman/SERS bioassays combine the vibrational information of microbead supports and SERS reporters to identify IgG, and thus free from photobleaching and fluorescence interference. Based on different Raman spectra of polymer beads and the large effective enhancement factors of SERS tags, we can explore the applications of such systems for multiplex analysis. Polymer beads together with various SERS tags can offer infinite Raman vibrational information with high accuracy, which can be used to identify different biomolecules simultaneously from one homogeneous immunoassay. Similarly, it can be envisaged that, by increasing the number of encoded Raman polymer microbeads and SERS nanotags, more codes could be produced for the multiplex analysis of many analytes, the number of which, in principle, equals the product of the Polymer micro-code and SERS nano-code capacity. In general, the drift of the Raman distinct peak position of polymer microbeads occupies a spectral window of 10 cm^{-1} for imaging, so that the codes capacity of Raman could go up to 140 in the range of 400 to 1800 cm^{-1}. For SERS codes, almost every molecule has a Raman signal and there are at least 100 Raman reporters without counting the number of their homologs. Therefore, the capacity of the as-proposed dual-encoding is at the level of more than 14,000. This is far more than that of the usually-used encoding methods involving fluorescence,[54] qualifying this method for high analyte throughput.

5.4. Conclusion

A novel technique is demonstrated for multiplexed IgG detection based on a Raman/SERS dual encoding suspension immunoassay. AuNPs, SERS-active molecules and antigens were used to prepare the core−shell−corona structured SERS-encoded reporters by the SAM and surface modification. The resulting SERS reporters are able to produce significant SERS signals. Various surface functionalized Raman-encoded polymer microbeads are used to immobilise

IgG for bead-based immunoassays. Raman spectroscopy and Raman imaging characterization demonstrate that both the SERS (from reporter) and Raman (from microbeads) signatures can be successfully readout in the presence of specific molecular recognition. Such systems offer high selectivity, high specificity, high multiplex, no photo-bleaching, narrow emission spectra, single excitation wavelength, when compared to traditional bead-based fluorescence imaging analysis. This dual encoded Raman/SERS immunoassay analysis has great potential for future high throughput screening and multiplexing of target analytes extorting a promising solution for early stage in-vitro disease detection.

Acknowledgement

References

1.   Hurley, I. P.; Coleman, R. C.; Ireland, H. E.; Williams, J. H., Measurement of Bovine IgG by Indirect Competitive Elisa as a Means of Detecting Milk Adulteration. *Journal of Dairy Science* **2004**, *87*, 543-549.

2.   Hurley, I. P.; Coleman, R. C.; Ireland, H. E.; Williams, J. H., Use of Sandwich Igg Elisa for the Detection and Quantification of Adulteration of Milk and Soft Cheese. *International Dairy Journal* **2006**, *16*, 805-812.

3.   Berg, B.; Cortazar, B.; Tseng, D.; Ozkan, H.; Feng, S.; Wei, Q.; Chan, R. Y.-L.; Burbano, J.; Farooqui, Q.; Lewinski, M., Cellphone-Based Hand-Held Microplate Reader for Point-of-Care Testing of Enzyme-Linked Immunosorbent Assays. *ACS Nano* **2015**, *9*, 7857-7866.

4.   Algaar, F.; Eltzov, E.; Vdovenko, M. M.; Sakharov, I. Y.; Fajs, L.; Weidmann, M.; Mirazimi, A.; Marks, R. S., Fiber-Optic Immunosensor for Detection of Crimean-Congo Hemorrhagic Fever IgG Antibodies in Patients. *Analytical Chemistry* **2015**, *87*, 8394-8398.

5.   Li, H.; Zhao, M.; Liu, W.; Chu, W.; Guo, Y., Polydimethylsiloxane Microfluidic Chemiluminescence Immunodevice with the Signal Amplification Strategy for Sensitive Detection of Human Immunoglobin G. *Talanta* **2016**, *147*, 430-436.

6.   Shi, H.; Yuan, L.; Wu, Y.; Liu, S., Colorimetric Immunosensing Via Protein Functionalized Gold Nanoparticle Probe Combined with Atom Transfer Radical Polymerization. *Biosensors and Bioelectronics* **2011**, *26*, 3788-3793.

7.   Li, H.; Wang, C.; Ma, Z.; Su, Z., Colorimetric Detection of Immunoglobulin G by Use of Functionalized Gold Nanoparticles on Polyethylenimine Film. *Analytical and Bioanalytical Chemistry* **2006**, *384*, 1518-1524.

8.   Linder, V.; Verpoorte, E.; Thormann, W.; de Rooij, N. F.; Sigrist, H., Surface Biopassivation of Replicated Poly (Dimethylsiloxane) Microfluidic Channels and

Application to Heterogeneous Immunoreaction with on-Chip Fluorescence Detection. *Analytical Chemistry* **2001**, *73*, 4181-4189.

9.   Wang, M.; Hou, W.; Mi, C.-C.; Wang, W.-X.; Xu, Z.-R.; Teng, H.-H.; Mao, C.-B.; Xu, S.-K., Immunoassay of Goat Antihuman Immunoglobulin G Antibody Based on Luminescence Resonance Energy Transfer between near-Infrared Responsive Nayf4: Yb, Er Upconversion Fluorescent Nanoparticles and Gold Nanoparticles. *Analytical Chemistry* **2009**, *81*, 8783-8789.

10.   Lyon, L. A.; Musick, M. D.; Smith, P. C.; Reiss, B. D.; Pena, D. J.; Natan, M. J., Surface Plasmon Resonance of Colloidal Au-Modified Gold Films. *Sensors and Actuators B: Chemical* **1999**, *54*, 118-124.

11.   Cao, C.; Sim, S. J., Signal Enhancement of Surface Plasmon Resonance Immunoassay Using Enzyme Precipitation-Functionalized Gold Nanoparticles: A Femto Molar Level Measurement of Anti-Glutamic Acid Decarboxylase Antibody. *Biosensors and Bioelectronics* **2007**, *22*, 1874-1880.

12.   Song, C.; Wang, Z.; Zhang, R.; Yang, J.; Tan, X.; Cui, Y., Highly Sensitive Immunoassay Based on Raman Reporter-Labeled Immuno-Au Aggregates and SERS-Active Immune Substrate. *Biosensors and Bioelectronics* **2009**, *25*, 826-831.

13.   Chon, H.; Lim, C.; Ha, S.-M.; Ahn, Y.; Lee, E. K.; Chang, S.-I.; Seong, G. H.; Choo, J., On-Chip Immunoassay Using Surface-Enhanced Raman Scattering of Hollow Gold Nanospheres. *Analytical Chemistry* **2010**, *82*, 5290-5295.

14.   Kim, K.; Lee, Y. M.; Lee, H. B.; Shin, K. S., Silver-Coated Silica Beads Applicable as Core Materials of Dual-Tagging Sensors Operating Via SERS and MEF. *ACS Applied Materials & Interfaces* **2009**, *1*, 2174-2180.

15.   Shin, M. H.; Hong, W.; Sa, Y.; Chen, L.; Jung, Y.-J.; Wang, X.; Zhao, B.; Jung, Y. M., Multiple Detection of Proteins by SERS-Based Immunoassay with Core Shell Magnetic Gold Nanoparticles. *Vibrational Spectroscopy* **2014**, *72*, 44-49.

16.   Song, C.; Min, L.; Zhou, N.; Yang, Y.; Su, S.; Huang, W.; Wang, L., Synthesis of Novel Gold Mesoflowers as SERS Tags for Immunoassay with Improved Sensitivity. *ACS Applied Materials & Interfaces* **2014**, *6*, 21842-21850.

17.   Zhang, X.; Du, X., Carbon Nanodot-Decorated $Ag@SiO_2$ Nanoparticles for Fluorescence and Surface-Enhanced Raman Scattering Immunoassays. *ACS Applied Materials & Interfaces* **2015**, *8*, 1033-1040.

18.   Han, X. X.; Chen, L.; Ji, W.; Xie, Y.; Zhao, B.; Ozaki, Y., Label-Free Indirect Immunoassay Using an Avidin-Induced Surface-Enhanced Raman Scattering Substrate. *Small* **2011**, *7*, 316-320.

19.   Israelsen, N. D.; Wooley, D.; Hanson, C.; Vargis, E., Rational Design of Raman-Labeled Nanoparticles for a Dual-Modality, Light Scattering Immunoassay on a Polystyrene Substrate. *Journal of Biological Engineering* **2016**, *10*, 2.

20.   Kang, T.; Yoo, S. M.; Yoon, I.; Lee, S. Y.; Kim, B., Patterned Multiplex Pathogen DNA Detection by Au Particle-on-Wire SERS Sensor. *Nano Letters* **2010**, *10*, 1189-1193.

21.   Zheng, J.; Hu, Y.; Bai, J.; Ma, C.; Li, J.; Li, Y.; Shi, M.; Tan, W.; Yang, R., Universal Surface-Enhanced Raman Scattering Amplification Detector for Ultrasensitive Detection of Multiple Target Analytes. *Analytical Chemistry* **2014**, *86*, 2205-2212.

22.   Valdez, J.; Bawage, S.; Gomez, I.; Singh, S. R., Facile and Rapid Detection of Respiratory Syncytial Virus Using Metallic Nanoparticles. *Journal of Nanobiotechnology* **2016**, *14*, 13.

23.   Wu, X.; Xia, Y.; Huang, Y.; Li, J.; Ruan, H.; Chen, T.; Luo, L.; Shen, Z.; Wu, A., Improved SERS-Active Nanoparticles with Various Shapes for CTC Detection without

Enrichment Process with Supersensitivity and High Specificity. *ACS Applied Materials & Interfaces* **2016**, *8*, 19928-19938.

24.   Li, J.; Zhu, Z.; Zhu, B.; Ma, Y.; Lin, B.; Liu, R.; Song, Y.; Lin, H.; Tu, S.; Yang, C., Surface-Enhanced Raman Scattering Active Plasmonic Nanoparticles with Ultrasmall Interior Nanogap for Multiplex Quantitative Detection and Cancer Cell Imaging. *Analytical Chemistry* **2016**, *88*, 7828-7836.

25.   Feng, J.; Xu, L.; Cui, G.; Wu, X.; Ma, W.; Kuang, H.; Xu, C., Building SERS-Active Heteroassemblies for Ultrasensitive Bisphenol a Detection. *Biosensors and Bioelectronics* **2016**, *81*, 138-142.

26.   Gellner, M.; Kömpe, K.; Schlücker, S., Multiplexing with SERS Labels Using Mixed Sams of Raman Reporter Molecules. *Analytical and Bioanalytical Chemistry* **2009**, *394*, 1839-1844.

27.   Doering, W. E.; Piotti, M. E.; Natan, M. J.; Freeman, R. G., SERS as a Foundation for Nanoscale, Optically Detected Biological Labels. *Advanced Materials* **2007**, *19*, 3100-3108.

28.   Wu, L.; Wang, Z.; Fan, K.; Zong, S.; Cui, Y., A SERS-Assisted 3D Barcode Chip for High-Throughput Biosensing. *Small* **2015**, *11*, 2798-2806.

29.   Li, M.; Kang, J. W.; Sukumar, S.; Dasari, R. R.; Barman, I., Multiplexed Detection of Serological Cancer Markers with Plasmon-Enhanced Raman Spectro-Immunoassay. *Chemical Science* **2015**, *6*, 3906-3914.

30.   Kang, H.; Jeong, S.; Park, Y.; Yim, J.; Jun, B. H.; Kyeong, S.; Yang, J. K.; Kim, G.; Hong, S.; Lee, L. P., Near-Infrared SERS Nanoprobes with Plasmonic Au/Ag Hollow-Shell Assemblies for in Vivo Multiplex Detection. *Advanced Functional Materials* **2013**, *23*, 3719-3727.

31. Lai, Y.; Sun, S.; He, T.; Schlücker, S.; Wang, Y., Raman-Encoded Microbeads for Spectral Multiplexing with SERS Detection. *RSC Advances* **2015**, *5*, 13762-13767.

32. Zheng, P.; Li, M.; Jurevic, R.; Cushing, S. K.; Liu, Y.; Wu, N., A Gold Nanohole Array Based Surface-Enhanced Raman Scattering Biosensor for Detection of Silver (I) and Mercury (Ii) in Human Saliva. *Nanoscale* **2015**, *7*, 11005-11012.

33. Dinish, U.; Balasundaram, G.; Chang, Y.-T.; Olivo, M., Actively Targeted in Vivo Multiplex Detection of Intrinsic Cancer Biomarkers Using Biocompatible SERS Nanotags. *Scientific Reports* **2014**, *4*.

34. Li, M.; Yang, H.; Li, S.; Zhao, K.; Li, J.; Jiang, D.; Sun, L.; Deng, A., Ultrasensitive and Quantitative Detection of a New B-Agonist Phenylethanolamine a by a Novel Immunochromatographic Assay Based on Surface-Enhanced Raman Scattering (SERS). *Journal of Agricultural and Food Chemistry* **2014**, *62*, 10896-10902.

35. Xu, L.; Yan, W.; Ma, W.; Kuang, H.; Wu, X.; Liu, L.; Zhao, Y.; Wang, L.; Xu, C., SERS Encoded Silver Pyramids for Attomolar Detection of Multiplexed Disease Biomarkers. *Advanced Materials* **2015**, *27*, 1706-1711.

36. Raez, J.; Blais, D. R.; Zhang, Y.; Alvarez-Puebla, R. A.; Bravo-Vasquez, J. P.; Pezacki, J. P.; Fenniri, H., Spectroscopically Encoded Microspheres for Antigen Biosensing. *Langmuir* **2007**, *23*, 6482-6485.

37. Wei, L.; Jin, B.; Dai, S., Polymer Microbead-Based Surface Enhanced Raman Scattering Immunoassays. *The Journal of Physical Chemistry C* **2012**, *116*, 17174-17181.

38. Song, J.-S.; Chagal, L.; Winnik, M. A., Monodisperse Micrometer-Size Carboxyl-Functionalized Polystyrene Particles Obtained by Two-Stage Dispersion Polymerization. *Macromolecules* **2006**, *39*, 5729-5737.

39. Turkevich, J.; Stevenson, P. C.; Hillier, J., A Study of the Nucleation and Growth Processes in the Synthesis of Colloidal Gold. *Discussions of the Faraday Society* **1951**, *11*, 55-75.

40. Schmidt, R., Colloidal Gold; Principles, Methods and Applications, Hayat Ma. Academic Press, Inc. Harcourt Brace Jovanovich, Publishers, Stuttgart-New York (1989), Price: Dm 144, 50. Urban & Fischer: 1990.

41. Jun, B.-H.; Kim, J.-H.; Park, H.; Kim, J.-S.; Yu, K.-N.; Lee, S.-M.; Choi, H.; Kwak, S.-Y.; Kim, Y.-K.; Jeong, D. H., Surface-Enhanced Raman Spectroscopic-Encoded Beads for Multiplex Immunoassay. *Journal of Combinatorial Chemistry* **2007**, *9*, 237-244.

42. McCabe, A. F.; Eliasson, C.; Prasath, R. A.; Hernandez-Santana, A.; Stevenson, L.; Apple, I.; Cormack, P. A.; Graham, D.; Smith, W. E.; Corish, P., SERRS Labelled Beads for Multiplex Detection. *Faraday Discussions* **2006**, *132*, 303-308.

43. Abdelrahman, A. I.; Ornatsky, O.; Bandura, D.; Baranov, V.; Kinach, R.; Dai, S.; Thickett, S. C.; Tanner, S.; Winnik, M. A., Metal-Containing Polystyrene Beads as Standards for Mass Cytometry. *Journal of Analytical Atomic Spectrometry* **2010**, *25*, 260-268.

44. Liang, C.; Krimm, S., Infrared Spectra of High Polymers. Vi. Polystyrene. *Journal of Polymer Science* **1958**, *27*, 241-254.

45. Weisbecker, C. S.; Merritt, M. V.; Whitesides, G. M., Molecular Self-Assembly of Aliphatic Thiols on Gold Colloids. *Langmuir* **1996**, *12*, 3763-3772.

46. Hung, Y.-L.; Hsiung, T.-M.; Chen, Y.-Y.; Huang, Y.-F.; Huang, C.-C., Colorimetric Detection of Heavy Metal Ions Using Label-Free Gold Nanoparticles and Alkanethiols. *The Journal of Physical Chemistry C* **2010**, *114*, 16329-16334.

47.   Neng, J.; Harpster, M. H.; Wilson, W. C.; Johnson, P. A., Surface-Enhanced Raman Scattering (SERS) Detection of Multiple Viral Antigens Using Magnetic Capture of SERS-Active Nanoparticles. *Biosensors and Bioelectronics* **2013**, *41*, 316-321.

48.   Park, H.; Lee, S. B.; Kim, K.; Kim, M. S., Surface-Enhanced Raman Scattering of P-Aminobenzoic Acid at Silver Electrode. *Journal of Physical Chemistry* **1990**, *94*, 7576-7580.

49.   Michota, A.; Bukowska, J., Surface-Enhanced Raman Scattering (SERS) of 4-Mercaptobenzoic Acid on Silver and Gold Substrates. *Journal of Raman Spectroscopy* **2003**, *34*, 21-25.

50.   Lin-Vien, D.; Colthup, N. B.; Fateley, W. G.; Grasselli, J. G., *The Handbook of Infrared and Raman Characteristic Frequencies of Organic Molecules*; Elsevier, 1991.

51.   Castro, J.; López-Ramírez, M.; Arenas, J.; Otero, J., Surface-Enhanced Raman Scattering of 3-Mercaptopropionic Acid Adsorbed on a Colloidal Silver Surface. *Journal of Raman Spectroscopy* **2004**, *35*, 997-1000.

52.   Camargo, P. H.; Cobley, C. M.; Rycenga, M.; Xia, Y., Measuring the Surface-Enhanced Raman Scattering Enhancement Factors of Hot Spots Formed between an Individual Ag Nanowire and a Single Ag Nanocube. *Nanotechnology* **2009**, *20*, 434020.

53.   Le Ru, E.; Blackie, E.; Meyer, M.; Etchegoin, P. G., Surface Enhanced Raman Scattering Enhancement Factors: A Comprehensive Study. *The Journal of Physical Chemistry C* **2007**, *111*, 13794-13803.

54.   Zhao, X.; Zhao, Y.; Gu, Z., Advances of Multiplex and High Throughput Biomolecular Detection Technologies Based on Encoding Microparticles. *Science China Chemistry* **2011**, *54*, 1185.

Chapter 6   Conclusions and Future Directions

6.1 Conclusions

This research focused on the preparation of suitable-sized gold nanoparticles (AuNPs) as the "hotspot" of SERS, various surface-functionalized copolymer microbeads with unique Raman signatures by two stage dispersion polymerisation, SAMs of Raman-active molecules, polymer microbead-based Raman/SERS immunoassay systems, which is finally aimed at multiplexed bioassay for immunoglobulin (IgG) detection through Raman spectroscopy and imaging.

6.1.1 Preparation of AuNP's and their SAMs

AuNPs were chosen as SERS-active substrates for the SERS tag preparation after self-assembled with different Raman-active molecules (4-ATP, 4-MBA and 3-MPA). Suitable-sized gold nanoparticles (AuNPs) as the "hotspot" for SERS were prepared by keeping the feed molar ratios of $HAuCl_4 \cdot 3H_2O/Na_3Ct$ as 1:2. As a result stable red coloured gold colloidal particles were achieved with approximate size of 25 nm. It was found these AuNPs with 25 nm average size gave a high Raman effective enhancement factor and is more suitable for producing significant SERS signals of the SAMs. This provides important information for the future utilisation of AuNPs as SERS substrate.

6.1.2 Synthesis of Surface Functionalized Polymer Microbeads.

Monodispersed copolymer microbeads with narrow size distribution and unique Raman signatures were fabricated using two stage dispersion polymerisation. Four different monodisperse copolymer microbeads, namely, poly(styrene-co-acrylic acid), poly(4-methylstyrene-co-acrylic acid), poly(4-tetrabutylstyrene-co-acrylic acid) and poly(glycidyl

methacrylate-co-acrylic acid), were produced with their particle sizes ranging from 1.1 to 1.7 µm. The surface carboxyl groups were introduced by the addition of functional comonomer (AA) during synthesis. The potentiometric and conductometric titrations indicated that carboxyl groups were present on the surface of the polymer microbeads, which render their possibility for further bioconjugation. The conversions for all the polymerisation for the microbeads fabrication was higher than 91% with less than 5% coefficient of variation (CV). The produced polymer microbeads were successfully used for high resolution Raman imaging with their narrow size distribution and specific spectroscopic properties.

6.1.3 Raman Analysis of Raman and SERS Dual Encoded Microbeads

SERS-tag molecules were conjugated to polystyrene (PS) or 4-tertbutylstyrene microbeads by conjugation chemistry to produce Raman and SERS dual encoded microbeads. The spectroscopic and imaging results reinforce the suitability of such dual coding systems. The result promises a substantial increase in the current combinatorial library for label free multiplexing in bioassays.

6.1.4 Highly Selective Multiplex Imaging from Raman/SERS Bioassays

An immunoassay system was developed for the multiplex, specific and sensitive detection of biological molecules. IgG was used as the model proteins. AuNPs, SERS-active molecules and antigens were used to prepare a core−shell−corona structured SERS-encoded reporters by the SAM and surface modification. The resulting SERS reporters are able to produce significant SERS signals. Various surface functionalized Raman-encoded polymer microbeads are used to immobilise IgG for bead-based immunoassays. Raman spectroscopy and Raman imaging characterization demonstrate that both the SERS (from reporter) and Raman (from microbeads) signatures can be successfully readout in the presence of specific molecular recognition. Such

systems offer no photo-bleaching, narrow emission spectra, single excitation wavelength when compared to traditional bead-based fluorescence imaging analysis.

This dual encoded Raman/SERS immunoassay analysis has great potential for future high throughput screening and multiplexing of target analytes extorting a promising solution for early stage in-vitro disease detection. In summary, a novel technique is demonstrated for multiplexed IgG detection based on a Raman/SERS dual encoding suspension immunoassay.

6.2 Future Directions

6.2.1 Dual Coding Systems for Immunoassays

As discussed in Chapter 4, SERS-active polymer microbeads with Raman signatures can be fabricated by the conjugation of AuNPs on the surface of polymer microbeads. Although a few copolymer microbeads with narrow size distribution and unique Raman fingerprints have been prepared in this study, the fabrication of different copolymer microbeads using dispersion polymerization still remains a challenge. In addition, Chapter 4 only chooses one aromatic thiol (4-ATP) as model Raman-active molecules to fabricate dual-encoded microbeads. Therefore, different Raman-active molecules, need to be self-assembled onto different *co*-functionalized polymer/AuNP composite microspheres in order to enhance the combinatorial library. This will require establishing detailed conjugation protocols for use of unique Raman active molecules.

6.2.2 Multiplex IgG Immunoassay Systems

Different SERS nanotags and Raman spectroscopic-encoded copolymer microbeads have been synthesized with unique Raman fingerprints. These microbeads were applied for the multiplex IgG detection system development based on Raman bio-imaging. By conjugating different

Raman spectroscopic-encoded microbeads with different antibodies, the microbeads specifically recognise the matched antigens after the formation of sandwich structures with SERS reporters. Because of the unique Raman spectra of microbeads and SERS reporters, the identification of each antigen was achieved by measuring the Raman signals of polymer microbead and SERS reporter combination. This can establish a major breakthrough in the field of bio-imaging for early stage cancer detection with minimal sample, high sensitivity, rapid diagnosis, multiplex and label-free bioassays. Future challenge remains in developing a Raman microscope capable of more rapidly acquiring the Raman image with higher plain coverage. This means advances in camera acquisition rates and digital processing speeds to enable faster analysis rates.

6.2.3 Raman Flow Cytometry System Based on Microfluidics

The Raman and SERS-active polymer microbeads have demonstrated their importance for multiplex detection. However, there is no commercial flow cytometry available to read these Raman/SERS signals. Therefore, requirement remains to demonstrate a system of sufficient sensitivity to acquire and analyse Raman/SERS spectra with good spectral resolution from samples consisting of nanoparticle SERS tags bound to Raman encoded microspheres. Challenges also remains in terms of speed and sensitivity whilst maintaining good resolution. The concept of lab-on-a-chip (microfluidics) devices takes advantage of the basic principles of flow cytometry (fluorescent) by a system of particularly shaped micro channels. Therefore, as part of future work for Raman/SERS based multiplex IgG detection, microfluidics could make it possible to quickly measure multiple analytes simultaneously and decrease related analytical cost.

Statement of Authorship

Title of Paper	Recent Advance of Surface Enhanced Raman Scattering for Bioanalysis
Publication Status	☐ Published ☐ Accepted for Publication ☐ Submitted for Publication ☑ Unpublished and Unsubmitted work written in manuscript style
Publication Details	Umar Azhar, Zeyad Alwahabi, Sheng Dai In preparation for submission.

Principal Author

Name of Principal Author (Candidate)	Umar Azhar		
Contribution to the Paper	Performed literature review and wrote the manuscript.		
Overall percentage (%)	70%		
Certification:	This paper reports on original research I conducted during the period of my Higher Degree by Research candidature and is not subject to any obligations or contractual agreements with a third party that would constrain its inclusion in this thesis. I am the primary author of this paper.		
Signature		Date	28th December 2018

Co-Author Contributions

By signing the Statement of Authorship, each author certifies that:

i.   the candidate's stated contribution to the publication is accurate (as detailed above).

ii. permission is granted for the candidate in include the publication in the thesis; and

iii. the sum of all co-author contributions is equal to 100% less the candidate's stated contribution.

Name of Co-Author	Professor Sheng Dai		
Contribution to the Paper	Supervision of manuscript preparation, evaluation and acting as the corresponding author.		
Signature		Date	2nd Jan 2019

Name of Co-Author	Associate Professor Zeyad Alwahabi		
Contribution to the Paper	Supervision of manuscript preparation, and evaluation.		
Signature		Date	Jan 3, 2019

Please cut and paste additional co-author panels here as required.

Statement of Authorship

Title of Paper	Identify Label-free Surface-functionalized Monodisperse Polymer Microbeads through Multiplex Raman Mapping
Publication Status	☐ Published ☐ Accepted for Publication ☑ Submitted for Publication ☐ Unpublished and Unsubmitted work written in manuscript style
Publication Details	Umar Azhar, Zeyad Alwahabi, Sheng Dai Submitted to ACS Langmuir for publication.

Principal Author

Name of Principal Author (Candidate)	Umar Azhar
Contribution to the Paper	Designed and performed the experiments. Interpreted data and wrote the manuscript.
Overall percentage (%)	70%
Certification:	This paper reports on original research I conducted during the period of my Higher Degree by Research candidature and is not subject to any obligations or contractual agreements with a third party that would constrain its inclusion in this thesis. I am the primary author of this paper.
Signature	Date 28ᵗ December 2018

Co-Author Contributions

By signing the Statement of Authorship, each author certifies that:

i.   the candidate's stated contribution to the publication is accurate (as detailed above);

ii. permission is granted for the candidate in include the publication in the thesis; and

iii. the sum of all co-author contributions is equal to 100% less the candidate's stated contribution.

Name of Co-Author	Professor Sheng Dai
Contribution to the Paper	Supervised development of work, data interpretation, manuscript evaluation and acting as the corresponding author.
Signature	Date 2nd Jan 2019

Name of Co-Author	Associate Professor Zeyad Alwahabi
Contribution to the Paper	Supervised development of work, manuscript evaluation and acting as the corresponding author.
Signature	Date Jan 3, 2019

Please cut and paste additional co-author panels here as required.

Statement of Authorship

Title of Paper	Synthesis and Spectroscopic Study of Dual-encoded Microbeads by Raman Scattering and Surface Enhanced Raman Scattering
Publication Status	☐ Published ☐ Accepted for Publication ☐ Submitted for Publication ☑ Unpublished and Unsubmitted work written in manuscript style
Publication Details	Umar Azhar, Aabhash Shrestha, Zeyad Alwahabi, Sheng Dai. In preparation for submission.

Principal Author

Name of Principal Author (Candidate)	Umar Azhar		
Contribution to the Paper	Designed and performed the experiments. Interpreted data and wrote the manuscript.		
Overall percentage (%)	70%		
Certification:	This paper reports on original research I conducted during the period of my Higher Degree by Research candidature and is not subject to any obligations or contractual agreements with a third party that would constrain its inclusion in this thesis. I am the primary author of this paper.		
Signature		Date	28th December 2018

Co-Author Contributions

By signing the Statement of Authorship, each author certifies that:

i. the candidate's stated contribution to the publication is accurate (as detailed above);

ii. permission is granted for the candidate to include the publication in the thesis; and

iii. the sum of all co-author contributions is equal to 100% less the candidate's stated contribution.

Name of Co-Author	Professor Sheng Dai		
Contribution to the Paper	Supervised development of work, data interpretation, manuscript evaluation and acting as the corresponding author		
Signature		Date	2nd Jan 2019

Name of Co-Author	Associate Professor Zeyad Alwahabi		
Contribution to the Paper	Supervised development of work, manuscript evaluation and acting as the corresponding author		
Signature		Date	Jan 3, 2019

Please cut and paste additional co-author panels here as required.

Statement of Authorship

Title of Paper	Sensitive Multiplex Imaging for Raman/SERS-Dual Encoded Bioassays
Publication Status	☐ Published ☐ Accepted for Publication ☐ Submitted for Publication ☑ Unpublished and Unsubmitted work written in manuscript style
Publication Details	Umar Azhar, Qazi Ahmed, Aabhash Shrestha, Zeyad Alwahabi, Sheng Dai In preparation for submission.

Principal Author

Name of Principal Author (Candidate)	Umar Azhar
Contribution to the Paper	Designed and performed the experiments. Interpreted data and wrote the manuscript.
Overall percentage (%)	70%
Certification:	This paper reports on original research I conducted during the period of my Higher Degree by Research candidature and is not subject to any obligations or contractual agreements with a third party that would constrain its inclusion in this thesis. I am the primary author of this paper.
Signature		Date	28ᵗʰ December 2018

Co-Author Contributions

By signing the Statement of Authorship, each author certifies that:

- i. the candidate's stated contribution to the publication is accurate (as detailed above);
- ii. permission is granted for the candidate in include the publication in the thesis; and
- iii. the sum of all co-author contributions is equal to 100% less the candidate's stated contribution.

Name of Co-Author	Professor Sheng Dai
Contribution to the Paper	Supervised development of work, data interpretation, manuscript evaluation and acting as the corresponding author.
Signature		Date	2nd June 2019.

Name of Co-Author	Associate Professor Zeyad Alwahabi
Contribution to the Paper	Supervised development of work and manuscript evaluation.
Signature		Date	Jan 3, 2019

Please cut and paste additional co-author panels here as required.